

MiCHe project

UNIBO UNIT CONTRIBUTION

Case study: Modena Cathedral

UNIBO Unit:

Prof. Tomaso Trombetti

Prof. Alberto Montanari

Ing. Michele Palermo

Ing. Simonetta Baraccani

Prof. Ing Giada Gasparini

Ing. Serena Ceola

Ing. Andrea Mazzola



Index

| | |
|--|-----------|
| Introduction | 6 |
| PART 1: APPROACHES AND METHODS..... | 8 |
| 1 HISTORICAL BUILDINGS: THE NEED OF SPECIFIC APPROACHES FOR A RELIABLE RISK ANALYSIS..... | 9 |
| 2 GUIDELINES FOR THE INTEGRATED KNOWLEDGE OF CULTURAL HERITAGE ASSETS..... | 11 |
| 3 MULTI- ANALYSIS INTEGRATED FOR SEISMIC VULNERABILITY ASSESSMENT | 13 |
| 4 A REVIEW OF STRUCTURAL INTERVENTIONS FOR THE CONSERVATION OF CULTURAL HERITAGE BUILDINGS..... | 14 |
| 4.1. Intervention on foundations | 14 |
| 4.1.1. Example: the Leaning Tower of Pisa | 19 |
| 4.1.2. Example: Intervention on the foundations of the Frari bell tower (Venice) | 21 |
| 4.2. Intervention techniques on masonry buildings | 22 |
| 4.2.1. Use of tie-rods to improve connections between masonry walls | 23 |
| 4.2.2. Ring and head beams | 23 |
| 4.2.3. Interventions to increase the masonry strength | 25 |
| 4.3. Arches and vaults..... | 29 |
| 4.3.1. Traditional consolidation procedures..... | 30 |
| 4.3.2. Consolidation with FRP and FRCM | 31 |
| 4.4. Intervention on roof structures..... | 32 |
| 4.4.1. Approach | 32 |
| 4.4.2. Example of "Collegiata di San Michele Arcangelo", Bagnacavallo (RA) | 34 |
| 5 PLUVIAL FLOOD HAZARD /RISK ASSESSMENT..... | 37 |
| 5.1 Preliminary hydraulic risk evaluation | 37 |
| 5.1.1 Flood hazard maps..... | 37 |
| 5.1.2 Flood risk maps..... | 41 |
| 5.1.3 Concluding remarks | 43 |
| 5.2 Pluvial flood hazard assessment..... | 45 |
| 5.2.1 Methods | 45 |



| | | |
|---|---|-----------|
| 5.2.2 | Required input data | 46 |
| 5.2.3 | Simulated rainfall events | 48 |
| 6 | MULTI-RISK ASSESSMENT | 50 |
| 6.1 | Single risk analysis | 50 |
| 6.1.1 | Introduction | 50 |
| 6.1.2 | Risk assessment approach for each individual hazard | 51 |
| 6.1.3 | Multi exposure analysis | 53 |
| 6.1.4 | Exposure factors for monumental buildings | 54 |
| 6.1.5 | Risk assessment for each individual hazard: the seismic hazard | 55 |
| 6.2 | Multi-risk analysis | 60 |
| PART 2: CASE STUDY- THE MODENA CATHEDRAL | | 61 |
| 1 | THE INTEGRATED KNOWLEDGE | 62 |
| 1.1 | The Cathedral of Modena | 62 |
| 1.2 | The actual state of the Cathedral..... | 64 |
| 1.2.1 | The construction phases and the main interventions | 64 |
| 1.2.2 | The reconstruction of the geometric configuration through laser scanner and the geotechnical investigations | 67 |
| 1.2.3 | Material properties..... | 69 |
| 1.2.4 | The actual state of degradation..... | 69 |
| 1.3 | Seismic Hazard analyses | 73 |
| 1.3.1 | Historical Deterministic Seismic Hazard Analysis (HDSHA) | 74 |
| 1.3.2 | Maximum Historical Earthquake Analysis (MHEA) | 76 |
| 1.3.3 | The 2012 Emilia's earthquake | 77 |
| 1.4 | Flood hazard assessment..... | 80 |
| 1.4.1 | Pluvial flooding closet o Modena Cathedral: results for the entire square | 80 |
| 1.4.2 | Pluvial flooding closet o Modena Cathedral: results for the Cathedral (inside and outside) | 84 |
| 1.5 | Concluding remarks..... | 94 |
| 2 | STRUCTURAL ASSESSMENT AND SEISMIC VULNERABILITY | 95 |



| | |
|---|------------|
| 2.1 Global structural behaviour | 95 |
| 2.1.1 Introduction | 95 |
| 2.1.2 The models and the simulations | 95 |
| 2.1.3 Static analyses | 96 |
| 2.1.4 Structural analysis with simple models | 97 |
| 2.1.5 Structural analysis with 3D finite element models | 102 |
| 2.2 Seismic behaviour: global analyses | 108 |
| 2.2.1 Natural frequency analysis | 108 |
| 2.2.2 Global seismic response | 109 |
| 2.2.3 Time history analyses: input the main shock recorded by the station of Modena | 114 |
| 2.2.4 The main vulnerabilities and conclusions | 117 |
| 2.3 Local structural analyses | 118 |
| 2.3.1 Introduction | 118 |
| 2.3.2 The models and the simulation | 118 |
| 2.3.3 Local collapse mechanisms | 119 |
| 2.3.4 The vault | 123 |
| 2.3.5 Summary of results from local analyses | 127 |
| 2.3.6 Structural analyses via Discrete Element Method | 129 |
| 2.3.7 Summary of results from Discrete Element Method simulations | 135 |
| 2.4 Structural Health Monitoring of the Cathedral of Modena | 138 |
| 2.4.1 Introduction | 138 |
| 2.4.2 Reference quantities | 138 |
| 2.4.3 Types and location of instruments | 139 |
| 2.4.4 Reference quantities | 143 |
| 2.4.5 Summary of results from SHM | 156 |
| 3 SEISMIC RISK ASSESSMENT | 157 |
| 3.1 Hazard curve | 157 |
| 3.2 Performance curves | 159 |
| 3.2.1 Accelerations that activate the different SL | 159 |
| 3.2.2 Fragility curves and performance curve | 163 |



| | | |
|---------------------------------|--|------------|
| 3.3 | Vulnerability curves..... | 164 |
| 3.4 | Risk curve L1..... | 170 |
| 4 | MULTI-RISK ASSESSMENT | 173 |
| 4.1 | Summary of Fire risk analysis | 173 |
| 4.2 | Total risk curve L1..... | 176 |
| PART 3: MITIGATION | | 179 |
| 1 | MAIN VULNERABILITIES RELATED TO EARTHQUAKE AND FIRE RISKS | 180 |
| 1.1 | Vulnerabilities from earthquake-risk analysis..... | 180 |
| 1.2 | Vulnerabilities from fire-risk analysis | 181 |
| 2 | SOLUTION STRATEGIES FOR SEISMIC RISK MITIGATION | 182 |
| 2.1 | Interventions..... | 182 |
| 2.1 | Performance curve | 186 |
| 2.2 | Risk curve L1..... | 188 |
| 3 | SOLUTION STRATEGIES FOR FIRE RISK MITIGATION | 189 |
| 3.1 | Interventions..... | 189 |
| 3.1.1 | Sprinkler system | 190 |
| 3.2 | Fire risk assessment..... | 192 |
| 4 | MULTI-RISK ASSESSMENT DUE TO EARTHQUAKE AND FIRE HAZARD | 195 |
| 4.1 | Total risk curve L1..... | 195 |
| BIBLIOGRAPHY..... | | 198 |



Introduction

Cultural heritage buildings represent inestimable values and not removable resources of most of European countries, which have to be preserved for future generations in order to transmit their history, culture, art. The correct management of cultural heritage buildings is a crucial issue: on one side, the conservative restoration requires compatible and limited intervention techniques in order to preserve the integrity of the monuments, and on the other side, this implies a profound knowledge of the structural behaviour, often difficult to understand and to predict for these complex buildings. The most widespread construction material used, especially in Italy, for the monumental buildings is the masonry that is characterized by a quite complex mechanical behaviour due to composite nature resulting from the interaction of bricks and mortar (both characterized by significantly different behaviour under tension and compression) thus leading to specific issues to be faced when analysing and modelling these constructions. Moreover, historical monuments are built and modified during the centuries by using various construction techniques, workmanships of different expertise, with the result of a complex fabric, characterized by a high degree of uncertainties, quite far from our modern buildings. In most cases, their actual configuration and the state of conservation are not only the result of the natural degradation due to aging effects, but also the consequence of the impact of past extreme natural events (such as earthquakes, floods, groundwater changes), which may sometime have caused partial or total collapses. The inherent complexity of historical buildings (due to the articulated geometrical configuration, the use of different construction techniques, different materials, the level of the connections between orthogonal walls), together with the natural material decay and the effects of natural hazards, makes the assessment the "structural health" extremely challenging. Furthermore, all the uncertainties due to this complexity render each monument a "unique". This means that there is no baseline directly applicable in order to obtain useful information concerning the "health" of the structure and the approach commonly used for the assessment of modern steel and concrete building (largely based on the use of computer software and well-established guidelines or codes) cannot be simply adopted for historical buildings. On the other hand such effects tend to inevitably reduce the level of safety and therefore increases the risks to future extreme events, but the monuments have also to meet the practical test of utility. Therefore, it clearly appears the need of a reliable estimation of the actual level of safety in order to plan effective interventions. In this respect, while for the case of conventional structures, a common strategy to reduce the uncertainties and therefore provide a reliable assessment of the "structural health" is based on the use of extended in situ experimental tests (destructive tests). For the case of cultural



heritage sites, the authorities responsible of monuments conservations in the spite of preserving the original integrity often prohibit this strategy.

An alternative approach to reduce the uncertainties in the knowledge of historical sites should be based on the development of a multidisciplinary approach aimed at providing an “integrated knowledge” through the mutual exchanging of expertise and capabilities offered by different fields. In this interdisciplinary knowledge process a fundamental contribution is played by the Structural Health Monitoring (SHM) whose aim is to evaluate the evolution of the structural health through a continuous real-time monitoring.

Hence, the main feature of Structural Health Monitoring strategy for monuments is to be geared towards a long-term evaluation of what is ‘normal’ structural performance or ‘health’. In this regard several studies available in the scientific literature, in fact, reported the main information obtained through structural health monitoring. However, such information are not so easy to compare given that a no unique approach is used for data analysis and interpretation.

Similarly, the assessment methods commonly used for the analyses of the “structural health” and for the evaluations of the effects of extreme events, consisting in the developments of single computer-based model and numerical simulations, do not always appear as appropriate for the case of historical monuments. Generally, only one model of the whole building is not able to capture all the structural peculiarities.

The research work developed by the UNIBO Unit focuses on:

- Development of guidelines for integrated knowledge of the cultural heritage buildings;
- Development of a framework of multi analyses for the assessment of the structural behaviour of monumental buildings;
- Review of structural solutions for the conservation of cultural heritage buildings;
- Simplified procedure for risk assessment of monumental buildings due to multiple hazards accounting for different sources of exposure;
- Multi-risk analysis for the Cathedral of Modena including earthquake, fire and flood hazards;



ALMA MATER STUDIORUM
UNIVERSITA' DI BOLOGNA

DICAM

Dipartimento di Ingegneria Civile,
Chimica, Ambientale e dei Materiali

MiChe

Mitigating the Impacts of natural hazards on Cultural Heritage
sites, structures and artefacts

PART 1: APPROACHES AND METHODS

Part 1 illustrates the approaches and methods that will be adopted to conduct the risk analysis for the case study of Modena Cathedral. After a brief introduction mentioning the main specific issues for a reliable risk analysis of a monumental building (chapter 1), chapter 2 will provides some general guidelines for a correct knowledge process. Chapter 3 will then introduce the basic concepts and approaches to conduct a seismic vulnerability assessment. Chapter 4 will give an overview on the main intervention strategies and solutions to mitigate the structural static and seismic vulnerabilities of monumental buildings. Finally, chapter 5 will introduce the methodology adopted for the hydraulic risk evaluation.



1 Historical buildings: the need of specific approaches for a reliable risk analysis

Historical masonry monuments are not only works of art, but also have to meet the practical test of utility and a suitable safety level. The efficient preservation of the structural health of these unique buildings presents several challenges. From a structural point of view, historical monuments are characterized by much larger uncertainties than ordinary buildings and conventional analysis tools may fail in providing a reliable characterization of their structural behaviour. According to the principles of restoration, only with a thorough knowledge it is possible to develop a consistent structural analyses (able to represent the real structural behaviour) and conceive, thus, intervention solutions targeted at preserving the integrity of the historical monuments. The concept of integrity, often, is only interpreted as the requirement of preserving the shape and the appearance of the monument. Instead, with reference to historical monuments, the requirement of integrity is not so simple because it also implies historic integrity, by considering the changes of the monument with time, as well as material integrity that means construction techniques, materials and structural scheme. Therefore, preserving integrity requires, beside an interdisciplinary approach, the development of a holistic approach in the monuments conservation. A possible approach to reduce the uncertainties in the knowledge of historical buildings and obtain the necessary information to evaluate its structural health should be based on the development of a multi-disciplinary research aimed at providing an "integrated knowledge" through the mutual exchange of expertise and capabilities of different disciplines and a real-time monitoring of the state of the buildings [1]. Moreover, as already briefly mentioned, approaches and tools commonly used in structural analysis of ordinary buildings, extensively based on numerical models, do not always seem to be appropriate for historical masonry monuments of unique features and are generally not able to provide convenient material models to describe highly nonlinear behaviour and masonry orthotropic. To conceive a unique tool valid to describe all possible structural responses of the historical masonry monuments is therefore complex, and most likely impossible. Quite often, more reliable results can be obtained by employing a multi-analysis method that integrates different approaches (from simple but more reliable limit schematizations, to more complex but, usually more sensible, finite element models) [2]. Figure 1.1.1 display an overview of the presented Multi-Disciplinary Multi Analyses approach for a proper assessment of the structural health of historical monuments.

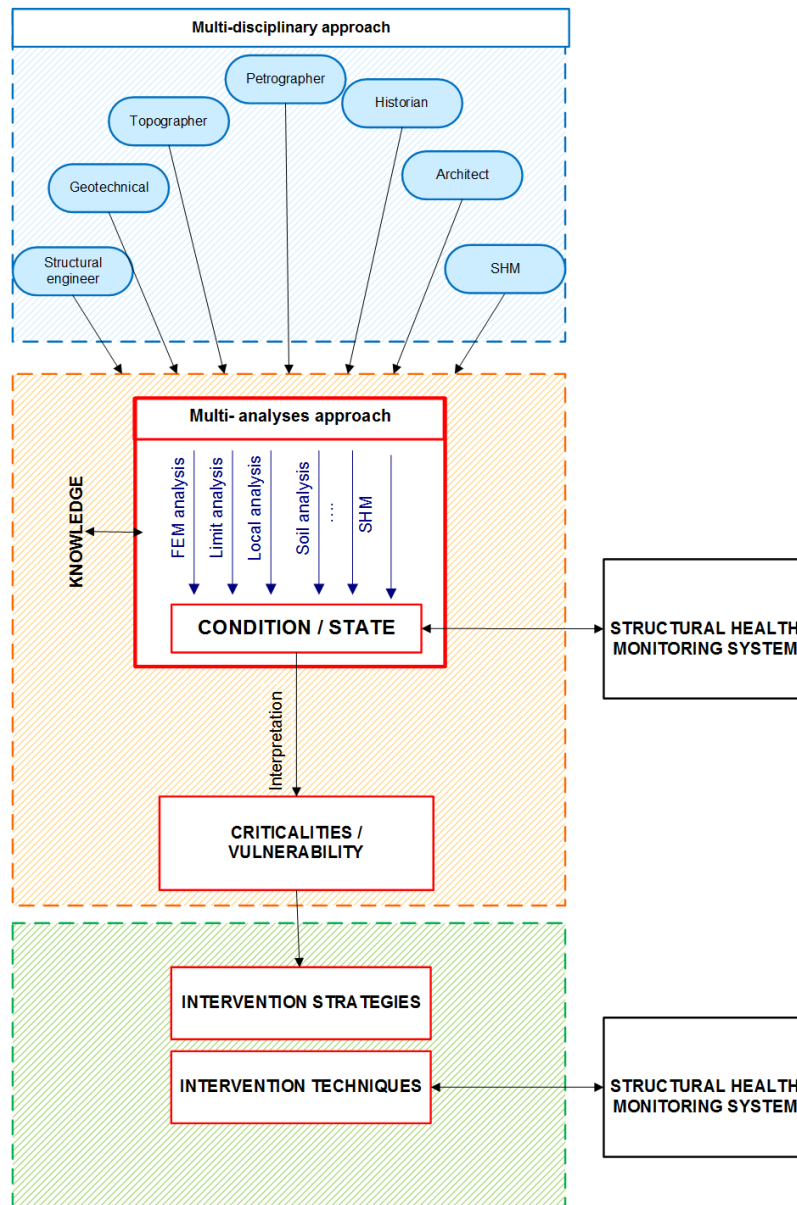


Figure 1.1.1-Overview of the MDMA approach



2 Guidelines for the integrated knowledge of cultural heritage assets

The current standard requirements recommend an interdisciplinary approach that thanks to an investigating team that incorporates a range of skills appropriate allows discovering phenomena involving structural behaviour of the monuments [1], [3]. A correct and complete analysis of an historical building have to be based on the historical, geometrical, material and structural knowledge of the structure in order to design strengthening interventions not only to guarantee safety, but also to respect the context, which surrounds them. Knowledge of the structure requires information on its conception, on its constructional techniques, on the processes of decay and damage, on changes that have been made and finally on its present state. The following steps can usually reach this knowledge [4]:

- definition, description and understanding of the historic and cultural significance of the buildings;
- a description of the original building materials and construction techniques;
- historical research covering the entire life of the structure including both changes to its form and any previous structural interventions;
- description of the structure in its present state including identification of damage, decay and possible progressive phenomena, using appropriate types of test;
- description of the actions involved, structural behaviour and types of materials;
- implementation of a SHM system.

The purpose of the historical investigation is to understand the conception and the significance of the building, the techniques and the skills used in its construction, the subsequent changes in both the structure and its environment and any events that may have caused damage (such as past earthquakes..). Knowledge of what has occurred in the past can help to forecast future behaviour and can be a useful indication of the level of safety provided by the current state of the structure. The direct observation and the survey of the structure is essential phase in order to identify decay and damage, geometric irregularities which can be the result of previous deformations (it can indicate the junction between different building phases or alterations to the fabric) and to determining whether or not the phenomena have stabilised. The identification of the mechanical characteristics of the materials should be investigated through non-destructive tests to avoid any alterations to a structure [4]. In addition to these remarks, it must be outlined the role of the monitoring, as an essential component of the integrated studies when exploring the long-term performances. SHM system can be very useful to acquire information of possible progressive phenomena, but also during and after



the implementation of strengthening interventions in order to evaluate their effectiveness. Figure 1.2.1 shows a schematic representation of the multi-disciplinary approach to obtain an integrated knowledge of the monuments.

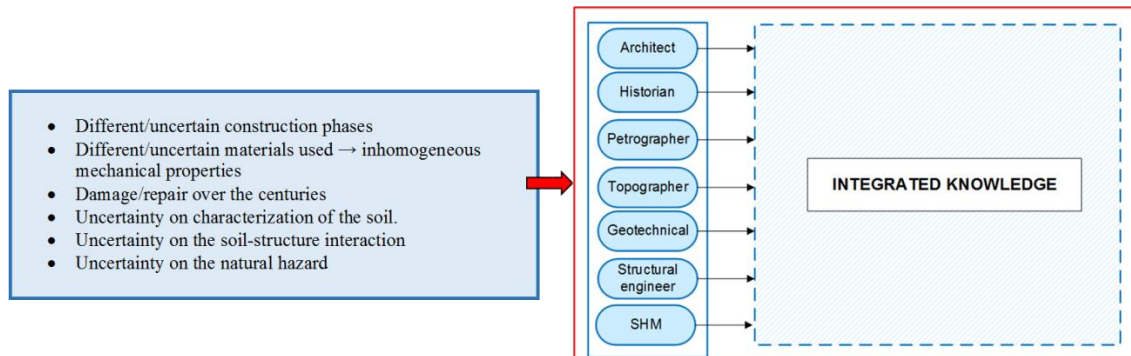


Figure 1.2.1- Schematic representation of the multi-disciplinary approach to obtain an integrated knowledge of the monuments

3 Multi- Analysis Integrated for seismic vulnerability assessment

The amount of data collected by the multi-disciplinary approach are used to develop reliable structural analyses in order to evaluate the safety levels of the monument. The structural behaviour of a monument is usually very complex and influenced by many factors. Therefore, only one model of the whole building generally is not able to capture all the structural peculiarities. The monument should be represented by different simplified 'structural scheme', (i.e. an idealisation of the building) with different complexity and different degrees of approximation to reality. Moreover, the model used has to take into account any alterations and weakening, such as cracks, disconnections, leanings, ..., whose effect may significantly influence the structural behaviour. Structural analyses of ancient masonry structures is very far from the modelling of ordinary buildings, and the most widespread tools generally based on Finite Element methods are affected by several limitations, that may be related to the material behaviour, the actual effectiveness of the connections, the effectiveness of the chains, the restraints provided by the soil. In addition, the dynamic properties of global models in terms of fundamental frequencies and modal shapes may be are very far from the real ones, provided that they are based on linear elastic analysis, whilst the masonry material is characterized by a highly non-linear response [5]. All these problems point to the need to develop a multiple analyses approach which integrating the potential of various methods of analyses, from simple but more robust ones, to more accurate but generally more sensible complex numerical simulations allows to assess the “structural health” of the monuments. The schematic representation of the concept of the multi analyses approach is shown in Figure 1.3.1

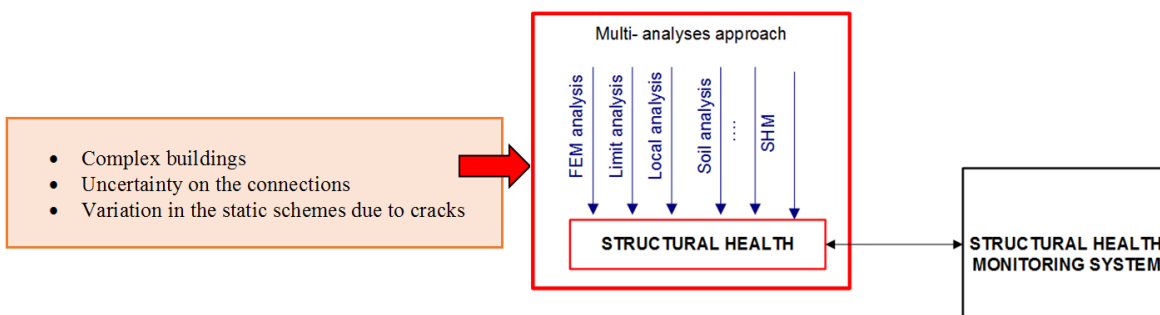


Figure 1.3.1: Schematic representation of the multi-analyses approach to evaluate the “structural health” of the monuments



4 A review of structural interventions for the conservation of cultural heritage buildings

Strengthening interventions on heritage buildings are generally necessary when one or more of the following circumstances occur:

- the presence of visible defects in the building;
- damages after a particular event that affects its stability (earthquake, etc.);
- the change of the use of the building for most severe conditions;
- the not negligible influence of the increase of specific action, such as traffic loads.

The implementation of rehabilitation interventions on heritage buildings requires, in general, the following steps:

- acquisition of the structural knowledge of the building;
- detailed survey of the present state of the building;
- evaluation of the mechanical properties of the materials;
- assessment of the structural safety;
- design of the solutions for the interventions;
- execution of the interventions.

The present chapter provides a brief review on the main solutions and strategies for structural interventions on existing masonry buildings with special attention on historical and monumental buildings.

4.1. Intervention on foundations

The assessment of the existing foundations of the historical building, in terms of geometry and material, is fundamental to design targeted interventions on these structural elements.

Moreover, the geotechnical characterization is also very important to understand the characteristics of the soil and to the water table, as well as to the presence of substances that can attack the building by capillary action (chlorides, nitrates, etc.). Particular attention will also be given to check the existence of embankments and to the identification of the drainage system of the building.

The TCs (technical committees) of the ISSMGE (International Society for Soil Mechanics and Geotechnical Engineering) are "a forum for discussing, developing and applying specialist



geotechnical knowledge related to the behavior of geo-materials, geotechnical engineering and engineering for society".

The TCs collected examples of preservation activities which may inspire the geotechnical engineer dealing with monuments and historic sites, suggesting an approach rather than a solution.

The basic principles for conservation of heritage structures and historical sites have been introduced in: ISO13822-2010: Assessment Of Existing Structures Defines in Annex I: Authenticity of Foundation of Heritage Structures.

Some interesting definitions are:

- "1.5.3 - Authenticity of foundation". From the point of view of conservation, foundations are not different from the rest of the structure and should be assessed and rehabilitated taking into consideration their heritage value. This involves the requirement to identify their authenticity and character-defining elements;
- "1.3.1 - Character-defining elements". Historic materials, forms, locations, spatial configurations, morphology, concept and details, structural design, uses and cultural associations that contribute to the heritage value of a structure that shall be retained in order to preserve its heritage;
- "1.9.2 - Minimal intervention for integrity". Intervention should be kept to the minimum level that needs structural requirements with the protection of character defining elements, in order to ensure the least harm to heritage values;
- "1.9.3 - Incremental approach for integrity". Step by step procedure in which the behavior of the structure is monitored at each step and the actual data are then used to provide the basis for further action.

Settlement most often occurs early in the life of a building or when there is a significant change in underground conditions (Figure 1.4.1). Often such settlement is associated with improper foundation design, particularly inadequate footers and foundation walls. Cracking is most likely to occur at corners and adjacent to openings, and usually follows a rough diagonal along mortar joints (although individual masonry units may be split).

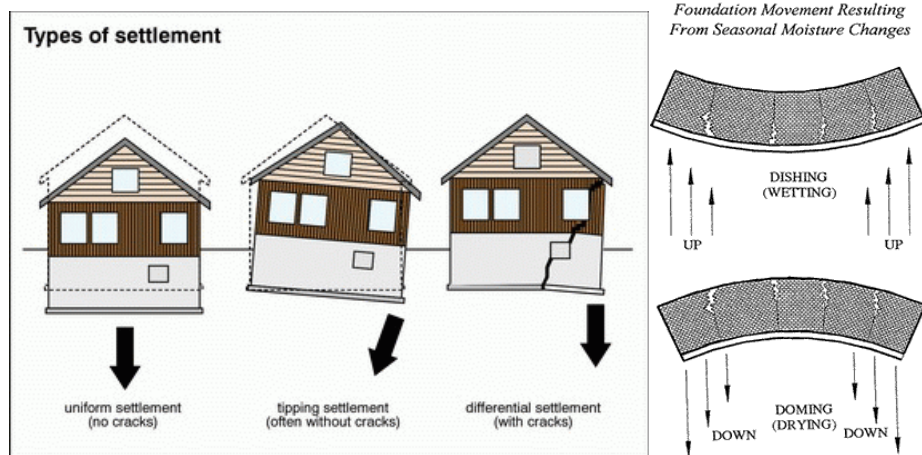


Figure 1.4.1: Different types of settlement.

Shallow soils are also generally affected by seasonal moisture changes. If the bearing soils consist of expansive clays that are subjected to changes in moisture content, differential foundation movement can occur if wetting and drying of the clays does not occur uniformly across the entire slab. This differential movement can result in "dishing" or "doming" of the foundation, and can become quite pronounced, especially in areas where the local climatic conditions include extended seasonal periods of both hot, dry weather and cooler, wetter weather.

In some cases, use of pressure-injecting concrete epoxy grout into the ground below the foundation can be sufficient. If movement continues and cracking is extensive, it is possible that the problem can only be rectified by underpinning.

Underpinning

The method of underpinning help to strengthen the foundation of an existing building through the installation of permanent or temporary support to the existing foundation so that additional depth and bearing capacity is achieved. Methods of base support include the construction of:

- footings,
- stem walls,
- driven piling or drilled piers.

Footings

This method is one of the most common, simple and ancient ones used in the history of buildings. It is based on the principle of carrying vertical loads on a larger base on the ground, in order to obtain a lower pressure, while maintaining the continuity of the material. It can be realized in different ways,

enlarging the foundation only on the external side, or when possible the foundation can be extended on both sides (internal and external), see Figure 1.4.1.

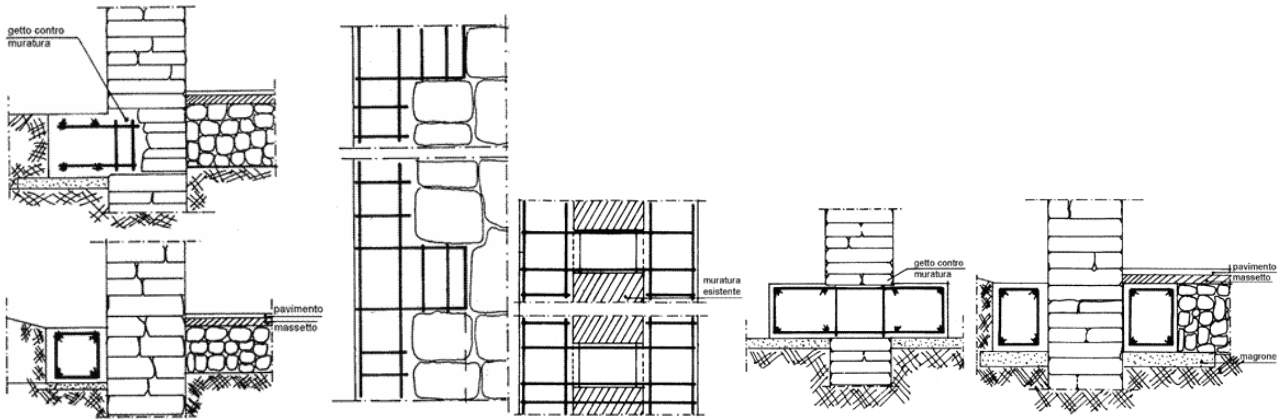


Figure 1.4.2: footing increasing by one side and both sides.

Stem walls

Stem or sister walls are used when the original foundation is insufficient and a deeper layer of soil had to be reached (Figure 1.4.2). With this application is important to provide good connections with the foundation and between wall sections for example using steel bars.

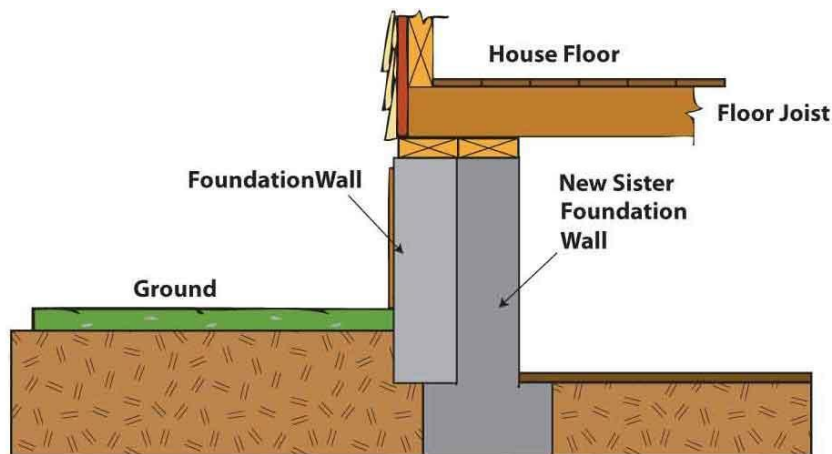


Figure 1.4.3: schematic of a typical intervention with a stem wall.

Underpinning with micropiles

Underpinning with micropiles is an intervention that allows a direct improvement of existing foundation for example crossing them or with realization of two concrete footing beams. As it can be noted in Figure 1.4.3 a, micropiles go through the existing masonry wall and several layers of soil in

order to reach the one with adequate consistency. In figure 2.11, micropiles are used together with the simultaneous enlargement of the base section of the foundation.

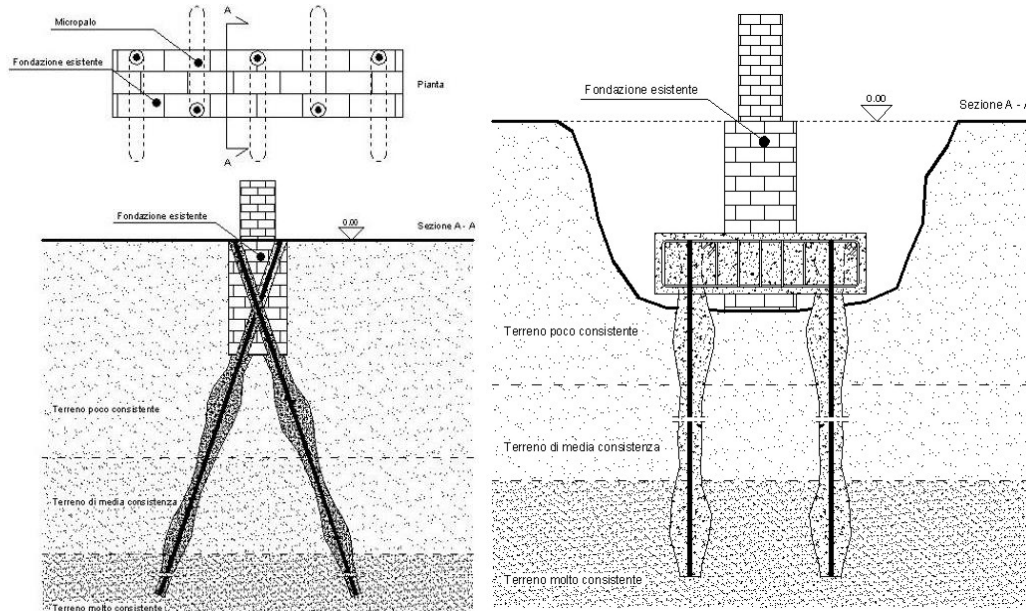


Figure 1.4.4: underpinning with micro-piles.

When the micropile is inserted in a cast of reinforced concrete it must be connected to it through metal elements, like steel bars, steel plates and for higher loads, steel profiles can be also adopted, they will be embedded in the casting concrete too.

Drilled piles require a clay ground to drill the pile and hydraulic jackets are used to apply a load on the steel piles after the realization of the concrete footing beam.

When underpinning with piles must be associated with an excavation to reach a lower level, the piles must be able to support a lateral loading and the ground in intermediate stages, this is the case of "Berlinese" Piles.

4.1.1. Example: the Leaning Tower of Pisa

The stabilization of the leaning Tower of Pisa is one of the best example of innovative method applied to the foundations. The foundations of tower were stabilised using the method of under excavation to reduce the southward inclination of the Tower.

The tower was constructed three phases between 1173 and 1370 [6], [7]. The Tower has a total height of 58.4 m measured from the base (56 m from ground level). The diameter of the superstructure is about 17 m including the external lodges and about 12 m without the lodges. The diameter of the central opening ranges from 7.3 to 7.7 m. The foundation of the Tower has a ring shape with an external diameter of 19.6 m [8].

In the early 1990s the leaning of the tower to the South increased up to 5.5° (leading to an overhang of around 5 m), seriously compromising the tower stability [9].

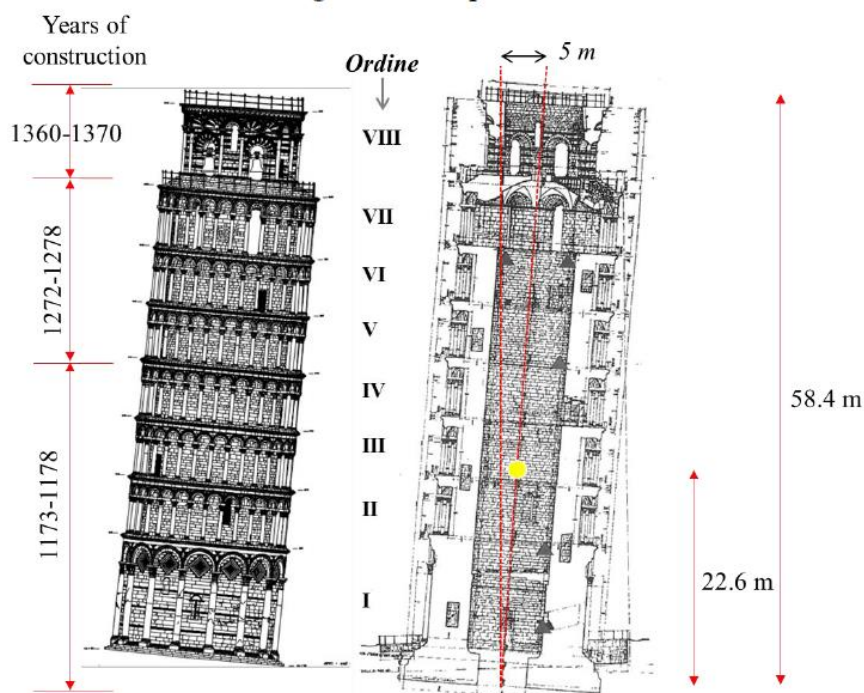


Figure 1.4.5: Side view and cross section of the Tower of Pisa with indication of the years of construction and the definition of the levels [9]

A soil extraction intervention was performed during years 1999-2001 involved the removal of small soil volumes from underneath the elevated part of the foundation. First of all cables were attached around third storey and tensioned to stabilise the Tower during drilling. Then drill were inserted at shallow angle to extract small volumes of soil on the North side of the Tower, in this way cavity fills under pressure of Tower, slowly reversing its southward tilt.



ALMA MATER STUDIORUM
UNIVERSITA' DI BOLOGNA

DICAM

Dipartimento di Ingegneria Civile,
Chimica, Ambientale e dei Materiali

MiChe

Mitigating the Impacts of natural hazards on Cultural Heritage
sites, structures and artefacts



Figure 1.4.6: Under-excavation work and tensioned cables

4.1.2. Example: Intervention on the foundations of the Frari bell tower (Venice)

The Basilica of Santa Maria Gloriosa dei Frari was built in Venice between the first half of the XIV and the second half of XV century. The adjacent Frari bell tower is the second tallest in the city after that of San Marco with a high of 65m. Originally the bell tower was conceived as a fully independent structure, but during the reconstruction of the Basilica, the bell tower was included into the masonry walls, at the south-east corner of transept and left aisle. The connection between the bell tower and the Basilica is at the origin of the subsequent problems that have always affected their structures. The bell tower showed the first documented signs of movements at the end of the XVI century [10]. Its movements (settlement and tilting) continued progressively and at the end of 19th century it was observed a differential settlement of about 40 cm between the bell-tower and the walls of the Basilica. At that time, the deviation from verticality, measured at a height of 42.50 m, was about 76.50 cm toward outside.



Figure 1.4.7: Santa Maria Gloriosa dei Frari church and adjacent bell tower

Between the end of 19th century and the first decade of 20th, several surveys, structural diagnosis investigation and strengthening interventions, were carried out.

From the results of the diagnostic investigations, it emerged that the interaction between the bell tower and the Basilica cannot bear further differential settlements without serious consequences.

To reduce the differential settlements of the bell tower, an innovative intervention of careful soil fracturing, also known as fracture grouting, was designed, in order to improve the mechanical characteristics of the soft silty clay.



The soil-fracturing technique consists in installing special injection tubes in the foundation soil, with valves at different depths. The careful and slow-rate injections of suitable cement and bentonite mixtures is repeated at successive stages, to obtain progressive increments in terms of mechanical characteristics [11].

The final outcome should be a reinforced soil, made up of the original material and an indented web of thin layers of injected grout.

4.2. Intervention techniques on masonry buildings

The structural behavior of a masonry walls depends on several factors:

- the masonry morphology (stonework, brickwork, single or multiple leaf walls, dry masonry or filled with mortar)
- the mechanical properties of masonry components (physical, chemical and mechanical characteristics of stones/bricks and mortar);;
- the quality index: conservation, stone/brick dimensions and shape, leaf connection, bed joints, vertical joints, mortar properties.

Historical structures are often characterized by a very complex geometry. The collapse mechanisms are strongly dependent on the construction techniques and on the connection details between orthogonal masonry walls and between the masonry walls and the possible restraining horizontal elements, such as tie-beams, well connected floors and roofs.

The most efficient structural configuration is the one in which the "box-like" behavior is ensured [12]. The connection systems to assure it are fundamental, they act as restraints with respect to orthogonal walls subjected to out of plane actions, preventing the activation of out-of-plan mechanisms and they connect parallel horizontal load-bearing walls, ensuring the redistribution of the horizontal actions between them and increasing the redundancy of the resisting system.

In order to ensure the "box-like" behavior vertical walls and horizontal structural elements should be properly connected for example with ring beams (at the floor level), connection systems (tie-rods) and efficient connections between orthogonal walls at the corners. Masonry walls and horizontal structural elements should have specific characteristics like adequate thickness and length, and proper stiffness and strength [13],[14].



4.2.1. Use of tie-rods to improve connections between masonry walls

In historical buildings, metallic tie-rods are largely used to improve their overall structural response [15]. The tie-rods are generally used to avoid the walls overturning and to sustain the thrust of arches and vaults.

A system of tie-rods can contrast the overturning of the façades or walls but the effectiveness of these devices depends on the integrity of the wall. For this reason, often it is necessary to combine the tie-rods with a strengthening intervention of the portion of facade using composite materials [16]

4.2.2. Ring and head beams

The box-behavior can be realized by means of a RC ring beam (or a reinforced masonry ring beam) at the floor level or the top of the walls. Realization of reinforced concrete ring beams can cause problems in the case of poor quality masonry. It is recommended to avoid the construction of ring beams within the thickness of the masonry in order to avoid disomogeneous loading of masonry walls and instability phenomena of the internal layer of the wall, to reduce the "pushing effect" of heavy slabs, the disgregation of masonry not well retrofitted and the sliding of the ring over the masonry wall.

The presence of a too rigid RC ring beam can cause the application of concentrated actions on the masonry, very dangerous if the quality of the masonry is bad. Local mechanisms like overturning of the wall, overturning of the corner, vertical bending of the wall and also damages like separation of the different layers of the wall can occur.

Steel belts, made with industrial production metal profiles, such as HEA, IPE or composite sections, resting directly on the top walls, are suitable for absorbing axial stresses, but have the defect of attributing the entire effort on the anchor to upstream and are not very compatible with the supporting wall structure.

A solution recently introduced and associated with the diffusion of composite materials, consists in the top dressing of masonry buildings with fiber ribbons arranged outside at the level of the eaves. The belts absorb the axial forces, counteract the swelling of the walls towards the outside, but are completely ineffective in the distribution of vertical loads.

A technique more compatible with the nature of traditional masonry construction and an alternative to RC ring beams, suitable for responding in a balanced way to all the static functions required, is represented by reinforced masonry "belts", made according to the technique proposed in the late 1980s in the "Manuale del Recupero di Città di Castello". This solution is highly appreciated by the protection agency ("soprintendenza") nowadays, as it performs the function of distributing vertical loads, creates a condition of collaboration between the walls and allows to counteract the out of

plane overturning of the walls, all thanks to the flexibility that determines a good adhesion to the masonry even in dynamic conditions. This type of curb differs from those in reinforced concrete in the construction principle and therefore in static operation. It contains the reinforcements prescribed by the standards but is made in layers and not through a concrete jet.

This allows to reduce the shear resistance between one row and another, making the structural element much more flexible. In conclusion is an intervention able to satisfy the technical requirements for restoration, like effectiveness, compatibility, durability and also important for the authenticity of the building.

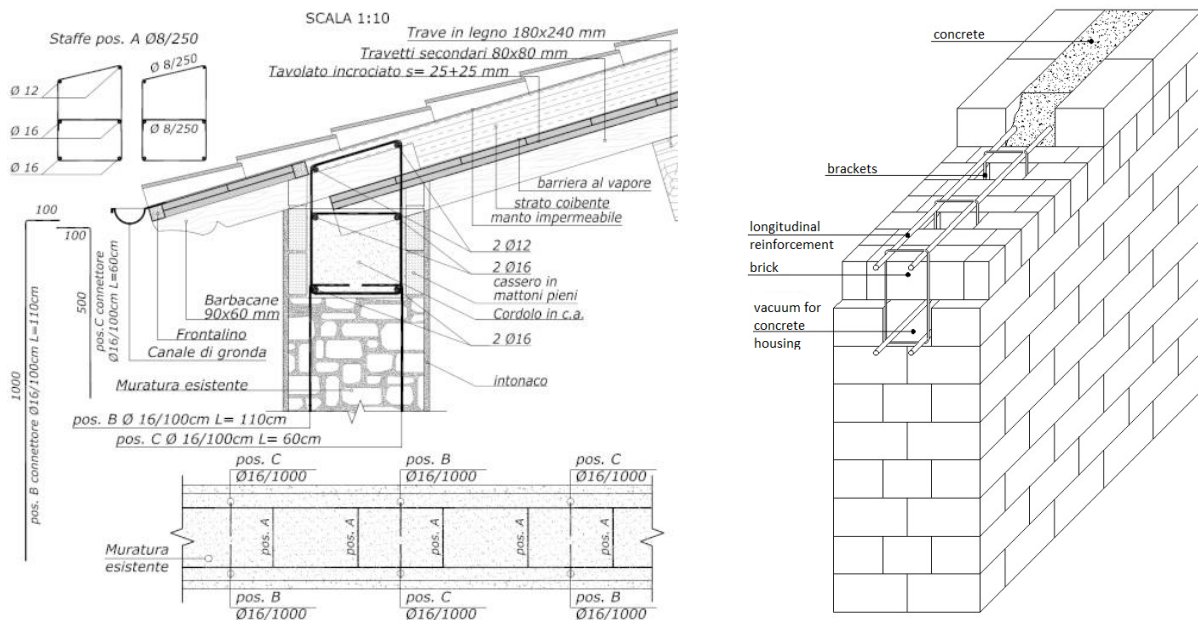


Figure 1.4.8: typical RC ring beam; typical reinforced masonry ring beam.



4.2.3. Interventions to increase the masonry strength

"Unstitch and stitch" local rebuilding

The local rebuilding "unstitch and stitch" methodology aims to restore the wall continuity along cracking lines (substitution of damaged elements with new ones, reestablishment of the structural continuity) and to recover heavily damaged parts of masonry walls. The materials used should be compatible with those employed in the original wall. The intervention is effective in the presence of elements of good quality, with good resistance and with similar characteristics in shape and size. First of all we need to prepare the wall by cleaning and setting up the wall face, in the second phase the wall must be supported in order to work in safety conditions. Then follow the removal of the damaged part and finally the reparation with new bricks and mortar.

Grout injections to consolidate the masonry walls

Often the masonry quality is very poor, and its consolidation is fundamental to carry effectively both vertical and seismic loadings. Block interlock is fundamental to allow a monolithic behavior of the masonry wall. The load transfer in a masonry wall takes place through the contact of the constituent blocks. The interlocking phenomenon is greater in presence of big blocks and for walls having an organized, regular texture. This consolidation method is usually called "passive" because it does not change the appearance of the building. The most suitable consolidation products are hydraulic lime-based fluid grouts, able to increase masonry strength with no relevant change in walls stiffness [17], [18].

The practical implementation of injections is articulated in the following phases:

- Opening the injection holes the drillings should be practiced in correspondence with mortar joints and with a distance of approximately 60 to 80 cm between them, depending on the thickness of the masonry; drill holes to, at least, half the thickness of the masonry; drilling of holes (usually 2 or 3 per m²);
- all cracks and small cracks, among the various elements, must be previously sealed;
- before performing the injection, the masonry should be washed up till saturation, using pure water, preferably deionized and free of soil matter;
- to control the volume of injected material, thin purge tubes should be used, through which excess material may exit;
- during the washing phase, additional operations must be performed (e.g.: joints repointing);



- pre-consolidation, leaving a very fluid slurry flow through a funnel or a wide pipe;
- injection of grouts within the holes at low pressure; injections from the bottom up, in order to avoid weight imbalances and unpredicted static changes;
- the injection pressure is conditioned to the depth to achieve and to the wall deterioration degree; maintain a tight control over the amount of injected material and the volume of the wall to inject. The pressure must be kept constant until the grout does not overflow out the adjacent holes to the pipes;
- after the grout had hardened, the pipes are removed and the holes sealed with suitable mortar.

Injections can be also localized interventions in the presence of cracks and very irregular masonry texture. Injections do not significantly change the stiffness of walls, differently from RC jackets, improving at the same time the strength and consistency of walls provided with voids and/or irregular morphology.

Joint repointing

Deep repointing is a repair and preventive technique for double leaf masonry walls carried out on the two faces of the masonry. The aim of this repair is to bond the stones of the external leaves, particularly in the case of badly bonded irregular stones and to obtain an external confinement of the wall in order to increase the masonry shear strength. The repointing can be carried out also in conjunction with grout injection [19].

This technique is often used in historic and monumental building often characterized by "rubble walls", with two external leaves of bricks or stones and an inner rubble core .

CAM System

In 1999, Dolce and Marnetto patented the CAM (Active Confinement of Masonry) system, to compact the irregular or double layer masonry systems, with lack of transverse connections, using a three-dimensional tying system [20], [21]. The use of a continuous three-dimensional system of pre-tensioned ties is able to "pack" the masonry structure, thus providing an advantageous state of tri-axial compression.

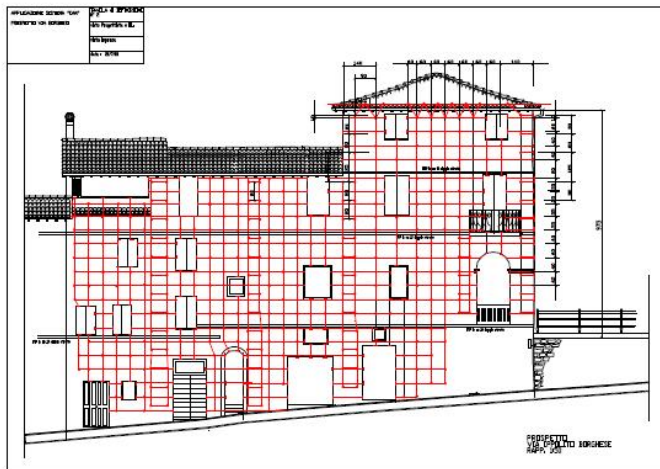


Figure 1.4.9: CAM arrangement in the façade [20]

The CAM system does not use bars to create ties: it consists of steel ribbons that form horizontal and vertical loops, passing through transverse holes. The flexibility of the system allows rectangular, rhombic, triangular, and irregular arrangements of the mesh.

Moreover, the use of two staggered meshes, with the holes arranged in quincunxes as in Figure 3.29b, minimizes the number of holes.

The ribbons (1-4 per loop) are clamped with a special tool that is able to apply a pre-stressing force, thus providing an active confinement to the masonry wall. Therefore, the CAM ribbons strengthen the masonry in the same way as the metallic straps strengthen the packages in heavy applications. Because of this analogy, the authors will call the tensioned ribbons of the CAM system "the straps". The pre-stressed steel ribbons behave like tie rods opposing to both deformation and disconnection of the building elements. In particular, since the straps form both horizontal and vertical closed loops, the CAM ribbons replicate the reinforcement scheme with horizontal and vertical ties. Nevertheless, the overall behavior of the CAM system is very far from that of traditional pre-tensioned horizontal and vertical ties, as the loop-shaped CAM ribbons bring several benefits:

- it is no longer necessary to anchor the ties into the masonry, because the ribbons close on themselves. This eliminates the problem of the excessive concentrations of stresses induced by the anchorages;
- the straps are made of stainless steel. This avoids the typical corrosion problems of tie rods, which need of a suitable covering or galvanization zinc plating;
- the cross-section of the straps is very small. This allows a moderate increase in the total weight of the structure, useful to not increase the attraction of seismic forces too much;



- each strap is a bi-dimensional device. This allows the ribbons to provide in-plane and transversal post-compression at the same time;
- the steel ribbons continue to wrap masonry even after masonry crushing. This is of fundamental importance for safeguarding life, as people do not risk that some part of the structure hits them, due to building collapse.

Reticulatus technique - example of the Castle of Compiano (Parma)

The technique is proposed for reinforcing rubble stone masonry walls, when the fair-face masonry must be kept. The reinforcement technique consists of embedding a continuous mesh of high strength steel cords in the mortar joints after a first repointing, and then anchoring this to the wall by means of steel eyebolts. A second repointing covers the cords and the heads of the eyebolts. This gives a reinforced fair-face masonry wall in which there is increased compression, shear and flexural strength, and the capacity to withstand tensile stresses, as was confirmed by the first tests. Furthermore, the small size of the reinforcement cords and the fact that they are easy to insert into the mortar joints makes it possible to apply this technique on an extensive, which avoids dangerous concentrations of stress.

More in detail, it consists in insertion of a continuous mesh made from high strength steel or composite cords in the mortar joints, stripped to a depth of 40-60 mm. The cords are arranged in vertical and horizontal directions, forming approximately square meshes, the dimensions of which, normally 300-500 mm wide, depend on the size of the stones in the masonry, and, as a rule, must not be greater than the thickness of the wall. The cords are connected to the transverse bars by means of eyelets in which the cords can slide: thus it is possible to apply a moderate tension, so as to make the mesh immediately functional. When the size of the stone walling material is such as to prevent the use of bars passing through the entire thickness of the masonry, the connection can be made with bars about 2/3 as long as the thickness of the wall, anchored with the injecting of non-shrink mortar or epoxy resin. With the aim at connecting the cord-reinforcement to the existing masonry and at increasing the level of connection between masonry wall leaves, it is advised to use an epoxy mortar, but when this is not possible a non shrink cement-based mortar could be also used. The final application of mortar, which completely covers both the cords and the heads of the transverse bars, makes it possible to preserve the fair-faced aspect of the masonry. All used mortars were lime-based, specifically designed for use with historic masonry. Because many historic buildings are restricted by protection and heritage conservation authorities, which in many cases do not authorize an extensive use of the repointing technique, the requirement for reversible

interventions as well as the use of historically or geographically-correct mortars, can limit the application of the Reticulatus technique.



Figure 1.4.10: Application of Reticulatus technique to the Castle of Compiano [22]

4.3. Arches and vaults

Since ancient times it is known that the arch shape, with the concavity downwards, is able to create the necessary compression between the segments of the wall structure subject to gravitational loads, up to completely cancel the eccentricity of the resultant if the shape of the arch coincides with the funicular of the loads.

In fact, a masonry arch reaches a failure condition essentially with 4 mode:

- for formation of a mechanism;
- for impost displacements;
- for sliding between the segments;
- by crushing the compressed masonry.

The failure due to the formation of a mechanism occurs when a number of internal hinges is formed in the arch in order to make the structure labile. Since a masonry arch is a 3 times hyperstatic structure in its plane, at least 4 internal hinges must be formed for a lability situation to arise, 5 in the symmetrical case.

The internal hinges are formed in the sections where the pressure curve is located near one end of the section: in them, in fact, the section is almost entirely cracked, and the compression effort is concentrated on a small part of the section, around at which rotation can take place.

This type of crisis presupposes that the compressive strength of the material that constitutes the segments is greater than the stresses and that it is therefore possible that a localized rotation occurs without the compression breaking of the reagent portion. It is also observed that in the event of



symmetrical loading, this mechanism can only occur if it causes the simultaneous removal of the imposts. The breakage due to the formation of a mechanism therefore, if not accompanied by displacement of the shutters, is typical of non-symmetrical load conditions, among which the condition under the earthquake must be included, due to the horizontal inertia forces at which the vault is subjected. The movement of the shutters forces the arch to form 3 internal hinges in order to adapt to the movement of its end points.

This failure mode is typical of the collapse of buildings in seismic conditions: in fact, the perimeter walls under the effect of the earthquake undergo horizontal displacements at the levels where the arches or vaults are set, while the internal ones, more closely related to the wall structure, do not move in synchrony with them. The third failure mode concerns the sliding of one ashlar on the other. In the first treatments on arches (De La Hire, 1699) it was considered the main failure mode, but in reality the sliding of the segments due to the shear stresses is rarely the cause of the failure of the arch or the vault. This sliding is observable in the vaults that have suffered an earthquake, due to the horizontal acceleration imposed on the masonry, but it is rarely of an entity such as to cause the collapse, being usually limited to a few millimeters. The last failure mode (crushing of compressed masonry) is actually very rare due to the high compressive strength of stone and brick.

4.3.1. Traditional consolidation procedures

To preserve the arches and vaults and thus the architectural integrity of the historical buildings, it is necessary to identify reliable reinforcement techniques. Strengthening masonry vaults remains a challenge since, in addition to identify reliable interventions, it is necessary to retain at the same time the architectural and historical value for the presence of ancient decorations, frescoes and painting that commonly cover the intrados of European vaults. Traditional reinforcement techniques used in the past to strengthen the arches and vaults are generally: tie-roads, reinforced concrete hoods applied at the extrados, addition of material fill in the corner area and construction of ribs at the extrados [23], [24], [25]. These techniques may guarantee an adequate increment in strength, stiffness, and ductility, but usually, especially the use of the concrete hoods, violate aesthetic requirements and conservation needs for historical monuments.

The insertion of tie rods, designed to collect the thrust of the arches and vaults is one of the first consolidation procedures to be applied and is one of the most effective.

Jurina [26] developed a techniques called “reinforced arch methods” to strength arches and vaults. The consolidation consist on placing cables alongside the extrados of arches and vaults providing strength whit minimum increase of mass. The cables are fixed to the masonry of the supporting walls

and then post-tensioned. The “reinforced arch method” has been applied for the conservation of several structures.



Figure 1.4.11: Application of “reinforced arch method” to the vaults of Casa Giacobbe (Milan) and Manta Castle (Cuneo) [26].

4.3.2. Consolidation with FRP and FRCM

Materials with very high performance in terms of tensile strength are obtained on the market today, by inserting appropriate fibers (carbon, basalt, steel, etc.) in a polymer matrix like FRP (Fibre Reinforced Polymers) or in an inorganic cementitious matrix like FRCM (Fibre Reinforced Cementitious Matrix).

Over the last 20 years, several researchers proposed the use of composite material to strengthen historical masonry structures arches [27], [28], vaults and domes [29],[30],[31],[32],[33], [34],[35], [36],[37].

The application of fibre reinforced polymers (FRP) for strengthening of masonry structures is very beneficial thanks to its easy installation, low self-weight that does not alter the mass of the structure, high strength, ability to preserve the initial geometrical configuration and reversibility. The FRP techniques have been widely used in recent years for the consolidation of arches and masonry vaults, especially inside to monumental buildings, i.e FRP strips have been used to strength the vaults of the town hall of Assisi, the San Barnaba church in Modena [36], [37], the San Petronio church in Bologna)



Figure 1.4.12: Application of FRP strips on the vaults of San Petronio church in Bologna and town hall of Assisi.

The use of polymeric resins is not always compatible with the preservation of historical masonry construction that requires the need of vapor permeability through the masonry and removable solutions. For these reasons, a new generation of composite materials were introduced, which are known as fabric reinforced cementitious mortars (FRCM) in which the fibers are embedded in a thick layer of inorganic plaster, without the massive use of polymer resins.

4.4. Intervention on roof structures

4.4.1. Approach

Traditional masonry buildings have timber floors and roofs, and they are typically flexible. The increase of the in-plane stiffness of floors is an evident and most effective method of improving the seismic behaviour of old masonry structures. This is mainly because the increase of in-plane stiffness of floors enables the structure to behave like a box, i.e. enables the horizontal forces to be redistributed between the different vertical structural elements, and then the horizontal forces of failing walls can be redistributed to the adjacent remaining walls. A significant role in the stability of the entire building is assigned to the floors and roofs. These structures are required, in addition to an adequate performance level, a remarkable rigidity and an efficient connection to the supporting walls, especially in what concerns seismic actions. For this reason, by strengthening a floor, one has an opportunity to improve the behaviour and efficiency of the entire structure. UNI 11138 - 2004 STANDARDS provides the basic criteria for the intervention in the wooden artefacts, no guidelines are given by Eurocode 5 or other codes.

The following steps are necessary:

- historical analyses (past interventions, failure, occurred damages, etc.);
- material characterization (according to UNI 11118 and UNI 11119);
- geometrical characterization;
- damage diagnosis;
- structural analysis (the reliability of the structural analysis depends on the accuracy of the previous steps).

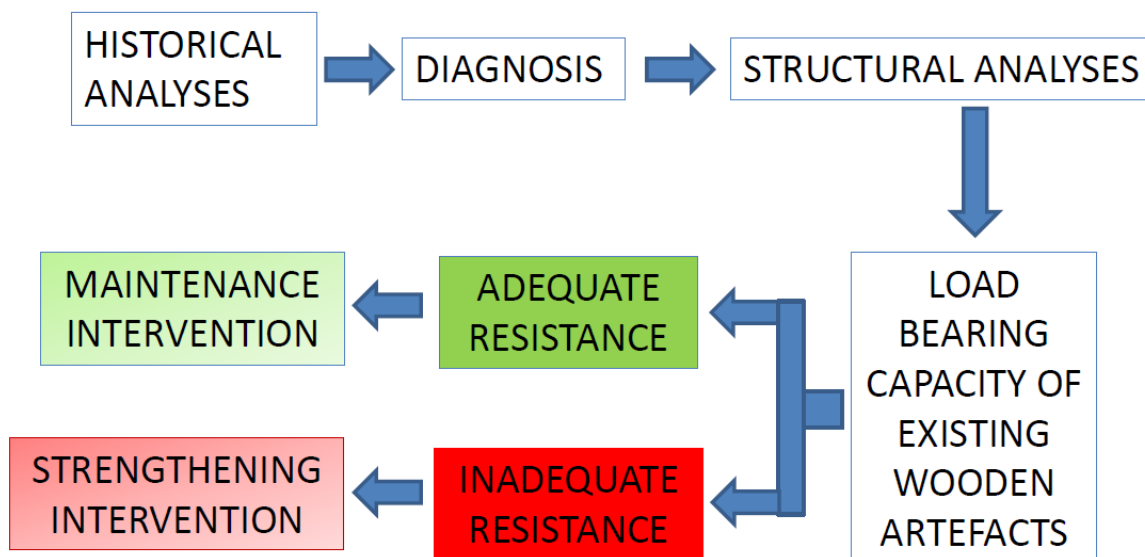


Figure 1.4.13: flow-chart-approach for roof strengthening

All the interventions have to satisfy these criteria: recognizability, replaceability, structural rehabilitation, preservation of historical features and can be realized by means of LOCAL strengthening INTERVENTIONS or DIFFUSE strengthening INTERVENTIONS.

Interventions include the following restoration techniques:

- material properties restorations;
- repairing and restoration of structural strength;
- repairing and restoration of joint functionality;
- intervention with imposed coaction states;
- structural behaviour improving against the accidental actions;
- surface treatment.

4.4.2. Example of "Collegiata di San Michele Arcangelo", Bagnacavallo (RA)

The church was built in 1741 and has undergone several renovations since then, the most important of which are related to the Second World War. The building consists of the church, the bell tower and a building used as a rectory and sacristy. The church has an almost rectangular plan with sides with maximum external dimensions of 21.30 m x 48.40 m and consists of three naves, one central and two lateral.



Figure 1.4.14: Collegiata di San Michele Arcangelo Church.

The central nave has a gable roof with a maximum height of about 20.00 m and about 17.00 m in the eaves. The presbytery has a four-pitched pavilion roof with a maximum height of 22.40 m and a gutter of 20.30 m. The apse has a roof with seven triangular pitches and with a maximum height of 18.20 m and a gutter of 15.50 m. The side aisles with an inclined pitch roof have a maximum height of 13.90 m and a eave of 10.00 m.

The load-bearing structure in elevation is entirely in solid brick masonry bonded with lime mortar, the roofs of the aisles, the apse and the presbytery are made with wooden structure, brick tiles and roof tiles. The bell tower and the building used as a sacristy and rectory are structurally independent of the church as they were built in different periods.

The main problem is found in the roof of the central nave. The trusses of the central nave have a clear out of plane movement in the direction of the main facade, due to the deformation of the pitch.

During an earthquake, this situation can increase phenomena of hammering and therefore overturning of the tympanum, and damage to the top of the longitudinal walls on which the trusses rest.

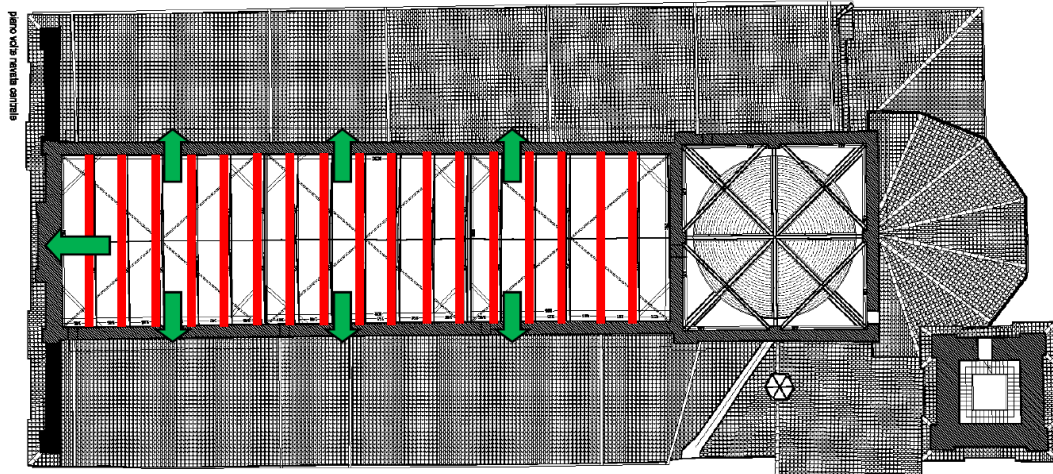


Figure 1.4.15: plan view of the roof system.

Looking at the wooden roof structure, it's observed that the trusses have undergone an out of plane movement, there are cracks in the walls near the heads of the wooden beams, portions of damaged beams and the roof is not effectively connected to the bearing walls.



Figure 1.4.16: details of the roof system.

To mitigate the critical issues described it's necessary to perform the following procedures:

- checking the state of degradation of the wooden trusses and perform the restoration of the damaged portions;
- checking the possible presence of mold, insects and pests etc. and select the specific treatment to avoid them;

- the realization of two cross bracing of the pitch of the wooden trusses with simple steel plates of the thinnest thickness possible to avoid a further out of plane heeling;
- the insertion of a ring beam on the extrados of the longitudinal and transverse walls on the side of the presbytery made with UPN 200 metal profile; this profile is connected with the masonry by means of threaded rods with a diameter of 16 mm with a pitch of 30/40 cm inserted in holes of appropriate diameter and length injected with specific consolidating grout and closed against the profile itself;
- the construction of a third S. Andrea cross brace to avoid the hammering action on the tympanum.

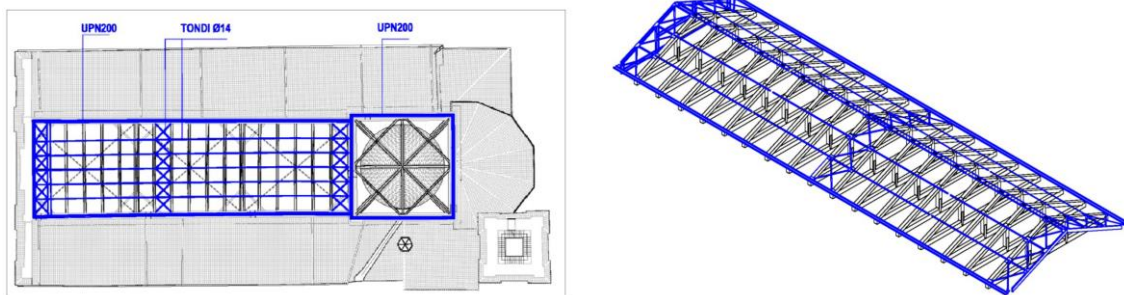


Figure 1.4.17: Overview of the interventions:



Figure 1.4.18: Details about the interventions



5 Pluvial flood hazard /risk assessment

5.1 Preliminary hydraulic risk evaluation

The European Directive 2007/60/EC establishes a “framework for the assessment and management of flood risks, aiming at the reduction of the adverse consequences for human health, the environment, cultural heritage and economic activity associated with floods in the Community” (Art 1).

According to this Directive, floods are defined as the “temporary covering by water of land not normally covered by water. This shall include floods from rivers, mountain torrents, Mediterranean ephemeral water courses, and floods from the sea in coastal areas, and may exclude floods from sewerage systems” (Art. 2).

A preliminary flood risk assessment is to be undertaken by considering each river basin district. In the context of the case study of Modena Cathedral, the results provided in the Flood Risk Assessment Plan for the Po River Basin are hereby considered (<http://pianoalluvioni.adbpo.it/il-piano/>). The Flood Risk Assessment Plan for the Po River Basin was compiled by the Po River Basin Authority.

This plan defines flood hazard maps and flood risk maps.

5.1.1 Flood hazard maps

As stated in the European Directive 2007/60/EC, flood hazard maps cover the geographical areas which could be flooded according to the following 3 scenarios:

- a) floods with a low probability, or extreme event scenarios;
- b) floods with a medium probability (likely return period ≥ 100 years);
- c) floods with a high probability, where appropriate.

In the context of the Flood Risk Assessment Plan for the Po River Basin, flood hazard maps consider different methodological approaches based on the following territorial classes:

- Main river reaches (RP, from the Italian *Reticolo idrografico principale*): it comprises the Po river and its main tributaries (total length of approximately 5000 km);
- Secondary river reaches across hills and mountains (RSCM, from the Italian *Reticolo secondario collinare e montano*): it comprises smaller streams and rivers across hills and mountains, but also mountain reaches of main rivers;



- Secondary river reaches across plains (RSP, from the Italian *Reticolo secondario di pianura*): it comprises artificial channels for irrigation purposes in the Po Plain, managed by Land Reclamation Bureaus;
- Coastal areas (ACM, from the Italian *Aree costiere marine*): it comprises areas close to the Po river delta in the Adriatic Sea;
- Lake areas (ACL, from the Italian *Aree costiere lacuali*): it comprises areas close to Maggiore Lake, Como Lake, Garda Lake etc.

Flood hazard maps identify the maximum extension of flooded areas associated with flood events with low, medium and high probability, as provided in Table 1.5.1 and 1. 5.2.

Table 1.5.1 – Summary of territorial classes and responsibility

| TERRITORIAL CLASS | RESPONSIBILITY |
|--|---|
| Main river reaches (RP) | Po River Basin Authority |
| Secondary river reaches across hills and mountains (RSCM) | Administrative regions |
| Secondary river reaches across plains (RSP) | Administrative regions and Land Reclamation Bureaus |
| Coastal areas (ACM) | Administrative regions |
| Lake areas (ACL) | Administrative regions, Regional agencies for Environmental Protection, Lake regulation consortia |



Table 1.5.2 – Summary of flood scenarios comparison between the European Directive 2007/60/EC and the Flood Risk Assessment Plan for the Po River Basin.

| FLOOD DIRECTIVE | | FLOOD RISK ASSESSMENT PLAN | |
|--------------------------|-------------------------|----------------------------|---|
| Scenario | Return Period (years) | Hazard class | Return period (years) for Main river reaches (RP) |
| High flood probability | 20-50 (frequent) | P3 High | 10-20 |
| Medium flood probability | 100-200 (less frequent) | P2 Medium | 100-200 |
| Low flood probability | > 500 (rare) | P1 Low | 500 |

Flood hazard maps for the city of Modena are available in the Flood Risk Assessment Plan for the Po River Basin in panel “RP_RSCM_Tavola_201SE”. An extract is reported in Figure 1.5.1, which shows that the city of Modena, and particularly the Cathedral area presents a low probability to be flooded (i.e. return period equal to 500 years).

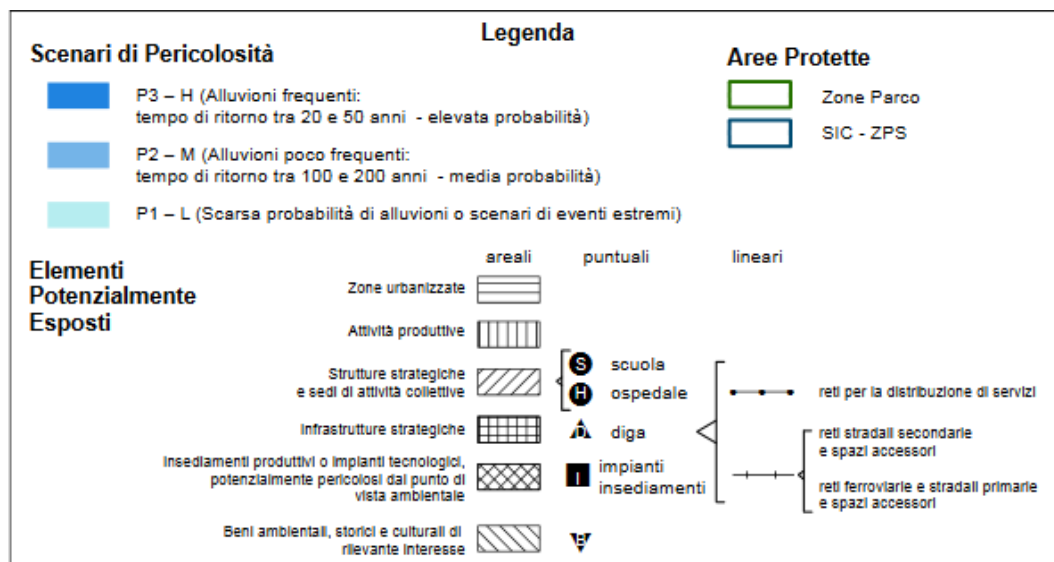
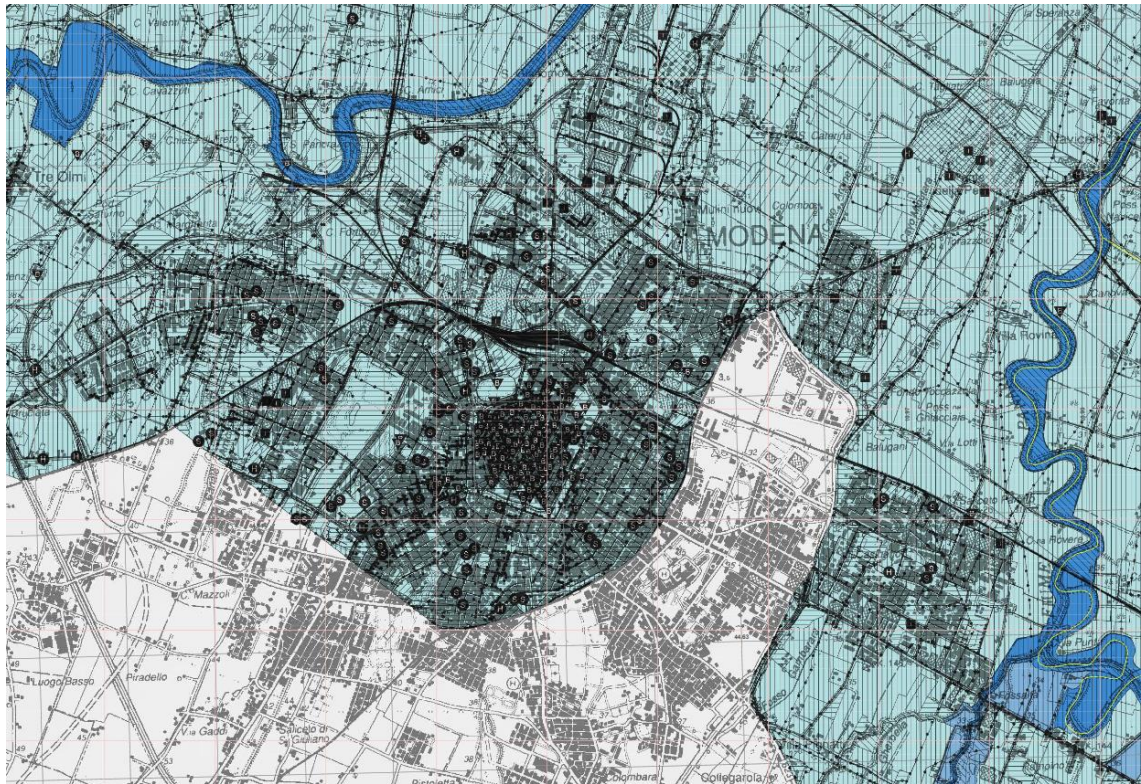


Figure 1.5.1 – Flood hazard map for the city of Modena



5.1.2 Flood risk maps

As stated in the European Directive 2007/60/EC, flood risk maps show the potential adverse consequences associated with flood scenarios (i.e. flood hazard) and also embed information about the indicative number of inhabitants potentially affected as well as the type of economic activity of the area potentially affected.

In the context of the Flood Risk Assessment Plan for the Po River Basin, flood risk maps identify 4 different classes of risk, by following Italian regulations (i.e. D.P.C.M. 29.09.98 and D.Lgs. 49/2010):

- R4 (very high risk): potential human losses, severe human injuries, severe damages to buildings, infrastructures and the environment, severe damages to socio-economic activities;
- R3 (high risk): potential injuries to people, damages to buildings and infrastructures, socio-economic activities brake-offs, damages to the environment;
- R2 (average risk): potential minor damages to buildings, infrastructures and the environment without affecting people safety;
- R1 (low or negligible risk): social, economic and environmental damages are negligible or null.

Flood risk (R) is defined by employing the following formula:

$$R = P \times E \times V = P \times D \quad (1)$$

where:

P (hazard): probability of occurrence, within a certain study area and time interval, of a flood with a given magnitude.

E (exposure): elements at risk, i.e. economic and intrinsic values that are present at the location involved. Population density, capital investment, and land or property value can be indicators of flood exposure. More specifically, the following categories are considered: (i) inhabitants (data gathered from Italian Statistical Analysis – ISTAT), (ii) economic-activities (data gathered from land use maps available from the EU CORINE LCL), (iii) Highly Pollutant Industrial Plants, as defined by the Industrial Emissions Directive (data gathered from the Italian Institute for Environmental Protection, ISPRA), (iv) protected areas (data gathered from Po River Basin Authority).

V (vulnerability): capacity of the society to deal with the flood event, namely, the state of susceptibility to harm from exposure to an undesired event, floods in this study, associated with environmental



and social change, and lack of capacity to adapt. Lack of flood defenses or protection of economic values and human lives susceptible to floods are indicators of vulnerability.

$D = E \times V$ (Potential damage): integrated measure of the environmental and socio-economic consequences of floods.

Estimates of potential damage D is not always easy to derive without any specific data concerning vulnerability, this variable V is assumed to be constant and equal to 1. Furthermore, potential damage assessment is performed by following a qualitative approach, also based on expert opinions, providing a value from $D1$ to $D4$, for less and more important land use classes, respectively. Higher values are assigned to residential classes, showing a constant human presence, whereas lower values are assigned to different kinds of economic activities, from industrial to agricultural ones. Higher values are also assigned to cultural heritage sites.

Flood risk analysis is then performed in a GIS environment by overlaying the following thematic maps: flood hazard and potential damages. This algorithm employs a matrix, which associates hazard classes $P1$, $P2$, $P3$ to damages classes $D1$, $D2$, $D3$, $D4$. Then, moving from the 3 hazard levels ($P1$, $P2$, $P3$) and the 4 damage levels ($D1$, $D2$, $D3$, $D4$), 4 risk levels are established ($R1$, $R2$, $R3$, $R4$) and flood risk maps are outlined. Figure 5.2 shows flood risk levels.

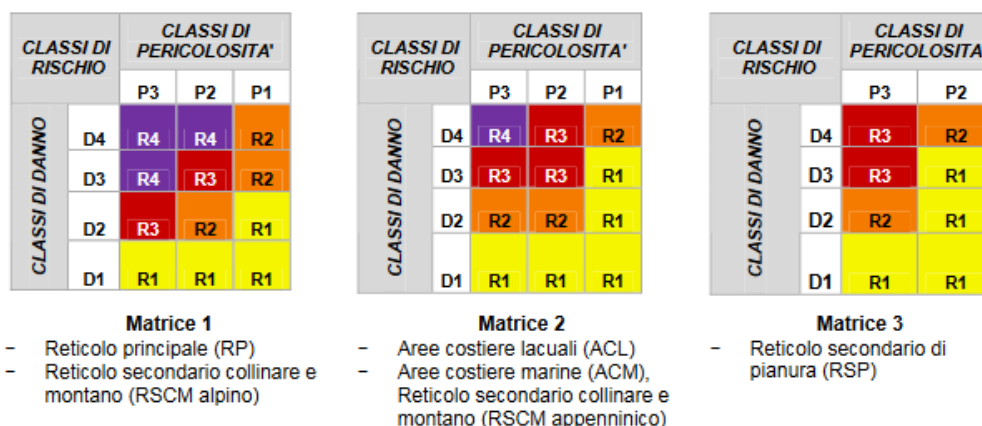


Figure 1.5.2 – Definition of flood risk levels, based on hazard levels ($P1$, $P2$, $P3$) and economic damages levels ($D1$, $D2$, $D3$, $D4$) for main river reaches (RP), secondary river reaches (RSCM and RSP).

The flood risk map for the city of Modena is shown in Figure 1.5.3 (extract from the Flood Risk Assessment Plan in the Po River Basin, panel “RP_RSCM_Tavola_201SE”).

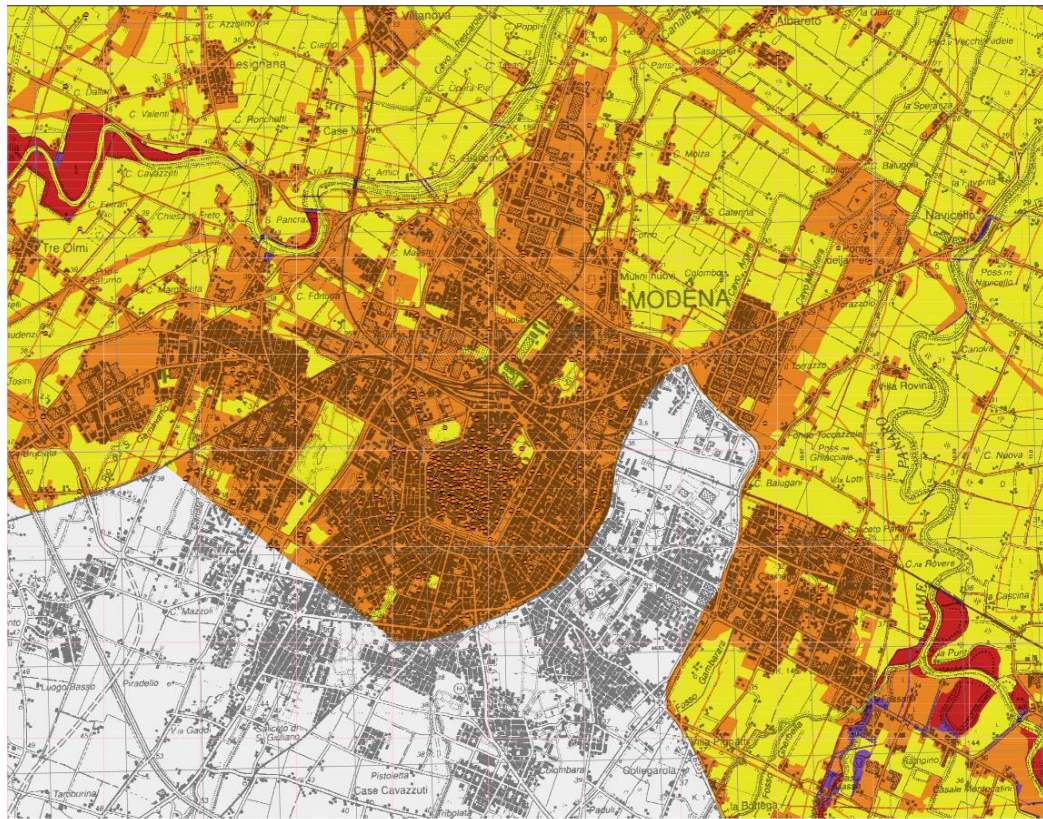


Figure 1.5.3 – Flood risk map for the city of Modena

5.1.3 Concluding remarks

Figures 5.2 and 5.3 clearly show the hazard and risk levels linked to flood events close to Modena Cathedral. Concerning flood hazard, Modena Cathedral is located in an area quite far from the river network: Secchia river is on the Western side of the city center, while Panaro river is on the Eastern side. As a consequence, the Modena city center shows a relatively low probability to be flooded (return period approximately equal to 500 years). Despite this situation, flood risk is classified as moderate due to the presence of cultural heritage sites such as Modena Cathedral.

Given the low hazard due to river flooding, it has been decided to evaluate the pluvial flood hazard. The pluvial flood refers to flood events caused by the concomitance of extreme precipitation events and land that is unable to effectively absorb rainwater. Modena Cathedral stands on a ground with these features.

Regarding precipitation trend, the annual average of the twentieth century series of rainfall in the province of Modena is 632.4 mm. If we consider the ten-year average, no particular variations occur, i.e. the average annual volume of rains did not change significantly.

When considering precipitation at a daily timescale, with a particular focus on extreme events, an increase of rainfall intensity emerges. Indeed, these events are growing since the exceptional event



ALMA MATER STUDIORUM
UNIVERSITA' DI BOLOGNA

DICAM

Dipartimento di Ingegneria Civile,
Chimica, Ambientale e dei Materiali

MiChE

Mitigating the Impacts of natural hazards on Cultural Heritage
sites, structures and artefacts

of October 5, 1990, which recorded a rainfall depth of 165.4 mm in 24 hours [38]. During 2019, several extreme meteorological events occurred, among which the one in November 15-17 caused various flooding phenomena from intense precipitation in Modena city. This event was characterized by an overall rainfall depth of 114.6 mm (89.1 mm on November 16-17 with a 12-hour duration, and 57 mm on November 17 only) [39].

Giving that Modena is located in an area where extreme meteorological events, and therefore pluvial flooding phenomena, occur more and more frequently, the flood hazard is assessed by implementing the Hierarchical Filling and Spilling methodology (HFS, Wu et al., 2015, 2018).



5.2 Pluvial flood hazard assessment

5.2.1 Methods

The HFS methodology has to be considered as a valid criterion for the rapid characterization of floodable areas due to the effect of intense rainfall. It provides flood maps with a good degree of detail and a low computational cost.

The HFS technique identifies areas subject to flooding due to intense rainfall based on the spatial distribution of the blue-spots within the study area and the volume of rain. Blue-spot is defined as a portion of depressed topographic surface, having a lower elevation than the surrounding areas.

The HFS methodology does not allow to simulate the flooding dynamics (speed and flooding times are not considered), however this simplification does not affect the results of the hazard characterization, as the speed of water depths eventually accumulated on the ground, can be reasonably considered negligible.

In particular, the HFS technique consists of two phases:

1. Pre-processing phase, identifying the depressions of the DEM and their hierarchical structure in the horizontal and vertical directions [40];
2. Flooding phase, consisting in the identification of flooded areas and water elevation on the ground next to the occurrence of a rainfall event of fixed intensity (i.e. of fixed precipitation volume).

Specifically, during the Flooding phase two different cases can occur. The first case occurs when the volume of water that could accumulate in a depression is greater than the volume of the depression itself. In this case the total filling of the depression (saturation) and the spillage of the water in excess towards the depressions, located hierarchically at a lower level occur (Filling-Spilling). The second case occurs instead when the volume of water that would accumulate in the depression is less than the volume of the depression itself, so the depression results partially filled. In the latter case the algorithm is able to define the Partial Filling volume [41].



5.2.2 Required input data

The implementation of HFS methodology involves the use of the following input data:

- DEM (Digital Elevation Model) of the areas affected by the potential flooding event. In the specific case, LiDAR was made available by the Italian Ministry of the Environment with a spatial resolution of 1 m (Lidar MATTM 2008 <http://www.pcn.minambiente.it/mattm/>);
- Events of intense precipitation, represented by volumes of rain (i.e. rain depths expressed in mm) with assigned return period (i.e. average number of years that elapses before an assigned event would be equalled or exceeded) for durations equal to 1, 3, 6, 12, 24 consecutive hours. In order to characterize the frequency trend of extreme rainfall events, rainfall data, made available by ARPAE (Regional Agency for the Protection of the Environment of Emilia-Romagna) and, relative to the rain station called Cognento, was analyzed. This rain station was chosen because it is the best representative of the area in which the Modena Cathedral is located (distance between pluviometer and Modena Cathedral is about 3.5 km). Also, it has available data appropriate for statistical analysis (20 years) registered in the exact period in which extreme rainfall events intensified (1975–2012).

By using the Gumbel formulation, depth duration-frequency curves (DDF) were defined based on the historical series of intense precipitation events recorded by Cognento station.

The distribution function of Gumbel's formulation, $P(x)$, defines the cumulative exceedance probability that the generic observation is less than or equal to an assigned x value:

$$P(x) = e^{-e^{-\frac{x-\xi}{\alpha}}} \quad (2)$$

where α e ξ indicate the distribution parameters, evaluated as follows.

$$\alpha = \frac{\sigma\sqrt{6}}{\pi} \quad (3)$$



$$\xi = \mu - 0.5772\alpha \quad (4)$$

where μ and σ respectively indicate the mean and standard deviation of the sample used (i.e. measured rainfall depths). Once the parameters are assessed, it is possible to estimate the rainfall depth associated to any given duration and return period and consequently derive the DDF curve. The return periods related to the precipitation depths were obtained using the probabilities of exceeding the limit states contained in the NTC2008 (Table 1.5.3) considering lifetime of 50 years.

Table 1.5.3 – Probabilities of exceeding the limit states (NTC2008).

| Limit states | | Probabilities of exceeding in a lifetime | Return period [years] |
|---------------------------|-----|---|--------------------------|
| Operating limit states | SLO | 81% | 30.6 |
| | SLD | 63% | 50.8 |
| Ultimate limit states | SLV | 10% | 475 |
| | SLC | 5% | 975 |

Table 1.5.4 shows the extreme rainfall depths for durations of 1, 3, 6, 12, 24 consecutive hours and for return periods of 30.6, 50.8, 475, and 975 years estimated from the Gumbel's formulation (equation (2)) for Cognento gauging station.

Table 1.5.4 – Precipitation depths [mm] for different durations [hours] and return periods [years] for Cognento gauging station.

| Return period [years] | Durations [hours] | | | | |
|--------------------------|----------------------|-------|--------|--------|--------|
| | 1 | 3 | 6 | 12 | 24 |
| 30.6 | 36.59 | 52.60 | 69.92 | 94.80 | 115.43 |
| 50.8 | 39.74 | 57.21 | 76.18 | 103.35 | 125.90 |
| 475 | 53.48 | 77.37 | 103.60 | 140.78 | 171.71 |
| 975 | 57.89 | 83.83 | 112.39 | 152.78 | 186.40 |

The corresponding DDF curves are shown in Figure 1.5.4.

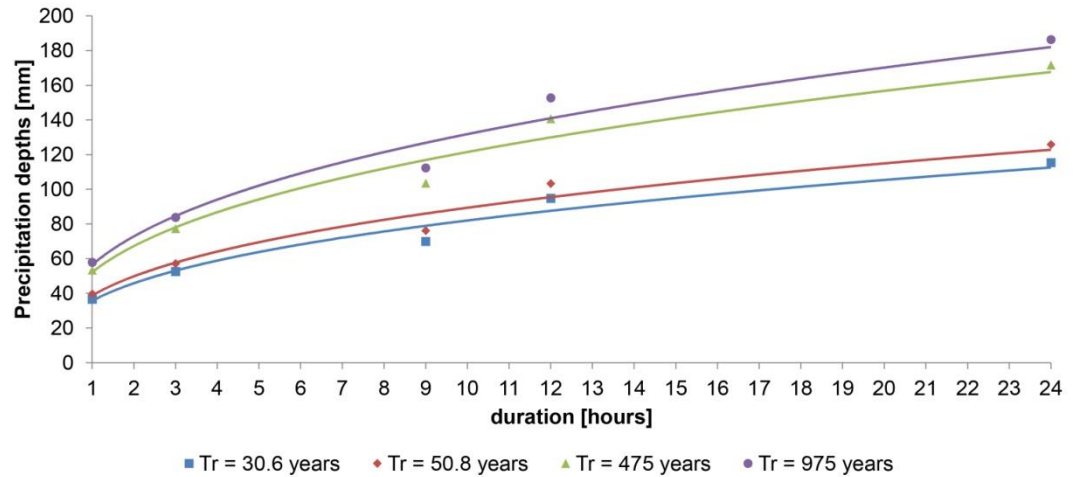


Figure 1.5.4 – DDF curve for Cognento gauging station.

The DDF curves express the relationship between the maximum annual rainfall depths and durations mentioned above that can occur in the study area, for an assigned return period.

5.2.3 Simulated rainfall events

The hydrological scenarios used for the characterization of the pluvial flood hazard consider a subset of all the scenarios shown in Table 1.5.4 and Figure 1.5.4. Specifically, the values shown in Table 1.5.5 are taken as a reference

Table 1.5.5 – Precipitation depth related to simulated events.

| Return period [years] | precipitation depth [mm] |
|--------------------------|-----------------------------|
| 30.6 | 36.59 |
| 50.8 | 39.74 |
| 475 | 53.48 |
| 975 | 57.89 |

For each return period considered, a rainfall depth was chosen in order to have sufficiently diversified flooding scenarios.



ALMA MATER STUDIORUM
UNIVERSITA' DI BOLOGNA

DICAM

Dipartimento di Ingegneria Civile,
Chimica, Ambientale e dei Materiali

MiChE

Mitigating the Impacts of natural hazards on Cultural Heritage
sites, structures and artefacts

During the simulation phase, a precipitation depth which does not cause any significant flooding, was also considered. This precipitation depth equals 29.53 mm and relates to a return period of 10 years with an exceeding probability equal to 99.5%.



6 Multi-risk assessment

To evaluate the risk associated with the different hazards that may have effects on historic monumental buildings (*multi-hazard analysis*), a simplified procedure is proposed which combines the results of mono-risk analysis developed for a monumental building.

For this aim first the approach for the evaluation of the risk associated to a single natural hazard is presented.

6.1 Single risk analysis

6.1.1 Introduction

To evaluate the risk associated with the different hazards that may have effects on historic monumental buildings (*multi-hazard analysis*), a simplified procedure is proposed based on two fundamental aspects:

- Introduction of exposure factors (multi-exposure analysis): in each mono-risk analysis the economic losses (direct + indirect) are assessed by introducing various exposure factors that explicitly refer to the specific characteristics of a monumental asset.
- Combination of the effects of the different hazards: the different hazards are combined in terms of economic losses referring to an observation time common to the different hazards, in the hypothesis of considering the hazards as statistically independent aleatory variables.

6.1.2 Risk assessment approach for each individual hazard

The logical process and the corresponding calculation path can be summarized briefly with reference to the figure below.

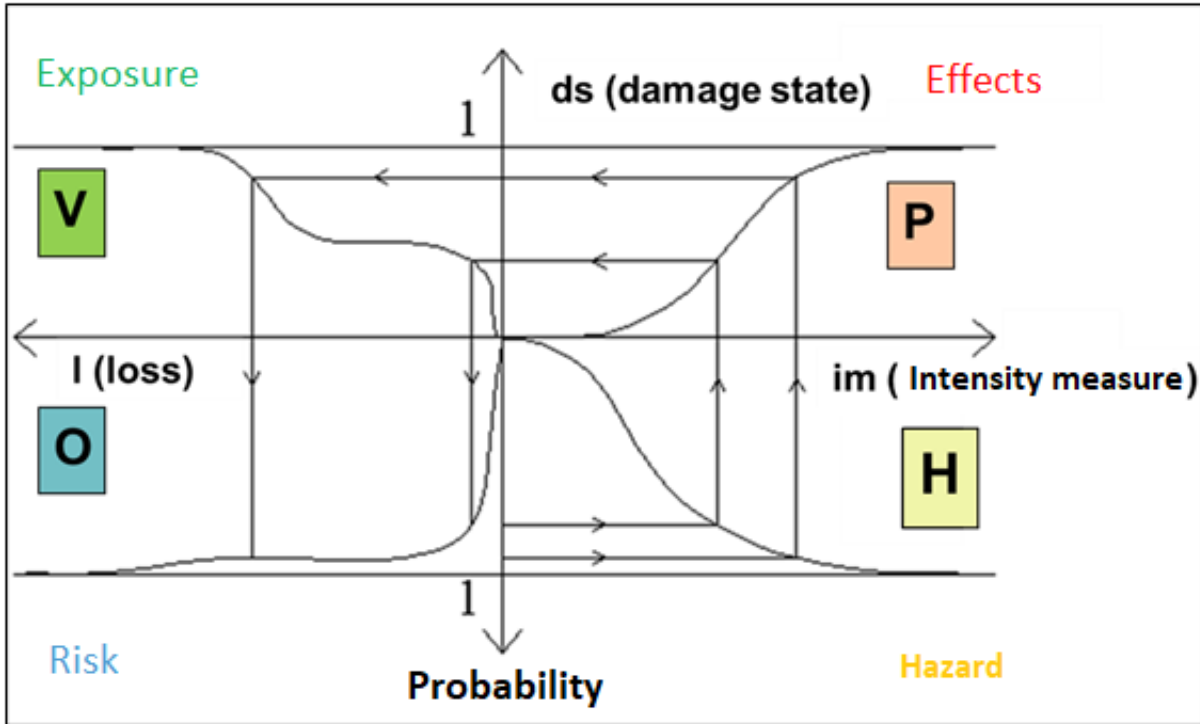


Figure 1.6.1 – Procedure for evaluation of risk due to natural hazard.

Where:

IM (intensity measure) = intensity of the event

ds = damage state

L (loss) = economic loss

H (hazard curve) = CDF(im)

P = performance curve

V (vulnerability) = vulnerability curve

O = CDF (I) = analysis output

Quadrant IV shows how the hazard analysis is taken into account (represented by probability of occurrence curves - PGA shaking index for the seismic case called "H"). The characterization of the site hazard is basically the probabilistic portion in the strict sense of the analysis, as it associates a precise probability with a macro-data identifying the shaking, the flooding, the fire ... With reference to earthquakes, the seismic hazard of the site is identified by the curves that associate a given probability (CDF and PDF) with a specific identifying parameter of telluric shaking (for example PGA).



ALMA MATER STUDIORUM
UNIVERSITA' DI BOLOGNA

DICAM

Dipartimento di Ingegneria Civile,
Chimica, Ambientale e dei Materiali

MiChE

Mitigating the Impacts of natural hazards on Cultural Heritage
sites, structures and artefacts

Quadrant I shows the ways in which the analysis of the **effects** of the hazard on the building is taken into account (through the performance or fragility curves called "**P**"). The curves associate in a deterministic way (even if based on statistical studies) to each value of the hazard identification parameter a corresponding damage index.

Quadrant II shows how the **exposure** is taken into account by associating to each value assumed by the damage index (d_s) a corresponding value capable of quantifying its effect on the specific exposed asset considered (the building-container, the good content, the usability of the structure, etc.) sometimes called "**vulnerability curves**". Due to the fact that different types of exposed assets are considered, different curves of this type can be implemented, globally called "**V_n**" and individually numbered progressively (**V1**, **V2**, etc.).

Quadrant III shows how the **risk** is assessed. This occurs through functions that associate specific non-exceeding probability values (in a given observation period) with the corresponding values that quantify the effect of the studied hazard (**economic damage**) on the specific exposed asset considered.



6.1.3 Multi exposure analysis

The multi-exposure analysis conceptually consists of two phases.

The first phase consists in **identifying the exposure factors** common to the different hazards. Each exposure factor is represented by:

- an aleatory variable that quantifies the economic loss associated with the i -th exposure factor (L_i);
- a function V_i which links the damage variable (d_s) to the expected economic loss (l_i).

The second phase of the multi-exposure analysis consists in **evaluating the vulnerability functions** related to each exposure. These vulnerability functions can be assessed through statistical data and / or analytical functions.

It should be noted here that, with specific reference to the seismic case, in the document "*Existing Empirical Vulnerability and Fragility Functions: Compendium and Guide for Selection*" [42], some examples of vulnerability curves analyzed are reported. There is no explicit mention of multi exposure but it is clearly noted that various elements can be analyzed, as shown in the extract of the document below.

To date, few direct vulnerability functions have been constructed due to the scarce availability of good quality empirical loss data. The majority of these existing functions correlate a measure of the cost of the **direct damage** to an intensity measure type. A small minority correlate a measure of casualty with intensity and only Comerio (2006) are found to correlate **downtime** with ground motion intensity. With regard to the form of these functions, discrete functions of loss are proposed by Scholl (1974) and Cochrane and Schaad (1992) in terms of **average economic** loss and by Comerio (2006) in terms of downtime. These are represented in similar matrix formats to DPMs with mean losses presented for each intensity level. Continuous functions have also been proposed to correlate the economic loss of the direct damage (Scawthorn et al. 1981; Petrovski et al. 1984) or **fatality ratio** (i.e. the deaths divided by the total exposed population of an area) (Jaiswal and Wald 2010) with a range of IM parameters. These take a range of forms, further discussed in Section 2.4.3.



6.1.4 Exposure factors for monumental buildings

The exposure represents all that can be negatively affected by hazard (seismic, flood, fire ..). The exposure is representable through homogeneous categories of effects of interest to the community and typically go to identify the losses that given systems can suffer following different hazards such as: seismic, flood, fire events

Some possible exposure factors are described below and the relative aleatory variable is associated which takes into account the relative / equivalent economic loss (L_i) associated to:

- **Structural damage:** damage to the structural element of the building (L_1)
- **Damage to Content:** damage to everything that is present inside the building (L_2)
- **Damage to goods of artistic value:** damage to goods of historical/artistic value present inside or outside the building such as statues, paintings, frescoes (L_3)
- **Non-usability:** months of non-use (L_4)
- **Economic losses due to non-usability :** economic losses associated to the months of non-use (L_5)
- **Social damage:** impact that the loss/damage of a cultural asset has on society (L_6)
- **Fatalities:** number of victims (L_7)
- **Economic losses due to fatalities:** economic losses associated to number of victims (L_8)
- **Damage due to interruption of viability:** road not practicable from collapse (L_9)

In addition to the losses associated with the individual exposure factors, it may be of interest to evaluate economic losses associated with specific combinations, for example:

- **Damage due the structural damage and contents:** $L_9=L_1+L_2$
- **Damage due the structural damage and goods of artistic value:** $L_{10}=L_1+L_3$
- **Damage to content and goods of artistic value:** $L_{11}=L_2+L_3$
- **Damage due the structural damage, content and goods of artistic value:** $L_{12}=L_1+L_2+L_3$

It is clear how additional categories (and specific L_i values) can be integrated with those.

From the point of view of the evaluation of the different aspects, while leaving each operator the specific evaluation method, the following approaches can now be suggested. Assessment of the "state" of the asset. From a seismic point of view, it is suggested to refer to the 4 states referred to the performance based design and Italian standards (SLO, SLD, SLV, SLC).



Various effects can easily be assessed from these 4 reference states. For example, there is no inhibition for the use of the property until the SLD. From the SLD onwards there are some inhibitions. Similarly, as regards casualties up to SLV, there are no inhibitions.

It is recommended to first evaluate the effects in a dimensionless way. For example, with reference to randomness, we can think of associating the number of causality as a linear progression in moving from SLV to SLC. With zero random number at the SLV earthquake and unit random value at the SLC earthquake. Once the dimensionless curve has been performed, it must be dimensioned. Where instead of passing from 0 randomness to 1, it passes from 0 to the actual maximum number assessed with specific reference to the specific case.

6.1.5 Risk assessment for each individual hazard: the seismic hazard

The risk analysis for buildings is carried out by calculating (combining) information related to the **probability** of having specific values of ground accelerations (for example of peak ground acceleration PGA, for the seismic case) represented by the **hazard curve H** (CDF of the intensity measurement) with information related to the behavior of the individual building under examination (**performance curve P**) and with specific curves that allow to correlate the behavior of the building (damage state ds) with specific data capable of quantifying the economic loss corresponding to the various factors of exposure such as damage to the container, contents, etc. (**vulnerability curves V1, V2** etc.). The **P** curve (specific of each analyzed building) allows to associate (for the examined building) to each value related to the analyzed hazard a precise value of structural damage index (ds). The structural damage index takes values between 0 (no damage to the structure) up to 4 (total damage to the structure). The damage index values have been defined in relation to the 4 structural performance levels on which the Performance Based Design procedures are structured (Vision 2000, FEMA 273 documents and subsequent additions):

- 1 = immediate occupancy (SLO),
- 2 = occupancy (SLD),
- 3 = life save (SLV),
- 4 = near collapse (SLC).

Using together the **H** and **P** curves allows to associate a precise probability to each damage index value.

Vulnerability curves **V1, V2, V3** etc. associate to each value assumed by the damage index a corresponding value capable of quantifying the economic loss associated with the corresponding exposure factor.

The probability curve (CDF and / or PDF) of the economic loss variables (I) represent the objective of the risk analysis and these functions associate specific non-exceedance probability values (in a given observation period) with the corresponding values that quantify the effect of the studied hazard (**economic damage**) on the specific exposed good considered.

The information provided by the various curves are "assembled" substantially through a process of "function of function" (numerical) conventionally called "**convolution**" and schematically represented in figure 1.6.1.

6.1.5.1 Hazard Curve

The **hazard** analysis allows to obtain **hazard curves H**: probability of occurrence curves - Hazard parameter (PGA for the seismic case). The hazard curve H, CDF of the seismic intensity measurement (PGA), represents the probability of having specific peak ground acceleration values PGA.

IM = Seismic intensity measure (PGA)

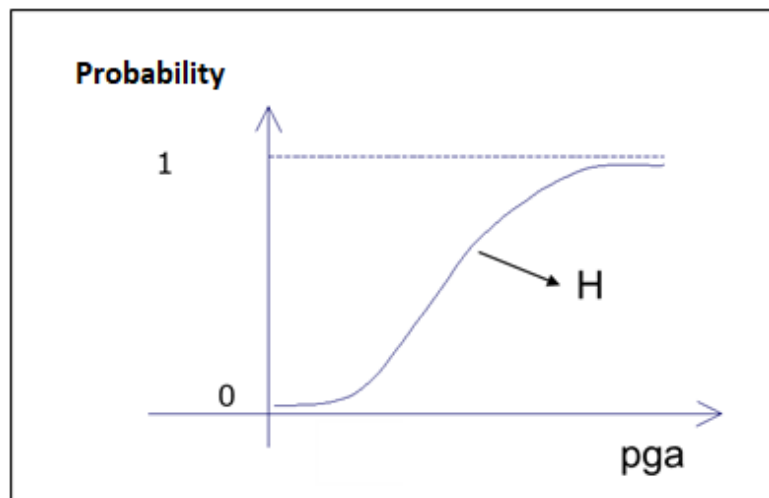


Figure 1.6.2 – Hazard curve.

The analytical expression that represents this hazard curve is the follow:

$$F_{IM}(im) = H$$

$$F_{PGA} = \Pr[PGA \leq \overline{pga}]$$

6.1.5.2 Performance curve

The performance curves associate in a deterministic way (even if based on statistical studies) to each value of the hazard identification parameter a corresponding damage index (ds). It should be noted that these curves could be obtained from specific fragility analysis.

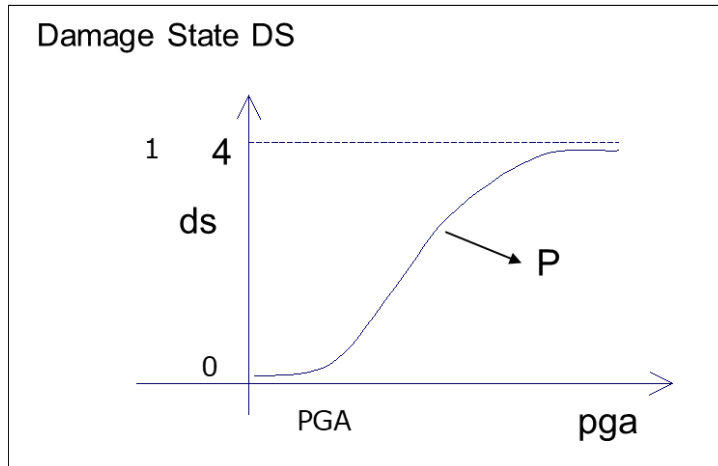


Figure 1.6.3 – Performance curve.

The analytical expression that represents the performance curve is:

$$P = E[DS / im]$$

The structural damage index, with specific reference to the seismic case, takes values from **0 (no damage to the structure) up to 4 (total damage to the structure)**. The damage index values have been defined in relation to the 4 structural performance levels on which the Performance Based Design procedures are structured (SLO, SLD, SLV, SLC).

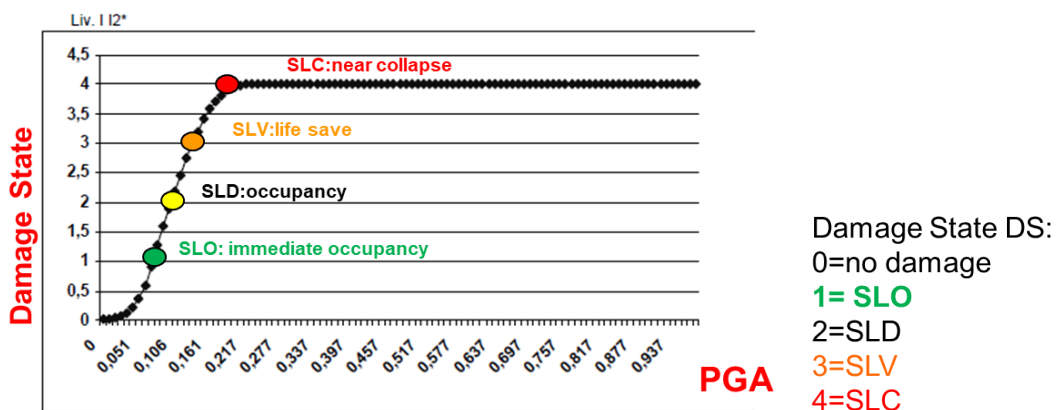


Figure 1.6.4 – Example of performance curve.

6.1.5.3 Vulnerability curves

The exposure is considered through the association of specific values of the damage index with the numerical quantification of the effect of this damage index on the specific exposed asset considered (for example the building, rather than its assets and functions). The set of pairs thus defined generically takes the name of "**vulnerability curve Vn**". From an operational point of view, exposure is taken into account by associating to each value assumed by the damage index a corresponding value capable of quantifying the economic loss connected to the corresponding exposure factor considered (the building-container, the asset-content , the usability of the structure, etc.). Due to the fact that different types of exposed goods are considered, different curves of this type can be implemented, globally called "Vn" and individually numbered progressively (V1, V2, etc.).

The following figure shows, for example, the vulnerability curve that takes into account the damage to the external casing of the building as an exposure factor (L1 = damage to the container).

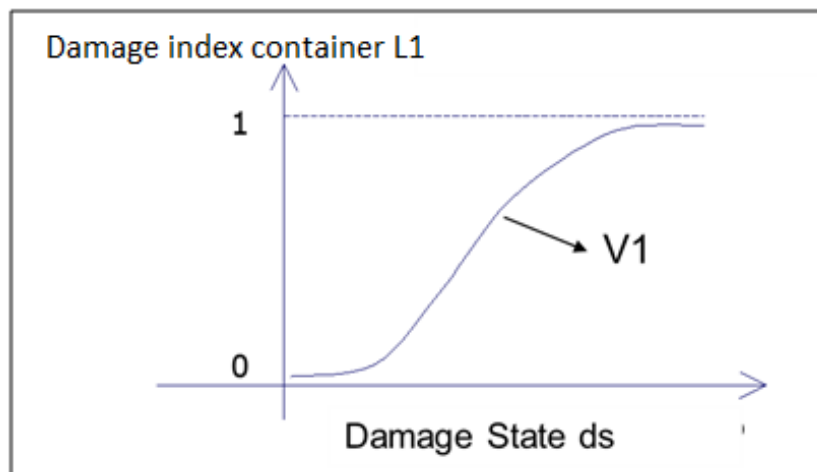


Figure 1.6.5 – Vulnerability curve V1.

The analytical expression that represents the performance curve is:

$$V_i = E[L_i / ds]$$

6.1.5.4 Risk curves - loss curves

The objective of the risk analysis is to obtain the probability curve (CDF - PDF) of the economic loss variables (loss- l) associated with each exposure factor considered.

These functions associate specific non-exceeding probability values (in a given observation period) with the corresponding values that quantify the effect of the studied hazard (**economic damage**) on the specific item exposed considered.

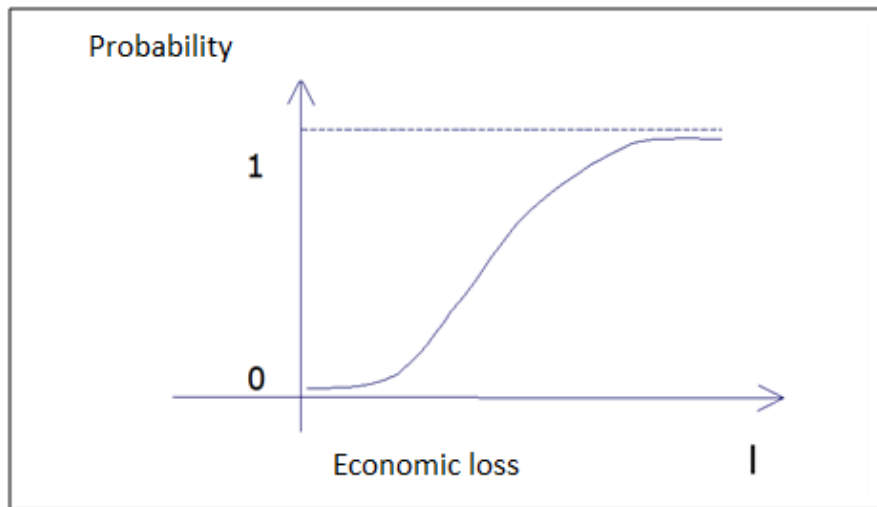


Figure 1.6.6 – loss curve.

Assuming that:

$$g_1 = E[DS / im] \quad \text{and} \quad g_2 = E[L / ds]$$

The analytical expression that represents the CDF of the risk curve (loss curves) is:

$$CDF(L) = F_L(l) = F_{IM}[g_1^{-1}(g_2^{-1}(L))] = F_{IM}[P^{-1}(V_n^{-1}(l))]$$

The analytical expression that represents the PDF of the risk curve (loss curves) is:

$$PDF(l) = f_L(l) = f_{IM}[g_1^{-1}(g_2^{-1}(l))] \cdot \frac{dg_1^{-1}(im)}{d(im)} \cdot \frac{dg_2^{-2}(ds)}{d(ds)}$$



6.2 Multi-risk analysis

The CDF and/or PDF probability curves of the loss variables calculated for the specific hazards (mono-risk analysis) can be identified as follows:

- L_i, E = CDF / PDF of the i -th loss variable for the seismic hazard (**Earthquake hazard**);
- L_i, FI = CDF / PDF of the i -th loss variable for the hydraulic hazard (**Flood hazard**);
- L_i, F = CDF / PDF of the i -th loss variable for the fire hazard (**Fire hazard**).

In the assumption that the events are statistically independent (there are no linked events), the multi-risk analysis relating to two specific hazards and the specific exposure factor is:

$$L_{i,m} = L_{i,E} + L_{i,FI} + L_{i,F};$$

Considering two random variables x_1 and x_2 representing the CDF and / or PDF probability curves of the loss variables calculated for the specific hazards (L_i, E, L_i, FI, L_i, F) the mathematical expression that combines **two** specific hazards can be developed as follows:

$$y = x_1 + x_2$$

$$F_Y(y) = \int_0^y \left\{ \int_{x_2}^y f_{X_1}(y - x_2) \cdot f_{X_2}(x_2) \cdot |J| dy \right\} dx_2$$

Where:

$$|J|=1$$

Similarly, the CDF probability curves of the losses linked to the combination of the 3 different hazards can be obtained as follows:

$$z = y + x_3$$

$$F_Z(z) = \int_0^z \left\{ \int_{x_3}^z f_Y(z - x_3) \cdot f_{X_3}(x_3) \cdot |J| dz \right\} dx_3$$



ALMA MATER STUDIORUM
UNIVERSITA' DI BOLOGNA

DICAM

Dipartimento di Ingegneria Civile,
Chimica, Ambientale e dei Materiali

MiChe

Mitigating the Impacts of natural hazards on Cultural Heritage
sites, structures and artefacts

PART 2: CASE STUDY- THE MODENA CATHEDRAL

Part 2 illustrates the main results of the studies conducted to assess the seismic and flood risk of the selected case study, namely the Cathedral of Modena. In particular, chapter 1 provides the summary of all research and studies conducted during the last decades to acquire knowledge related to the behaviour of the monument and site hazard including: construction phases, geometrical configurations, material properties and their state of degradation, soil conditions, seismic hazard, flood hazard. Chapter 2 illustrates the main results of the structural analyses conducted to assess the static and seismic behaviour of the monument. Chapter 3 and 4 gives the main results of the risk analysis associated to both seismic and fire hazards.

1 The integrated knowledge

1.1 The Cathedral of Modena

The Cathedral of Modena and the adjacent Ghirlandina Tower are part of the UNESCO site of Piazza Grande, since 1997. The Cathedral is a masterpiece of Romanesque architecture and sculpture of northern Italy (Figure 2.1.1). Its construction was realized between 1099 (the date of its foundation is marked on a stone on its façade) and 1319, when the construction of the Ghirlandina was completed. Inscriptions on the façade and on the central apse celebrate respectively the sculptor Wiligelmo and the architect Lanfranco. As it will be better explained later, the actual Cathedral rise up on the ruins of three previous Cathedrals [43], the first one containing the tomb of St. Geminianus (the Modena city's patron). The in-plan geometry is approximately 25 m wide, in the transversal direction, and 66 m long, in the longitudinal direction, for an area of roughly 1650 m². The maximum roof height is approximately 24 m (Figure 2.1.2). The Cathedral has a Latin cross plant with three naves, a false transept and the chancel (the area of the liturgical altar) in an elevated position, due to the presence of a crypt containing the corpse of the city's patron, Saint Geminianus.



(a)



(b)

Figure 2.1.1: Photographs of Cathedral of Modena: (a) view of the apses and (b) view of the facade.

The structural configuration consists of heavy masonry walls, sturdy masonry and stone piers supporting the weight of impressive thin masonry vaults, added in the XV century. Both the central nave and the side aisles have four spans. The vaults of the central nave have double length span

with respect to the length span of the vaults of the aisles. The maximum height of the vaults of the central nave is around 20 m, while that of the side aisles is approximately 13 m. Next to the Cathedral, there is the Ghirlandina Tower, a high tower of roughly 88 m high whose construction proceeded in parallel with that of the Cathedral up to the fourth level. The upper part of the Tower was built later, between 1261 and 1319 [44].

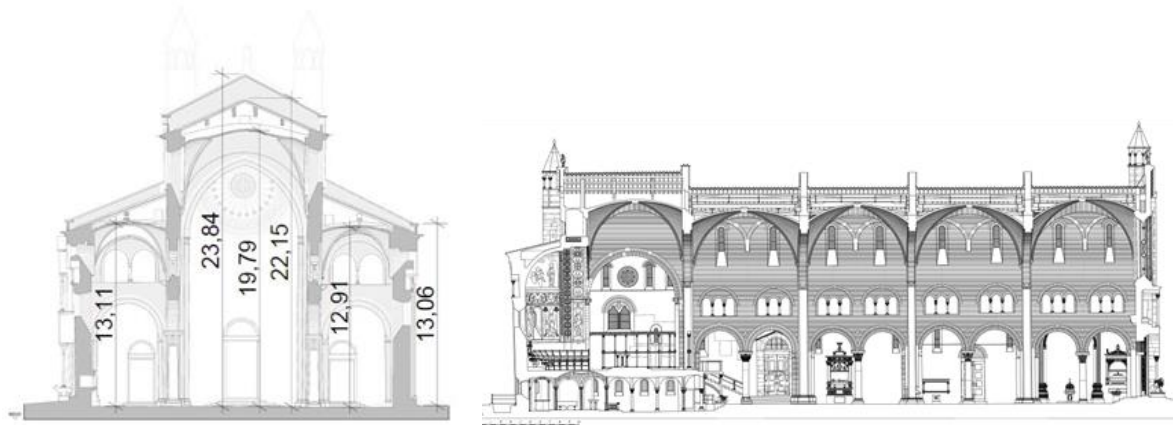


Figure 2.1.2: Cross-section of the Cathedral of Modena.

1.2 The actual state of the Cathedral

1.2.1 The construction phases and the main interventions

The current configuration of the Cathedral is the result of various transformations and interventions that occurred on the fabric during centuries. These changes did not only affect the architecture of the Cathedral, but also influenced significantly its structural behavior. In the light of this, it is of fundamental importance to have a clear view of the most significant construction phases. Before the present Cathedral, three ones were built on the necropolis containing the tomb of St. Geminianus (the founder of the church of Modena) which is the only remaining evidence of the first one. A second Cathedral was erected in the same place around the VIII-IX century. The archaeological remains indicate that this church had a length of around 32 m and width of 18 m. The presence of polylobate piers [45], discovered during past excavations, allow to suppose the existence of another Cathedral, presumably built around the XI century (Figure 2.1.3) [46].

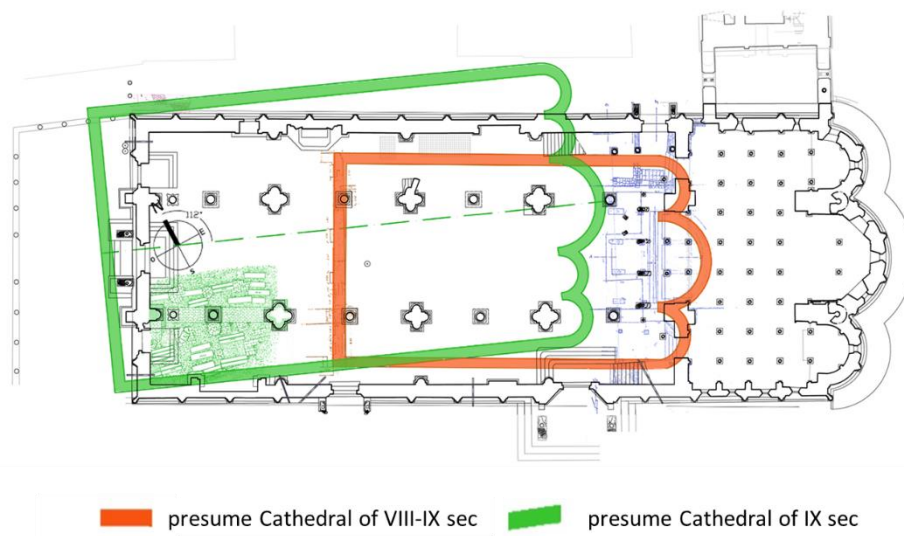


Figure 2.1.3: The pre-existing Cathedrals

There is an open debate about the construction phases leading to the actual fabric [47], [48], [49], [50],[51]. According to the hypothesis of Porter [52], confirmed later by other researchers, the construction began in 1099, almost in parallel, from the apses and, just few years later, from the main façade. At 1130, the complex knew the construction of the clerestory and the joining of the lateral naves where, according to Peroni (1989 and 1999) and Lomartire (1989), the initial construction was interrupted in order to maintain the portions of the pre-existing Cathedral. More recent historical studies [51] suggest that the construction of the outer perimeter did not proceed in parallel from the two sides, specifically the main façade and the apses, but started from the apses

(phases A) to end with the main façade (phases B), (Figure 2.1.4: The construction phases Figure 2.1.4). In light of this alternative hypothesis, the phase C was remarked by the repair of some damages due to early soil settlements manifested during the first two phases. This reconstruction may be further supported by the analysis of the cracking pattern. Figure 2.1.4 graphically represents the three construction phases according to this last hypothesis.

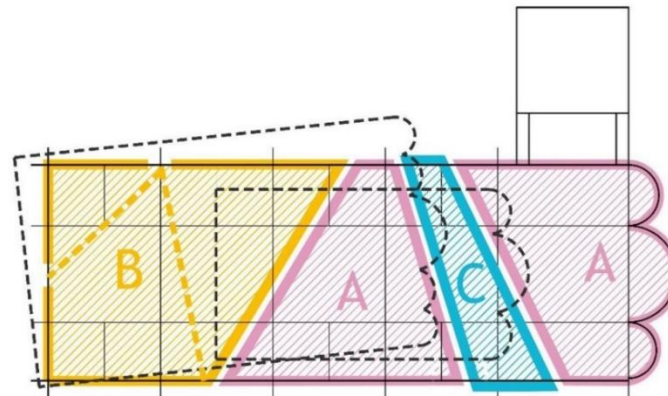
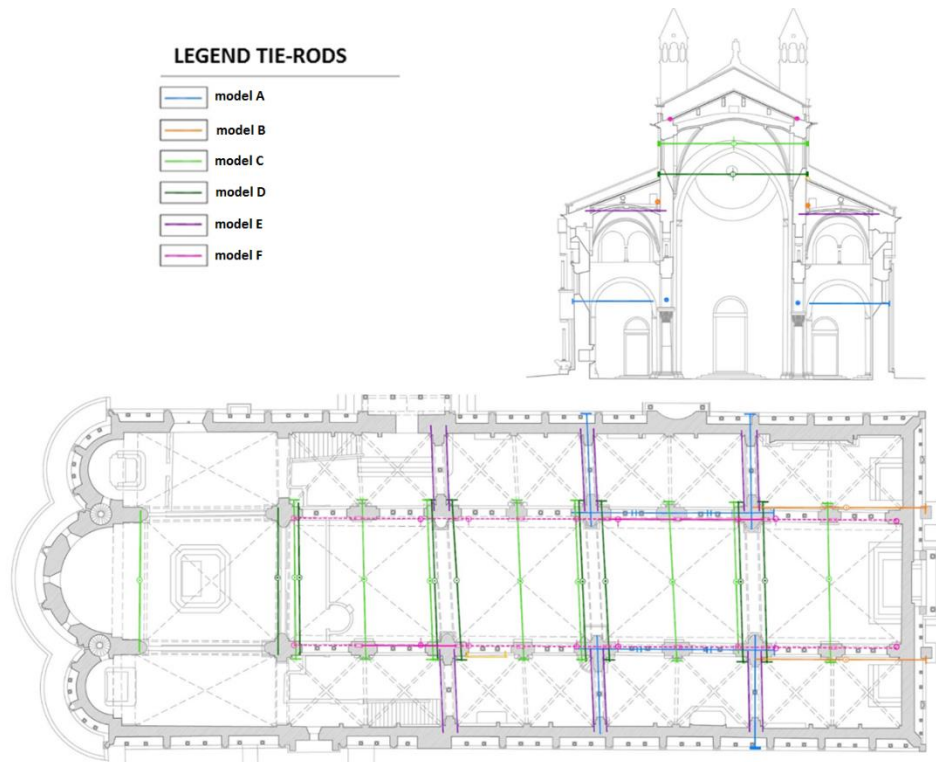


Figure 2.1.4: The construction phases

After the end of the construction, several interventions were carried out during the years. The elevation of the Tower in the following years caused the lowering and slight rotation of the apses due to differential soil settlements. The presbytery appeared so slanted that it was necessary to realize many reparations and reconstructions according to a new verticality and horizontality. This was one of the principal intents of the architectural renovation applied by the Campionesi masters at the Cathedral of Modena during the years 1180-1220. In the light of the studies on the construction phases, the 3D laser scanner survey was able to measure the different inclinations of the masonry walls belonging to the different phases, thus dating the successive increases of the foundation settlements along the centuries. According to several historians, the original roof system, made of timber trusses (“capriate”) arranged in the transversal direction, was rebuilt after 1413. The orientation of the principal beams was changed when the vaults of the naves were constructed. Probably during this phase, the original timber beams were replaced causing deformations of the longitudinal walls. Later on, other interventions proved to be necessary after the earthquake events occurred in the 1501, 1505 1671 and 1832. The main interventions affected the vaults, the arches, the façade and the portions of walls adjacent to the Ghirlandina Tower [53]. In the following years, additional strengthening interventions were performed, such as refilling the main cracks, repairing the roof (new wood structures connected to the masonry wall by iron chains) and connecting the walls through iron chains in the naves at different heights (Figure 2.1.5). At the beginning of the XX century, all the constructions built next and into the Cathedral during the years (rectory, cluster,

sacristy and internal chapels) were demolished in order to restore the original Romanesque aspect. In 1975, Modena and its Cathedral were affected by the soil subsidence. During the recent years, starting from the 2006, a restoration campaign has interested the external stone facade, until the earthquakes of the 2012 shifted the attention to the damages of the interior, principally the vaults, as it will be better explained in § 1.2.4.



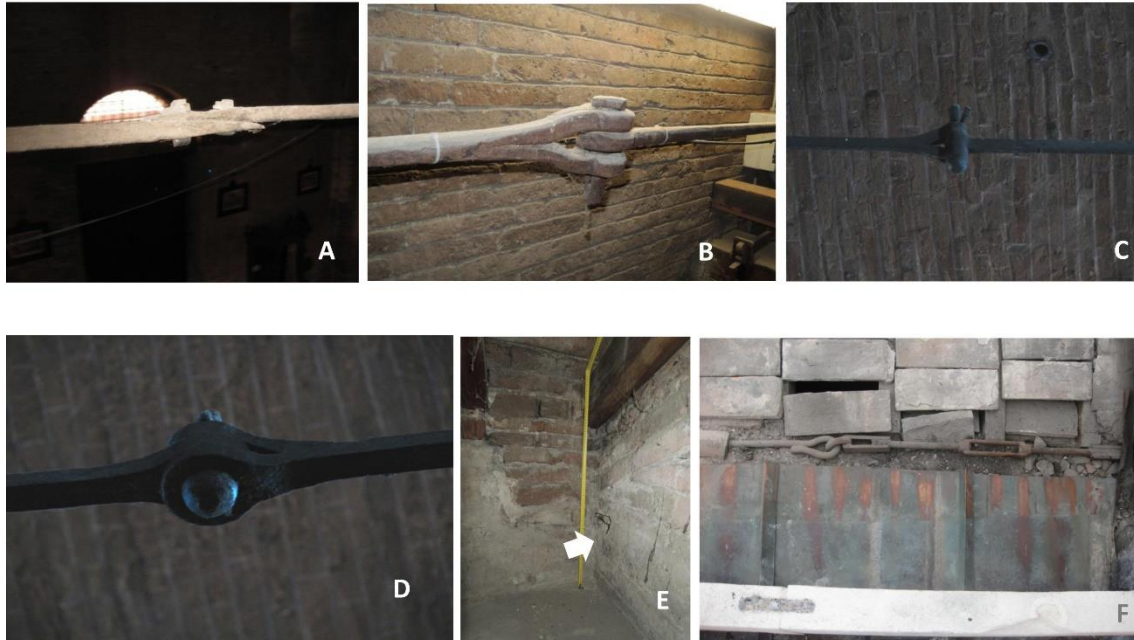


Figure 2.1.5: Survey of the tie-rods installed on the Cathedral during the years and respective photographers.

1.2.2 The reconstruction of the geometric configuration through laser scanner and the geotechnical investigations

A 3D laser scanner of the Cathedral was carried out to identify with accuracy walls dimensions and deviation from verticality [54]. Figure 2.1.6 displays the inclinations of the external wall and internal pillars as obtained from the 3D laser scanner. In general, excluding the area of the South transept, the walls are inclined towards the outside. As already clear by simple visual inspection, the overhanging increases moving closer to the Ghirlandina Tower, thus indicating a strong interaction between the Tower and the Cathedral. Notably, this interaction caused so important damages to the two masonry arches connecting the Tower with the Cathedral, at the point that they were completely reconstructed at the beginning of the last century.

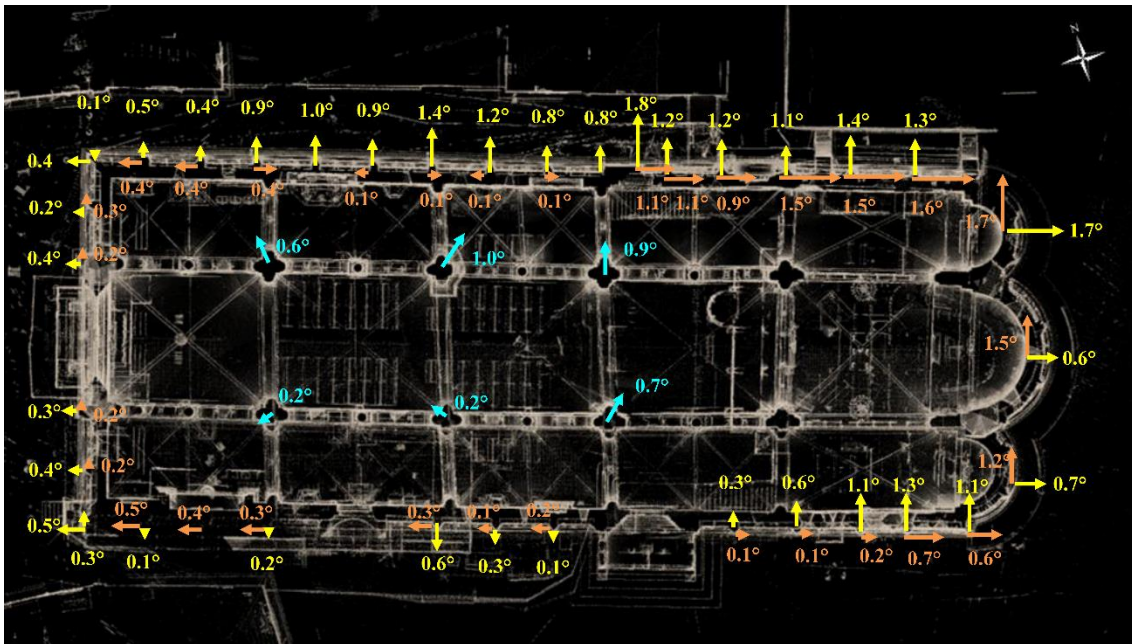


Figure 2.1.6: The inclinations of the external walls and internal pillars as so obtained from the 3D laser scanner.

In addition to the differential settlements induced by the interaction between the Tower and the Cathedral, also a discontinuity in the soil stiffness due to the presence of the ruins in only one portion of the plan (see Figure 2.1.3), could have significantly contributed to the walls deformation. Since that soil has “memory” of its previous loading history [55], due to loading-unloading (as consequence of sequences of construction and demolitions), the soil response of these portions would be much stiffer than those parts that never experienced any previous loading-unloading. Therefore, this loading history could contribute to explain why the Cathedral suffered uneven settlements not only moving from South towards North (due to the presence of the Tower, as before explained), but also moving from East towards West. These differential settlements were also more pronounced due to the nature of the foundation soil. The soil profile were investigated up to a depth of 80 m resulting in a sequence of recently deposited alluvial horizons. The first horizon is made of medium to high-plasticity inorganic clays with a number of millimeter-thick laminas of sands and peats. The upper portion of this horizon, which has a thickness of about 5 m to 7 m, is known as the Modena unit and it is linked to flooding events (of post-Roman era) produced by minor streams. Geological and geotechnical studies [56],[57],[58] have shown events of exposition during deposition and generate layers that therefore were slightly over consolidated by desiccation. From these geotechnical investigations, also the soil mechanical properties useful for the structural analysis have been obtained. For instance, two different values of the Winkler constant may be assumed to account for the presence of a portion of more consolidated soil (see Figure 2.1.7).

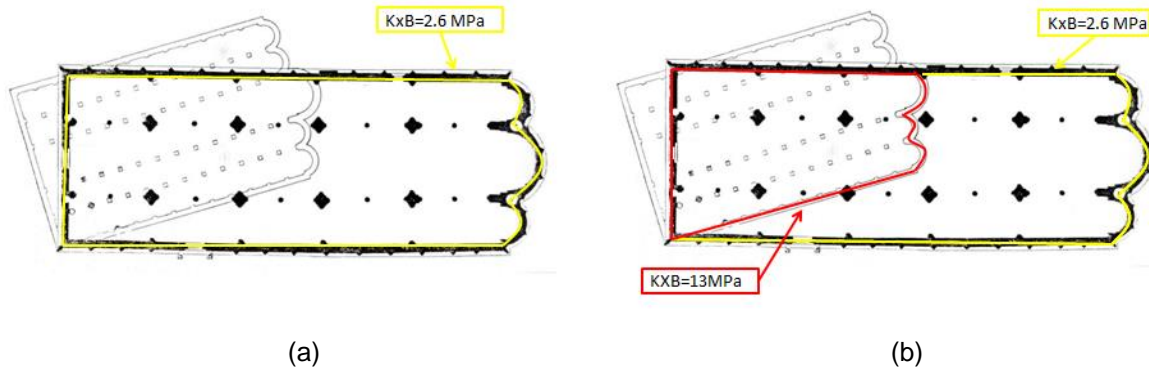


Figure 2.1.7: (a) Uniform distribution of Winkler's constant (W1) and (b) Non Uniform distribution of Winkler's constant (W2).

1.2.3 Material properties

It is a matter of well consolidated knowledge that the assessment of material properties of historical masonries is a rather challenging problem. Extensive destructive and non-destructive tests are typically used to evaluate material properties of ordinary existing buildings. Nonetheless, for important monuments, only limited tests are usually allowed by the local authorities in charge of the conservation of the monument. Moreover, the mechanical parameters as obtained from few non-destructive tests provide only partial and local information. This means that these few data must be critically analyzed in terms of their reliability. Therefore, experimental data have to be compared not only with values suggested by the codes or literature but as well as with values based on material models. This approach was already successfully applied to the ancient masonry "Asinelli" Tower in Bologna [59] and has been also used in the present case. The results of video-endoscopic investigations on the facade and sonic and radar tests on the remaining walls and piers, were integrated and validated with the values suggested by the scientific literature [60],[61] or by codes (Circ. n. 617, 2009) leading to masonry and stone Young's modulus equal to $E_m = 1800-4000$ MPa, and $E_s = 25000$ MPa, respectively. For the timber beams, considering aging effects, the lower bounds mechanical properties have been used as suggested by the document CNR-DT 206 [62]: Young's modulus $E = 600$ MPa, compression strength $f_m = 14$ MPa and mean density $\rho_m = 350$ Kg/m³.

1.2.4 The actual state of degradation

A first detailed survey of the cracking pattern was carried out in the 2010. After the 2012 Emilia Earthquakes, the Cathedral suffered minor damages, mainly localized in the vaults. Therefore, a second survey was carried out to detect in detail the damages caused by the earthquake sequence.

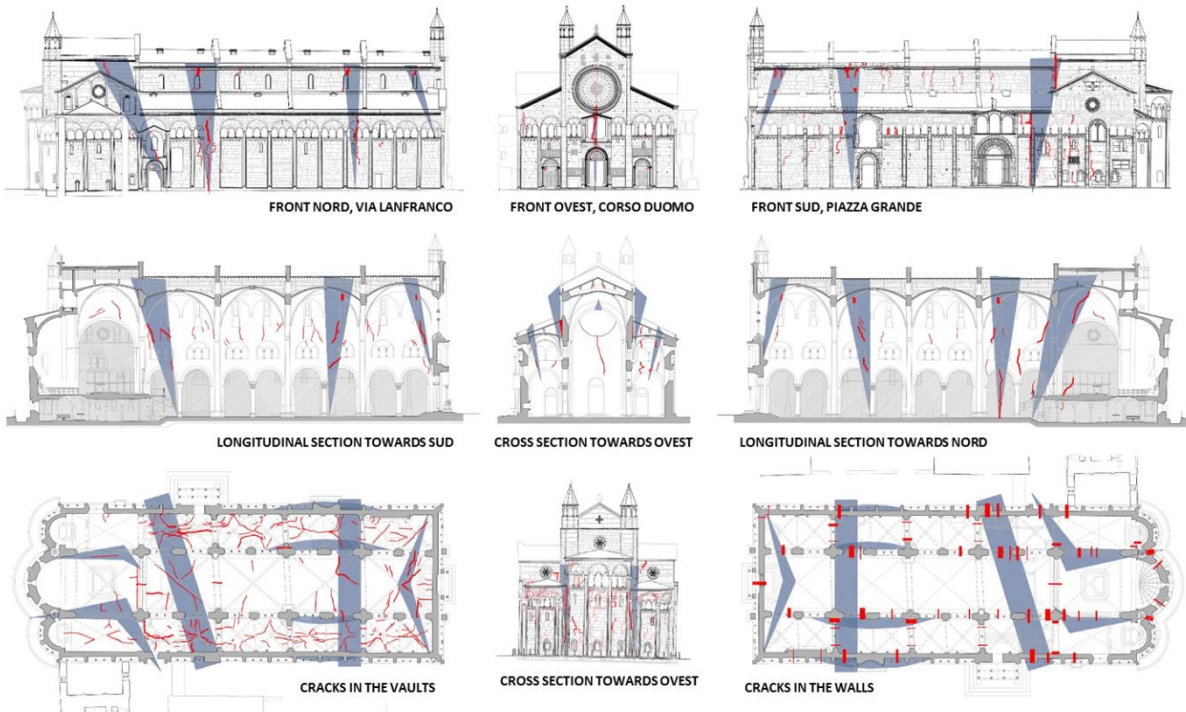


After this detailed survey, a strengthening intervention has been planned and the design is actually under development.

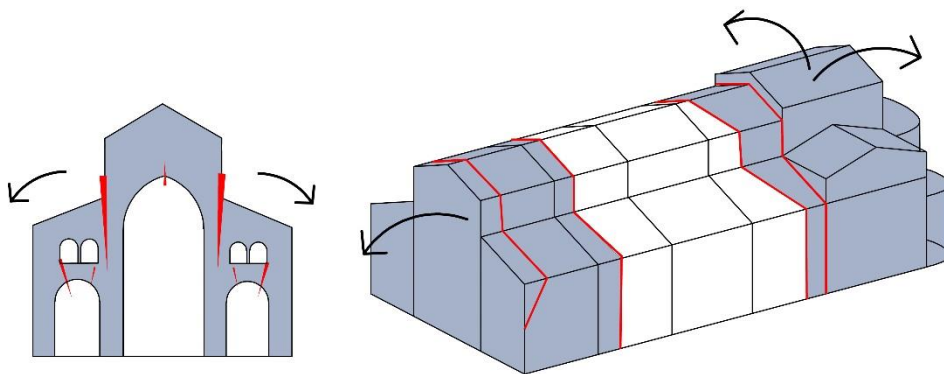
The initial crack pattern (2010) has been studied not only to monitor the state of the main cracks but also to correlate their location within the construction phases and main interventions. The analyses of past studies also helped in the classification of the cracks. In particular, the correlation between the damage and the past interventions allow to identify the probable causes and distinguish between stable cracks and still evolutionary situation. The major cracks are displayed in Figure 2.1.8. The main cracks are indicated in red, while grey areas indicates the zones of diffused cracks with potential high vulnerabilities. It can be noted that:

- a large vertical crack is located in the main facade, just below the big rose window;
- a concentration of cracks has been identified in the connection between the walls, all along the portion of the building constructed during the phase C, in the fourth span from the west;
- another cracks concentration appears near the main facade, along a line parallel to the façade, in the second span from the west;
- vertical cracks along the main transversal walls and arches separate the central naves from the lateral naves.

The grey areas are mainly located in the portion of the Cathedral coinciding with the location of the old Cathedrals. During the survey after the 2012 Emilia Earthquakes, new cracks appeared in the intrados of the main vaults. Moreover, an evolution of some existing cracks has been also observed (Figure 2.1.9).



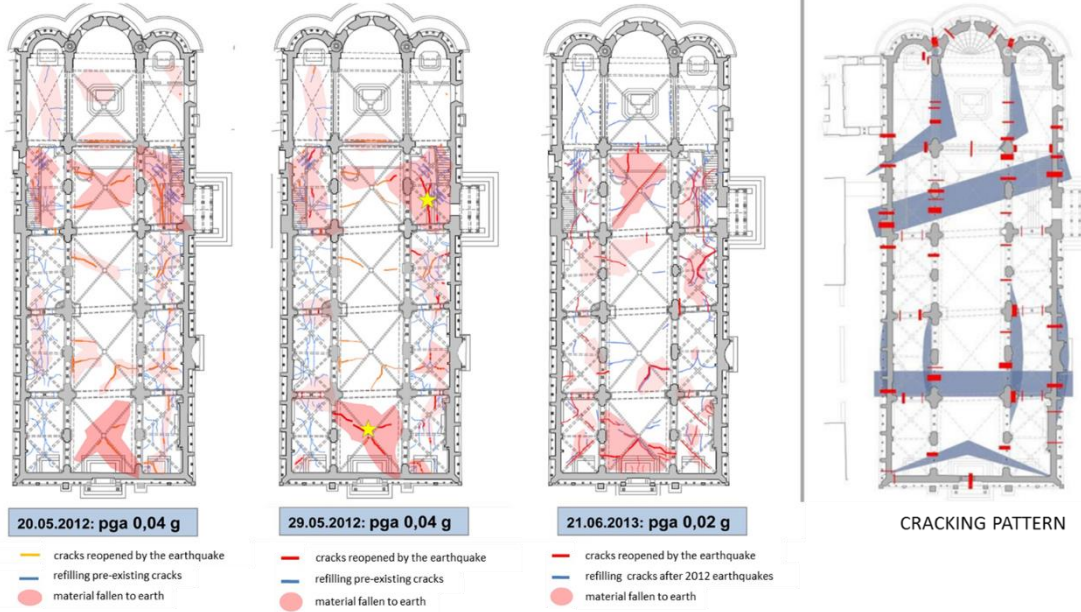
a)



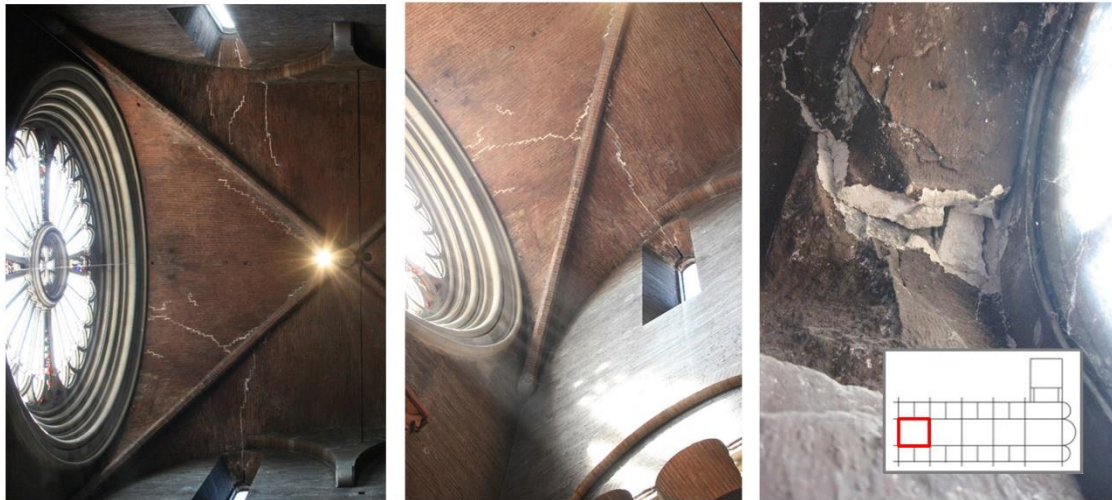
b)

Figure 2.1.8: (a) Crack pattern of the Cathedral of Modena and (b) main failure mechanisms of the Cathedral on the longitudinal and transverse direction

MAPS OF THE CRAKS DETECTED ON THE VAULTS-earthquakes of the 20, 29 may 2012 and 21 June 2013



a)



b)

Figure 2.1.9: (a) Maps of the cracks detected on the vaults after the earthquakes of the 20 and 29 May 2012 and 21 June 2013 and comparison with the crack pattern and (b) photographs on the damage caused by recent earthquakes.



1.3 Seismic Hazard analyses

The objective of the seismic hazard analysis is to compute, for a given site over a given observation time, the probability of exceeding any particular value of a specified ground motion parameter (commonly the Peak Ground Acceleration, PGA). In the case of monumental buildings, seismic hazard analysis does not allow only to predict the characteristics of possible future earthquakes, but also to obtain information on the characteristics of already occurred past earthquakes. The past seismic input has been studied through the reconstruction and the position of the historical earthquakes that have affected the Cathedral. This analysis allows to collect information useful for the identification of the historical periods of specific cracks and failures or interventions and for the reconstruction of the history of the building. The possible future seismic input has been studied through probabilistic and deterministic seismic hazard in order to identify the most probable earthquake scenarios which can shake the site of the monuments. Typical probabilistic seismic hazard analysis (as performed according to the approach suggested by Cornell) [63] assume that, in each point of the seismic zone area, the probability of occurrence of an earthquake is uniform. Thus, this approach is suitable for designing new buildings and for regional planning. However, it is not adequate for the identification of the seismic input to be adopted in the studies of monumental buildings, where the consequences of failure are intolerable and protection is needed against the worst that can be reasonably expected to occur. In these cases, the deterministic method is strongly recommended [64]. Two kinds of deterministic seismic hazard analyses have been performed for the site of the Cathedral of Modena:

- Historical Deterministic Seismic Hazard Analysis (HDSHA);
- Maximum Historical Earthquake Analysis (MHEA);

These analyses have been based on the following data: the ZS9 zoning (subdivision of the Italian Territory):

- the Cathedral of Modena is located in the zone 912 (<http://zonesismiche.mi.ingv.it/>);
- the CPTI04 earthquake catalogue (<http://emidius.mi.ingv.it/CPTI04/>);
- the Sabetta-Pugliese attenuation law [65];
- the Gutenberg-Richter recurrence law [66].



1.3.1 Historical Deterministic Seismic Hazard Analysis (HDSHA)

HDHSA has the objective to reconstruct the intensity of historical earthquakes that have actually affected the Cathedral of Modena in the past centuries. Significant historical earthquakes have been selected from the CPTI04 earthquake catalogue, through the following criteria:

- earthquakes that occurred within 20 km from the Cathedral;
- earthquakes characterised by the greater magnitude that occurred in the ZS9 seismogenetic zones near to the site of the Cathedral;
- significant earthquakes in relation to the historical information.

Table 2.1.1 shows these significant earthquakes of the past and the reconstruction of their Peak Ground Accelerations, in correspondence of the site of the Cathedral, as obtained using the Sabetta-Pugliese attenuation law. Based on the five past earthquakes with epicentre in Modena (4 earthquakes with epicentre in Modena respectively in the years 1249, 1474, 1660, 1850 and the earthquake of the Appennino Modenese of 1501), it can be stated that the cathedral might have been hit by accelerations around 0.15 g. The earthquake of 1249 was the most violent and might have rocked the Cathedral with an acceleration of approximately 0.20 g. Figure 2.1.10 shows the reconstruction of the median of the PGA, obtained considering the epistemic uncertainty associated to the Sabetta-Pugliese ground motion prediction model, for all earthquakes of the CPTI04 earthquake catalogue. Inspection of indicates that, looking at the past, the earthquake with acceleration between 0.15 g and 0.20 g is characterized by a return period of about 200-250 years.



Table 2.1.1- Reconstruction of peak Ground Acceleration (PGA) in correspondence of the site of the Cathedral of Modena for the selected earthquakes

| Selection criteria | N. | Year | Location Name | Seismogenetic zone (ZS9) | R [Km] (distance) | Msp (magnitude) | PGA mode | PGA median | PGA mean value | PGA percentile 80% |
|---|-----|---------|------------------|--------------------------|-------------------|-----------------|----------|------------|----------------|--------------------|
| Earthquakes that occurred within 20 km from the Cathedral | 53 | 124 | Modena | 912 | 0.65 | 4.80 | 0.20 | 0.245 | 0.27 | 0.360 |
| | 171 | 147 | Modena | 912 | 0.12 | 4.61 | 0.17 | 0.211 | 0.23 | 0.310 |
| | 195 | 150 | Appennino | 913 | 16.37 | 5.82 | 0.14 | 0.170 | 0.18 | 0.250 |
| | 279 | 158 | Spilambert | 913 | 10.86 | 4.53 | 0.07 | 0.083 | 0.09 | 0.120 |
| | 362 | 166 | Modena | 912 | 0.12 | 4.25 | 0.13 | 0.156 | 0.17 | 0.230 |
| | 374 | 167 | Rubiera | 912 | 14.26 | 5.23 | 0.10 | 0.117 | 0.12 | 0.170 |
| | 720 | 181 | Sassuolo | 913 | 23.49 | 5.09 | 0.05 | 0.066 | 0.07 | 0.100 |
| | 871 | 185 | Modena | 912 | 5.66 | 4.53 | 0.11 | 0.131 | 0.14 | 0.190 |
| | 984 | 187 | Reggiano | 913 | 25.29 | 4.93 | 0.04 | 0.053 | 0.05 | 0.080 |
| | 173 | 192 | Formigine | 913 | 15.20 | 5.05 | 0.08 | 0.095 | 0.10 | 0.140 |
| | 180 | 192 | Carpi | 912 | 17.83 | 4.54 | 0.04 | 0.054 | 0.05 | 0.080 |
| | 185 | 193 | Modenese | 913 | 15.80 | 4.54 | 0.05 | 0.060 | 0.06 | 0.090 |
| | 189 | 193 | Vignola | 913 | 19.38 | 4.06 | 0.03 | 0.033 | 0.03 | 0.060 |
| | 223 | 196 | Formigine | 913 | 9.21 | 4.09 | 0.05 | 0.065 | 0.07 | 0.100 |
| Earthquakes characterised by the greater magnitude that occurred in the ZS9 seismogenetic zones near to the site of the Cathedral | 393 | 168 | Romagna | 912 | 116.68 | 5.85 | 0.02 | 0.025 | 0.02 | 0.390 |
| | 30 | 111 | Veronese | 906 | 82.03 | 6.49 | 0.05 | 0.062 | 0.06 | 0.090 |
| | 776 | 182 | Valle dello | 911 | 209.68 | 5.55 | 0.01 | 0.011 | 0.01 | 0.050 |
| | 195 | 150 | Appennino | 913 | 16.37 | 5.82 | 0.14 | 0.170 | 0.18 | 0.250 |
| | 278 | 158 | Appennino | 914 | 147.54 | 5.99 | 0.02 | 0.023 | 0.02 | 0.230 |
| | 170 | 192 | Garfagnana | 915 | 88.64 | 6.48 | 0.05 | 0.057 | 0.06 | 0.090 |
| Significant earthquakes in relation to the historical information | 988 | 187 | Liguria | 916 | 73.43 | 5.47 | 0.02 | 0.029 | 0.03 | 0.060 |
| | 47 | 122 | Basso | 906 | 96.77 | 6.05 | 0.03 | 0.036 | 0.04 | 0.060 |
| | 202 | 150 | Bologna | 913 | 40.57 | 5.41 | 0.04 | 0.050 | 0.05 | 0.080 |
| | 149 | 190 | Bassa | 912 | 85.20 | 5.48 | 0.02 | 0.026 | 0.02 | 0.400 |
| | 168 | 191 | Mugello | 915 | 99.06 | 6.18 | 0.03 | 0.040 | 0.04 | 0.060 |
| | 250 | 199 | Correggio | 912 | 30.95 | 5.26 | 0.05 | 0.058 | 0.06 | 0.090 |
| | | 201 | Finale | 912 | 43.42 | 5.90 | 0.06 | 0.071 | 0.07 | 0.110 |
| | 201 | Medolla | 912 | 28.97 | 5.80 | 0.08 | 0.097 | 0.10 | 0.150 | |

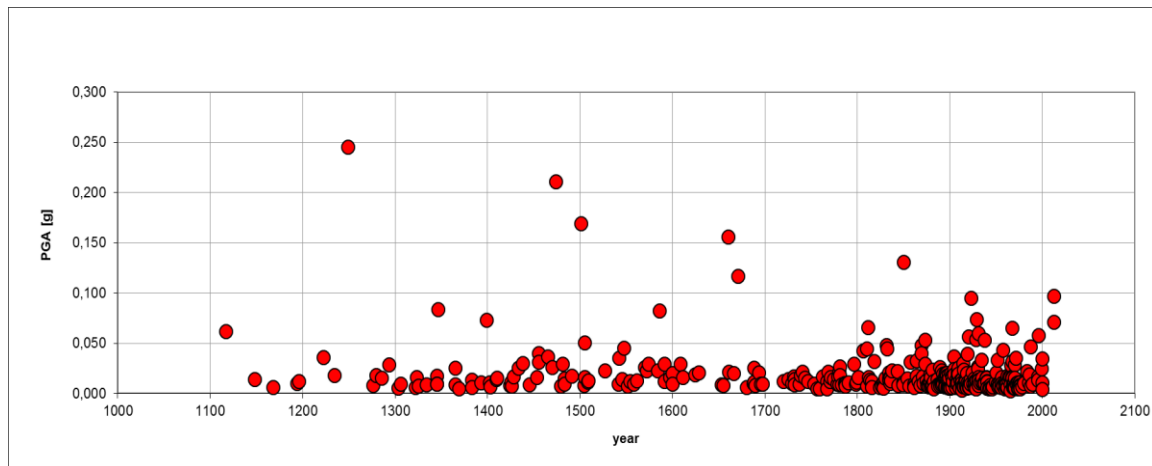


Figure 2.1.10: Reconstruction of the median of the PGA, obtained considering the epistemic uncertainty associated to the Sabetta-Pugliese ground motion prediction model, for all earthquakes of the CPTI04 earthquake catalogue.

1.3.2 Maximum Historical Earthquake Analysis (MHEA)

The MHEA is aimed at estimating the most violent earthquake that could occur in the future on the specific site of the Cathedral. The PGA recorded in a specific site during an earthquake depends on two factors: the magnitude and the distance between the epicentre and the site. Therefore, the worst seismic scenario for a specific site occurs with the combination of the high magnitude and null epicentre-site distance. The maximum magnitudes recorded in the past in the seismic zone (912) of the Cathedral and in the adjacent zones (913, 914, 915, 916, 911 and 906) were obtained from the earthquake catalogue. Then, it is assumed that earthquakes of such magnitudes could occur at zero distance from the Cathedral, and the intensity of the earthquake worse future is reconstructed considering the epistemic uncertainty associated to the Sabetta-Pugliese ground motion prediction model. Table 2.1.2 shows the list of the highest magnitudes occurred in all the considered zones and the reconstructed median, mode, mean values and 80% percentile values of the PGA variable. According to seismic activity of the two areas 912 and 913, it can be stated that a future earthquake with acceleration of about 0.50 g can occur, as shown in the Figure 2.1.11.

Table 1.1.2- Estimation, through MHEA, of the PGA that can occur in the future in the site of the Cathedral of Modena

| ZS zoning | Rmin from Cathedral | Mas max | Msp max | Mode | Median | Mean value | 80% percentile |
|-------------------------|---------------------|---------|---------|------|--------|------------|----------------|
| 912 (zone of Cathedral) | 0.00 | 5.85 | 5.85 | 0.49 | 0.60 | 0.65 | 0.87 |
| 913 | 2.96 | 5.82 | 5.82 | 0.41 | 0.50 | 0.55 | 0.73 |
| 914 | 67.50 | 5.99 | 5.99 | 0.04 | 0.05 | 0.05 | 0.08 |
| 915 | 54.67 | 6.48 | 6.48 | 0.08 | 0.09 | 0.10 | 0.14 |
| 916 | 75.48 | 5.32 | 5.47 | 0.02 | 0.03 | 0.03 | - |
| 911 | 99.35 | 5.55 | 5.55 | 0.02 | 0.02 | 0.03 | - |
| 906 | 72.12 | 6.49 | 6.49 | 0.06 | 0.07 | 0.08 | 0.11 |

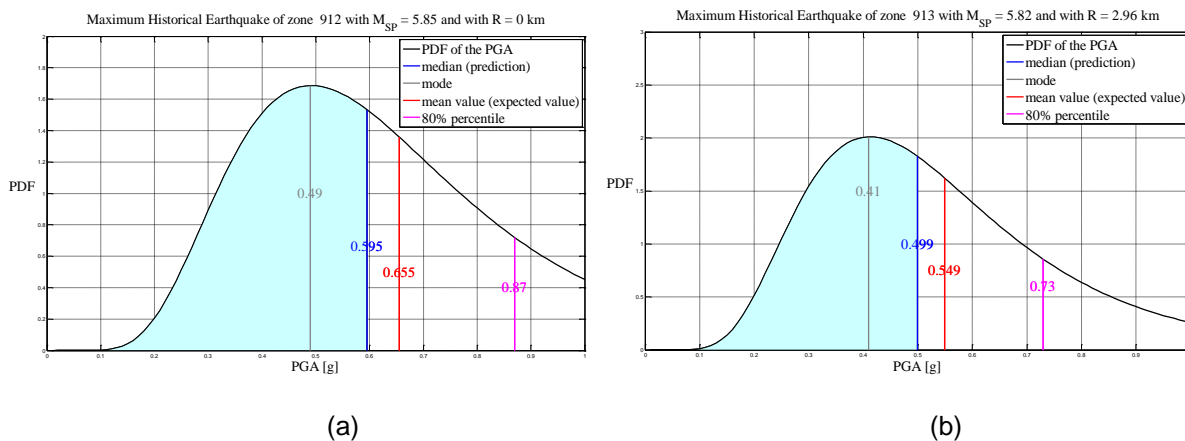


Figure 2.1.11: Probability density function (PDF) of the PGA in the site of the Cathedral of Modena as a result of seismic activity of zones: (a) zone 912, (b) zone 913.

1.3.3 The 2012 Emilia's earthquake

The 20th May 2012, at 02:03:53 (UTC), Emilia Romagna region (Northern Italy) was struck by an earthquake of magnitude $M=5.9$ (latitude 44.890 longitude 11.230). The main shock was preceded by a $M=4.1$ event on 19th May and followed on the 29th May 2012 by a 5.8Mw earthquake with epicentre 15km North West of the former event (Figure 2.1.12a). Several events with magnitude $4.0 \leq M_l \leq 4.5$, plus several other minor earthquakes, occurred in the same area the following days, as reported in Italian Instrumental and Parametric Data-Base (ISIDe),[67]. As reported, this earthquake sequence has caused a lot of damage / collapse in the monumental building, including the Cathedral of Modena. The cathedral has been considered, first, as a model of itself with the purpose of understanding its intrinsic structural behaviour. For this reason, the strong motions of the main shock recorded by the station of Modena (code MDN) have been used in some of the next analyses

developed on the Cathedral. The localization of the recording station MDN is reported in Figure 2.1.12.

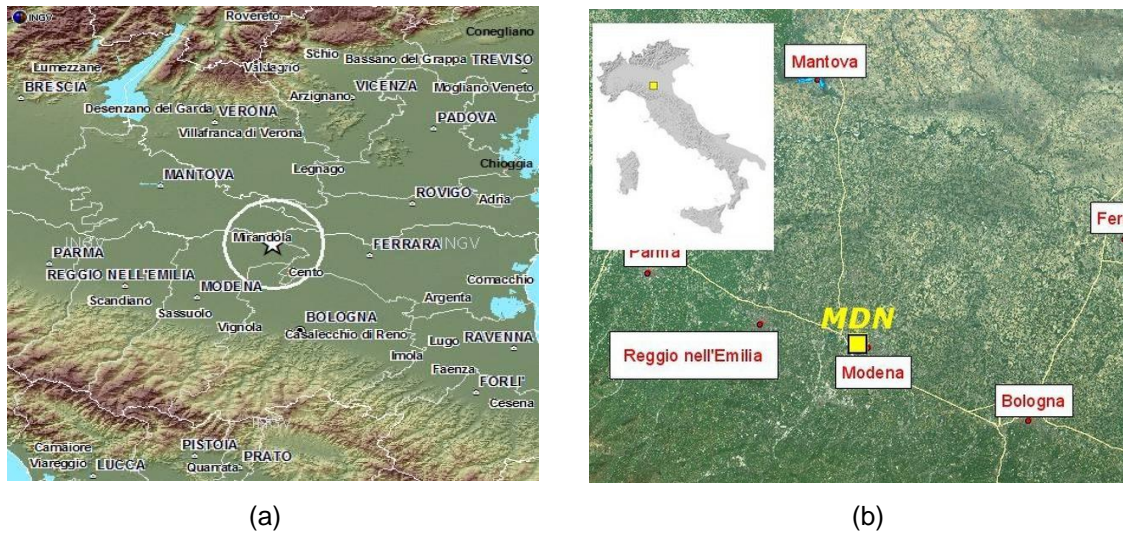
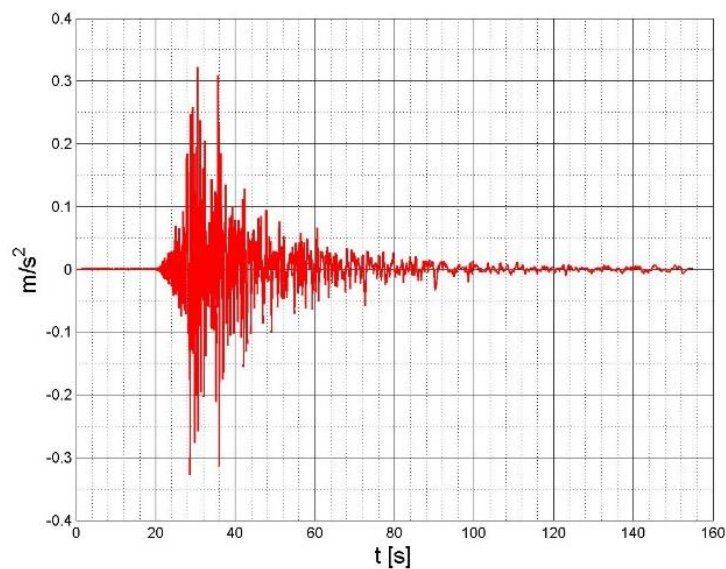
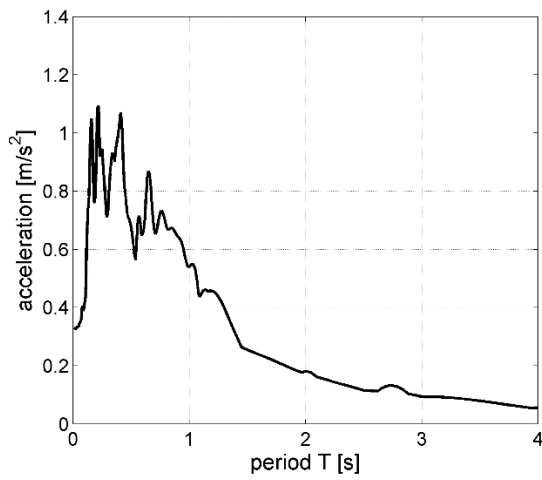


Figure 2.1.12 (a) Location of epicentre of May 29th earthquake (INGV), (b) Localization maps of the recording station in Modena (MND)

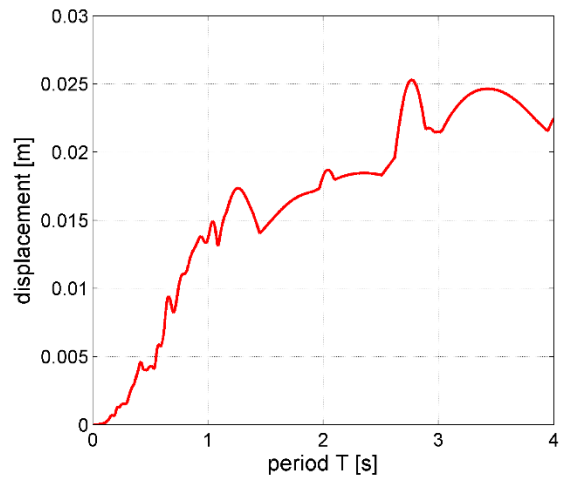
Figure 2.1.13 display the acceleration as recorded by MDN station during the main shock of 20th May and used in the dynamic analyses of the Cathedral and the corresponding spectral acceleration and the spectral displacement.



(a)



(b)



(c)

Figure 2.1.13: (a) The acceleration recorded by the station MDN during the main shock of 20th May 2012, (b) the corresponding spectral acceleration and (c) the corresponding spectral displacement



1.4 Flood hazard assessment

1.4.1 Pluvial flooding closet o Modena Cathedral: results for the entire square

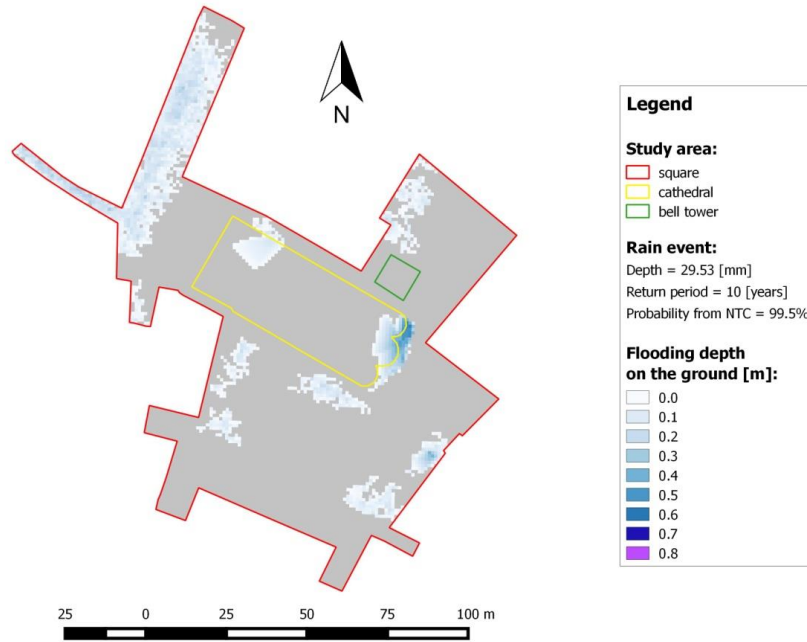


Figure 2.1.14- Maximum flooding depth on the ground for a precipitation depth equal to 29.53 mm.

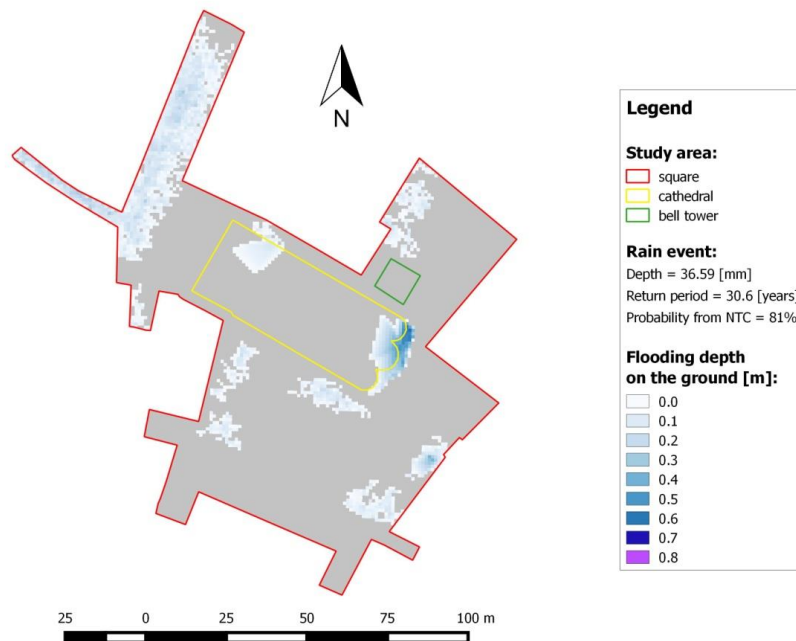


Figure 2.1.15- Maximum flooding depth on the ground for a precipitation depth equal to 36.59 mm.

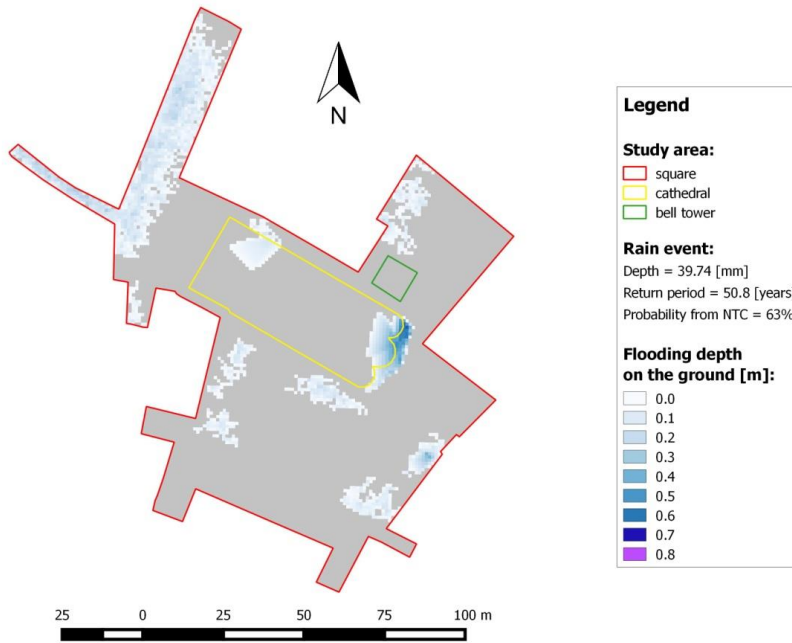


Figure 2.1.16- Maximum flooding depth on the ground for a precipitation depth equal to 39.74 mm.

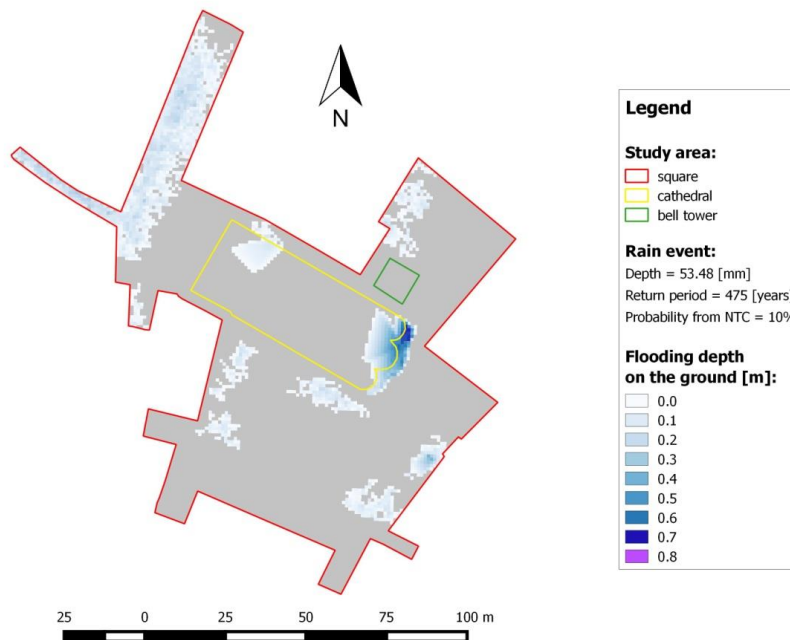


Figure 2.1.17- Maximum flooding depth on the ground for a precipitation depth equal to 53.48 mm.

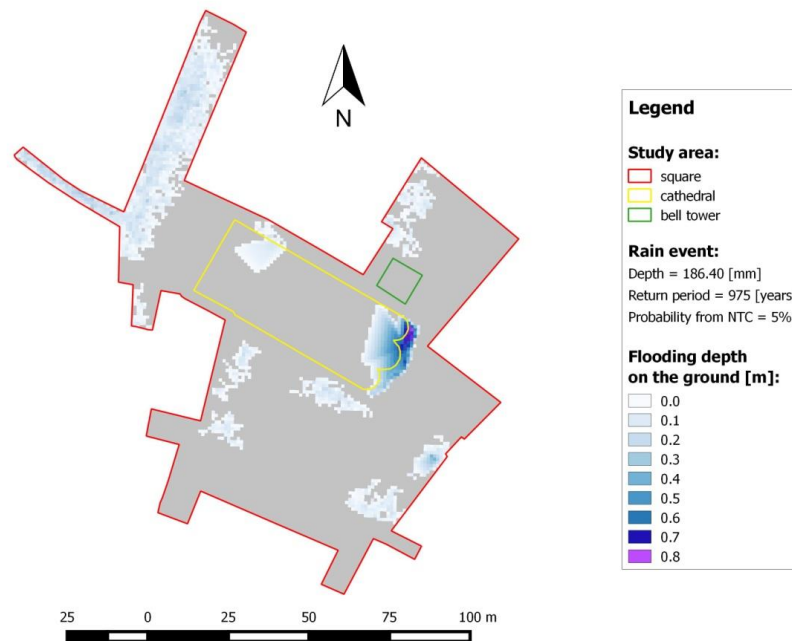


Figure 2.1.18- Maximum flooding depth on the ground for a precipitation depth equal to 186.40 mm.

Figure 2.1.15 shows the maximum flooding depths [m] for a rainfall event with a depth equal to 36.59 mm and a return period of 30.6 years. As represented in the image, in the 80% of cases, the flooding depths on the ground are in the range 0 - 14 cm. The average flooding depth on the ground is 8.9 cm. Only locally, in topographically depressed areas, these depths can reach values 61 cm.

Figure 2.1.16 shows the maximum flooding depths [m] for a rainfall event with a depth equal to 36.59 mm and a return period of 30.6 years. As represented in the image, in the 80% of cases, the flooding depths on the ground are in the range 0 - 14 cm. The average flooding depth on the ground is 8.9 cm. Only locally, in topographically depressed areas, these depths can reach values 61 cm.

shows the maximum flooding depths [m] for a rainfall event with a depth equal to 39.74 mm and a return period of 50.8 years. As represented in the image, in the 80% of cases, the flooding depths on the ground are in the range 0 - 14 cm. The average flooding depth on the ground is 9.0 cm. Only locally, in topographically depressed areas, these depths can reach values 63 cm.

Figure 2.1.17 shows the maximum flooding depths [m] for a rainfall event with a depth equal to 36.59 mm and a return period of 30.6 years. As represented in the image, in the 80% of cases, the flooding depths on the ground are in the range 0 - 14 cm. The average flooding depth on the ground is 8.9 cm. Only locally, in topographically depressed areas, these depths can reach values 61 cm.

shows the maximum flooding depths [m] for a rainfall event with a depth equal to 53.48 mm and a return period of 475 years. As represented in the image, in the 80% of cases, the flooding depths on



the ground are in the range 0 - 14 cm. The average flooding depth on the ground is 9.8 cm. Only locally, in topographically depressed areas, these depths can reach values 71 cm.

Figure 2.1.18 shows the maximum flooding depths [m] for a rainfall event with a depth equal to 36.59 mm and a return period of 30.6 years. As represented in the image, in the 80% of cases, the flooding depths on the ground are in the range 0 - 14 cm. The average flooding depth on the ground is 8.9 cm. Only locally, in topographically depressed areas, these depths can reach values 61 cm.

shows the maximum flooding depths [m] for a rainfall event with a depth equal to 186.40 mm and a return period of 975 years. As represented in the image, in the 80% of cases, the flooding depths on the ground are in the range 0 - 15 cm. The average flooding depth on the ground is 10.6 cm. Only locally, in topographically depressed areas, these depths can reach values 79 cm.

When comparing the results, a substantial invariance of the flooded areas emerges. This result is due to the fact that the HFS methodology assume a flooding condition only in the local depressions within the study area. The excess water volume is transferred to other depressions located further downstream, which are external to the study area.

Table 2.1.3 shows non-exceedance the probabilities relate to the maximum flooding depths (a spatially averaged value is reported) for the analysis performed by considering the entire square close to Modena Cathedral.

| 1-P (NTC) [%] | Maximum flooding depth on the ground (spatial average) [m] |
|------------------------------|---|
| 0.5 | 0.086 |
| 19 | 0.089 |
| 37 | 0.090 |
| 90 | 0.098 |
| 95 | 0.106 |

Table 2.1.3 Non-exceedance probabilities related to the maximum flooding depths for the analysis performer by considering the entire square closet to Modena Cathedral.

The same values are shown in Figure 2.1.19.

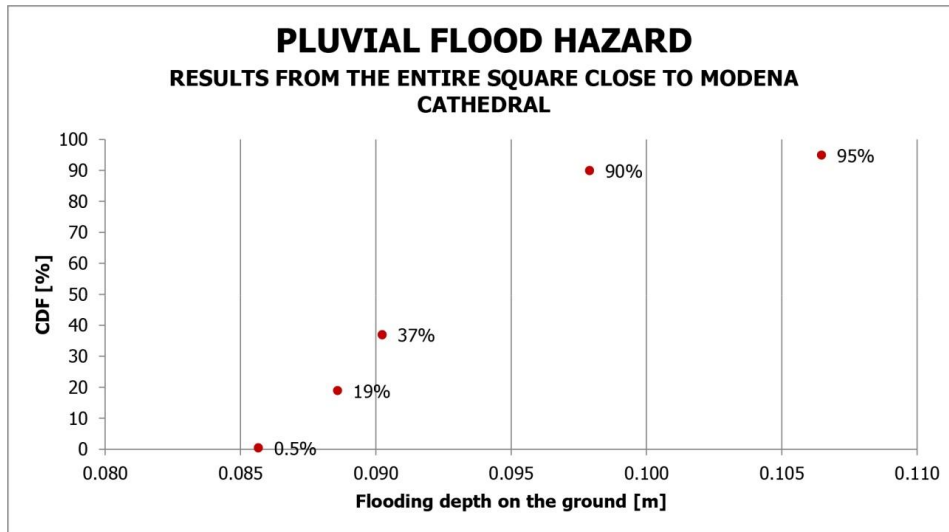


Figure 2.1.19 - Non-exceedance probabilities related to the maximum flooding depths for the analysis performed by considering the entire square close to Modena Cathedral.

1.4.2 Pluvial flooding closet o Modena Cathedral: results for the Cathedral (inside and outside)

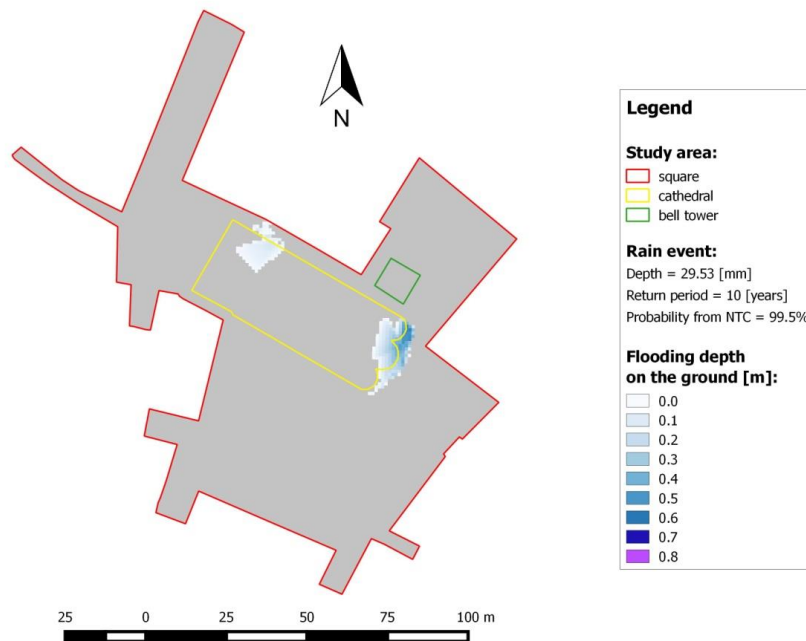


Figure 2.1.20- Maximum flooding depth on the ground for a precipitation depth equal to 29.53 mm.

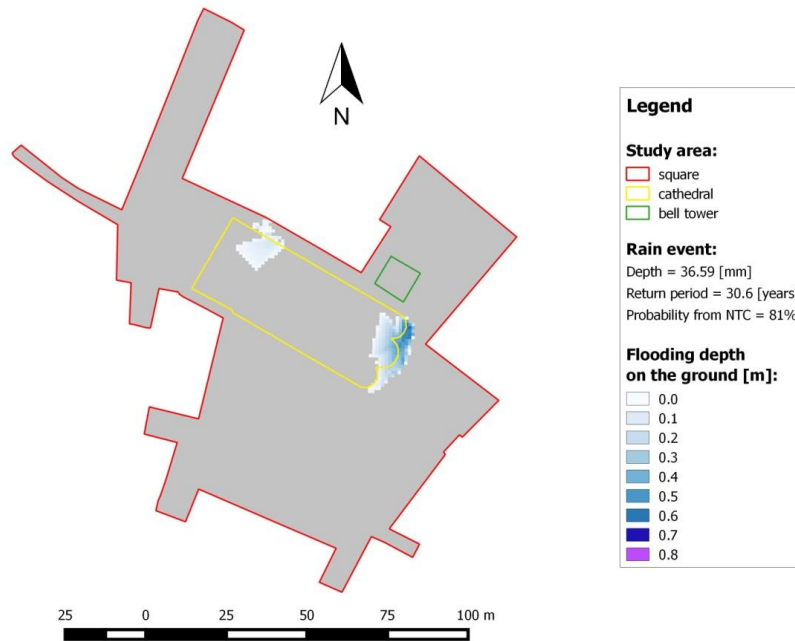


Figure 2.1.21- Maximum flooding depth on the ground for a precipitation depth equal to 36.59 mm.



Figure 2.1.22- Maximum flooding depth on the ground for a precipitation depth equal to 39.74 mm.

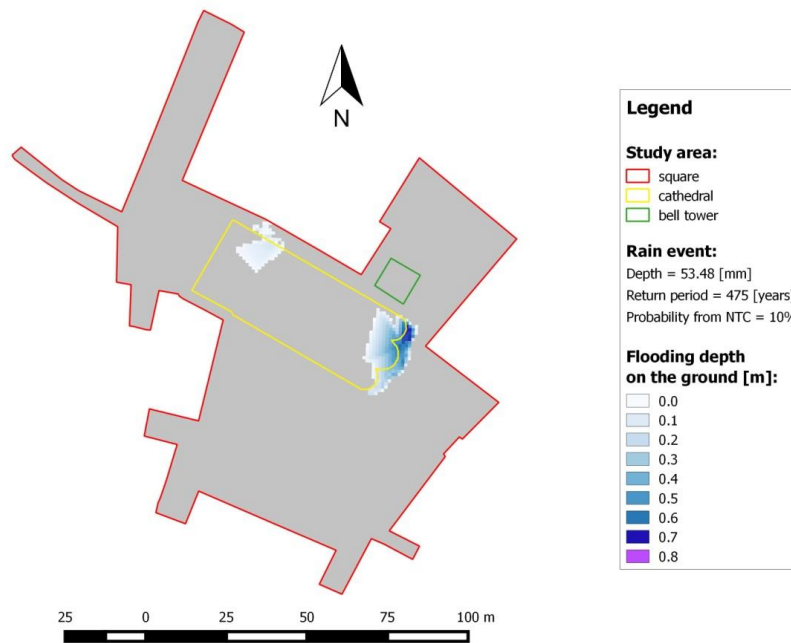


Figure 2.1.23- Maximum flooding depth on the ground for a precipitation depth equal to 53.48 mm.

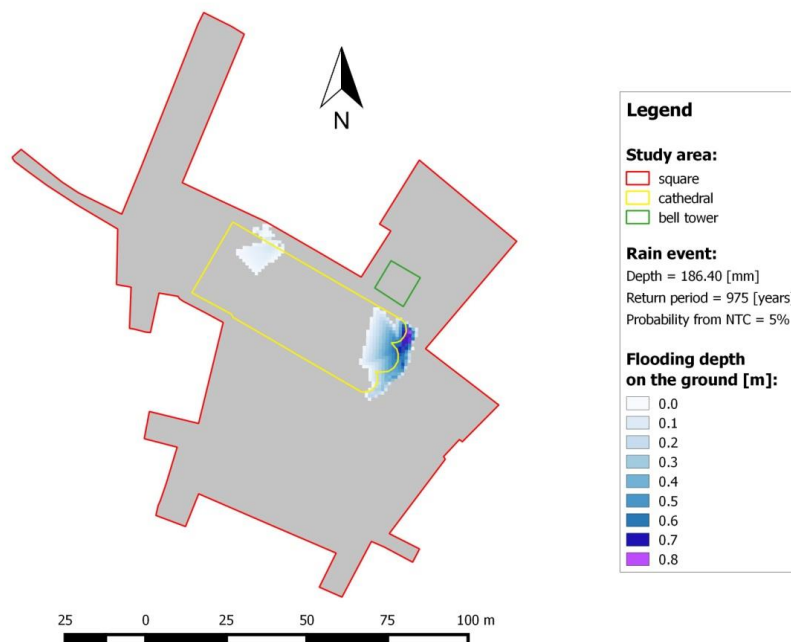


Figure 2.1.24- Maximum flooding depth on the ground for a precipitation depth equal to 186.40 mm.



Figure 2.1.20 shows the maximum flooding depths [m] for a rainfall event with a depth equal to 29.53 mm and a return period of 10 years. As represented in the image, in the 80% of cases, the flooding depths on the ground are in the range 0 – 29.1 cm. The average flooding depth on the ground is 15.2 cm. Only locally, in topographically depressed areas, these depths can reach values 57 cm.

Figure 2.1.21 shows the maximum flooding depths [m] for a rainfall event with a depth equal to 36.59 mm and a return period of 30.6 years. As represented in the image, in the 80% of cases, the flooding depths on the ground are in the range 0 – 32.1 cm. The average flooding depth on the ground is 16.7 cm. Only locally, in topographically depressed areas, these depths can reach values 61 cm.

Figure 2.1.22 shows the maximum flooding depths [m] for a rainfall event with a depth equal to 39.74 mm and a return period of 50.8 years. As represented in the image, in the 80% of cases, the flooding depths on the ground are in the range 0 – 42.1 cm. The average flooding depth on the ground is 17.4 cm. Only locally, in topographically depressed areas, these depths can reach values 63 cm.

Figure 2.1.23 shows the maximum flooding depths [m] for a rainfall event with a depth equal to 53.48 mm and a return period of 475 years. As represented in the image, in the 80% of cases, the flooding depths on the ground are in the range 0 – 39.1 cm. The average flooding depth on the ground is 20.4 cm. Only locally, in topographically depressed areas, these depths can reach values 71 cm.

Figure 2.1.24 shows the maximum flooding depths [m] for a rainfall event with a depth equal to 186.40 mm and a return period of 975 years. As represented in the image, in the 80% of cases, the flooding depths on the ground are in the range 0 – 45.1 cm. The average flooding depth on the ground is 23.9 cm. Only locally, in topographically depressed areas, these depths can reach values 79 cm.

When comparing the results, a substantial invariance of the flooded areas emerges. This result is due to the fact that the HFS methodology assume a flooding condition only in the local depressions within the study area. The excess water volume is transferred to other depressions located further downstream, which are external to the study area.

Table 2.1.4 shows non-exceedance the probabilities relate to the maximum flooding depths (a spatially averaged value is reported) for the analysis performed by considering the area inside and outside to Modena Cathedral.



Table 2.1.4 Non-exceedance probabilities related to the maximum flooding depths for the analysis performed by considering the area inside and outside to Modena Cathedral.

| 1-P (NTC) [%] | Maximum flooding depth on the ground (spatial average) [m] |
|---------------------|---|
| 0.5 | 0.152 |
| 19 | 0.167 |
| 37 | 0.174 |
| 90 | 0.204 |
| 95 | 0.239 |

The same values are shown in Figure 2.1.24.

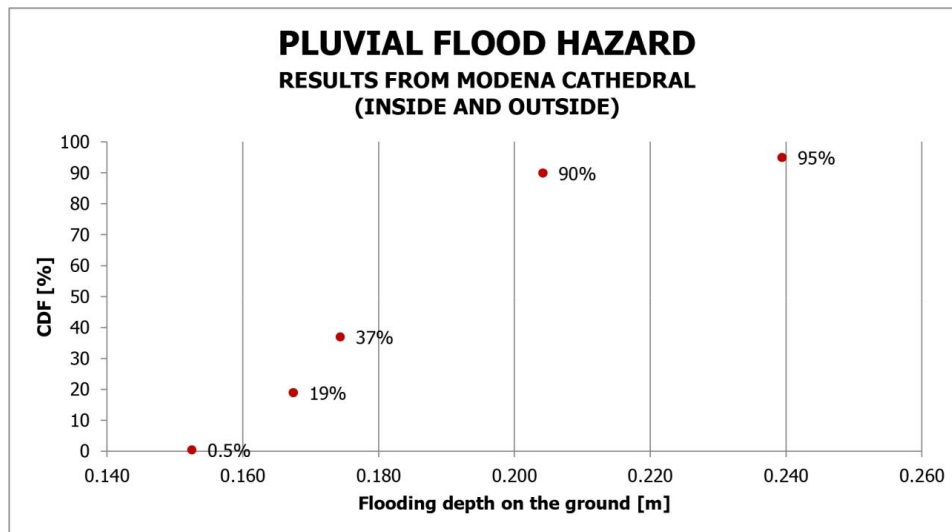


Figure 2.1.24 - Non-exceedance probabilities related to the maximum flooding depths for the analysis performed by considering the area inside and outside to Modena Cathedral

1.4.1. Pluvial flooding closet o Modena Cathedral: results for the Cathedral (only inside)



Figure 2.1.25 - Maximum flooding depth on the ground for a precipitation depth equal to 29.53 mm.

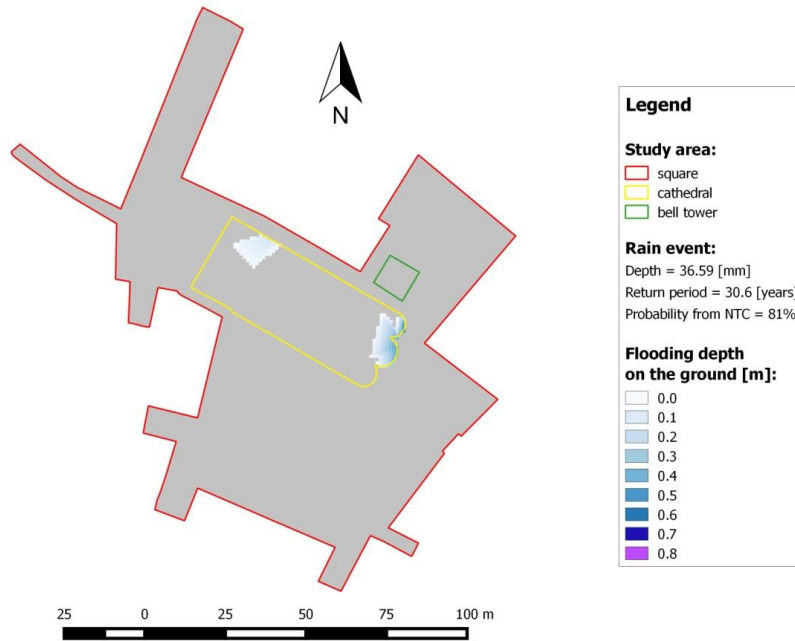


Figure 2.1.26- Maximum flooding depth on the ground for a precipitation depth equal to 36.59 mm.

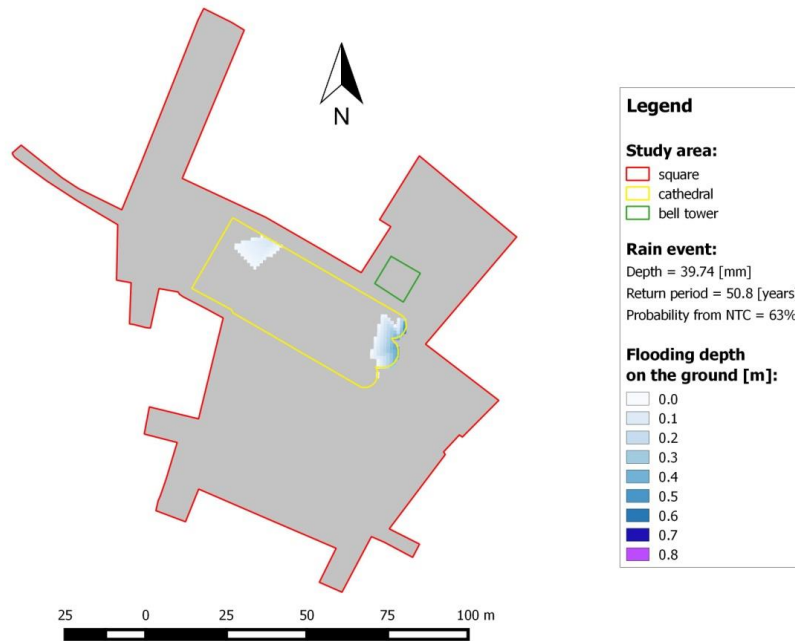


Figure 2.1.27 - Maximum flooding depth on the ground for a precipitation depth equal to 39.74 mm.



Figure 2.1.28 - Maximum flooding depth on the ground for a precipitation depth equal to 53.48 mm.



Figure 2.1.29 - Maximum flooding depth on the ground for a precipitation depth equal to 186.40 mm.

Figure 2.1.25 shows the maximum flooding depths [m] for a rainfall event with a depth equal to 29.53 mm and a return period of 10 years. As represented in the image, in the 80% of cases, the flooding depths on the ground are in the range 0 – 26.1 cm. The average flooding depth on the ground is 11.8 cm. Only locally, in topographically depressed areas, these depths can reach values 49.1 cm.

Figure 2.1.26 shows the maximum flooding depths [m] for a rainfall event with a depth equal to 36.59 mm and a return period of 30.6 years. As represented in the image, in the 80% of cases, the flooding depths on the ground are in the range 0 – 27.1 cm. The average flooding depth on the ground is 13.4 cm. Only locally, in topographically depressed areas, these depths can reach values 53.1 cm.

Figure 2.1.27 shows the maximum flooding depths [m] for a rainfall event with a depth equal to 39.74 mm and a return period of 50.8 years. As represented in the image, in the 80% of cases, the flooding depths on the ground are in the range 0 – 27.0 cm. The average flooding depth on the ground is 14.6 cm. Only locally, in topographically depressed areas, these depths can reach values 55.1 cm.

Figure 2.1.28 shows the maximum flooding depths [m] for a rainfall event with a depth equal to 53.48 mm and a return period of 475 years. As represented in the image, in the 80% of cases, the flooding depths on the ground are in the range 0 – 31.1 cm. The average flooding depth on the ground is 16.5 cm. Only locally, in topographically depressed areas, these depths can reach values 63.1 cm.

Figure 2.1.29 shows the maximum flooding depths [m] for a rainfall event with a depth equal to 186.40 mm and a return period of 975 years. As represented in the image, in the 80% of cases, the



flooding depths on the ground are in the range 0 – 39.1 cm. The average flooding depth on the ground is 19.4 cm. Only locally, in topographically depressed areas, these depths can reach values 71.1 cm.

When comparing the results, a substantial invariance of the flooded areas emerges. This result is due to the fact that the HFS methodology assume a flooding condition only in the local depressions within the study area. The excess water volume is transferred to other depressions located further downstream, which are external to the study area.

Table 2.1.5 shows non-exceedance the probabilities relate to the maximum flooding depths (a spatially averaged value is reported) for the analysis performed by considering the area only inside to Modena Cathedral.

Table 2.1.5 Non-exceedance probabilities related to the maximum flooding depths for the analysis performer by considering the area only inside to Modena Cathedral.

| 1-P (NTC) [%] | Maximum flooding depth on the ground (spatial average) [m] |
|------------------------------|---|
| 0.5 | 0.118 |
| 19 | 0.134 |
| 37 | 0.146 |
| 90 | 0.165 |
| 95 | 0.194 |

The same values are shown in Figure 2.1.30.

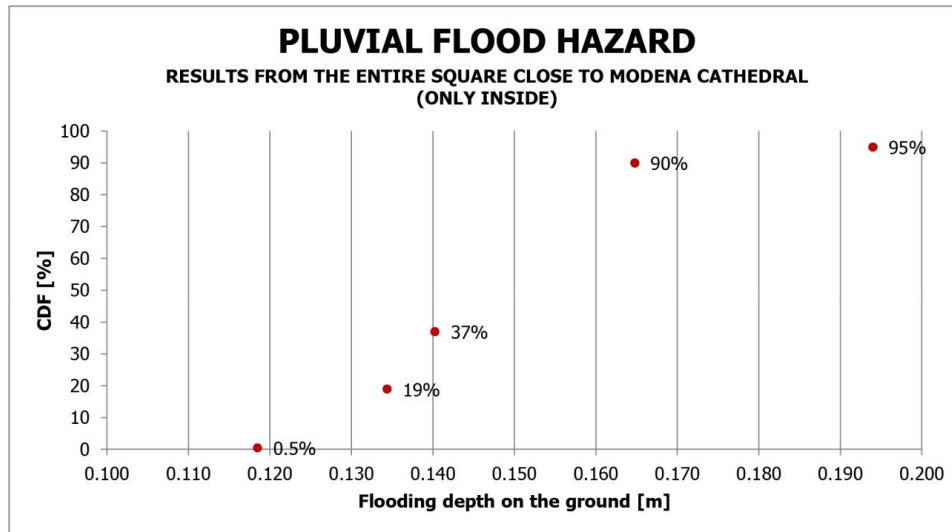


Figure 2.1.30 - Non-exceedance probabilities related to the maximum flooding depths for the analysis performed by considering the area only inside to Modena Cathedral



1.5 Concluding remarks

The integrated knowledge of a monument is the first step to develop consistent risk analyses and, thus, to evaluate correctly its structural health and reliability. The knowledge process developed for the cathedral highlighted the important role played by the following aspects

- the presence of previous Cathedrals that gave rise to uneven settlements of the actual one, due to the influence of soil behaviour as a “material with memory”;
- the construction phases; and
- the interaction with the Ghirlandina Tower.
- assessment of main natural hazards

These aspects strongly influence the structural behaviour of the cathedral and must to be considered in the structural analyses. Moreover, the seismic hazard analyses allowed reconstructing the intensity of the earthquakes that occurred on the cathedral in the past. Historical Deterministic Seismic Hazard Analysis has highlighted that four important earthquakes (peak ground acceleration around 0.15 and 0.25g) and 20 earthquakes of medium intensity (peak ground acceleration around 0.05 g e 0.10) have hit the cathedral during its life. The comparison with the historical evidence revealed that for the important earthquakes the Cathedral has reported consistent damages, which interested particularly the vaults and slender pinnacles. For earthquakes of medium-low intensity (as the 2012 earthquake) slight damages have been detected always mainly on the vaults and slender pinnacles.



2 Structural assessment and seismic vulnerability

2.1 Global structural behaviour

2.1.1 Introduction

The information obtained from the integrated knowledge have been used to study the global structural behaviour of the cathedral, i.e. recognize the structural elements and the actual load paths, to identify the materials properties and the appropriate restraint at the base. Different analyses (simple, but more reliable limit schematizations, and more complex, but too much sensitive to uncertainties, computer-based models) have been conducted on the global structure of the masonry fabric in order to identify the main static and seismic vulnerabilities.

2.1.2 The models and the simulations

The static behaviour of the cathedral has been investigated through simple limit schematizations and Finite Element models of increasing complexity (2D models, 3D models with fixed base, 3D models accounting for the soil-structure interaction). Due to the complexity of the monument and the relevant influence of different factors (such as construction phases, soil properties, existing cracks, interaction with the Tower), instead of a unique 3D FE model in which all factors are simultaneously taken into account, several specific 3D FE models have been performed to separately investigate, the effects of each single factor. The results of the static analyses as obtained from FE models, validated through the simple static analyses performed on the substructures, have been used to interpret the cracking patterns as obtained from in situ surveys and the deformations related to changes in the geometrical configuration as obtained from the topographic survey. In addition, on the 3D FE model able to better represent the static behaviour of the cathedral various seismic analyses have been carried out in order to assess its seismic vulnerabilities. The analyses developed are summarized in Table 2.2.1.

Table2.2.1- The different analyses developed

| Model-Element | Analysis |
|---|-----------------|
| Hand –made schematization of the roof system | Static analysis |
| Hand –made schematization of the main vertical elements | Static analysis |
| 2D FEM model of the vertical elements | Static analysis |

| | |
|---|--|
| 3D FEM models with different restraint at the base and load cases | Static analysis |
| 3D FEM models | Natural frequency analysis |
| 3D FEM models-input consistent with the SHA §1.3 | Response spectrum, time history analysis |
| 3D FEM models-input recorded during the 2012 earthquake§1.3.3 | Time history analysis |

2.1.3 Static analyses

2.1.3.1 The applied loads/actions

The effect of the gravity loads (also considering thermal effects) have been considered in the structural static analysis. The assessment of the monument against the other possible environmental loads is out of the scope of the present work. The vertical load due to snow has been estimated equal to 1.20 kN/m² according to the Italian building code (NTC 2008). In addition to the above described loads also the interaction between the Cathedral and the adjacent Ghirlandina Tower has been accounted for (even if, at this stage, in a rather simple way) by imposing a profile of differential vertical displacements at the base of the Cathedral, as provided by the geotechnical studies mentioned in §1.2.2. In detail, the differential displacements have been imposed in the portion closest to the Ghirlandina Tower (Figure 2.2.1), the vertical displacements being equal to 20 cm at corner H, 27 cm at corner G, and 30 cm at corner F. Linear variations of vertical imposed displacements have been assumed between the above mentioned points, as well as moving from the side to the center of the Cathedral.

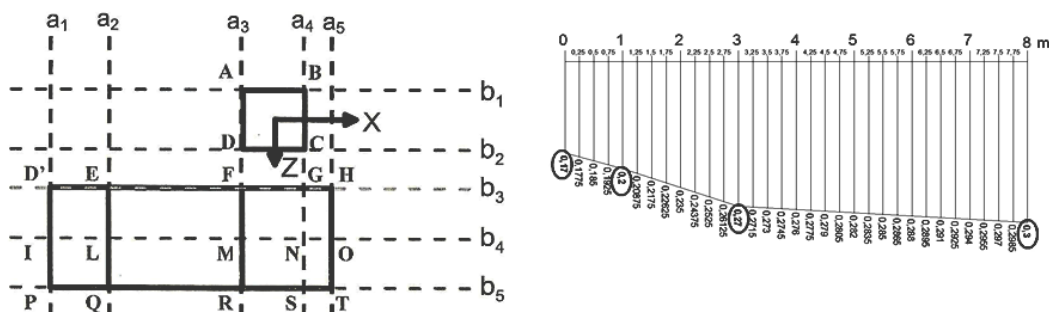


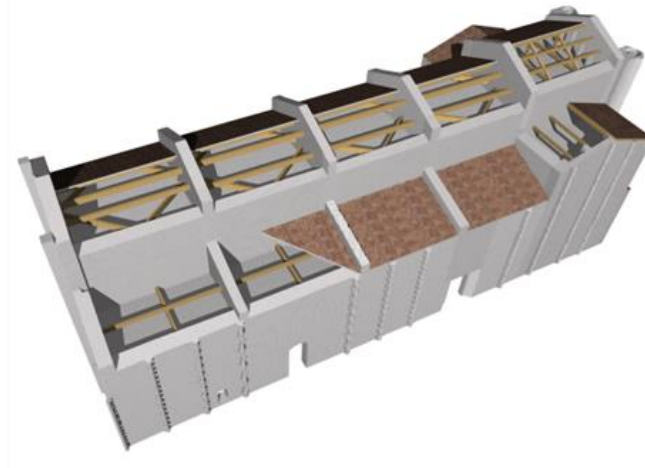
Figure 2.2.1: Imposed vertical differential displacements at the base due to the interaction between the Cathedral and the Ghirlandina Tower

2.1.4 Structural analysis with simple models

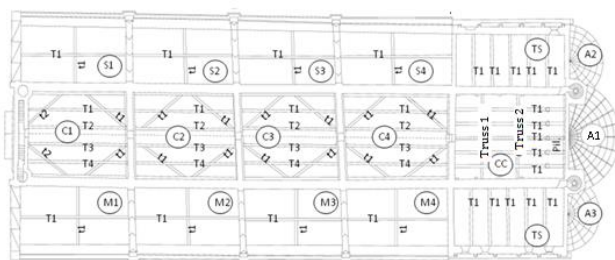
Simple limit schematizations have been developed for a preliminary structural analysis of the roof system and the main vertical resisting elements (i.e. walls and stone piers). Each substructure is analyzed with the purpose of obtaining the stress state of the main structural elements.

2.1.4.1 The roof system

The roof (Figure 2.2.2) is made of timber principal beams arranged in the longitudinal direction (indicated as T_i), which find additional supports on underlying timber beams or timber trusses - "capriate" - (indicated as t_i). The roof system, transferring the gravity loads directly to the masonry walls and stone piers, is covered by thin-masonry non-structural vaults withstanding only their self-weight. It should be noted that the increment of loads (both vertical loads and thrusts) due to the presence of the vaults is negligible.



a)



a)



b)

Figure 2.2.2: a) A 3D view of the roof system; b) Structural roof elements and c) Main beams (T_i) and trusses system (t_i)

Making use of this geometry, a simple static analysis has been performed of the roof system solely in order to evaluate the stress levels and the reactions at the base of the roof (which are then applied as loads on the masonry walls). The maximum normal stresses for the main timber beams due to self-weight only are about 5 MPa for the beams of central nave, 8 MPa for the beams in the transept, 10 MPa for the beams of the aisles. The addition of the snow load lead to an increase in the maximum stresses of about 35% leading to stresses close to the material strengths. In detail, Figure 2.2.3 shows the stress levels (in a color scale) of the roof beams. The stress levels in the secondary elements (trusses) are about 1 and 1.5 MPa, well below the material strengths. It is worth to note that, due to the absence of specific tests performed on the wood elements, the assumed strength is conservative.

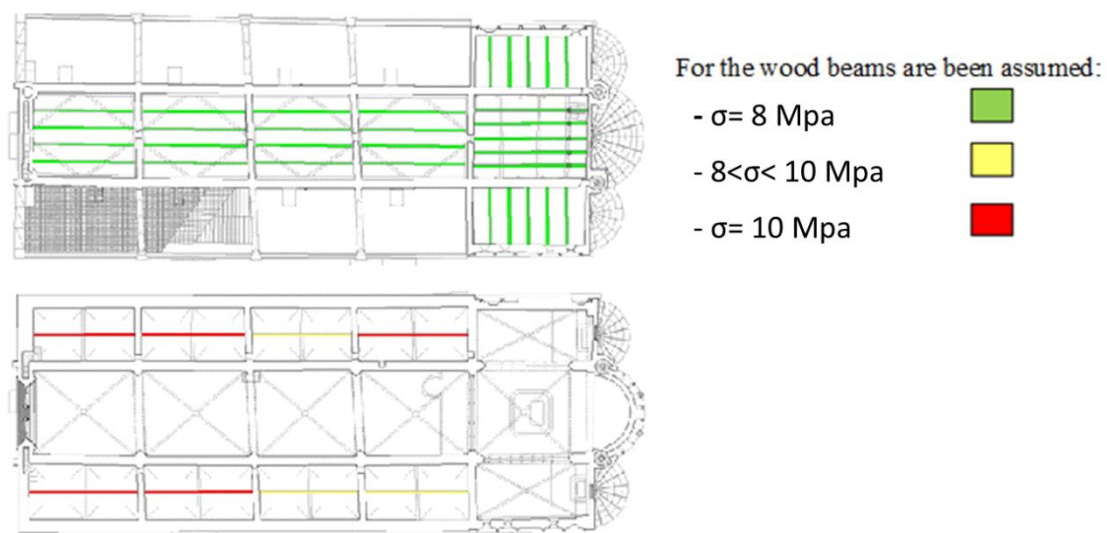


Figure 2.2.3: Stress level of the roof elements

2.1.4.2 The vertical resisting elements

The vertical resisting elements of the Cathedral are the masonry walls, the masonry piers and the stone columns. The masonry elements are characterised by non-uniform geometry (variations in thickness) and non-uniform mechanical properties. These discontinuities may lead to significant stress concentrations, and, in order to account for the presence of these geometrical discontinuities, in addition to homogeneous regular hand-made schematization, 2D FE models of each single wall have been also developed, assuming an ideal vertical configuration. These planar models are used to develop in-plane analysis aimed at evaluating the stress levels in the walls.

The hand-made schematizations of the single walls are used to calculate the stresses at the wall base, according to the Navier - de Saint Venant formulation, due to the self-weight, the weight of the vaults and the reactions of the roof system. In detail, the following assumptions have been made: (i) two limiting conditions: full cross-section and hollow cross-section (or “a sacco”, i.e. two exterior masonry layers plus an interior layer composed of chaotic stones and filling materials; in the “a-sacco” configuration the wall inertia is equal to the inertia of the two exterior layers only); (ii) constant wall thickness equal to the average wall thickness; (iii) the presence of decorative elements has been neglected; (iv) each wall has been subdivided into homogeneous portions (i.e. same cross-section, referred to as a_i , $i=1, \dots, 28$) for the evaluation of the normal average stresses at the base, (iv) perfect verticality of the masonry walls. In the limiting case of full cross-section, the normal stresses due to the gravity loads are between 0.3 and 0.8 MPa for exterior walls and between 1 and 1.4 MPa for masonry piers. On the other hand, in the limiting case of hollow cross-section (“a sacco” masonry), the normal stresses due to the gravity loads double both for the external walls and the internal piers. The maximum stress at the base of the stone columns is around 3.2 MPa. The increase due to the snow load is about 2.5% of the stresses due to gravity load. These stresses levels at the walls base obtained from simple hand-made models (Figure 2.2.4) have then been compared with those obtained from the 2D FE models, which are reported in terms of contour maps in Figure 2.2.5. This comparison indicates a good agreement between the two analyses.

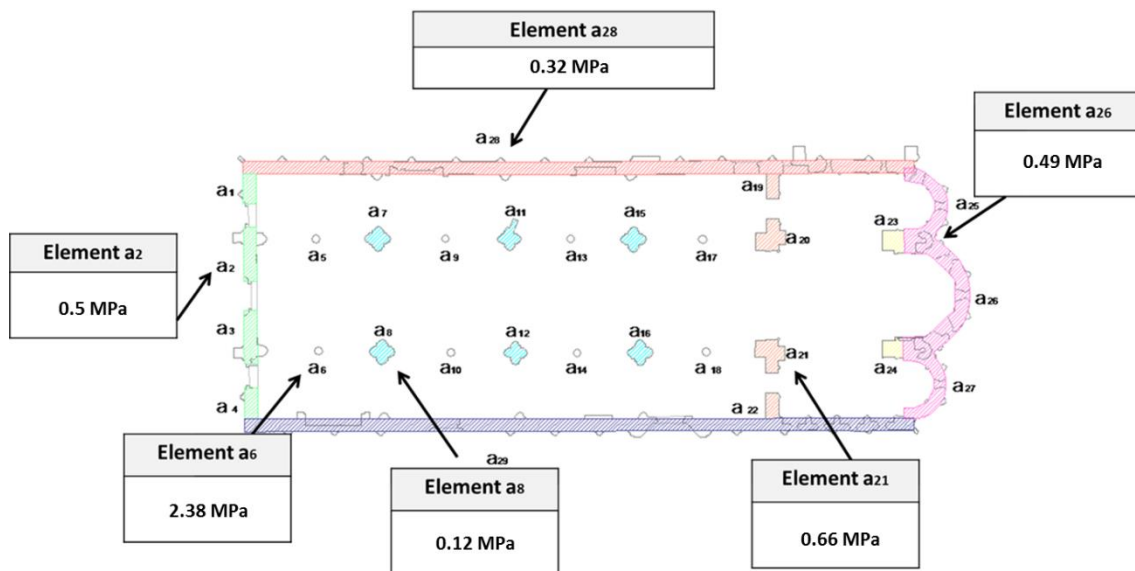


Figure 2.2.4: Reference values of the stress level at the base of the principal structural elements.

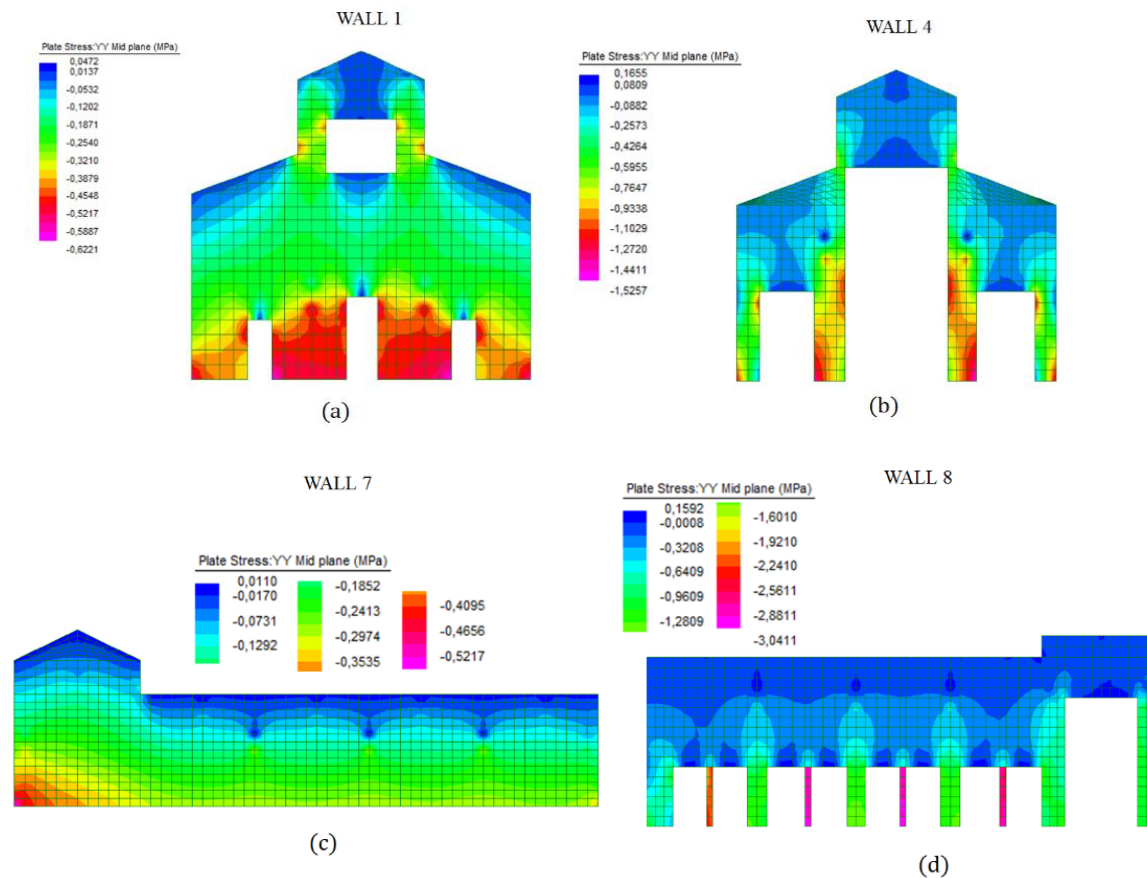


Figure 2.2.5: Contour maps of the normal stresses at the base of some walls obtained with two-dimensional FE models: (a) Wall 1; (b) Wall 4; (c) Wall 7; (d) Wall 8;

The 3D laser scanning showed significant inclinations of the longitudinal walls. Consequently, the walls are subjected to additional stresses due to the imperfect verticality. To account for this effect in a rather simplified way, the second order bending moments due to the eccentricity corresponding to the measured overhangs (Figure 2.2.6) have been included in the evaluation of the stresses. Figure 2.2.7 provides a schematic plan indicating the percentage increment of the normal stresses at the base of the walls and pillars due to their inclination (values are evaluated with reference to the hand-made models). The green color represents increments below 30%, the yellow color represents increments between 30% and 70%, while the red color represents increments larger than 70%. The ranges of the normal stresses at the base of the masonry walls and pillars, including also the effect of walls inclinations, are provided in the plan schematization displayed in Figure 20. Maximum stresses are around 1.5 MPa for the masonry walls and 9 MPa for the stone pillars. All values are well below material strengths.

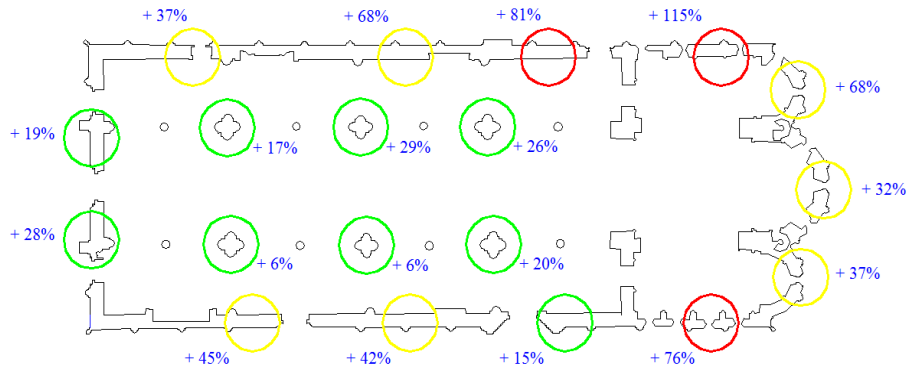


Figure 2.2.6: Increments of the stress at the base of the walls due to the inclination of the vertical elements.

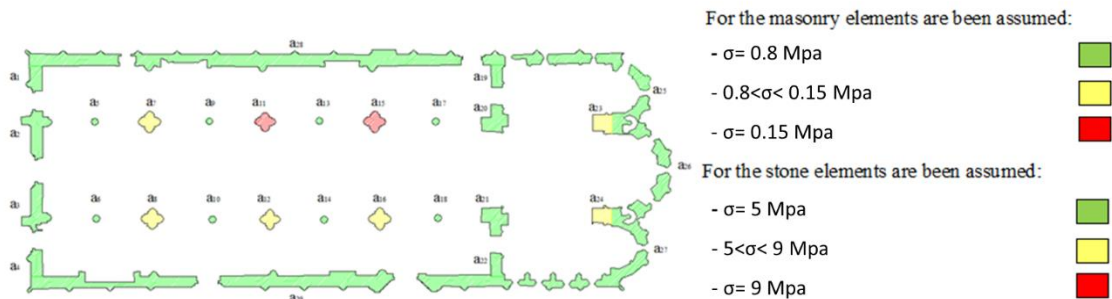


Figure 2.2.7: Level of stress at the base of the vertical elements including the effects of the inclinations

To simply evaluate how the presence of the arches in the transversal walls may contribute in the overall inclination of the wall, the thrusts of the arches have been calculated by assuming a simply supported arch schematization subjected to a uniform distributed load (due to the loads transmitted by the roof and the vaults). Then, the lateral forces corresponding to the calculated thrusts have been applied at the top of each corresponding wall in order to evaluate the lateral deflection, assuming a cantilever configuration and a tributary resisting wall width of 1.25 m, and thus neglecting the presence of the chains. The angle of inclination corresponding to the lateral deflection (with reference to the chord) has been compared with the measurements from the 3D laser scanning (Figure 2.2.8). It can be noted that the contribution due to the thrusts, in the case of not effective chains, is significant and, in the undisturbed areas (near the façade, where the interaction with the Ghirlandina Tower is weak and the soil is more uniform) is close to the measured one. Larger discrepancies appear in the areas closer to the Ghirlandina Tower where the interaction with the Tower is more relevant or where the chains could be more effective. It has to be noted that the choice of the tributary width significantly affects the estimation of the maximum out-of-plane deformations. A tributary length of 1.00 m can be considered as a lower bound, thus leading to conservative (i.e. reasonably larger) estimations.

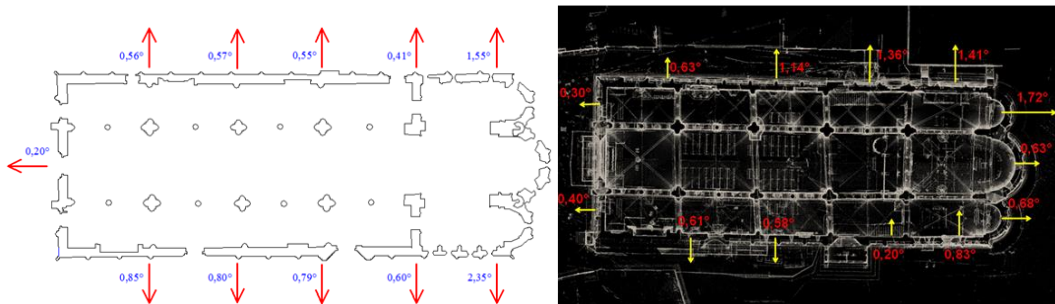


Figure 2.2.8: Comparison between the calculated inclinations due to only the lateral thrusts of the arches and those measured by 3D laser scanner

2.1.5 Structural analysis with 3D finite element models

Several 3D FE models have been developed to separately investigate, the effects of each single factor that could be influence the structural response of the cathedral. Once the importance of each single effect has been quantified, a unique 3D FE model has been developed in order to account for the interaction of all effects. All the models have been developed assuming: (i) homogeneous and elastic material characterized by the properties summarized §1.2.3; (ii) full cross-section masonry walls; (ii) average value of the thickness for each wall; (iii) architectural elements are not included in the model; (iv) the roof system and the vaults are not directly modeled and considered only in terms of applied vertical loads (in this respect, note that, on the contrary, the masonry arches both in the longitudinal and in transversal directions have been directly modeled). In more detail, the following types of restraints at the base have been considered to progressively investigate the soil-structure interaction:

- Fixed-base condition (F): the soil is assumed to be infinitely stiff in both vertical and horizontal directions;
- Roller-type base supports (R): the soil is assumed to be rigid in the vertical direction and with negligible lateral stiffness;
- Winkler type 1 base supports (W1): all the foundation soil is assumed to have a unique constant vertical stiffness (i.e. Winkler spring constant equal to $KxB=2.6$ MPa as displayed in Figure 2.1.7 (a), with B equal to the wall thickness); the lateral stiffness is assumed to be proportional to the applied axial load up to an horizontal displacement equal to 4 mm (i.e. a non-linear spring characterized by an elastic-perfectly plastic behavior has been assumed, as shown in Figure 2.2.9);

- Winkler type 2 base supports (W2): two different vertical stiffness values are used to account for the presence of the ancient Cathedral of the XI century (i.e. Winkler spring constants equal to $K_{xB}=2.6$ MPa and $K_{xB}=13$ MPa as displayed in Figure 2.1.7 (b); the same non-linear horizontal springs adopted in the W1 type supports have been used.

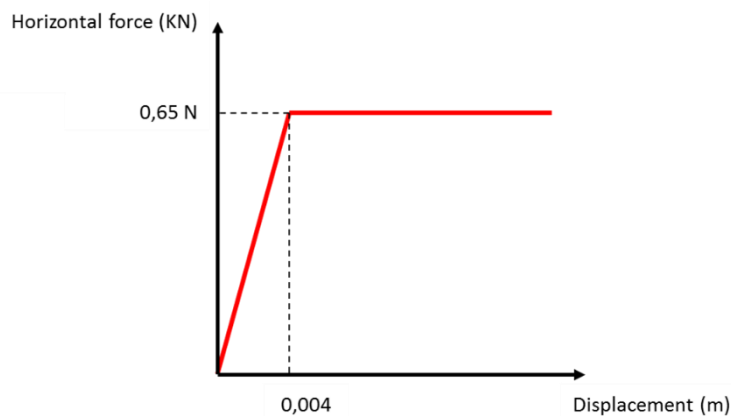


Figure 2.2.9: Elastic-perfectly plastic behaviour of the soil

Two geometrical configurations have been developed:

- Undamaged configuration (UD-C);
- Cracked configuration (C-C).

In the C-C configuration, the walls are characterized by discontinuities, which represent the main existing cracks as obtained from the in-situ inspections §1.1.4.

The response to the following single load cases have been evaluated for all models:

- Vertical loads (V);
- Thermal effects (T);
- Imposed differential Displacements (D) at the base representing the interaction between the Cathedral and the Ghirlandina Tower.

As above explained, the separate analyses of each single load case and the successive combination of these elementary contributions allow a more in-depth interpretation of the possible causes of the main cracks. Table 2.2.2 summarizes the different models, constraints imposed at the base and the different load cases used to perform the static analyses. For instance, in order to better clarify the nomenclature introduced in Table 2.2.2, the response of the undamaged configuration with the fixed based condition subjected to vertical loads will be referred to as UD-C+F+V.



First, a brief overview of the most relevant aspects of the single models is presented. Then, the most relevant results of the more representative models are reported. As expected, the restraints at the base which better allow to simulate the actual behaviour of the Cathedral (i.e. to provide the most reasonable justification of the main cracks detected with the survey) is the one referred to as W2. In general, the models, which account for the initial presence of the main cracks does not lead to significant discrepancies in terms of maximum stresses. Therefore, in the following the attention will be focused on the W2 restraint and on the UD-C configuration.

Table 2.2.2- Summary of the specific models with a specific restraint and a specific load cases provide a specific response developed.

| Model and Base Restraints | Model Response | | | |
|------------------------------|--------------------|----------------------|-------------------|----------------------------|
| | Vertical loads (V) | Thermal stresses (T) | Imposed disp. (D) | Combination (C = V+T+D) |
| UD-C + F | UD-C + F+V | UD-C + F+T | UD-C + F+D | UD-C + F+C |
| UD-C + R | UD-C + R+V | UD-C + R+T | UD-C + R+D | UD-C + R+C |
| UD-C + W1 | UD-C + W1+V | UD-C + W1+T | UD-C + W1+D | UD-C + W1+C |
| UD-C W2 | UD-C + W2+V | UD-C + W2 | UD-C + W2+D | UD-C + W2+C |
| C-C + F | C-C + F+V | C-C + F+T | C-C + F+D | C-C + F+C |
| C-C + R | C-C + R+V | C-C + R+T | C-C + R+D | C-C + R+C |
| C-C + W1 | C-C + W1+V | C-C + W1+T | C-C + W1+D | C-C + W1+C |
| C-C W2 | C-C + W2+V | C-C + W2 | C-C + W2+D | C-C + W2+C |

The stress state for a specific longitudinal wall and transversal wall as obtained from the UD-C + W2 considering all single load cases is summarized in Figure 2.2.10 and Figure 2.1.11. It can be noted that the locations of the peaks of the tensile stresses are in good agreement with the location of the main cracks.

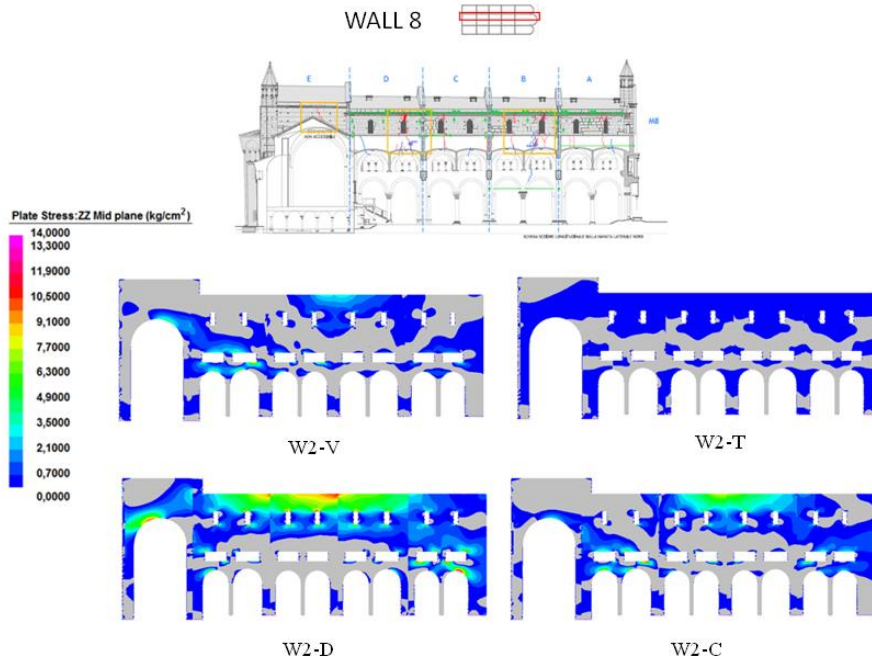


Figure 2.2.10: Stress of Wall 8 obtained from the W2 model with the different load cases and compared with the observed cracking patterns.

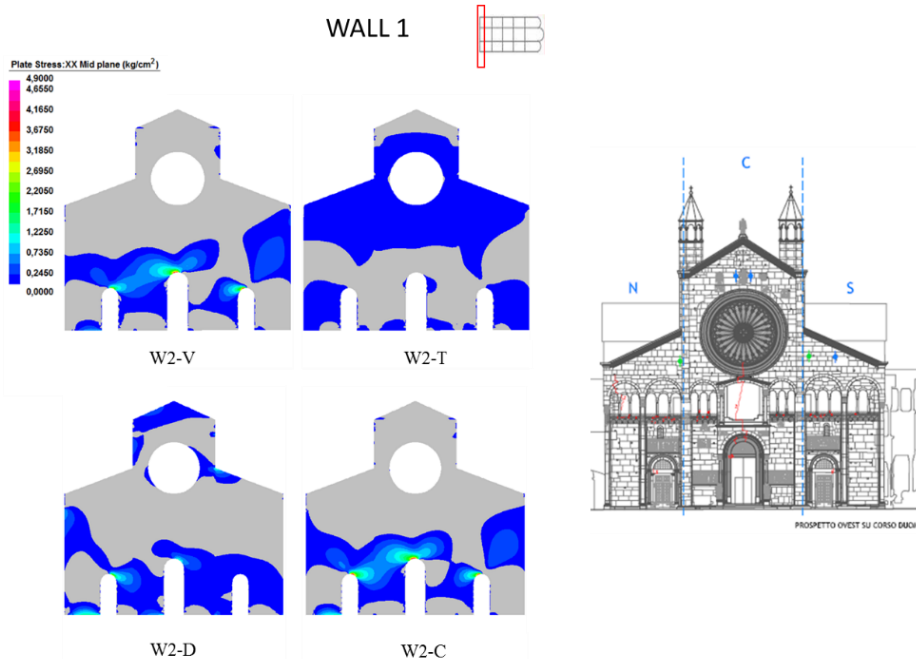


Figure 2.2.11: Stress of Wall 1 obtained from the W2 model with the different load cases and compared with the observed cracking patterns.

The in-plane and out-of-plane deformed shapes of a specific longitudinal wall are represented in and compared with the results of the 3D laser scanning. The deformed shapes are qualitatively consistent with the 3D laser scanning indicating that:

- the presence of the ancient ruins of the pre-existing churches reduces the vertical deformations in proximity of the facade (as indicated in Figure 2.2.12);
- the interaction between the Cathedral and the Ghirlandina Tower causes significant out-of-plane displacements (Figure 2.2.12) of the longitudinal walls, especially for those walls closer to the Tower.

Nonetheless, the maximum out-of-plane wall deformations leads to maximum out-of-plane inclinations of about 0.5° , thus smaller than those obtained from the 3D laser scanner and also from the simple hand calculations (see Figure 2.2.8). This can be explained by considering that in the FE models the entire inertia of the global wall as inserted in the whole structural context is considered. In summary, a sketch which schematically shows the main deformations is represented in Figure 2.2.13: (a) out-of-plane deformation of the longitudinal walls, (b) global inclination towards the Ghirlandina Tower due to differential soil settlements, which is contrasted by (c) the reactions of the masonry arches which link the Cathedral and the Tower.

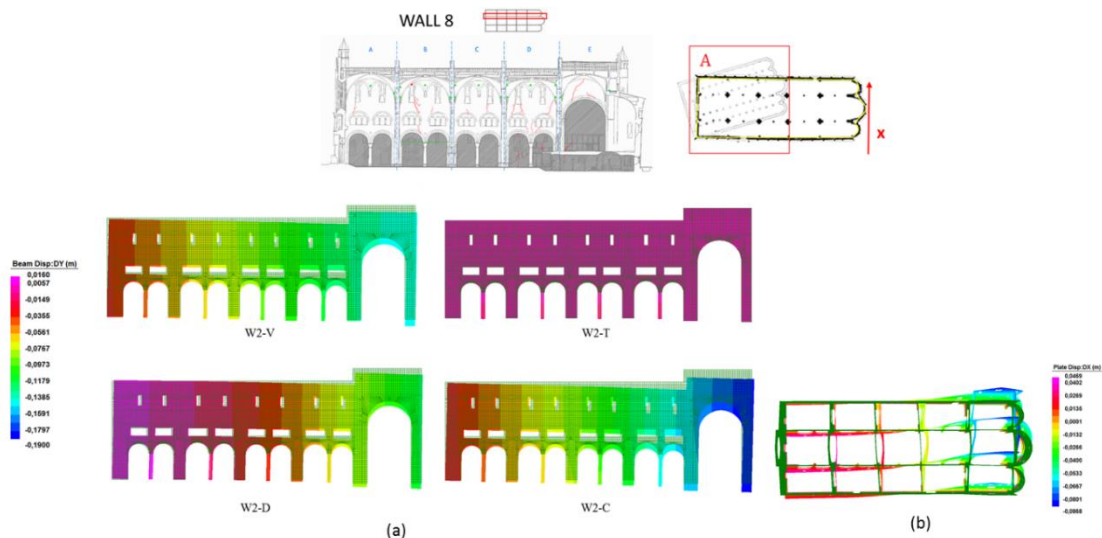


Figure 2.2.12: (a) in-plane deformed shape for Wall 8; (b) out-of-plane deformed shape (x direction) for all walls.



ALMA MATER STUDIORUM
UNIVERSITA' DI BOLOGNA

DICAM

Dipartimento di Ingegneria Civile,
Chimica, Ambientale e dei Materiali

MiChE
Mitigating the Impacts of natural hazards on Cultural Heritage
sites, structures and artefacts

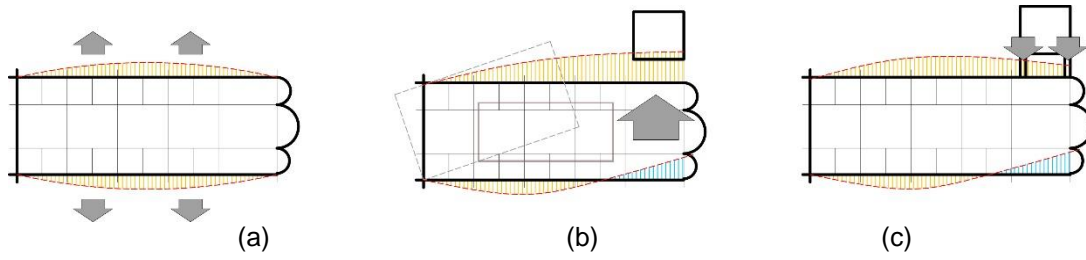


Figure 2.2.13: Sketch of the main global movements of the Cathedral as reconstructed by integrating the surveys with the results of the structural analyses.

2.2 Seismic behaviour: global analyses

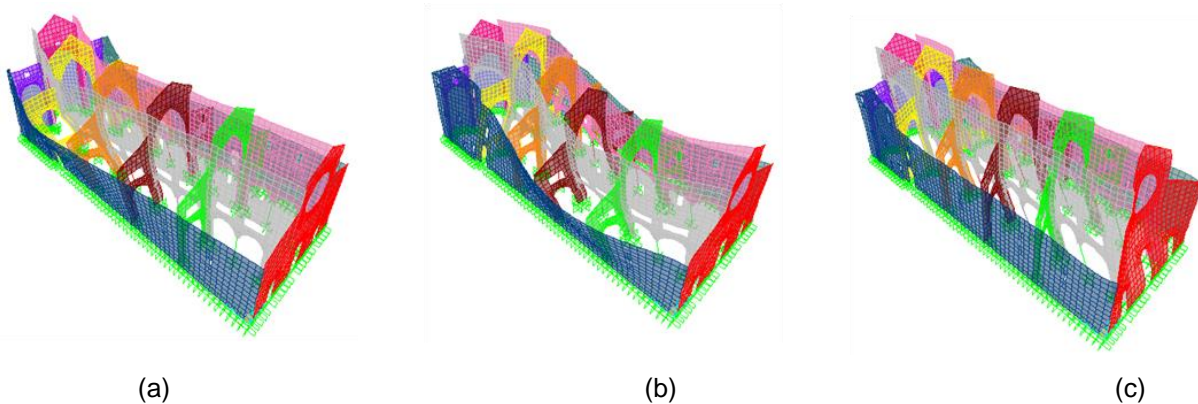
First, the dynamic properties of the monument (natural periods and mode shapes) have been identified through a natural frequency analysis performed on the 3D finite element model which was considered the more representative of the structure, as identified in the previously section. Then, the seismic behaviour of the whole structure have been investigated considering that the seismic response of the cathedral can involve mainly two types of mechanisms:

- in-plane mechanisms and
- out-of-plane mechanisms.

Finally, time history analyses on the 3D finite element models, considering as input the acceleration recorded during the 2012 earthquake §1.3, have been developed to identify the displacements/shearing deformation at the top of the walls and piers (springings of the vaults).

2.2.1 Natural frequency analysis

Since the stress-strain constitutive of masonry structures is yet non-linear for small values of deformation, the reliability of the modes of vibration is to be taken with caution. The common design codes, such as the Italian D.M. 14/01/2008 [68], prescribe that the participating mass must exceed 85%; therefore, in the consecutive seismic analyses 20 mode shapes have been considered in order to satisfy this requirement. The fundamental periods are in the range of 0.25-0.35 s. Figure 2.2.14 shows the first five mode shapes. This analysis shows that the first mode shape is characterized by a translation in the transverse direction of the Cathedral more pronounced in the area of the heavy apses than the area of the nave and the facade. The third mode shape is characterized by a translation along the longitudinal direction.



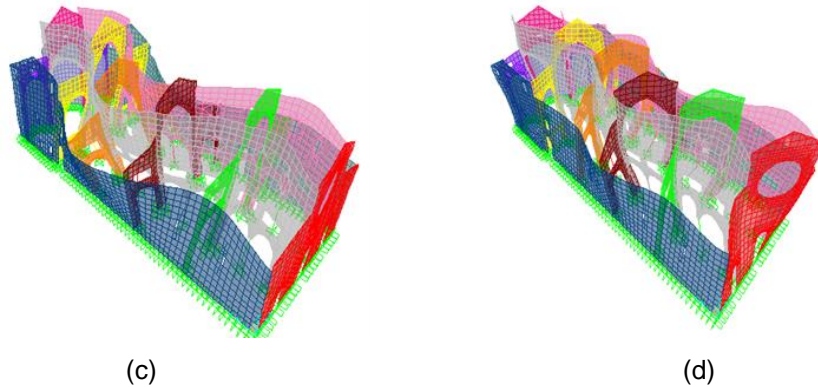


Figure 2.2.14: Mode shapes; (a) T=0.35 sec ;(b) T=0,31sec;(c) T=0,28sec;(d) T=0,28sec; (e) T=0,26sec

2.2.2 Global seismic response

Response spectrum and time history analysis have been performed on the 3D finite element model (called UD-C + W2). The analysis have been devoted to the identification of the criticalities in terms of:

- in-plane mechanisms caused by high shear force (causing possible diagonal cracks or horizontal sliding);
- out-of-plane mechanisms caused by high eccentricity, defined as the ratio between the bending moment and the axial force (causing possible stress concentration at the base or overturning of the wall).

The study of the in-plane mechanisms has been conducted by evaluating the tensile stresses in the walls (diagonal cracking check) and the shear stresses at the base of the walls (sliding check). Figure 2.2.15 shows the comparison between the tensile stresses and the cracking patterns for the wall 1 (façade wall). In general, the results obtained from tensile stresses show a high validation with the cracking patterns. The majority of the lesions seems to be caused by the accumulation of damage over time caused by various earthquakes. The sliding check at the base is performed as follows:

$$\tau < \tau_{di}$$

where

τ is the tangential mean stress and τ_{di} is the shear strength of the masonry, as evaluated according the two diagonal cracking and (friction) sliding mechanisms:

$$\tau_{di} = \tau_{od} \sqrt{1 + \frac{\sigma_{oi}}{1,5\tau_{od}}}$$

$$\tau_{di} = \tau_{od} + 0,4\sigma_{oi}$$

where:

τ_{od} = shear strength of the masonry ($\tau_{od}=1\text{kg/cm}^2$);

σ_{oi} = mean compressive stress.

Figure 2.2.16 shows the tangential stresses calculated for wall 1 and Table 2.2.3 reports the values obtained for the sliding check. Figure 2.2.17 summarizes the results obtained for all the walls of the cathedral and highlights that the greatest criticalities are related to the in the internal transversal walls.

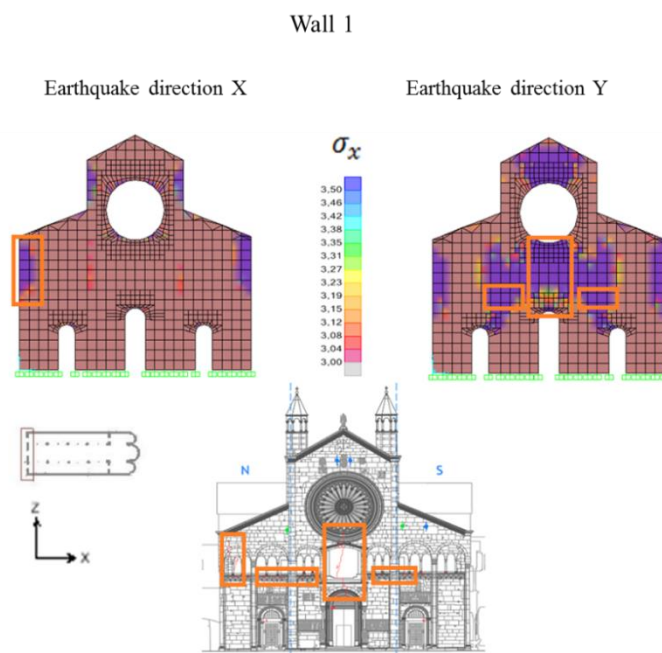


Figure 2.2.15: Comparison between tensile stresses and the cracking patterns

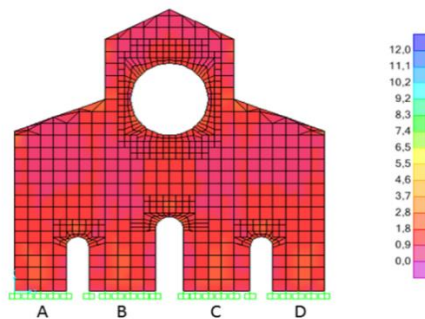


Figure 2.2.16: Tangential stresses

Table 2.2.3 - Verification of the shear strength for the wall 1

| | Compressive mean stress | Shear strength Eq. (2.2) | Shear strength Eq. (2.3) | Tangential mean stress (Demand) | Demand/ Capacity ratio Eq. (2.2) | Demand/ Capacity ratio Eq. (2.3) |
|----------------|----------------------------|--------------------------------|--------------------------------|--|--|--|
| | [Kg/cm ²] | [Kg/cm ²] | [Kg/cm ²] | [Kg/cm ²] | [] | [] |
| Section cut 1A | 6.95 | 2.37 | 3.78 | 1.25 | 0.53 | 0.33 |
| Section cut 1B | 4.66 | 2.03 | 2.86 | 1.36 | 0.67 | 0.47 |
| Section cut 1C | 4.66 | 2.03 | 2.87 | 1.37 | 0.68 | 0.48 |
| Section cut 1D | 7.06 | 2.39 | 3.82 | 1.25 | 0.52 | 0.33 |

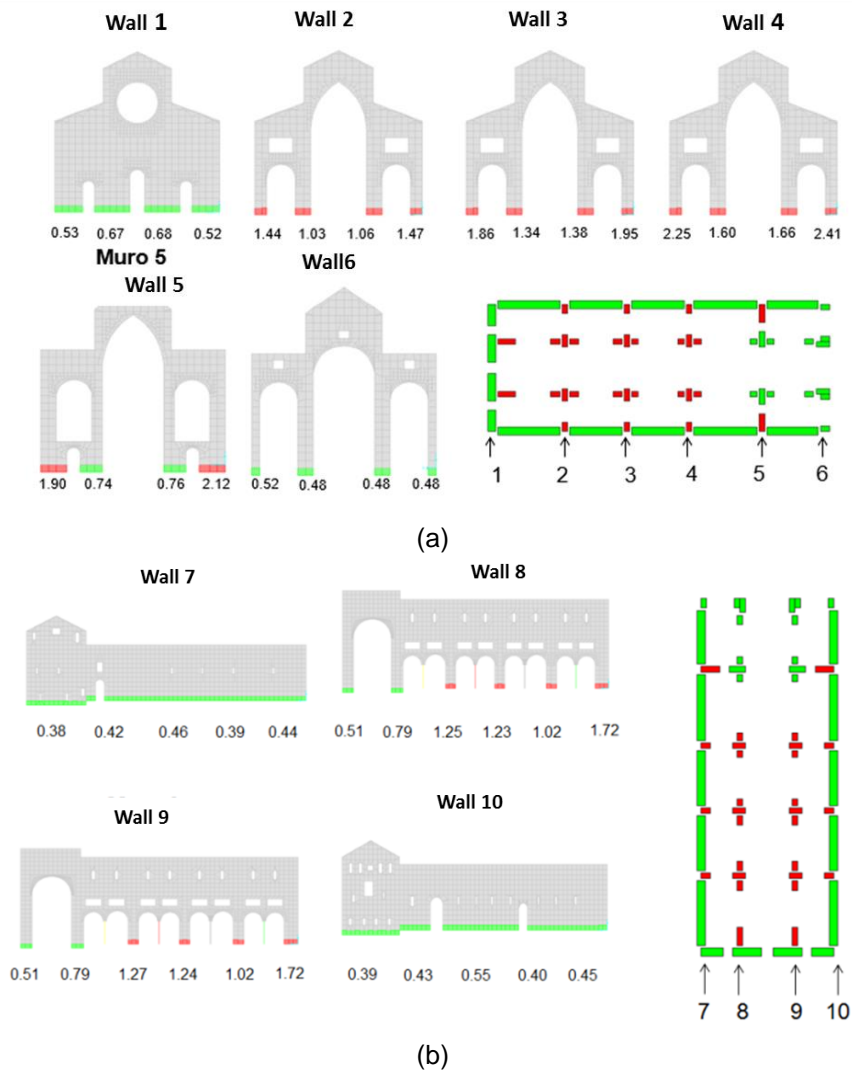


Figure 2.2.17: Sliding check for all the walls of the cathedral: (a) transversal walls and (b) longitudinal walls

Out-of-plane mechanisms have been identified by first evaluating the eccentricity at the base of the walls, as defined as the ratio between the bending moment and the axial force in seismic conditions, and then checking that:

- the eccentricity is below the usual reference values $s/6$ and $s/2$ (with s indicating the thickness of the wall) and
- the lateral shear stresses developed on the two vertical lateral sides of the considered wall are below some reference values (i.e. connection capacity).

In detail, the eccentricity at the base of each wall has been calculated by considering both the static loads (self weight and dead loads) and the seismic actions (that, in the case of a dynamic time-history analysis, are function of time) for each section (Figure 2.2.18):

$$e(t) = \frac{M_{static} + M_{seismic}(t)}{N_{static} + N_{seismic}(t)}$$

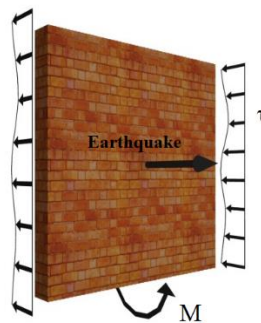
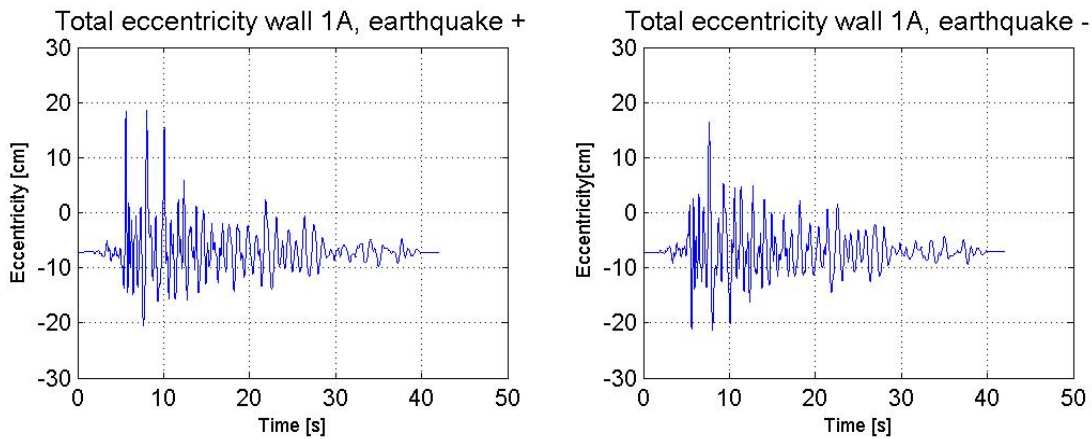


Figure 2.2.18: A schematic representation of a single wall with the indication of the out-of-plane seismic action, the base moment and the transversal actions due to the interaction between the orthogonal walls

The time history of the eccentricity has then been evaluated using 9 recorded accelerograms (selected from the P.E.E.R. strong motion database) consistent with the results of the seismic hazard analyses §1.3. Then the maximum absolute eccentricities have been used to check the out of plane stability of the walls. Two limit cases regarding the quality of the connection between orthogonal walls have been considered to compute the eccentricities: good connections (perfect continuity between orthogonal walls) and bad connections (partial continuity between orthogonal walls, modelled by inserting more flexible elements). Figure 2.2.19 a shows the time history of the eccentricity for the 1A section of the wall 1 whereas Figure 2.2.19 b shows the shear stresses, exchanged between the considered and the adjacent walls, obtained from the time history analysis for the wall 1. 2.2.4 shows the values of the eccentricity calculated for the various sections of the wall 1 and verify that these values are lower than $s/2$. Figure 2.2.20 provides a summary of the results obtained for all the walls of the cathedral. In can be noticed that, the study of the out of plane

collapse mechanisms showed criticality in the transversal walls especially in the control sections B-C. However, the values of the shear stresses for each wall suggest that, even leading to cracked conditions at the base of the walls, the connections are able to keep the wall in a stable configuration. In two longitudinal walls, instead, the results indicate both cracked conditions at the base and values of shear stresses greater than the shear strength of the masonry in the absence of vertical loads.



(a)

Wall 1, thickness $s = 145$ cm

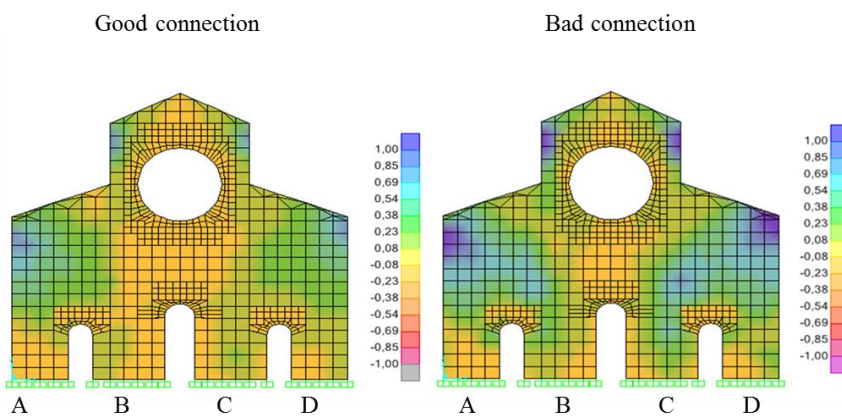


Figure 2.2.19: (a) The time history of the eccentricity on the 1A section (b) Tangential stresses for the wall 1

Table 2.2.4- Verification of the eccentricity for the wall 1

| | Good connection | Bad connection | | Good connection | Bad connection | Central core of inertia | s/2 |
|----------------|-----------------|----------------|--|-----------------|----------------|-------------------------|------|
| | Mean + [cm] | Mean + [cm] | | Mean - [cm] | Mean - [cm] | [cm] | [cm] |
| Section cut 1A | 50,10 | 120,04 | | -26,15 | -51,02 | 24,17 | 72,5 |
| Section cut 1B | 1183,40 | 412,82 | | -28,70 | -99,75 | 24,17 | 72,5 |
| Section cut 1C | 1386,93 | 470,64 | | -28,60 | -102,97 | 24,17 | 72,5 |
| Section cut 1D | 57,03 | 151,55 | | -26,20 | -53,51 | 24,17 | 72,5 |

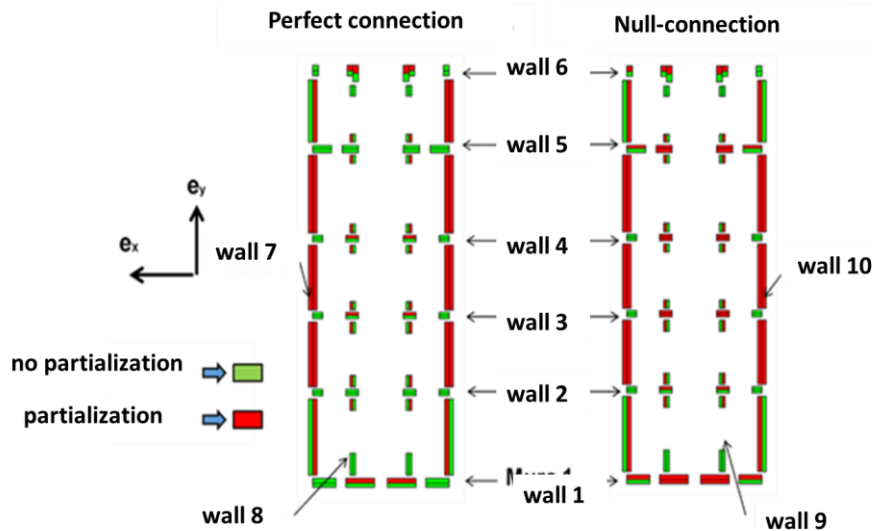


Figure 2.2.20: Vulnerability for the out-of-plane mechanisms in the walls

2.2.3 Time history analyses: input the main shock recorded by the station of Modena

Time history analyses on the 3D FEM model of the Cathedral, has been developed to identify the displacements/shearing deformation at the springings of the vaults (top of the walls and piers). The input considered in the analyses is the acceleration recorded by the station close to Modena (MDN) during the 2012 Emilia earthquake (with a pick ground acceleration around 0.04g). The main purpose of these analyses is the assessment of the correlation between the displacements of the springings of the vaults, due to the vibration of the underneath structures, and the damages detected. Figure 2.2.21 shows the nomenclature used for the vaults of the cathedral and the displacements that can interest the vaults (shearing displacement referred to VNC1 and widening referred to VNC3). Table

2.2.5 and Table 2.2.6 collect the displacements (widening and closing) and the shear displacement at the springings of the central and lateral vaults. It can be noticed that during the 2012 Emilia earthquake the springings of the vaults of the cathedral suffered shear imposed displacement lower than 1 cm and negligible widening and closing displacements.

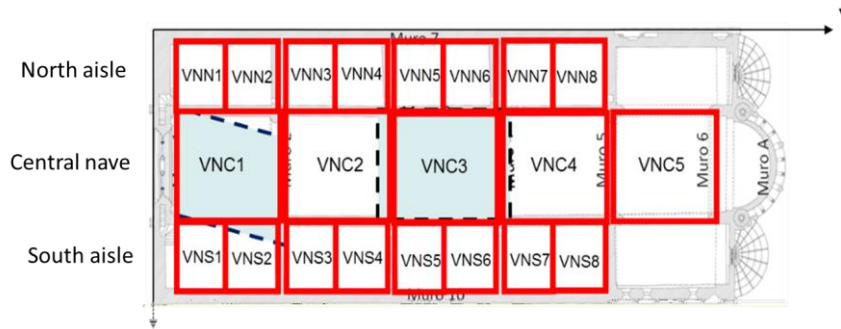


Figure 2.2.21: The nomenclature of the vaults of the cathedral

Table 2.2.5- The displacement at the springings of the central vaults as obtained from the time history analyses

| Central Vault | Displacement [cm] | Shear Displacement[cm] |
|---------------|-------------------|------------------------|
| VNC1 | 0.014 | 0.43 |
| VNC2 | 0.020 | 0.39 |
| VNC3 | 0.03 | 0.39 |
| VNC4 | 0.03 | 0.48 |
| VNC5 | 0.037 | 0.43 |

Table 2.2.6- The displacement at the springings of the lateral vaults as obtained from the time history analyses

| Lateral Vault | Displacement [cm] | Shear Displacement [cm] |
|---------------|-------------------|-------------------------|
| VNN1-S1 | 0.014 | 0.43 |
| VNN2-S2 | 0.020 | 0.39 |
| VNN3-S3 | 0.03 | 0.39 |
| VNN4-S4 | 0.03 | 0.48 |
| VNN5-S5 | 0.037 | 0.43 |
| VNN6-S6 | 0.014 | 0.43 |
| VNN7-S7 | 0.020 | 0.39 |
| VNN8-S8 | 0.03 | 0.39 |

The results obtained in terms of shear displacement are compared with the survey of the damage observed after the 2012 earthquakes (Figure 2.2.22). It can be noticed that generally the vaults mainly damaged correspond at the vaults that suffered the major shear displacement at the springings due to the vibration of the underneath walls and piers.

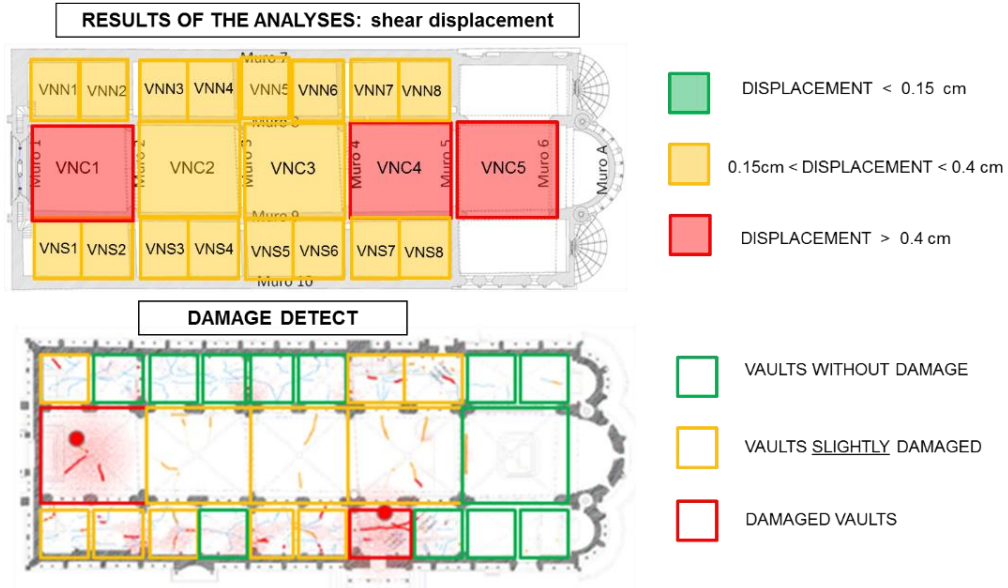


Figure 2.2.22: The comparison between the shear displacements and the damage detected on the vaults after the 2012 earthquake



2.2.4 The main vulnerabilities and conclusions

Starting from the knowledge acquired by the multi-disciplinary approach, the structural behaviour of the Cathedral has been investigated in order to identify the more vulnerable elements of the building. The multi-analyses method which aims at integrate the results obtained by different models, (characterized by different level of accuracy according to typology of problems to be investigated) appears fundamental in order to obtain a consistent assessment of the structural behaviour of the monuments.

The results of the static analyses reveals that the different soil stiffness at the base of the cathedral strongly influence its structural behaviour. Indeed, the model, which considers the soil-structure interaction, is able to provide with more accuracy a state stress congruent with the cracks pattern detected.

Moreover, from the static analyses it can be recognized that the main vulnerabilities are:

- the tendency of the longitudinal perimeter walls to develop out-of-plane movements, as revealed by the 3D laser scanner, probably due to the unconstrained thrusts of the arches and differential settlements;
- the overall rotation movement towards the Ghirlandina Tower, caused by the strong interaction between the Cathedral and the Tower, that promotes differential soil settlements (note that the portion of the apses is significantly heavier than the other portions);
- the concentration of cracks and peaks of the tensile stresses in the portion coinciding with the location of the old Cathedrals.

The results of the seismic analyses reveal vulnerabilities of the perimeter walls with respect to out-of-plane overturning. These numerical results have been confirmed by the experimental evidences of the damages observed after the recent 2012 Emilia Romagna earthquake sequence.



2.3 Local structural analyses

2.3.1 Introduction

The seismic performances of historical masonry buildings are closely related to the behaviour of each substructure. In general, the horizontal seismic forces cause damages and/or collapses mainly in the following specific elements: large space without structural walls, arches, vaults, domes, ... , which are common in the historical churches. The analysis of the main damages suffered by Italian churches due to the recent earthquakes (L'Aquila 2009, Emilia 2012, Umbria-Marche 2016) has shown a number of common collapse mechanisms, which may involve the local response of single structural elements [69], [67]. In particular, the information on damage location and extent, collected after these violent earthquakes, highlighted that, among all structural elements, the most vulnerable one are masonry vaults.

In this chapter, the local collapse mechanisms of the main substructures of the Cathedral have been studied. In addition, 3D Finite element models of the most damaged vaults, after the 2012 Emilia Romagna earthquake, have been developed in order to provide information on the stress and deformation state.

2.3.2 The models and the simulation

The local collapse mechanisms which aim at providing the value of the load that activates the failure mechanisms of each elements through kinematics models (both in-plane and out-of-plane mechanisms) have been evaluated for the single sub-elements of the cathedral. Then, the stress levels of vaults under dynamic excitation and displacement imposed at their springings have been investigated making use of 3D linear Finite element models. The analyses developed are summarized in Table 2.2.7.

Table 2.2.7- The different analyses developed

| Model-Element | Analysis |
|---|---------------------------|
| Sub-elements: façade, nave, vaults, aisles... | local collapse mechanisms |
| 3D FEM models of the vaults | Static analyses |
| 3D FEM models of the vaults | Seismic analyses |



2.3.3 Local collapse mechanisms

The local collapse mechanisms are strongly dependent on the construction techniques and on the connection details between orthogonal masonry walls and between the masonry walls and the possible restraining horizontal elements, such as tie-beams, well connected floors, The cathedral has been divided into sub-elements, i.e. structural elements characterized by an autonomous structural behaviour: the façade, the nave, the aisles, the vaults, the longitudinal perimeter walls, the columns, the transept, the triumphal arch and the apses. For each one of these sub-elements, when applicable, out-of-plane mechanisms and in-plane mechanisms have been considered. As far as the out-of-plane mechanisms are concerned, the limit analysis approach has been applied. Each sub-element is assumed to be composed by a number of stiff, incompressible and infinitely-resistant blocks, and the limit load multiplication coefficient (λ) is calculated by means of equilibrium equations. Limit load is the maximum seismic horizontal load that the structure can safely carry. In general, the limit analysis of masonry structures involves the following assumptions [70]: (i) masonry has no tensile strength, (ii) stresses are so low that masonry has effectively an unlimited compressive strength, (iii) sliding failure does not occur. Here, only the calculations related to the evaluation of the limit load multiplication coefficient of the façade are entirely presented. The crack pattern shows lesions in the orthogonal longitudinal walls next to the facade Figure 2.2.23a) that suggest a good connection between these elements. However, three different hypotheses of connections are here considered : (1) good connection between orthogonal masonry walls , (ii) bad connection (negligible connection between orthogonal masonry walls) and (III) reasonable estimation of the connection. The following mechanisms have been taken into account:

- overturning of the whole façade (Figure 2.2.23b and Figure 2.2.24– mechanism 1);
- overturning of the left portion of the façade (Figure 2.2.24– mechanism 2);
- overturning of the central portion of the façade (Figure 2.2.24-mechanism 3);
- overturning of the right portion of the façade (Figure 2.2.24– mechanism 4-5).

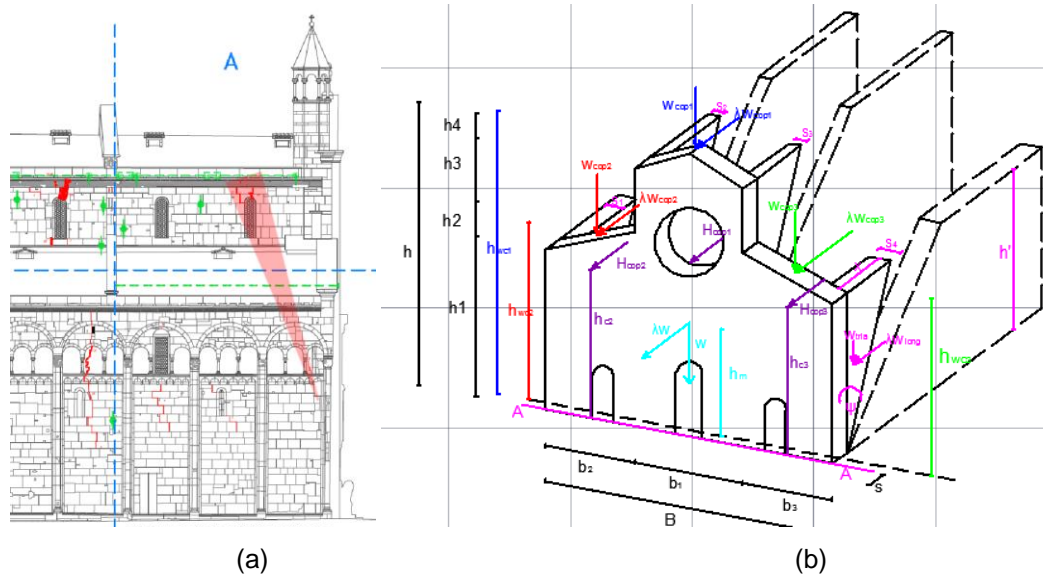


Figure 2.2.23: (a) Cracks in longitudinal walls of Cathedral, (b) Overturning of global facade around the base dashed straight line.

The behaviour of the wall in limit equilibrium conditions has been simulated by applying the principle of virtual works, i.e. equating the overturning moment (due to horizontal loads) and the stabilizing moment (due to self-weight):

$$M_{overturning} = M_{stabilizing}$$

$$\left[\left((W - W_{holes}) \cdot \frac{s}{2} + W_{cop} \cdot d_c - H_{cop1} \cdot h_c + W_{tria} \cdot \left(s + \frac{1}{3} x_i \right) \right) \right] -$$

$$-\lambda \cdot \left[W_{wall} \cdot h_m - W_{holes} \cdot h_f + W_{cop1} \cdot h_{wc1} + W_{long} \cdot \left(\frac{2}{3} \cdot h'_i \right) \right] = 0$$

The limit load corresponding to the spectral acceleration that activates the local mechanism of collapse has been obtained from the previously Equation.

$$\lambda = \frac{\left[(W - W_{holes}) \cdot \frac{s}{2} + W_{cop1} \cdot d_{c1} + W_{cop2} \cdot d_{c2} + W_{cop3} \cdot d_{c3} - H_{cop1} \cdot h_{c1} - H_{cop2} \cdot h_{c2} - H_{cop3} \cdot h_{c3} \right]}{\left[W_{wall} \cdot h_m - W_{holes} \cdot h_f + W_{cop1} \cdot h_{wc1} + W_{cop2} \cdot h_{wc2} + W_{cop3} \cdot h_{wc3} \right]} = 0,22$$

$$a_0 = \lambda \cdot g = 0,22g$$

Figure 2.2.24 shows the acceleration values that activate overturning mechanisms of the different portions of the façade for the different connection considered. These values, also considering the good connection, are higher than the acceleration reference values for the past earthquakes obtained from HDSHA §1.3.1 (0.15-0.20 g), but lower than the acceleration estimates for the possible future earthquakes obtained from MHEA §1.3.2 (0.50 g).

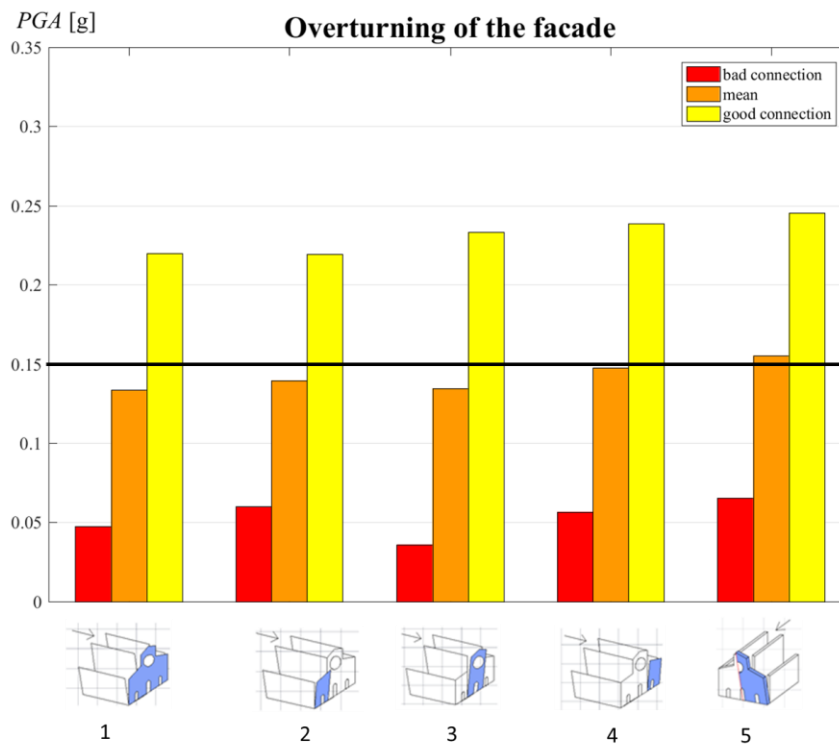
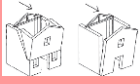
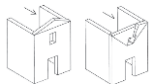




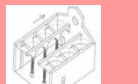
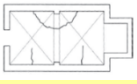
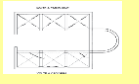
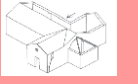

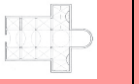

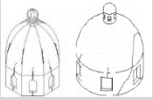
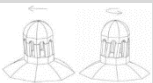

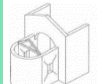






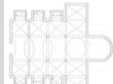


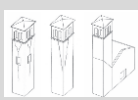
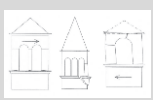


Figure 2.2.24: Comparison between the accelerations that activate the 4 mechanisms of collapse for the façade

The results obtained for the other substructures are summarized in Table 2.2.8. The acceleration that activates the failure mechanisms reported in Table 2.2.8 are referred to the most unfavourable condition of each elements (bad connections, more susceptible element).

In general, the study of the local mechanism of other sub-elements reveal that the main local vulnerabilities are relevant to the façade (as described above), the top façade (with trigger accelerations around 0.06 g), the cross vaults (with trigger accelerations around 0.12 g), the triumphal arch (0.07 g), the transversal response of the columns (0.14 g) and the out-of-plane behaviour of the apse walls (0.13 g).

Table 2.2.8-The acceleration that activates the failure mechanisms for each sub structures

| | | | | | | |
|---|--|--|--|--|---|---|
| 1. OVERTURNING OF THE FACADE  0.13 g | 2.OVERTURNING TOP OF THR FACADE  0.06 g | 3. IN OLANE MECHANISMS OF THE FACADE  0.33 g | 4. PROTHYRUM  0.17 g | 5. TRANSVERSAL RESPONSE OF THE AULA  0.31 g | 6. SHEAR IN THE LATERAL WALLS  0.14 g | 7. LONGITUDINAL RESPONSE OF THE COLUMNS  0.19 g |
| 8.VAULTS OF THE CENTRAL NAVE  0.21 g | 9. VAULTS OF THE AISLES  0.13 g | 10. OVERTURNING TRANPSET WALLS  0.24 g | 11. SHEAR IN THE TRANSEPT  0.12 g | 12. VAULTS OF THE TRANSEPT  0.07 g | 13. TRIUMPHAL ARCHES  0.15 g | 14. DOME  0.37 g |
| 15. LANTERNA  0.34 g | 16. OVERTURNING OF THE APSE  0.21 g | 17. SHEAR MECHANISMS ON THE APSE  0.15 g | 18. VAULTS OF THE APSE  0.21 g | 19. ROOF SYSTEM  0.21 g | 20. ROOF OF THE TRANSEPT  0.21 g | 21. ROOF OF THE APSE  0.21 g |
| 22. OVERTURNING OF THE CHAPEL  0.21 g | 23. SHEAR MECHANISMS ON THE CHAPEL  0.21 g | 24. VAULTS OF THE CHAPEL  0.21 g | 25. PLAN AND HEIGHT IRREGULARITIES  0.21 g | 26. AGGETTI (PINNACLES)  0.21 g | 27. BELL TOWER  0.21 g | 28. CELL BELL  0.21 g |

| |
|---|
| $a < 0.15 g$ |
| $0.15g < a < 0.25 g$ |
| $a > 0.25 g$ |
| <i>Not present, or static patterns insufficiently representative of reality</i> |

2.3.4 The vault

The investigation of the structural behavior of the cross vaults under earthquake excitation is a fundamental issue in order to plan effective structural interventions. However, the evaluation of their seismic response is severely complex and depends on several factors, such as the three-dimensional geometry, the mechanical properties of the constituent materials and the behavior of the underneath vertical elements (lateral walls and piers) [71]. A vault under earthquake excitation is mainly subjected to two different phenomena (Figure 2.2.25):

- pseudo-static response of the vault to the relative displacements imposed at its springings, due to the horizontal movements of the underneath structures (walls and piers).
- dynamic response of the vault to the acceleration imposed at its springings due to the seismic vibration of the underneath structures (walls and piers);

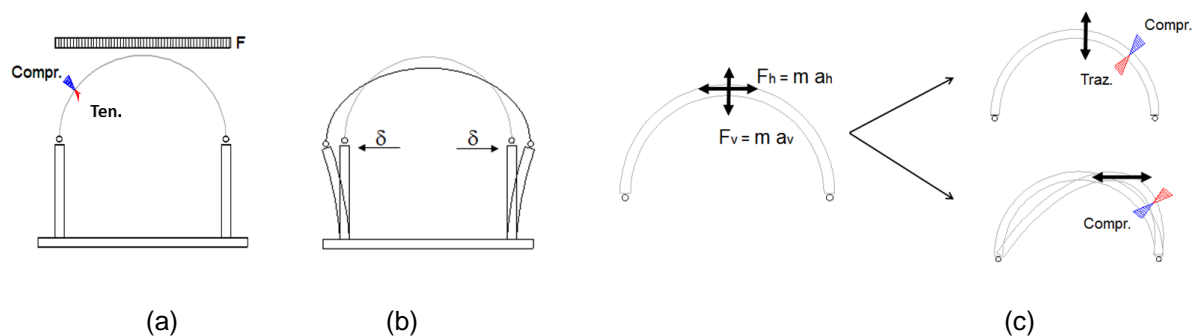


Figure 2.2.25: Schematization of the effects used for the assessment of the seismic response of the vaults: (a) vault undergo to vertical loads, (b) vault subject to imposed displacement at the springings and (c) vault under earthquake excitation

In this section the structural behavior of the vaults of the cathedral has been investigated. First, static analyses have been developed in order to identify the stress level due to the self-weight and displacement imposed at their springings (as obtained in § 2.2.3). Then, linear time history analyses, using the acceleration recorded by the MDN station §1.3.3, have been performed.

2.3.4.1 3D FE models of the vaults

Static and dynamic analyses have been developed on the 3D FE models of the two most damaged vaults (VNC1 and VNS7) after the 2012 earthquake of the cathedral. The FE models reproduce the actual geometry of the groin vaults, which has been determined by means of laser scanning surveys, paying particular attention to the restraining given by the support and contrast elements (Figure 2.2.26). The information regarding the geometry of the two vaults are reported in Table 2.2.9. In the FE modelling the masonry is modelled as homogeneous continuum. For this reason, the FE models are not suitable to capture the expected failure modes but may give indications on the level of stress

on the vaults. High tensile stress resulting from static and dynamic loads are assumed to indicate cracking due to material failure.

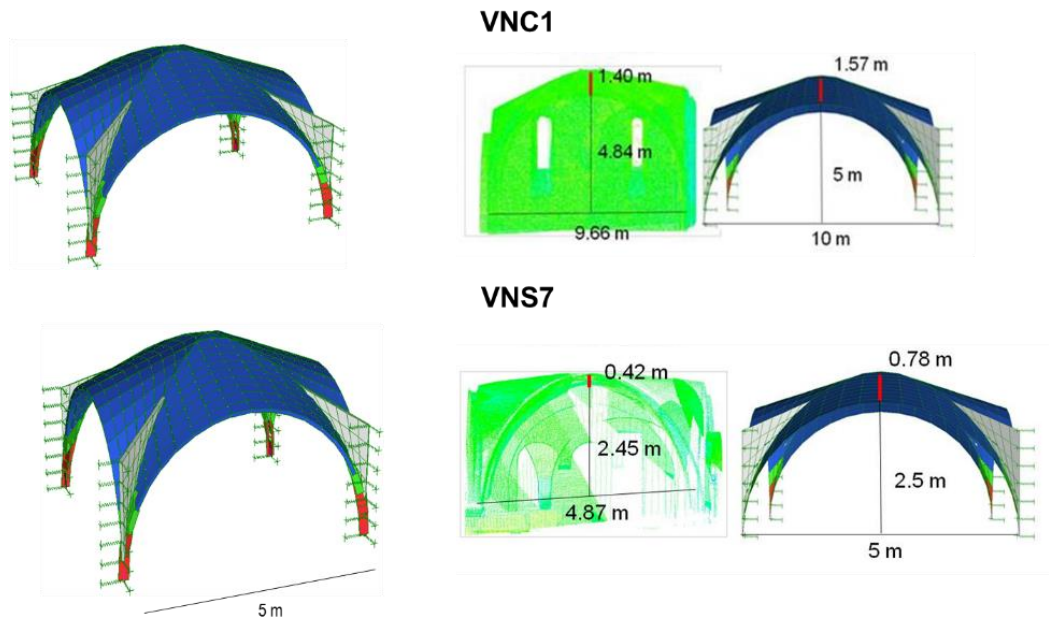


Figure 2.2.26: The actual geometry of the central and lateral vaults (VNC1 and VNS7) and the corresponding 3D FE models

Table 2.2.9: The geometry of the central and lateral vault of the cathedral

| CENTRAL VAULT (VNC1) | | | | | | |
|----------------------|----------|------------------------|---------------|-------------------------------|-------------|---------|
| Base [m] | High [m] | Area [m ²] | Thickness [m] | γ [kg/m ³] | Weight [KN] | E [KPa] |
| 9.1 | 10.2 | 211 | 0.12 | 1800 | 7.9 | 4144000 |
| LATERAL VAULT (VNS7) | | | | | | |
| Base [m] | High [m] | Area [m ²] | Thickness [m] | γ [kg/m ³] | Weight [KN] | E [KPa] |
| 5.2 | 5.6 | 70 | 0.12 | 1800 | 150 | 4144000 |

Static analyses considering also imposed displacements at the springings of the vaults, as obtained by the time history analyses on the global model of the cathedral, have been conducted. The increment of the level of stress (both compression and tensile stress) due to the widening and closing displacements imposed at the springings are substantially irrelevant. On the other hand, however, the shear displacements imposed causes a not negligible increment of the tensile stress at the extrados of the vaults (it can reach $2/3 \text{ kg/cm}^2$), with particular concentrations along the diagonals. The maximum compressive stresses remain instead contained within limits compatible with the resistance of the materials characteristics (below 10 kg/cm^2) (Figure 2.2.27 and Figure 2.2.28).

VNC1: SELF-WEIGHT AND SHEAR DISPLACEMENT

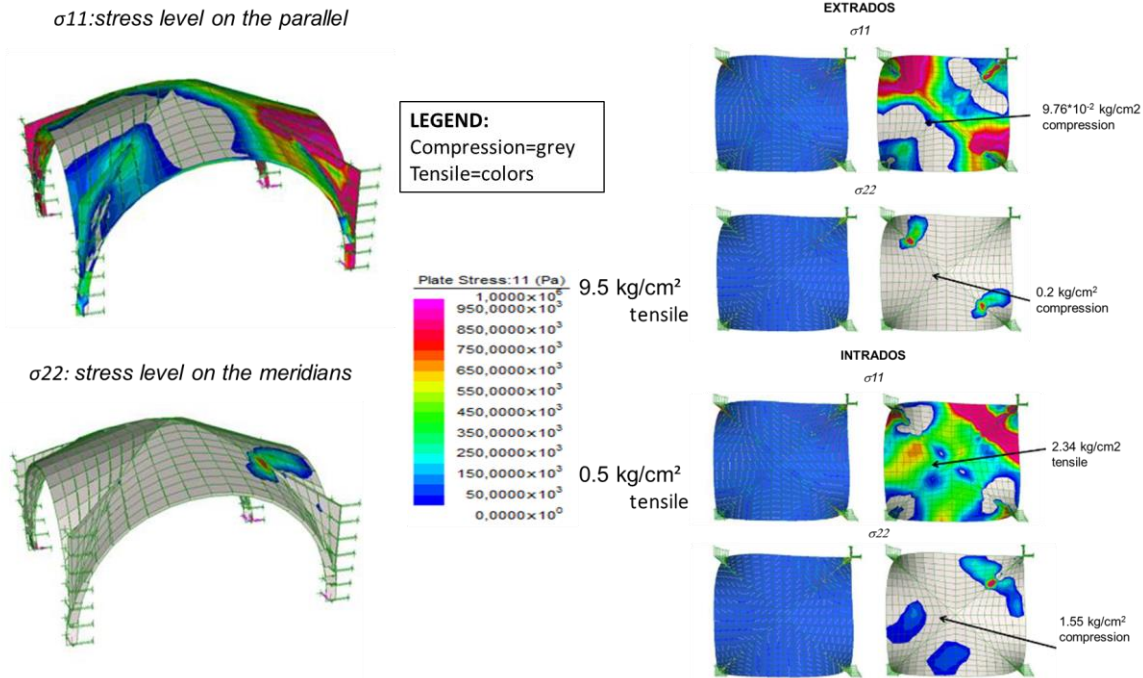


Figure 2.2.27: Stress levels of the vault VNC1 obtained from the static analyses considering the self-weight and the shear imposed displacements

VNN7: SELF-WEIGHT AND SHEAR DISPLACEMENT

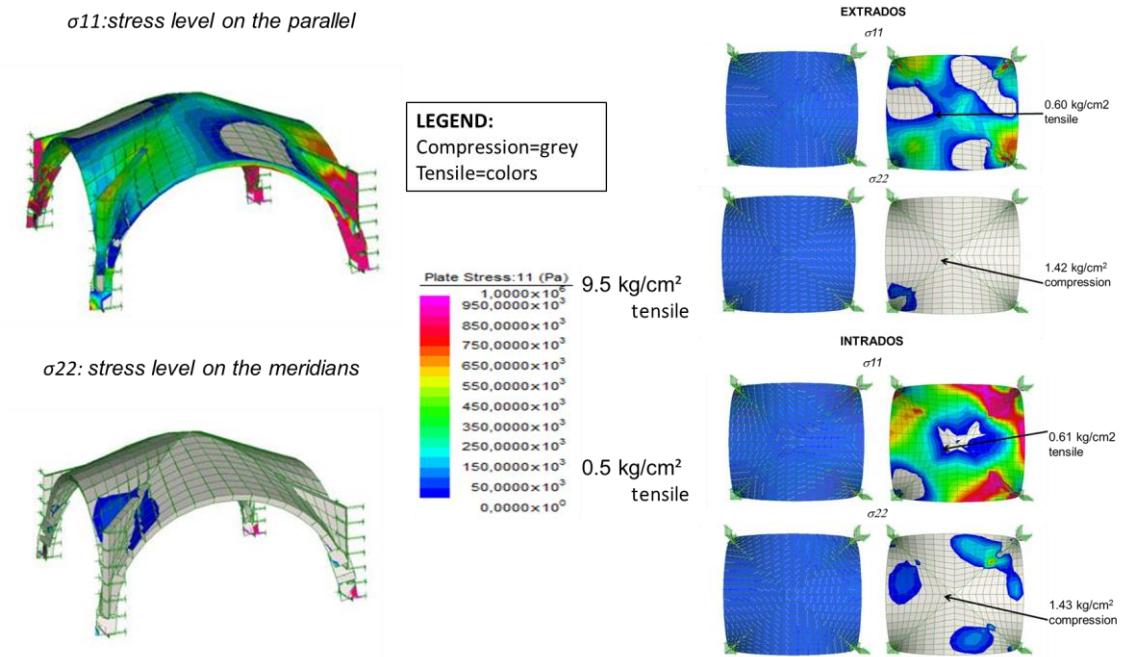


Figure 2.2.28: Stress levels of the vault VNN7 obtained from the static analyses considering the self-weight and the shear imposed displacements

Linear time history analyses on the 3D FE models of the vaults have been also developed applying as input the acceleration recorded by the station close to Modena during the 2012 earthquake. Figure 2.2.29 and Figure 2.2.30 display the stress level on the vault VNC1 and the vault VNN7 obtained from the dynamic analyses considering the self-weight and the seismic load. These analyses show that the effect of the dynamic response of the vaults is substantially comparable in terms of maximum tensile stresses to that induced by the shear displacements imposed at the springings.

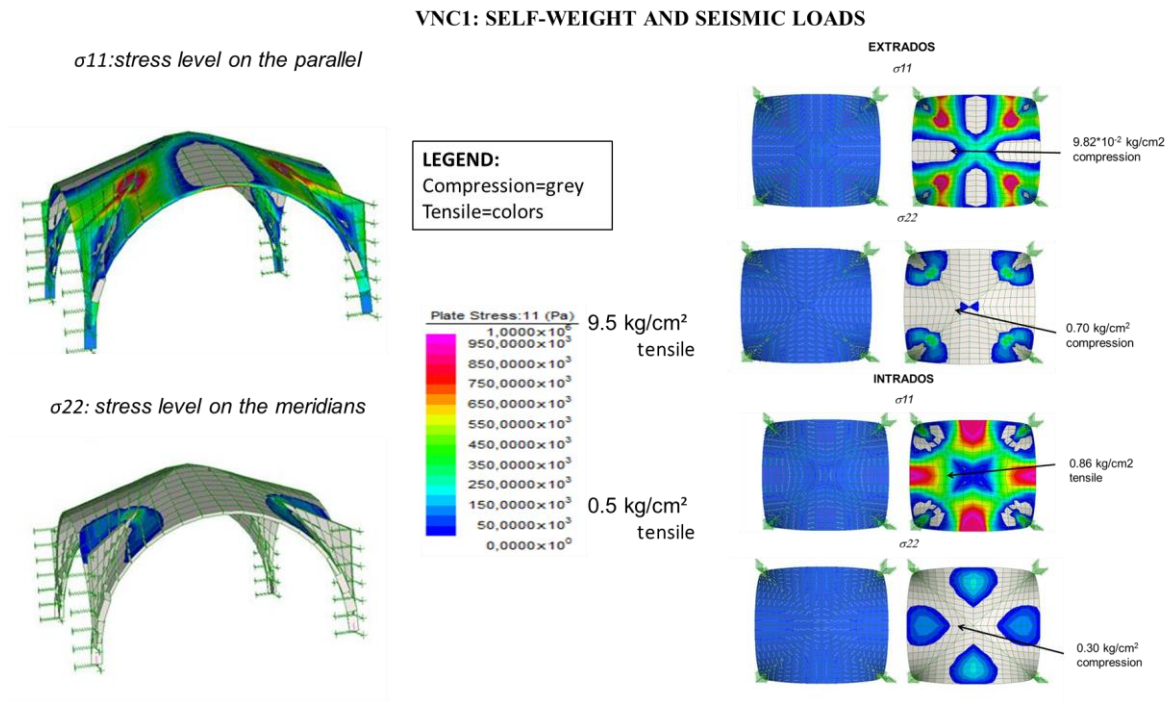


Figure 2.2.29: Stress levels of the vault VNC1 obtained from the dynamic analyses considering the self-weight and the seismic loads

VNN7: SELF-WEIGHT AND SEISMIC LOADS

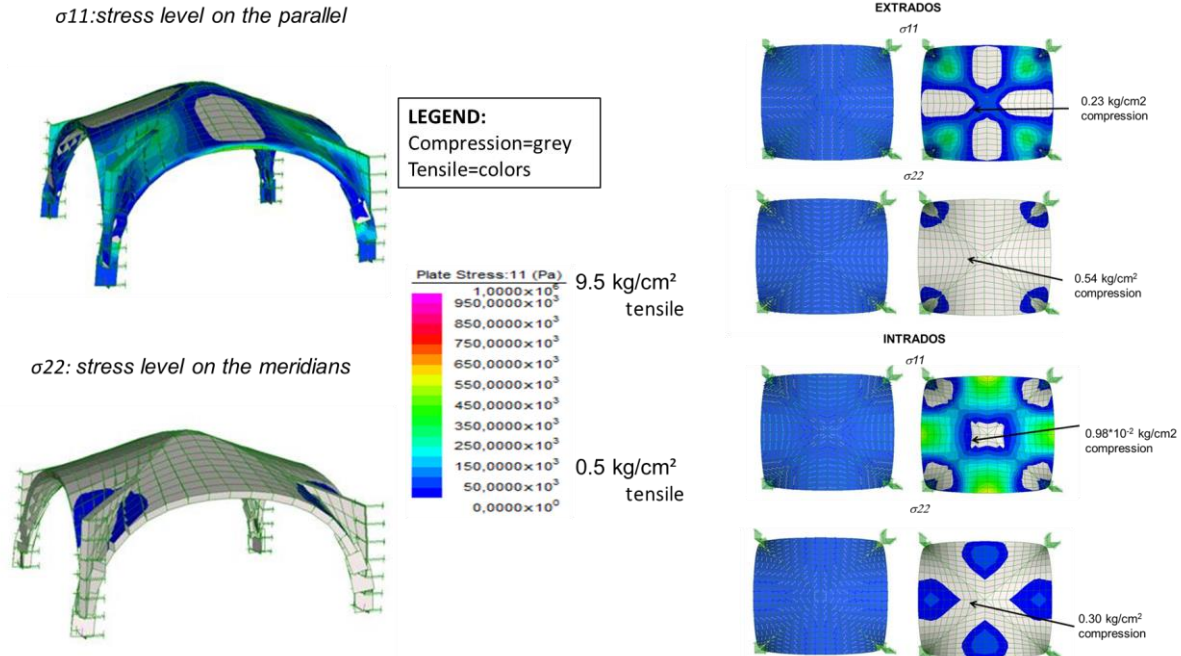


Figure 2.2.30: Stress levels of the vault VNN7 obtained from the dynamic analyses considering the self-weight and the seismic loads

2.3.5 Summary of results from local analyses

The local collapse mechanisms allowed to identify the most vulnerable sub-structures of the cathedral of Modena. In detail, these analyses reveals that, considering a negligible connection between orthogonal masonry walls and between the masonry walls and the possible restraining horizontal elements (“bad connection”) the most vulnerable elements are:

- the top of the façade: the overturning could be occur for acceleration around 0.06g;
- the triumphal arch: the collapse could be occur for acceleration around 0.07g;
- cross vaults: the collapse could be occur for acceleration around 0.12g;
- the apse walls: the out-of-plane behaviour could be occur for acceleration around 0.13g;
- the façade: the overturning could be occur for acceleration around 0.13g;
- longitudinal response of the columns: the mechanism could be occur for acceleration around 0.14g;

It is noted that, considering a good connection, the local mechanisms of collapse for the elements analysed could be activated for highest acceleration values. For this reason, it seems essential to ensure good connection between the orthogonal walls through appropriate interventions.



The static and dynamic analyses developed on the 3D model of the two most damaged vaults, after the 2012 earthquake, reveal that:

- the increment of the stress level (both compression and tensile stress) because of the widening and closing displacements imposed at the springings due to the horizontal movements of the underneath structures (walls and piers). are substantially irrelevant;
- the increment of the stress level because of the shear displacements imposed at the springings due to the horizontal movements of the underneath structures are not negligible. The increment of the tensile stress at the extrados of the vaults can reach $2/3 \text{ kg/cm}^2$, with particular concentrations along the diagonals. The maximum compressive stresses remain instead contained within limits compatible with the resistance of the materials characteristics (below 10 kg / cm^2);

The increment of the stress level because of the acceleration imposed at the springings due to the seismic vibration of the underneath structures (walls and piers) are substantially comparable in terms of maximum tensile stresses to that induced by the shear displacements imposed.

2.3.6 Structural analyses via Discrete Element Method

In the light of the results obtained in the previous section, the cross section located in the fourth span from the west and characterized by different soil stiffness and absence of tie-rods appears the most vulnerable portion of the cathedral (Figure 2.2.31). This cross section has been investigated in order to evaluate the interactions between the vaults and the longitudinal walls under seismic loads.

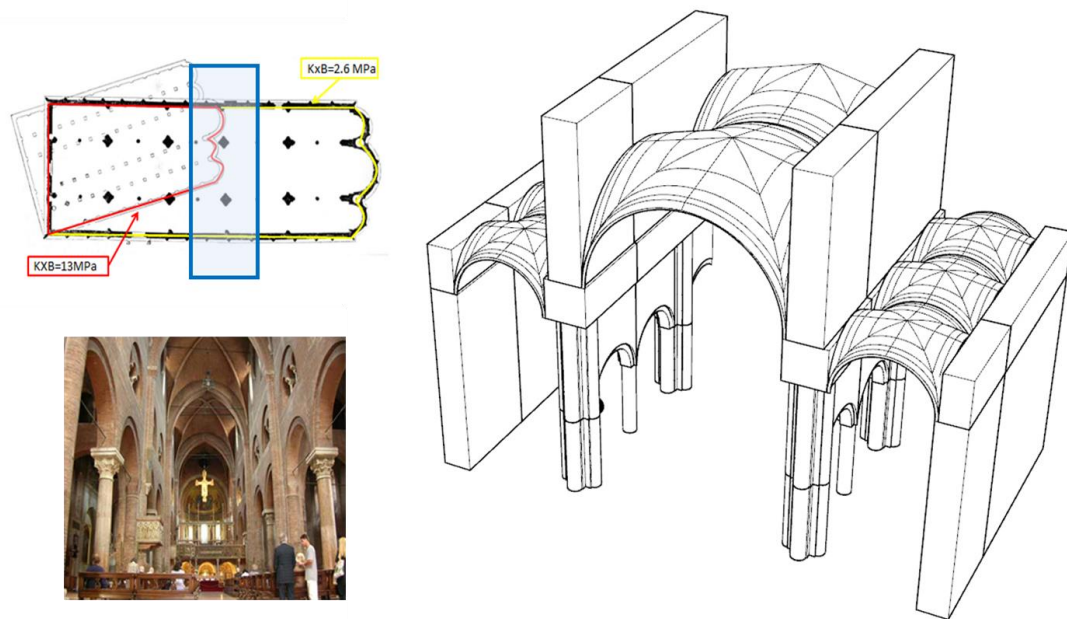


Figure 2.2.31: Position of the cross section studied

2.3.6.1 The model and the analyses

The cross section has been investigated through 2D models (where the density of the blocks and the stiffness at the interfaces takes into account the depth of 10 meters of the walls and of the vaults and the weight of the overlying non-structural elements) in order to evaluate the dynamic response of this portion of the Cathedral and the interaction between the vaults and the longitudinal walls. Figure 2.2.32 schematizes the structural elements of the portion of the Cathedral investigated. Two-limit schematizations have been considered in the analyses:

- (i) 2D cross section modelling the longitudinal walls, the vaults and also the transversal walls (hereinafter called "COMPLETE DEM" and represented in Figure 2.2.32 b) and
- (ii) 2D cross section schematizing only the longitudinal walls and the vaults (hereinafter called "SIMPLIFIED DEM" and represented in Figure 2.2.32 c). The transversal walls are here considered only as weight applied.

The COMPLETE DEM model is analyzed under static loads only, given the onerous computational time required to develop an earthquake time-history analysis. The main issue is to evaluate the detachment of the blocks (corresponding to the cracks openings) and compare them with the observed crack patterns. The SIMPLIFIED DEM model is analyzed under both static gravity loads and earthquake ground motion.

It has to be noted that the complete model is able to account for the lateral thrust exerted by the lower arches, which is not considered in the simplified model. Such a discrepancy may affect the lateral displacement induced by both vertical and horizontal loads.

In the case of dynamic analyses, after the application of the gravity loads, the ground motion recorded in Modena during the 2012 Emilia's earthquake is applied to blocks 9,10,11. The analyses developed are summarized in Table 2.2.10.

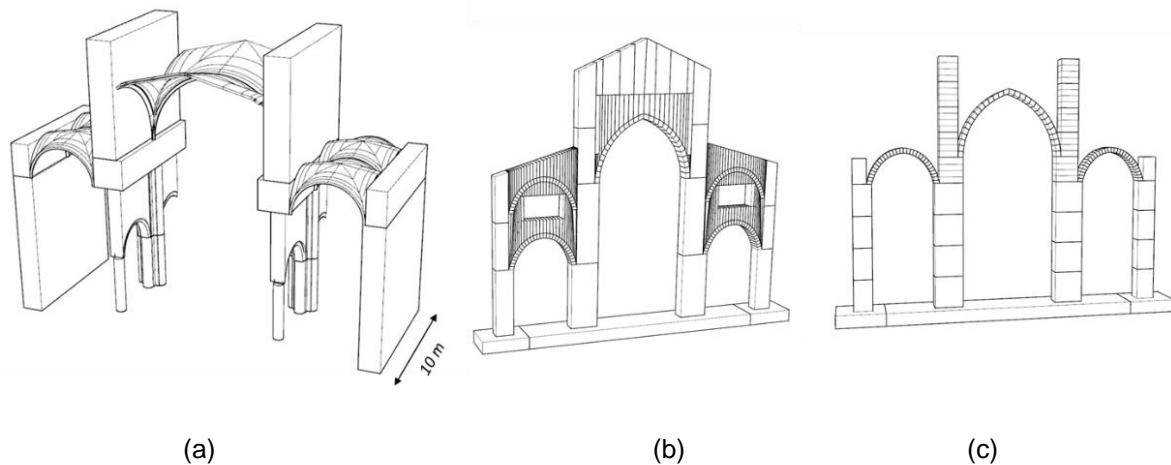


Figure 2.2.32: (a) The investigated cross-section of the Cathedral of Modena: representation of the structural elements, (b) the "COMPLETE DEM", (c) the "SIMPLIFIDE DEM"

Table 2.2.10- The different analyses developed

| Model | Static analysis | Dynamic analysis (Acceleration recorded in Modena) |
|----------------|-----------------|--|
| COMPLETE DEM | x | |
| SIMPLIFIED DEM | X | X |

2.3.6.2 The modelling parameters of the three numerical models

In the next sections, the modelling parameters used in the analyses are only synthetically shown.

Complete DEM model

Figure 2.2.33 a shows the “COMPLETE DEM” model analysed and the names of the elements used in the calculation of the properties of the blocks and interfaces. In particular, Figure 2.2.33 a displays the rendering made with the software Rhinoceros 5 and imported in 3DEC. The specific number of blocks in which the elements have been subdivided is shown in Figure 2.2.33 b (that represents the 3DEC model). It can be noticed that the arches were schematized with six blocks. The modelling parameters used are reported in the Table 2.2.11, Table 2.2.12 and Table 2.2.13.

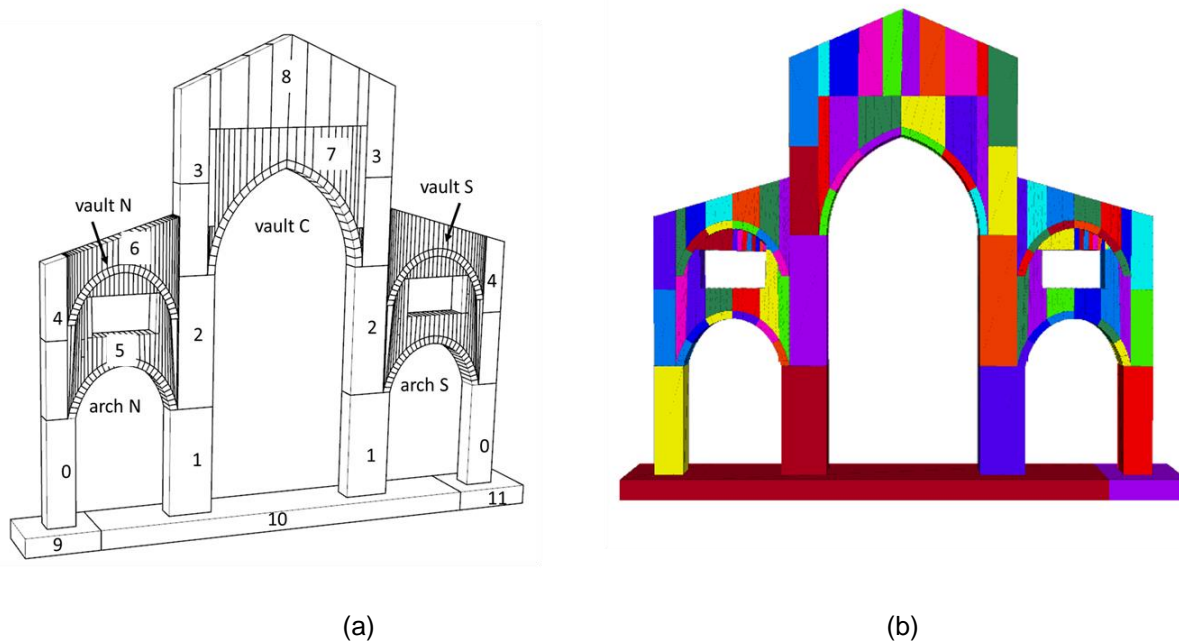


Table 2.2.33: The “COMPLETE DEM” model analysed: (a) The Rhinoceros rendering and the name of the element used in the following calculation, and (b) the 3DEC model



Properties of the blocks:

Table 2.2.11- The properties of the blocks used in the analyses of the “complete cross-section”

| Element | Weight per unit volume [KN/m ³] | *Elastic Modulus [KPa] | Dimension of the blocks [m] | Density [10 ³ Kg/m ³] |
|-------------------|--|---------------------------|--------------------------------|---|
| Wall ₀ | 119 | 4144000 | 1.5·1·5.05 m | 11.9 |
| Wall ₁ | 39 | 1727000 | 2.3·1·5.05 m | 3.9 |
| Wall ₂ | 80 | 1727000 | 1.9·1·1.08 | 8.0 |
| Wall ₃ | 105 | 1727000 | 1.5·1·4.0 | 10.5 |
| Wall ₄ | 144 | 4144000 | 1.1·1·2 | 14.4 |
| Wall ₅ | 17 | 4144000 | | 1.7 |
| Wall ₆ | 19 | 4144000 | | 1.9 |
| Wall ₇ | 24 | 4144000 | | 2.4 |
| Wall ₈ | 17 | 4144000 | | 1.7 |
| Vault N-S | 141 | 4144000 | 0.4·1·0.27 m | 2.44 |
| Vault C | 159 | 4144000 | 0.4·1·0.27 | 4.07 |
| arch N-S | 17 | 4144000 | | 1.7 |

*Elastic modulus used in the calculation of the interfaces stiffness (the blocks are here considered rigid)

Joint stiffness of the interfaces

Table 2.2.12- The properties of the interfaces in the vertical direction used in the analyses

| Interface | Joint Kn [KPa/m] | Joint Ks [KPa/m] |
|--------------------------------------|----------------------|---------------------|
| Wall ₀ –Wall ₄ | 4.4 10 ⁶ | 1.9 10 ⁶ |
| Wall ₁ ·Wall ₂ | 6.5 10 ⁵ | 2.8 10 ⁵ |
| Wall ₂ ·Wall ₃ | 2.7 10 ⁶ | 1.9 10 ⁶ |
| Wall ₄ | 9.7 10 ⁶ | 4.1 10 ⁶ |
| Wall ₇ ·Wall ₈ | 9.98 10 ⁵ | 4.2 10 ⁵ |
| Vault N-S | 3.0 10 ⁷ | 1.3 10 ⁷ |
| Vault C | 1.8 10 ⁷ | 7.5 10 ⁶ |
| Wall ₇ ·Vault C | 1.5 10 ⁶ | 6.3 10 ⁵ |
| Wall ₆ ·Vault N-S | 1.8 10 ⁶ | 7.6 10 ⁵ |
| Wall ₅ ·Vault N_S | 1.97 10 ⁶ | 8.3 10 ⁵ |
| Arch N-S | 1.99 10 ⁷ | 8.4 10 ⁶ |
| Wall ₀ –9 | 5.1 10 ⁴ | 1.3 10 ⁶ |
| Wall ₁ –10 | 1.1 10 ⁴ | 3.0 10 ⁶ |
| Wall ₀ –11 | 2.0 10 ⁴ | 1.3 10 ⁶ |



The equivalent normal stiffness at the base of walls of the cross-section have been used in the analysis and are calculated in the follow Equations:

$$k_{ntot_wall_{0-9}} = k_n + \Delta k_n = 5.1 \cdot 10^4 + 2.6 \cdot 10^6 = 2.7 \cdot 10^6 \frac{kPa}{m}$$

$$k_{ntot_wall_{1-10}} = k_n + \Delta k_n = 1.1 \cdot 10^4 + 6.0 \cdot 10^6 = 6.0 \cdot 10^6 \frac{kPa}{m}$$

$$k_{ntot_wall_{0-11}} = k_n + \Delta k_n = 2.0 \cdot 10^4 + 2.6 \cdot 10^6 = 2.6 \cdot 10^6 \frac{kPa}{m}$$

Table 2.2.13- The properties of the interfaces in the horizontal direction used in the analyses

| Interface | Joint Kn [KPa/m] | Joint Ks [KPa/m] |
|--------------------------------------|-----------------------------|-----------------------------|
| Wall ₃ –Wall ₇ | 4.2 10 ⁶ | 1.810 ⁶ |
| Wall ₇ | 1.8 10 ⁶ | 8 10 ⁵ |
| Wall ₃ -Wall ₆ | 5.5 10 ⁶ | 2.310 ⁶ |
| Wall ₆ | 3.2 10 ⁶ | 1.4 10 ⁶ |
| Wall ₄ -Wall ₅ | 5.5 10 ⁶ | 2.3 10 ⁶ |
| Wall ₂ -Wall ₅ | 5.5 10 ⁶ | 2.3 10 ⁶ |
| Wall ₅ | 3.2 10 ⁶ | 1.4 10 ⁶ |
| Wall ₃ –Wall ₈ | 1.5 10 ⁶ | 6.2 10 ⁵ |

Simplified DEM model

Figure 2.2.34 shows the “SIMPLIFID DEM” model analysed and the names of the elements used in the calculation of the properties of the blocks and interfaces. Also in this case the Figure 2.2.34 b displays the 3DEC model with the respective subdivision in blocks of the elements used in the analyses. The modelling parameters used are reported in the Table 2.2.14 and Table 2.2.15.

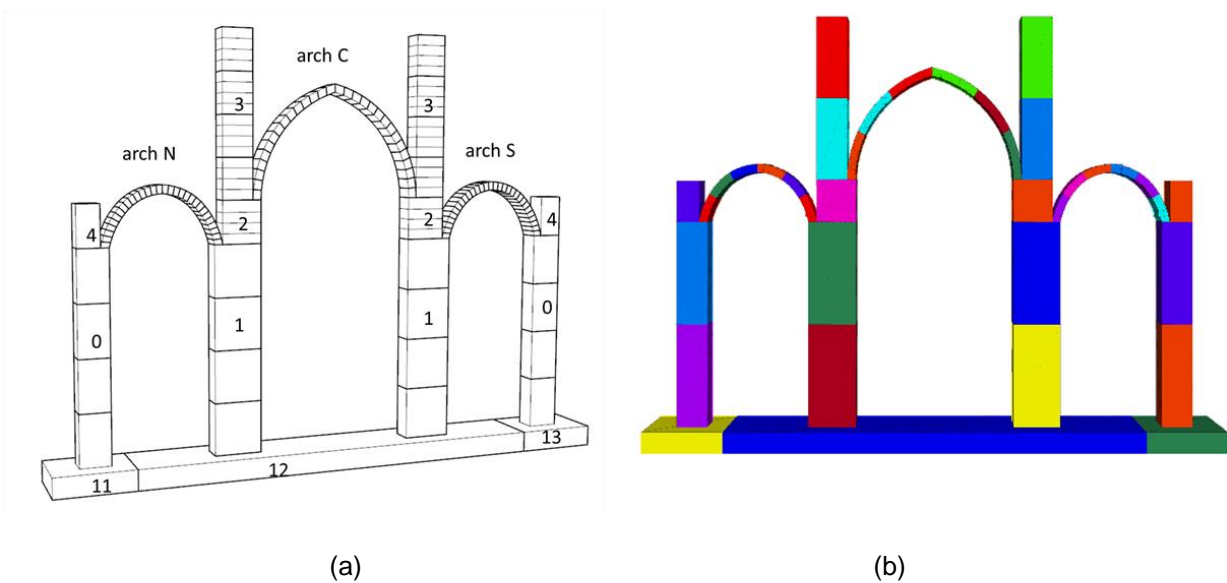


Figure 2.2.34: The “SIMPLIFIED DEM” model analysed: (a) The Rhinoceros rendering and the name of the element used in the following calculation, and (b) the 3DEC model

Properties of the blocks:

Table 2.2.14- The properties of the blocks used in the analyses of the “simple cross section”

| Element | Weight per unit volume [KN/m ³] | *Elastic Modulus [KPa] | Dimension of the blocks [m] | Density [10 ³ Kg/m ³] |
|-------------------|---|------------------------|-----------------------------|--|
| Wall ₀ | 125 | 4144000 | 1.5·1·5.05 m | 12.5 |
| Wall ₁ | 50 | 1727000 | 2.3·1·5.05 m | 5.0 |
| Wall ₂ | 127 | 1727000 | 1.9·1·1.08 | 12.7 |
| Wall ₃ | 140 | 1727000 | 1.5·1·4.0 | 14.0 |
| Wall ₄ | 213 | 4144000 | 1.1·1·2 | 21.3 |
| ArchN-S | 141 | 4144000 | 0.4·1·0.27 m | 14.1 |
| Arch C | 159 | 4144000 | 0.4·1·0.27 | 15.9 |

*Elastic modulus used in the calculation of the interfaces stiffness (the blocks are here considered rigid)



Joint stiffness of the interfaces:

Table 2.2.15- The properties of the interfaces used in the analyses of the “simple cross-section”

| Interface | Joint Kn [KPa/m] | Joint Ks [Kpa/m] |
|--------------------------------------|---------------------------|---------------------------|
| Wall ₀ | 8.2 10 ⁶ | 3.5 10 ⁶ |
| Wall ₀ -Wall ₄ | 1.2 10 ⁷ | 5.0 10 ⁶ |
| Wall ₁ | 7.8 10 ⁵ | 3.3 10 ⁵ |
| Wall ₁ -Wall ₂ | 1.1 10 ⁶ | 4.7 10 ⁵ |
| Wall ₂ -Wall ₃ | 1.3 10 ⁶ | 5.5 10 ⁵ |
| Wall ₃ | 1.2 10 ⁶ | 4.2 10 ⁵ |
| Arch N-S | 3.0 10 ⁷ | 1.3 10 ⁷ |
| ArchN-S-Wall ₀ | 1.3 10 ⁷ | 5.5 10 ⁷ |
| Arch C | 1.8 10 ⁷ | 7.5 10 ⁶ |
| Arch C-Wall ₁ | 1.9 10 ⁷ | 7.9 10 ⁶ |
| Wall ₀ -11 | 2.7 10⁶ | 1.3 10⁶ |
| Wall ₁ -12 | 6.0 10⁶ | 3.0 10⁶ |
| Wall ₀ -13 | 2.6 10⁶ | 1.3 10⁶ |

Damping

$$f_{crit} = \frac{\omega_e \sqrt{2}}{2\pi} = \frac{1391\sqrt{2}}{2\pi} = 222 \text{ cycles / second}$$

2.3.7 Summary of results from Discrete Element Method simulations

Static analyses

Contour maps of the lateral displacements along x direction are reported in Figure 2.2.35. The maximum displacement in the x direction of the longitudinal walls obtained from the static analyses of the COMPLETE DEM model is around 0.012 m (Figure 2.2.35a). Instead, the SIMPLIFIED DEM model provides a maximum displacement by around 0.004m (Figure 2.2.35b). As expected, the COMPLETE DEM model gives larger lateral displacements probably due to the lateral thrust exerted by the lower arches (not modelled in the SIMPLIFIED DEM model).

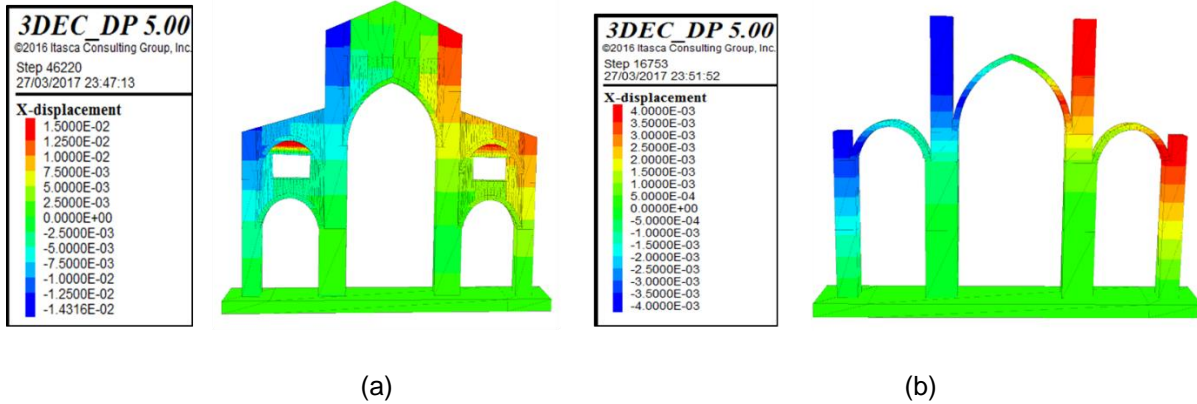


Figure 2.2.35: Contour maps of the lateral displacements along x direction obtained by : (a) COMPLETE DEM model and (b) SIMPLIFIED DEM model

Figure 2.2.36 displays the contour plot of the interfaces, relative block-to-block, displacement (blue indicate an opening between the blocks). The contour plot is qualitatively compared with the crack patterns as observed before the 2012 Emilia Earthquake (see §1.2.4). It can be noted that the block openings agrees with the location of the main cracks. It reminds that the model takes into account of the different soil stiffness at the base of the walls that are probably the first cause of the crack patterns detected before the 2012.

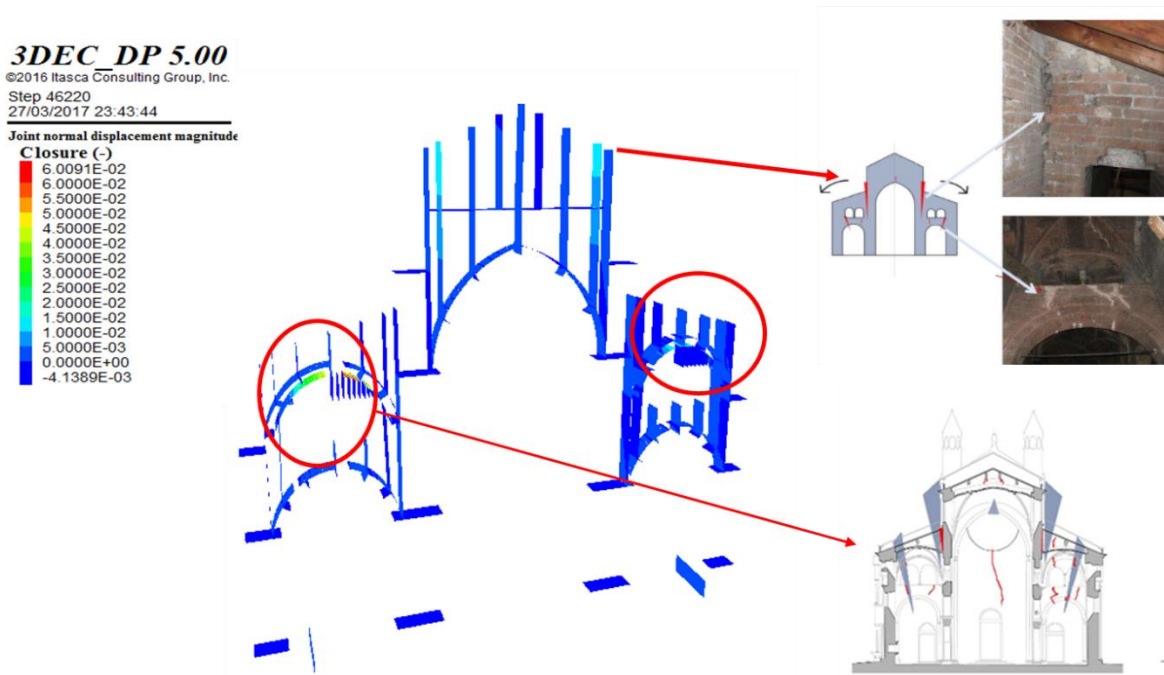


Figure 2.2.36: Contour plot of the interfaces of the COMPLETE DEM model and the crack pattern detected in the 2010

Dynamic analyses

As expected the dynamic analyses performed on the SIMPLIFIED DEM model considering the ground motion recorded in Modena during the 2012 Emilia's earthquake (§1.3.3) do not lead to the collapse of the structure. Figure 2.2.37 displays the contour plot of the interfaces, relative block-to-block, displacement (orange and red colors indicate an opening between the blocks) obtained by the SIMPLIFIED DEM model. It can be noticed that under the seismic loads several new openings appear mainly concentrated on the arches (that schematized the vaults). These openings are in good agreement with the cracks observed after the Emilia Earthquake (own concentrated predominantly in the vaults §1.2.4).

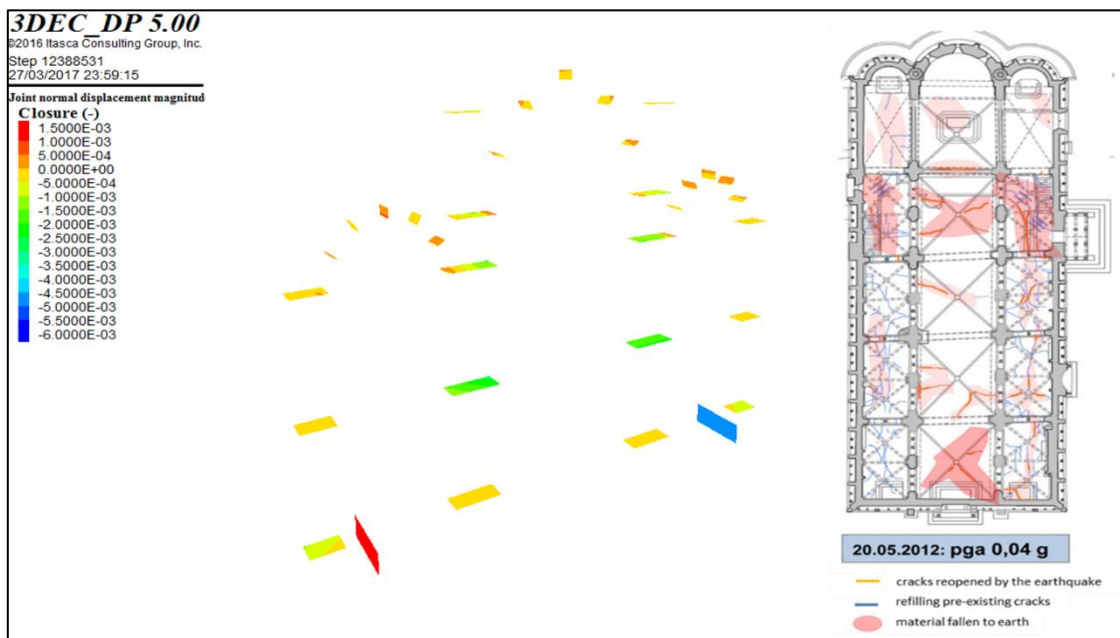


Figure 2.2.37: Contour plot of the interfaces of the SIMPLIFIED DEM model and the crack pattern detected in after the 2012 Emilia earthquake



2.4 Structural Health Monitoring of the Cathedral of Modena

2.4.1 Introduction

In the 2003, a static SHM system has been installed on the Cathedral of Modena.

The large amount of data recorded by the monitoring system has been analyzed, using a simple approach proposed by the authors that relying on a time-domain data processing through the introduction of so-called "reference quantities", which can be interpreted as the "main descriptors" of the recorded data [72],[73].

2.4.2 Reference quantities

A useful analysis of the data from a SHM system have to focus on the identification of the potential evolutionary trends of response, which typically oscillates following the daily and seasonal thermal excursions. To do that, it is first necessary to characterize these seasonal and daily effects by introducing appropriate descriptors, hereafter referred to as "reference quantities"

The collection of these "reference quantities" constitute a specific nomenclature for an interpretation of the data obtained from a structural monitoring that also allow to collect data in a systematic fashion and thus compare them with those of similar structural typologies. The systematic identification of the "reference quantities" from the recorded data allows to identify the presence of potential evolutionary trends of the monitored state by the specific sensor. In effect, the "reference quantities", extracting useful information of the data recorded in a daily and annual span of time, allow to compare these values over all the period of monitoring.

Table 2.2.16 collects the "reference quantities" defined. Sudden drops may be present in the recorded time series. These sudden drops may be related either to an instrument malfunctioning, either to external factors, or to extreme events (such as earthquakes, hurricanes, ...) and are here identified through the letter Δ .



Table 2.2.16- The introduced “reference quantities” for the analysis of the recorded data.

| Reference quantity | Definition | Mean value within the observation period Δt |
|--|---|--|
| Daily Amplitude | $\delta_{day,j} = [\max x(t_i) - \min x(t_i)] \quad \forall t_i \in \text{j-th day}$ | $\bar{\delta} = \frac{1}{N_{\Delta t}} \sum_{j=1}^{N_{\Delta t}} \delta_{day,j}$ |
| Mean Daily Value | $\mu_{day,j} = \frac{1}{n_j} \sum_{i=1}^{n_j} x(t_i) \quad \forall t_i \in \text{j-th day}$ | $\bar{\mu} = \frac{1}{N_{\Delta t}} \sum_{j=1}^{N_{\Delta t}} \mu_{day,j}$ |
| Absolute Daily Residuals of the Mean Value | $r_{\mu day,j(k-k_0)} = \mu_{\mu day,j(k)} - \mu_{\mu day,j(k_0)}$ | $\bar{r}_{\mu} = \frac{1}{N_{\Delta t}} \sum_{j=1}^{N_{\Delta t}} r_{\mu day,j(k-k_0)}$ |
| Progressive Daily Residuals of the Mean Value | $rp_{\mu day,j(k_{+1}-k)} = \mu_{day,j(k_{+1})} - \mu_{day,j(k)}$ | $\bar{rp}_{\mu} = \frac{1}{N_{\Delta t}} \sum_{j=1}^{N_{\Delta t}} rp_{\mu day,j(k_{+1}-k)}$ |
| Annual Amplitude | $\Sigma_{year,y} = [\max x(t_i) - \min x(t_i)] \quad \forall t_i \in \text{y-th year}$ | $\bar{\Sigma} = \frac{1}{N_{\Delta t}} \sum_{y=1}^{N_{\Delta t}} \Sigma_{year,y}$ |
| Mean Annual Value | $M_{year,y} = \frac{1}{n_y} \sum_{i=1}^{n_y} x(t_i) \quad \forall t_i \in \text{y-th year}$ | $\bar{M} = \frac{1}{N_{\Delta t}} \sum_{y=1}^{N_{\Delta t}} M_{year,y}$ |
| Absolute Annual Residuals of the Mean Value | $R_{M year,(k-k_0)} = M_{year,k} - M_{year,k_0}$ | $\bar{R}_M = \frac{1}{N_{\Delta t}} \sum_{y=1}^{N_{\Delta t}} R_{M year,(k-k_0),y}$ |
| Progressive Annual Residuals of the Mean Value | $Rp_{M year,(k_{+1}-k)} = M_{year,k_{+1}} - M_{year,k}$ | $\bar{Rp}_M = \frac{1}{N_{\Delta t}} \sum_{y=1}^{N_{\Delta t}} Rp_{M year,(k_{+1}-k),y}$ |
| Drop | Δ | |

2.4.3 Types and location of instruments

The monitoring system allows monitoring the main cracks across the walls and vaults, the relative displacements between the cathedral and the Ghirlandina tower, the inclination of the external longitudinal walls, and the temperature. Most of the instruments were installed in 2003, while others (such as the deformers and inclinometers) were installed at the end of 2010. Data are acquired at time intervals of 30 minutes. The following symbols have been used to indicate the type of instrument:

D=deformer, **MGB**=biaxial joint meter, **MGT**= triaxial joint meter, **FP**=inclinometer, **T**= thermometer.

The different instruments installed on the Cathedral are displayed in Figure 2.2.38.

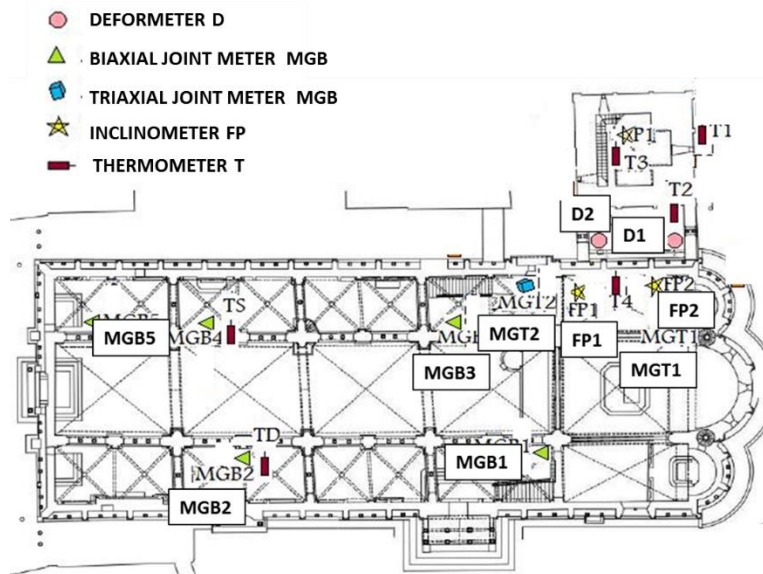


Figure 2.2.38: Location of the sensors.

The instruments installed on the Cathedral are briefly described below.

Invar Deformeter

The deformeters were placed on the buttresses between the Cathedral and the Ghirlandina Tower (Figure 2.2.39). They are designed to perform the deflection measurements of a structure of a substantial amount (in this case have an overall length of 5 meters). They consist of Invar rods having a low coefficient of thermal expansion. On the wall of the Ghirlandina tower was put the anchor support, while on the Cathedral wall is anchored to a non-contact sensor of the inductive type with 8 mm theoretical measurement range with a resolution of 0.01 mm. They are fed to a continuous voltage of 24 Vdc and the analog output signal is between 4 and 20 mA proportional to the distance between the transducer and the target. Conventionally the positive values on the graphs, which will be explained later, correspond to an estrangement between the Tower and the Cathedral, while negative values correspond to a rapprochement of the two.

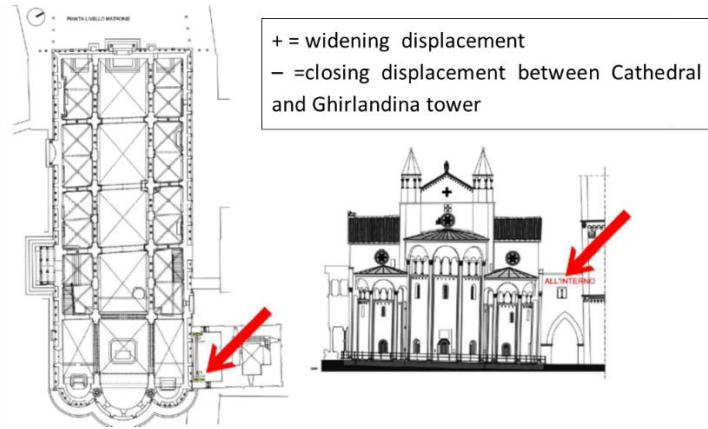


Figure 2.2.39: Deformer installed on the buttress of the Cathedral (D1)

Biaxial joint meter- Triaxial joint meter

The variation in the opening of cracks in the bearing elements, due in most cases to the interaction with the ground and / or to an intrinsic degradation of materials is carried out by means of measuring instruments such as joint meters or deformeters. The joint meters are bound rigidly to the wall using anchors at the turn of the crack to be monitored. They may be biaxial, in this case the measure movements detected are in a plane (for example, a wall surface) (Figure 2.2.40) or triaxial if are able to detect also the displacements orthogonal to the plane (Figure 2.2.41). Seven main cracks of the Cathedral have been monitored through these sensors. In particular, in 2003, four biaxial joint meters were installed in the central nave and a triaxial joint meter were installed in the wall close to the two buttresses that link the Cathedral and the Tower. In December 2010, other two joint meters were installed.

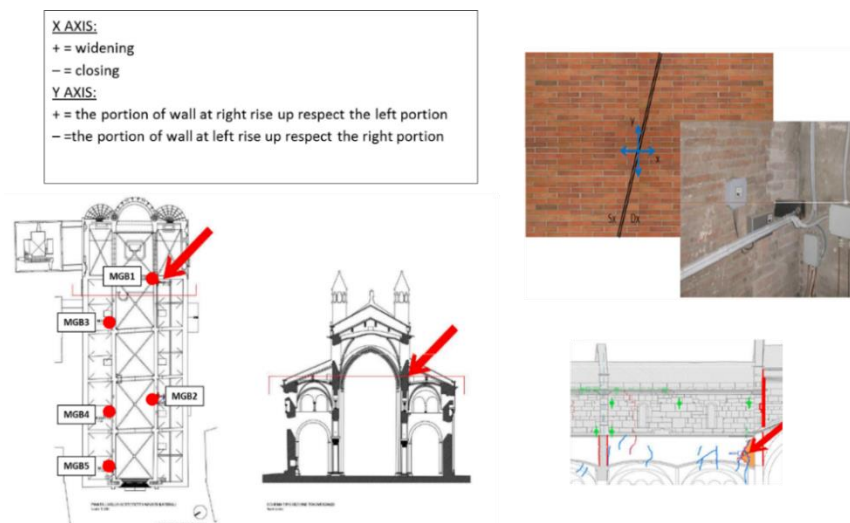


Figure 2.2.40: Biaxial joint meter installed in the central nave of the Cathedral (MGB1)

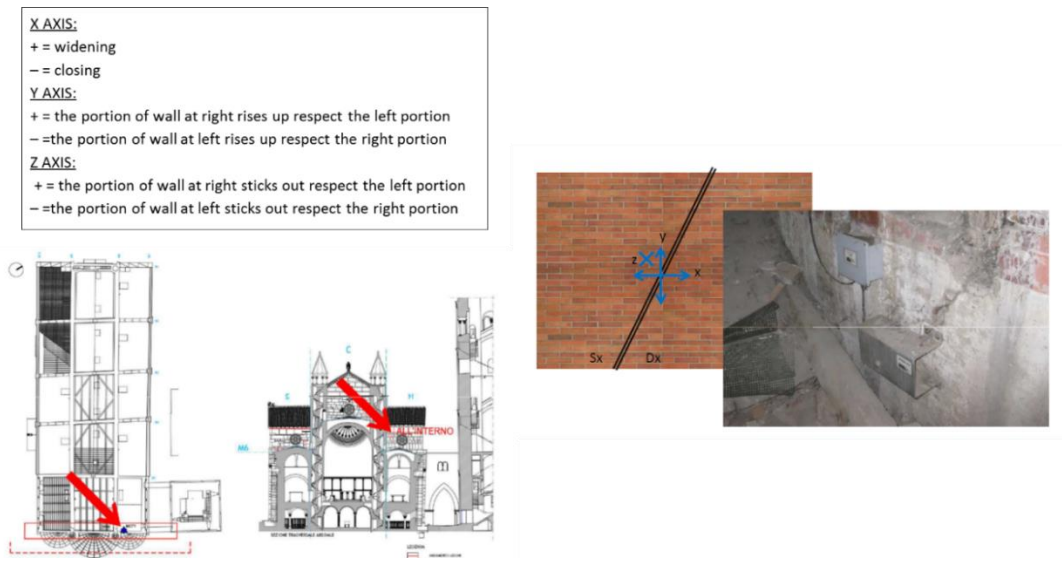


Figure 2.2.41: Triaxial joint meter installed in the longitudinal wall of the Cathedral (MGT1)

Inclinometer

The inclinometers (or pendulums) installed on the cathedral are designed for the control of the stability of the buildings, and their operation is based on the principle of a plumb line (Figure 2.2.42). It consists of: an upper berth, to the plumb bob (consists of Invar alloy to contain the thermal expansions), and the measuring instrument (that allows to perform the automatic measurement of the plumb line portion). This data allow analysing the slope changes of the Cathedral, both periodic (due to temperature variations) and permanent ones due to real structural behaviour.



Figure 2.2.42: Inclinometer installed on the longitudinal wall of the cathedral (close to the buttress) FP1 and the conventional signs used.



2.4.4 Reference quantities

The reference quantities defined in § 2.4.2 have been identified for all the data recorded by sensor of the monitoring system installed on the Cathedral of Modena.. In the next section, the salient results, obtained from the interpretation of the static monitoring data through the proposed procedure, are illustrated.

Invar deformer

The deformers Di and D2, placed on the buttresses between the Cathedral and the Ghirlandina Tower in order to monitor the movements between the two structures, recorded significant drops during the seismic event that hit the Emilia Romagna in May 2012. In particular, the drops corresponding to the two days where the tremors of greatest intensity were recorded (20th and 29th May 2012). As mentioned above, positive values on the graph correspond to an estrangement between the Tower and the Cathedral, while negative values correspond to a rapprochement of the two.

Deformers D1

From 1th January 2011 until 20th May 2012, D1 records a slight estrangement between the Cathedral and the tower. After the 2012 earthquake, the trend recorded by this device changes considerably. On days 20th and 29th May it has recorded two drops of $\Delta_{20\text{may}} = 0.53\text{mm}$ and $\Delta_{29\text{may}} = 0.3\text{ mm}$, respectively, that indicate an approaching of the two structures (Figure 2.2.43). After the seismic event, the recorded data are negative, indicating a progressive approach between Ghirlandina and Cathedral. This sensor is characterized by several missing data; therefore, the systematic identification of the reference quantities does not lead to significant results. However, it is interesting to note that the mean value of the daily amplitude, not considering the data recorded in the 2012, is around of 0.03 mm. The daily amplitudes recorded on 20th and 29th May are, thus, around 20 times more than the mean value of the daily amplitude recorded in the other years.

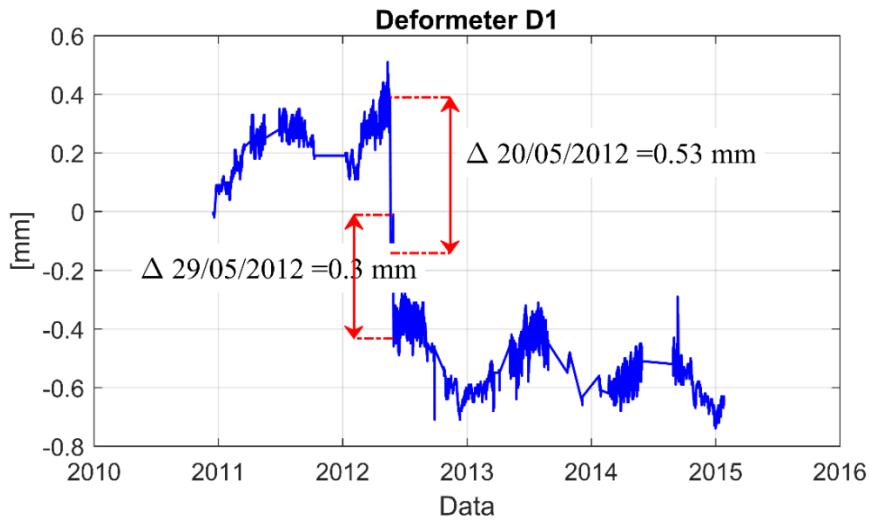


Figure 2.2.43: Data recorded by the deformer D1 installed on the buttresses between the Cathedral and the Ghirlandina Tower

Deformeters D2

The deformer D2 does not record specific anomalies during the main shocks of the 2012 Emilia earthquake. However, a drop was recorded in 27th August 2012 (August $\Delta 27 = 0.4$ mm). On that date it is detected a earthquake of much lower intensity compared to those of May during which the device did not show significant changes. It excludes, therefore, that the cause of this drop is due to slight earthquake but it's probably due to interference. Before and after the drop, the device has recorded a cyclical trend. The negative values on the graph correspond to a rapprochement between the cathedral and the tower (Figure 2.2.44).

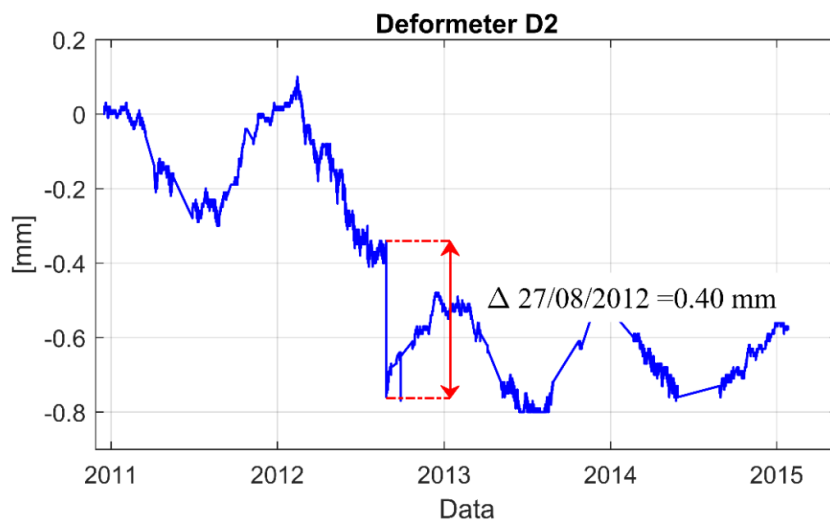


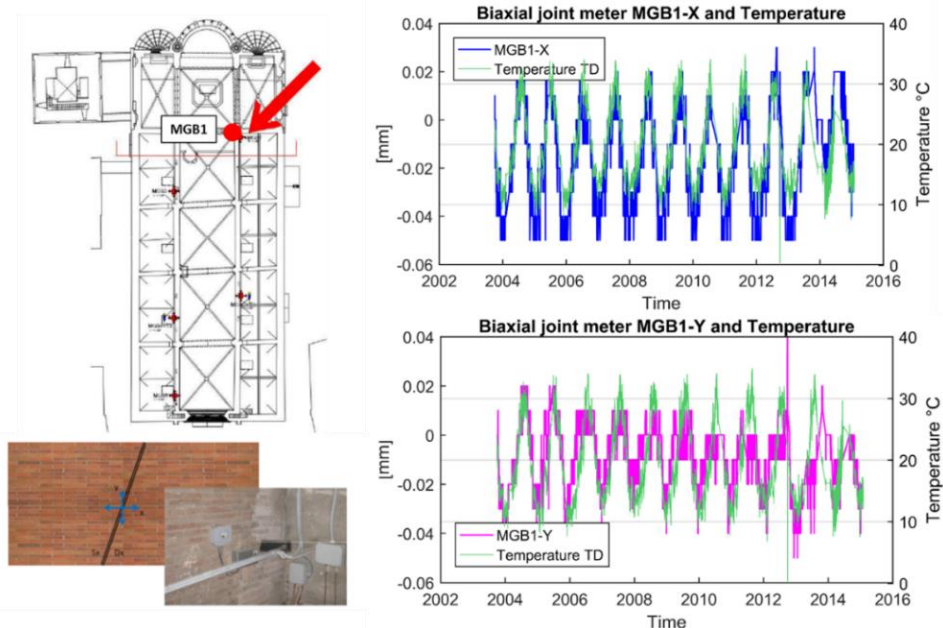
Figure 2.2.44: Data recorded by the deformer D2 installed on the buttresses between the Cathedral and the Ghirlandina Tower

Joint meter

The biaxial joint meters MGB1, MGB2, MGB3, MGB4 and the triaxial joint meter MGT1 were installed in October 2003 while MGB5 and MGT2 was added later in 2010. It is noted that MGT2 is characterized by many missing data. For this reason its data are not reliable in order to perform evaluations on the structural health and their will not considered in the following analyses.

Biaxial joint meter MGB1

The sensor MGB1 monitors the movements of a crack located in the South aisle, apse side in correspondence with the cracks area which transversely crosses the fourth nave. The temperature effect is significant and the recorded data evidence a high direct correlation with respect to the temperature data (Figure 2.2.45 a). When the temperature increases, in fact, the wall tends to expand with consequent closure of the crack and, vice versa, with the decrease of the temperature, the masonry walls tends to compresses with a widening of the crack. The absolute daily residuals reveal that the crack under observation has opened of 0.02 mm and the portion of wall at right of the crack rise up of 0.03 mm respect the left portion, during all years of monitoring (Figure 2.2.45 b, c).



(a)

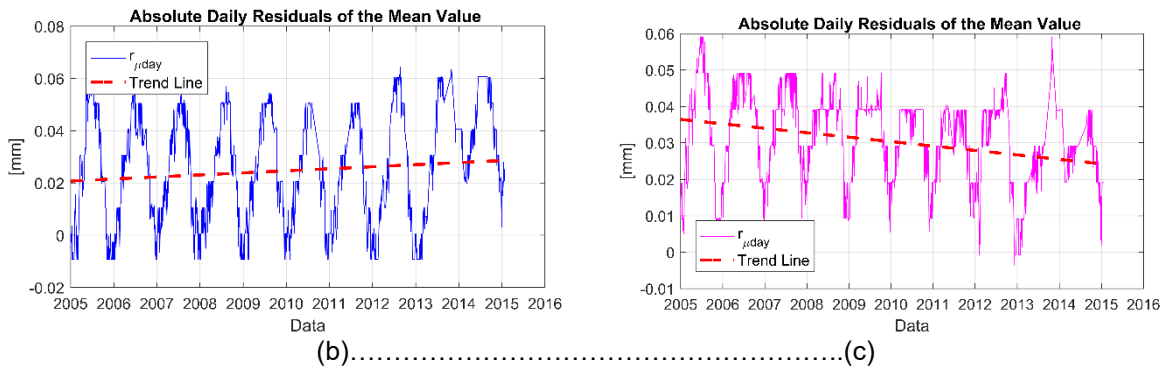


Figure 2.2.45: Biaxial joint meter MGB1: row-data recorded by MGB1 considering also the temperature variation, as recorded by the thermometer TD, and (b),(c) the absolute daily residuals evaluated for both X and Y direction

Biaxial joint meter MGB2

The sensor MGB2 monitors the movements of a crack located in the South aisle in correspondence with the cracks area, which transversely crosses the second nave. The data recorded are in phase with respect to temperature data (Figure 2.2.46 a). MGB2 records a cyclical trend that is repeated for all the years and, as already seen for MGB1, probably due to the correlation with the thermal variations. The trend of the daily amplitudes is, in fact, regular. Unlike what was seen for the previous device, MGB2 shows a decreasing trend over the years for both the X component that Y. This indicates that the lesion tends progressively to open up and the portion of wall at left of the crack rises up compared to the wall at the right. However, the absolute daily residuals reveal that the movements are small: a cumulative trend of -0.04 mm in both the directions is recorded (Figure 2.2.46 b, c).

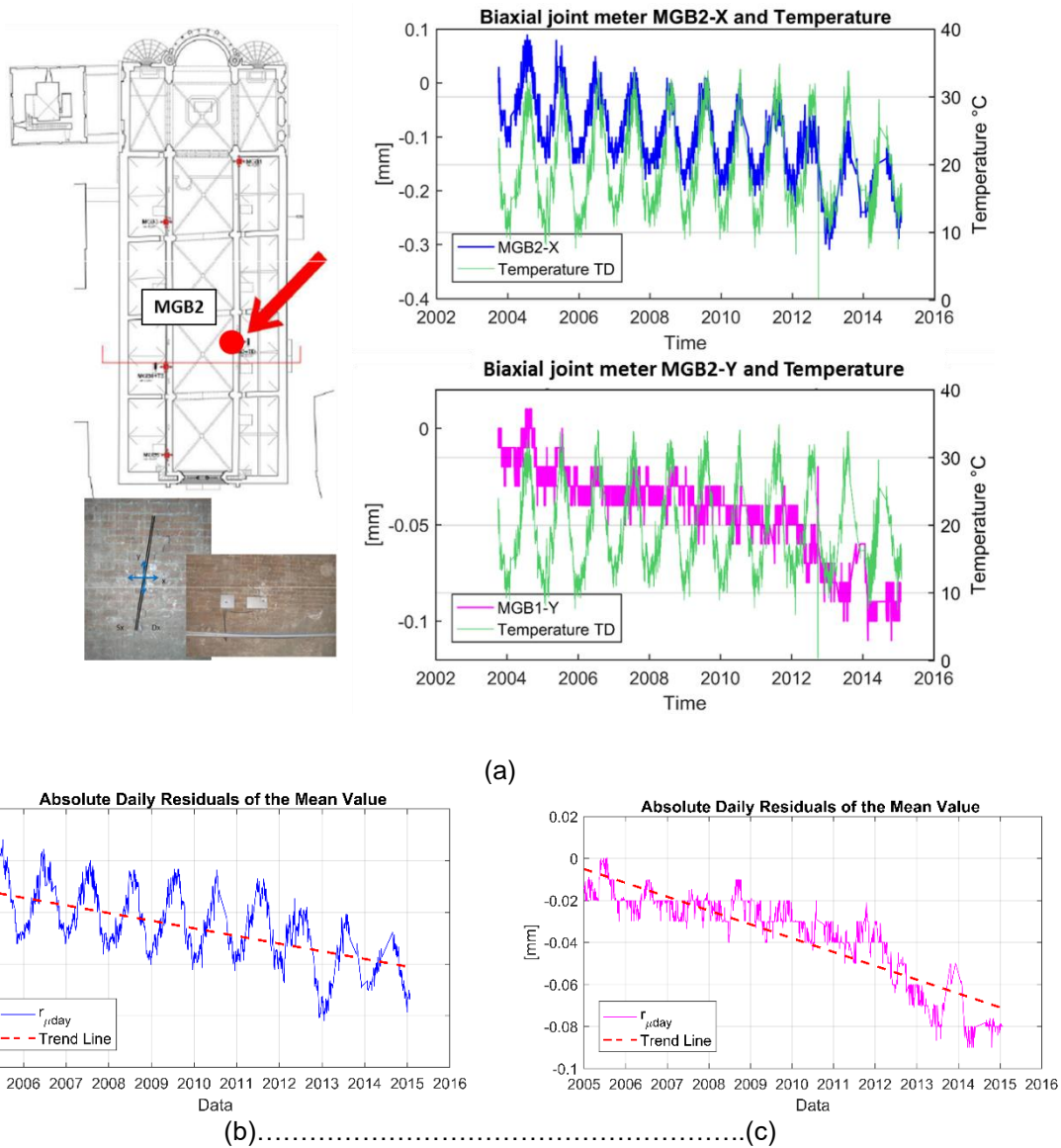


Figure 2.2.46: Biaxial joint meter MGB2: row-data recorded by MGB2 considering also the temperature variation, as recorded by the thermometer TS, and (b),(c) the absolute daily residuals evaluated for both X and Y direction

Biaxial joint meter MGB3

The sensor MGB3 monitors the movements of a crack located in the North aisle, apse side in correspondence with the cracks area, which transversely crosses the second nave. The recorded data for the x component evidence a high direct correlation with respect to the temperature data. The data recorded for the y component appears to be out of phase with the temperature data (Figure 2.2.47a). The x component recorded a decreasing trend throughout the observation period, and then a gradual opening of the crack (with a cumulative trend of -0.03 mm), (Figure 2.2.47b). The y component, instead, recorded an increasing trend that indicates that the portion of the wall at the left

of the crack rise up with respect to that of the right. Then until 2014, a decreasing trend has been recorded. The absolute daily residuals reveal for the y component a cumulative trend of +0.05mm (Figure 2.2.47 c).

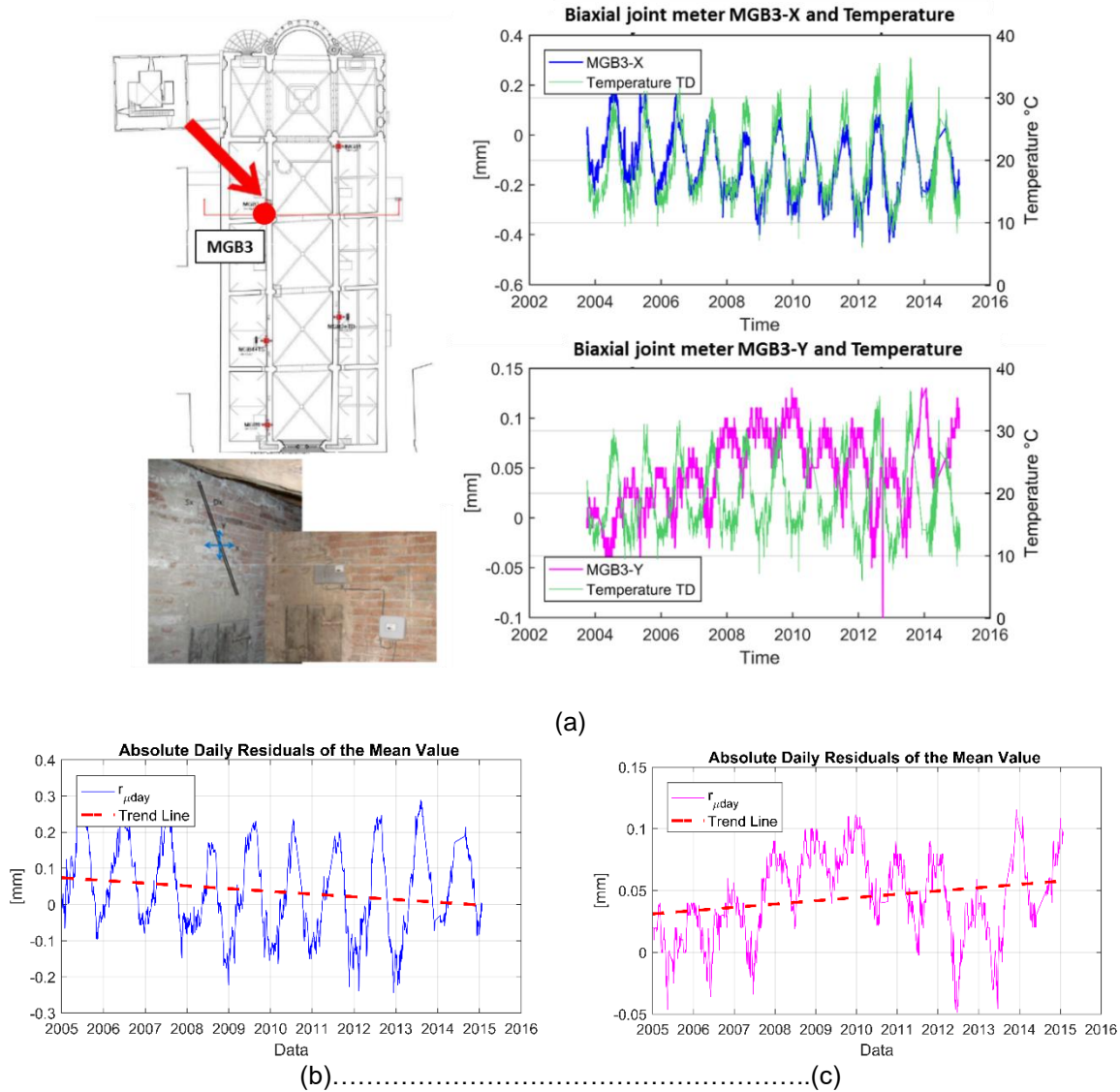


Figure 2.2.47: Biaxial joint meter MGB3: row-data recorded by MGB3 considering also the temperature variation, as recorded by the thermometer TS, and (b),(c) the absolute daily residuals evaluated for both X and Y direction

Biaxial joint meter MGB4

The sensor MGB4 monitors the movements of a crack located in the North aisle. The recorded data are in phase with respect to the temperature data recorded by the thermometer TS (Figure 2.2.48 a). The x component shows a decreasing trend, which indicates a slight opening of the crack. The absolute daily residuals reveal for the x component a cumulative trend of -0.1 mm (Figure 2.2.48 b).

Even the y component registers a decreasing trend (the portion of wall at left of the crack tends to rise compared to the wall at the right). Moreover, three drops are recorded in 20th, 29th May and 28th September 2012, respectively of $\Delta_{20\text{May}} = 0.05$ mm, $\Delta_{29\text{May}} = 0, 08$ mm and $\Delta_{28\text{September}} = 0.10$ mm. The first two drops correspond with the tremors of greatest intensity of the seismic event of May 2012. The list of earthquakes recorded in Modena does not present significant earthquakes in September. The absolute daily residuals reveal for the y component a cumulative trend of -0.13 mm (Figure 2.2.48 c).

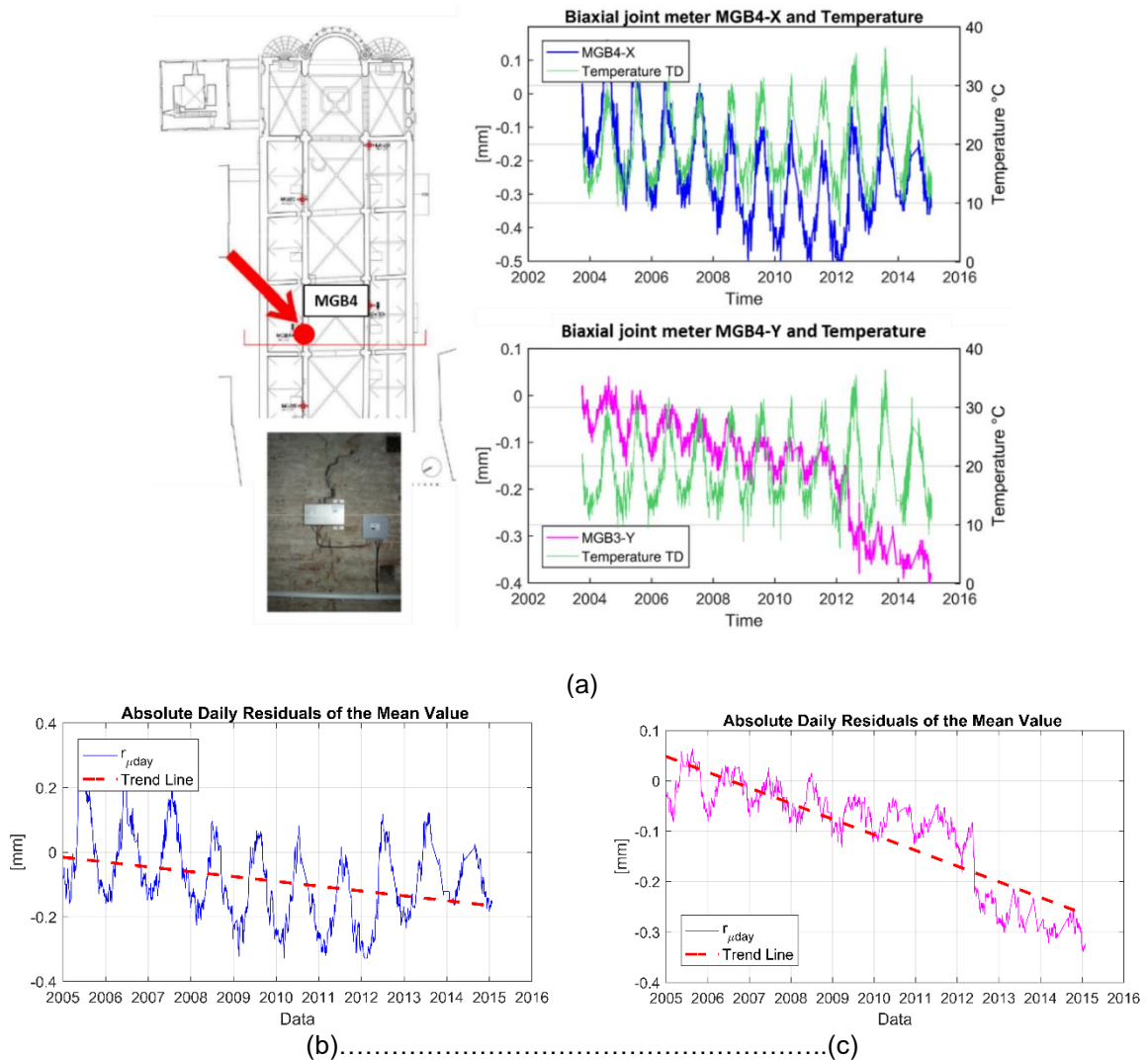
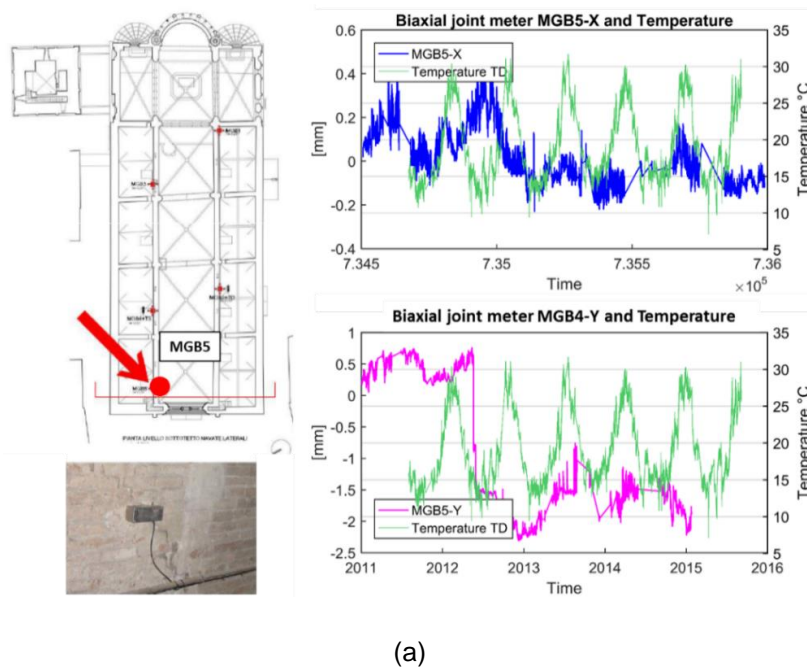


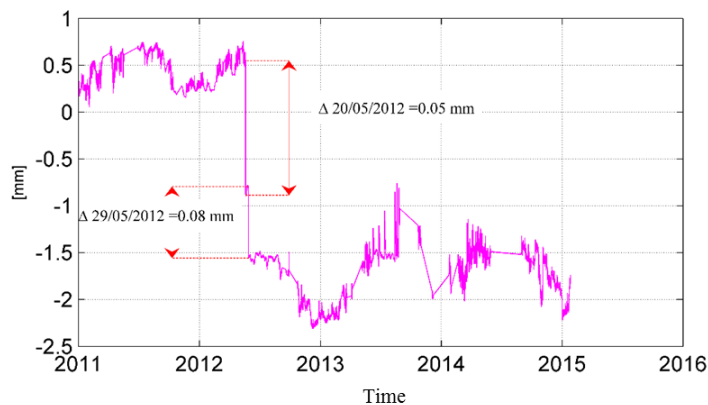
Figure 2.2.48: Biaxial joint meter MGB4: row-data recorded by MGB4 considering also the temperature variation, as recorded by the thermometer TS, and (b),(c) the absolute daily residuals evaluated for both X and Y direction

Biaxial joint meter MGB5

The sensor MGB5 was installed in 2010 to monitor a crack present in North aisle. The recorded data indicate that the opening of the crack (x-direction) has followed a cyclical pattern substantially due to thermal variations (Figure 2.2.49 a). The y component instead shows, in addition to cyclical trends relate to the temperature, two significant drops in correspondence of 20 and 29 May 2012 (Figure 2.2.49 b). These drops indicate that seismic events in May 2012 have led to an, albeit slight, changes in the relative quota between the two walls close to the crack, with the portion of the wall to the left of the crack that is rise up of approximately 1.5 mm with respect to the right.



(a)

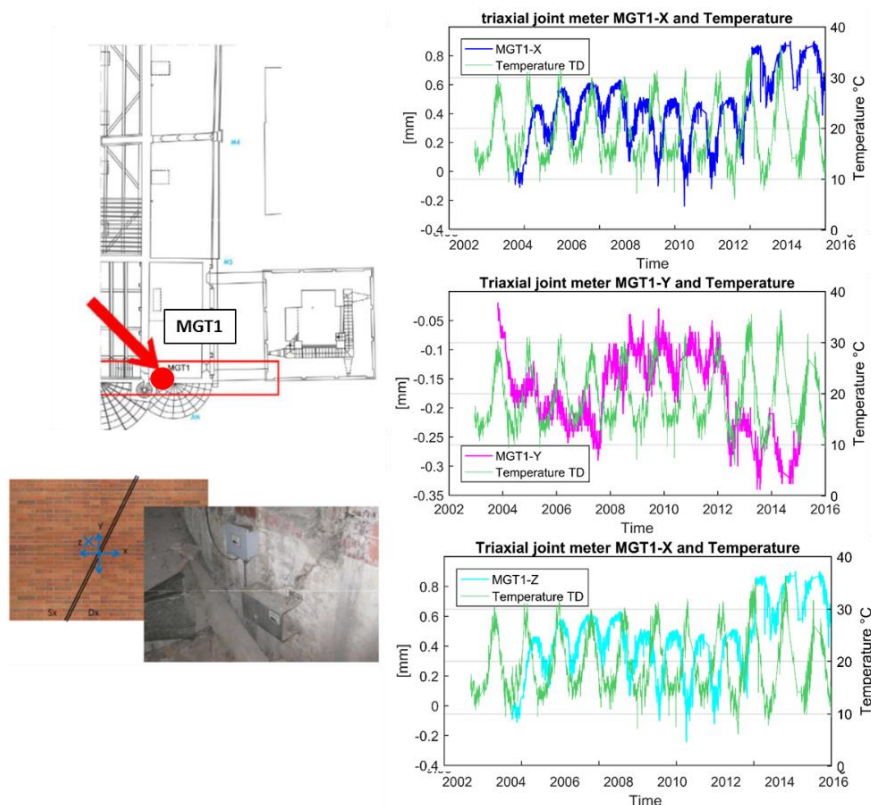


(b)

Figure 2.2.49: Biaxial joint meter MGB5: row-data recorded by MGB5 considering also the temperature variation, as recorded by the thermometer TS and (b) the drops recorded in the y direction during the seismic events of May 2012

Triaxial joint meter MGT1

The sensor MGT1 monitors the movements of a crack located in the transversal wall close to the apses. The recorded data are in phase with respect to the temperature data recorded by the thermometer TS (Figure 2.2.50 a). In the x direction, MGT1 records a cyclical trend substantially related to the effects of temperature variations. However, a slight increasing trend concentrated in the last years is recorded indicating the tendency of the crack to close over the time. The absolute daily residuals reveal a cumulative trend of -0.5 mm (Figure 2.2.50 b). The y component shows a decreasing trend until 2008 (the portion of the wall to the left of the crack rise up compared to that of the right). From 2008 until 2012, the device recorded a recovery indicated by the increasing trend. During seismic events, a total drop of $\Delta = 0.13$ mm has been recorded indicating a further lifting of the left wall compared to that of the right . The absolute daily residuals reveal a cumulative trend of -0.1 mm in the thirteen years of monitoring (Figure 2.2.50c). The recordings detected in the Z direction (perpendicular to the plane) show an increasing trend, indicating, therefore, an increase in the protrusion of the right wall compared to that of the left with a cumulative residua of 0.14 mm (Figure 2.2.50 a, d).



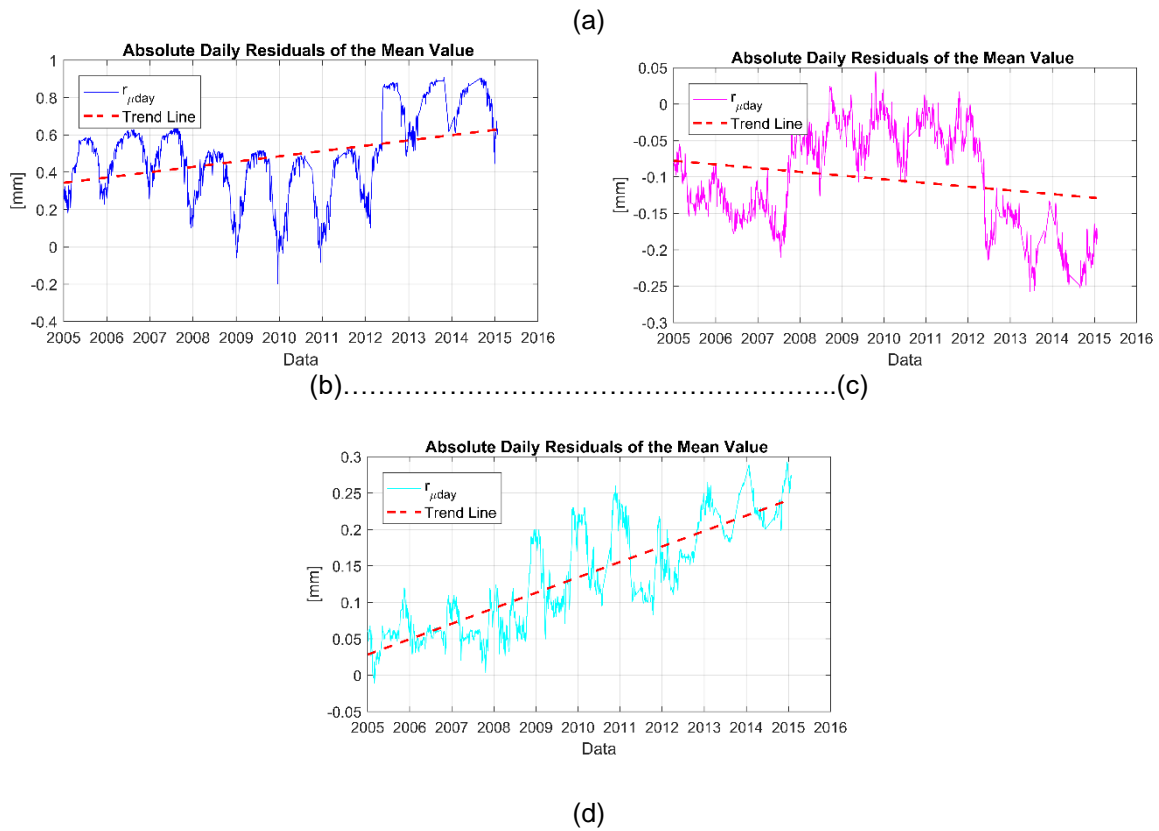


Figure 2.2.50: Triaxial joint meter MGT1: row-data recorded by MGT1 considering also the temperature variation, as recorded by the thermometer TS, and (b),(c), (d) the absolute daily residuals evaluated for both X, Y and Z direction

The mean values over the entire observation period of the reference quantities are collected in Table 2.2.17 for all the joint meters.

Table 2.2.17- Mean values of the reference quantities over the thirteen years of monitoring for the joint meters

| Sensor | Year | $\delta_{day,j}$ [mm] | $rp_{\mu day}$ [mm] | $r_{\mu day}$ [mm] | M_{year} [mm] | Σ_{year} [mm] | Rp_{Myear} [mm] | R_{Myear} [mm] |
|--------|------|--------------------------|------------------------|-----------------------|--------------------|-------------------------|----------------------|---------------------|
| MGB1-X | mean | 0.006 | 0.000 | 0.024 | -0.016 | 0.078 | 0.001 | 0.013 |
| MGB1-Y | mean | 0.005 | -0.001 | 0.029 | -0.010 | 0.053 | 0.000 | 0.013 |
| MGB2-X | mean | 0.020 | -0.014 | -0.043 | -0.124 | 0.200 | -0.016 | -0.061 |
| MGB2-Y | mean | 0.005 | -0.006 | -0.042 | -0.049 | 0.038 | -0.007 | -0.037 |
| MGB3-X | mean | 0.022 | -0.009 | 0.033 | -0.129 | 0.408 | -0.006 | -0.005 |
| MGB3-Y | mean | 0.007 | 0.005 | 0.048 | 0.053 | 0.098 | 0.009 | 0.048 |
| MGB4-X | mean | 0.018 | -0.015 | -0.095 | -0.250 | 0.376 | -0.017 | -0.114 |



ALMA MATER STUDIORUM
UNIVERSITA' DI BOLOGNA

DICAM

Dipartimento di Ingegneria Civile,
Chimica, Ambientale e dei Materiali

MiChE

Mitigating the Impacts of natural hazards on Cultural Heritage
sites, structures and artefacts

| | | | | | | | | |
|---------------|------|-------|--------|--------|--------|-------|--------|--------|
| MGB4-Y | mean | 0.007 | -0.024 | -0.129 | -0.174 | 0.108 | -0.030 | -0.142 |
| MGB5-X | mean | 0.059 | -0.041 | -0.104 | 0.011 | 0.333 | -0.051 | -0.198 |
| MGB5-Y | mean | 0.085 | -0.457 | - | -0.954 | 0.707 | -0.239 | - |
| MGT1-X | mean | 0.035 | 0.035 | 0.501 | 0.462 | 0.536 | 0.050 | 0.484 |
| MGT1-Y | mean | 0.012 | -0.008 | -0.113 | -0.184 | 0.398 | -0.017 | -0.140 |
| MGT1-Z | mean | 0.011 | 0.016 | 0.146 | 0.179 | 0.125 | 0.024 | 0.159 |

Inclinometer

Inclinometer FP1

The sensor FP1, located in the longitudinal wall close to the buttressed, measures the variation of the inclination of the wall. FP1 pendulum recorded a constant trend, in both the directions, up to 20 May 2012. During the 2012 earthquake, and particularly in the two days where the most significant tremors are recorded, two drops in both directions were recorded (Figure 2.2.51). The drops recorded on 20 and 29 May indicate a movement of the top of the wall of about 1.0 mm in the South-West direction, and equal to about 1.3 mm in the southeast. It is noted that in the months following the earthquake sequence have been recorded jumps probably due to interference in the instrument recording because there have been no significant seismic events on those dates. In particular, the 24th October 2014 the device records a drop that allows to recover most of the overhangs recorded during the earthquake of May 2012.

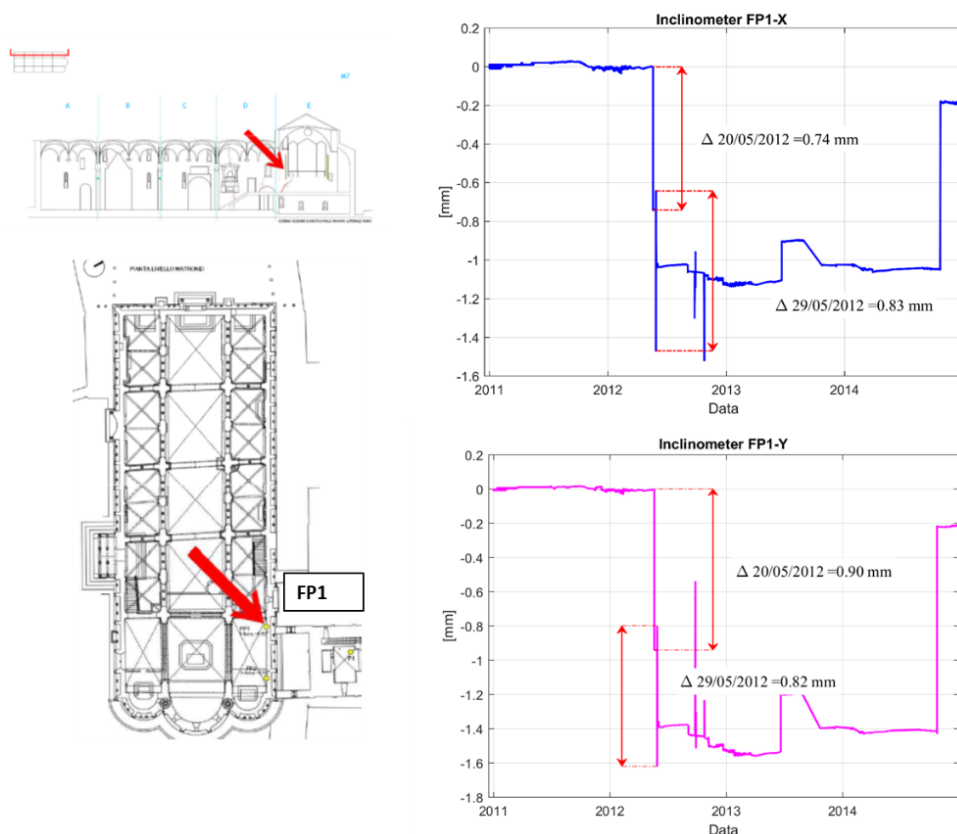


Figure 2.2.51: Inclinometer FP1: row-data recorded by FP1 highlighted the drops recorded during the 2012 earthquake

Inclinometer FP2

The sensor FP2 is located in the some longitudinal wall of FP1, close to the buttressed. FP2 has recorded a similar behaviour to that recorded by FP1. Before the 2012 earthquake, FP2 recorded a regular trend with very small daily amplitudes oscillations. On 20th and 29th May 2012, drops in both the directions were recorded. The drops recorded indicate movements of the top of the wall to the South-West direction (towards the inside of the Cathedral) of about 1.68 mm. On 28th September 2012 was registered another drop probably due to interference, given that it has been fully recovered on the same day, while the 21 June 2013 is recorded a drop in both the directions, indicating a further movements of the top of the wall toward the inside of the Cathedral (Figure 2.2.52)

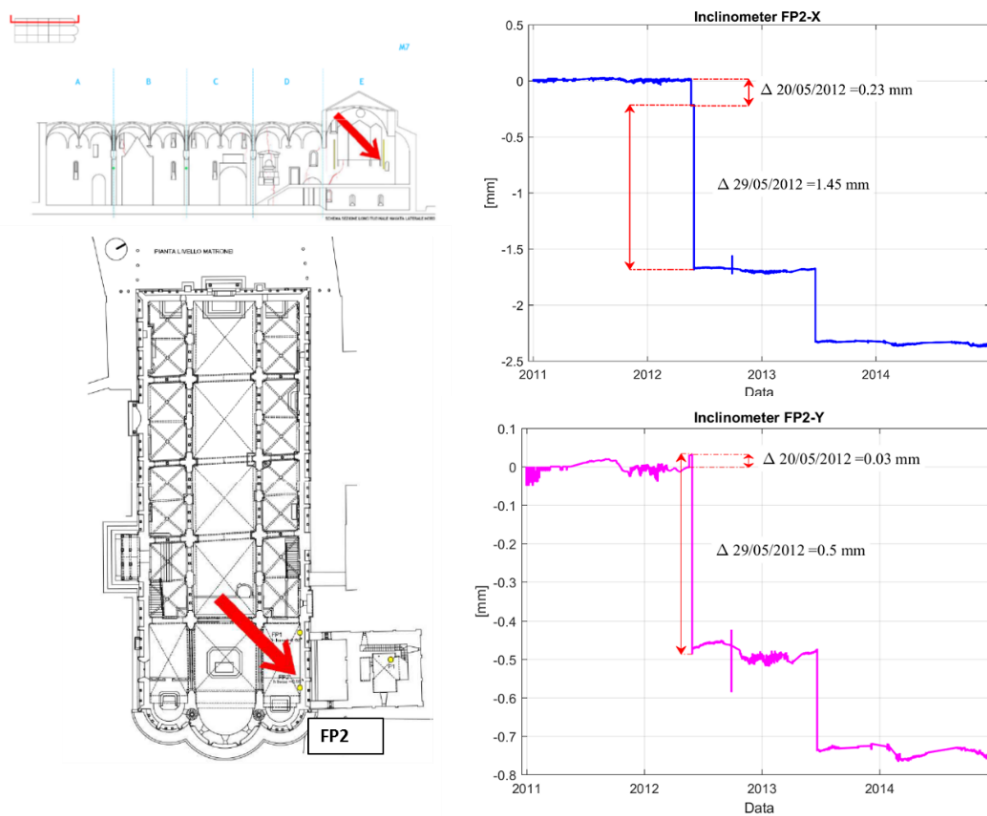


Figure 2.2.53 Inclinometer FP2: row-data recorded by FP2 highlighted the drops recorded during the 2012 earthquake



2.4.5 Summary of results from SHM

The interpretation of the data recorded (from 2004 to 2015) by the static monitoring system installed on the Cathedral of Modena allows to draw the following concluding remarks :

- the data recorded by the devices installed on the Cathedral have allowed to control the condition of the structure after the 2012 Emilia earthquake. In particular, the analyses of the data made it possible to understand their possible evolutionary trends triggered by the seismic load.
- The invar deformeters and the inclinometers, while not recording data continuously, have caught some movements caused by the 2012 earthquake. In more detail, the invar deformeters have recorded a rapprochement between the cathedral and the Ghirlandina tower during the earthquake. These movements are not recovered later, but the devices, after the earthquake, record again a cyclical trend meaning that the movements triggered by the earthquake are not evolving. A similar condition has been recorded by the inclinometers.
- The joint meters, which measure the movements of some cracks, display a high direct correlation with the temperature. It should be noted that some of the joint meters record an evolutionary trend (MGB2, MGB3 and MGB4). The "evolutionary" phenomenon noted suggests the need for a precise control of the specific cracks in order to exclude dangerous amplification of the phenomenon under observation. At the moment, however, the situation appears substantially "not alarming". The order of magnitude of the cumulative residues reveals in fact small movements in the thirteen years of monitoring. Moreover, these trends showing an analogy with the main movements identified through the integrated knowledge and the structural analyses performed on the Cathedral.

The main periodicity of the recorded data by the joint meters have been investigated through the signal frequency analyses and reveal the predominant component with period close to $T = 365$ days. Other important amplitudes are observed for periods equal to 170 days and 500 days.

3 Seismic risk assessment

This chapter provides a summary of the results of the seismic risk analysis developed according to the simplified approach presented in chapter 6 of part 1 of the report.

3.1 Hazard curve

The seismic hazard curve for the site of the Modena Cathedral has been evaluated according to the procedure presented in part 1.

Figure 2.3.1 shows the hazard curve has obtained considering an observation period of 50 years.

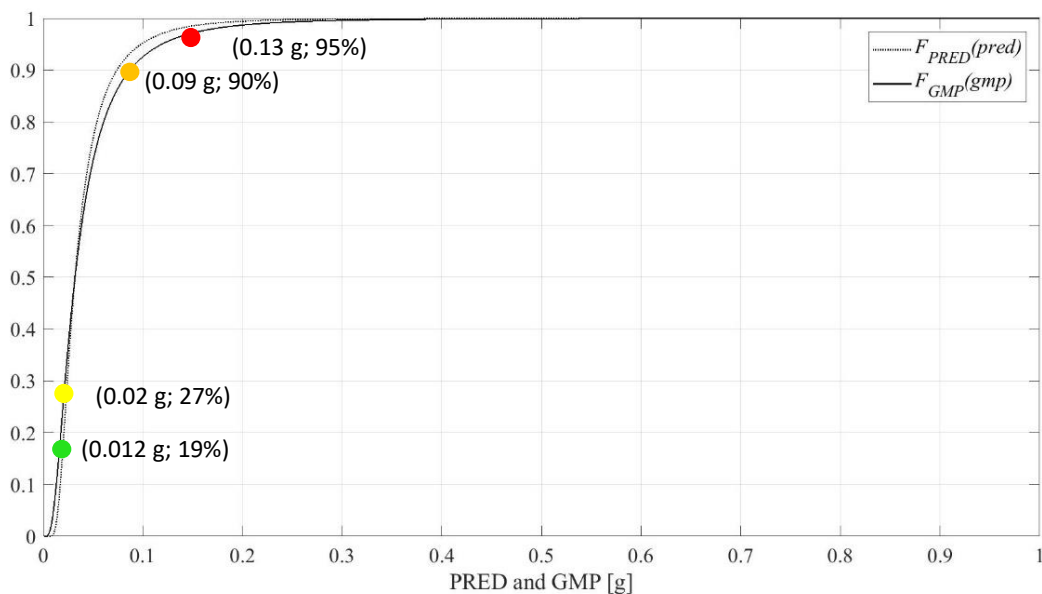


Figure 2.3.1.- Hazard curve for the site of Modena Cathedral (for a reference period of 50 years).

The coloured circles indicates the values of acceleration at specific not exceeding probabilities of corresponding to the typical values suggested by codes at each relevant limit state:

- P=19% corresponds to the probability of occurrence of a frequent event (81% within the reference period) generally associated with a so called fully operation limit state; the point is identified as SLO limit state according to the Italian building code NTC18.
- P=27% corresponds to the probability of occurrence (63% within the reference period) of an occasional event generally associated with a so called operation limit state; the point is identified as SLD limit state according to the Italian building code NTC18.



ALMA MATER STUDIORUM
UNIVERSITA' DI BOLOGNA

DICAM

Dipartimento di Ingegneria Civile,
Chimica, Ambientale e dei Materiali

MiChE

Mitigating the Impacts of natural hazards on Cultural Heritage
sites, structures and artefacts

- $P=90\%$ corresponds to the probability of occurrence (10% within the reference period) of a rare event generally associated with a so called life safety limit state; the point is identified as SLV limit state according to the Italian building code NTC18.
- $P=95\%$ corresponds to the probability of occurrence (5% within the reference period) of a very rare event generally associated with a so called near-collapse limit state; the point is identified as SLC limit state according to the Italian building code NTC18.



3.2 Performance curves

The performance curve provides the values of accelerations associated to the damage state variable DS with values between 0 and 4. The following specific values of DS corresponding to the following limit states:

1= SLO : no damage.

2=SLD: cracks to arches and vaults.

3=SLV significant damages_(such as partial collapses of vaults).

4=SLC extensive or total collapses

The following sections provides a summary of the main results of the structural analyses which allowed to obtain the values of acceleration corresponding to each identified limit state.

3.2.1 Accelerations that activate the different SL

The seismic response of the Cathedral of Modena was analyzed considering the actual response of the monument to past seismic events (based on historical data) and through assessments of the seismic response to hypothetical future earthquakes.

Seismic response based on historical data

The intensity of the **specific historical earthquakes** that occurred in the past and actually affected the structures of the Cathedral of Modena have been reconstructed through a historical deterministic analysis §1.3.1. This type of analysis allows you to collect important information obtained from the correlation between this hazard study and the analysis of historical documents that represent the cracks, the collapses, the interventions that have occurred over time on the factory elements of the Cathedral. The historical deterministic analysis shows that in the approximately **1000 years of the Cathedral "life"**, at its base, the following occurred:

- 4 seismic shaking characterized by maximum ground acceleration (PGA) values between **0.15 g** and **0.25 g**. On average, therefore, an "important" shaking occurred every 250 years, the last of these shaking occurred around the middle of 1600, more than 400 years ago.
- 20 seismic shaking characterized by maximum ground acceleration (PGA) values between **0.05 g** and **0.15 g**. On average, therefore, a "not negligible" shaking occurred every 50 years.

Historical evidence has shown that for "important" earthquakes (characterized by an acceleration between **0.15 g** and **0.25 g**), the Cathedral has suffered **significant damages** which mainly involves the towers and vaults.



For frequent earthquakes (characterized by an acceleration between **0.05 g** and **0.15 g**), such as that of May 2012, **minor damages were found mainly on the vaults.**

Seismic response based on LV1

To obtain a first indication of the seismic vulnerability level of the current state of the entire building, an LV1 analysis was developed. This analysis, although more appropriate for the assessment of the vulnerability of cultural heritage on a territorial scale, was developed as it allows to obtain a preliminary assessment of the global vulnerability of the building through an estimate of the ground acceleration corresponding to the achievement of the SLV limit state (substantially corresponding to the activation of the first partial collapse mechanisms).

The analysis performed on the Modena Cathedral showed that the **acceleration value on the ground corresponding to the achievement of the SLV condition is equal to 0.205 g**. It is interesting to note that this acceleration value is coherent with what emerged from the historical deterministic analysis of seismic hazard (above) and by comparing the survey of the crack pattern and the documentation of historical damage induced by seismic events.

Seismic response based on LV2

Level 2 analyzes (LV2) are carried out by dividing the structure into macroelements, or in architectural portions characterized by a substantially autonomous structural response, with recurring phenomenologies. In the case of Modena Cathedral, the following eight macroelements were taken into consideration: the facade, the hall, the longitudinal walls, the colonnade, see §2.3.3. For each of these macroelements, the corresponding collapse mechanisms and the corresponding acceleration were identified. Recalling that for this analysis, assumptions were made in favor of safety on the degree of connection between the wall facings, the elements that are most vulnerable are, in descending order:

- **top of the facade:** the overturning mechanism could be activated with an estimated acceleration of about 0.06g;
- **triumphal arches:** this mechanism could be activated with an estimated acceleration of about 0.07g;
- **transept vaults:** the overturning mechanism could be activated with an estimated acceleration of about 0.12g;
- **facade:** the overturning mechanism could be activated with an estimated acceleration of about 0.13g;



- **walls of the transept:** the overturning mechanism could be activated with an estimated acceleration of about 0.13g;
- **longitudinal response of the colonnade:** the overturning mechanism could be activated with an estimated acceleration of about 0.14g.

These elements are vulnerable to earthquakes characterized by accelerations lower than 0.15 g, which are characterized by a return period of approximately 50 years. For earthquakes characterized by an acceleration of between 0.15 g - 0.25 g and with a return period of 250 years, the following elements are also vulnerable: **turrets, transept apses and hall**. The masonry walls do not show any particular problems, although it is appropriate to highlight how the largest deformation gradient is reached in the first and last span transversely for earthquakes acting in a transverse direction.

Seismic response based on LV3

LV3 seismic vulnerability assessments estimate the seismic safety of the construction as a whole, identifying the soil acceleration that leads to the ultimate limit state of the global construction or of significant individual parts of it through the development of representative finite element numerical modeling of the whole structure.

Time history seismic analysis were therefore developed through finite element modeling, with the specific aim of investigating: (i) the in-plan mechanisms due to shear and eccentric axial force, and (ii) the out of plan mechanisms due to loss of balance of the walls, see § 2.2.

With regards to the in-plan analysis, the average tangential stresses (assessed by the analysis carried out on FEM 3D models) were compared with the corresponding shear strength values estimated on the basis of the results of the non-destructive investigations developed. This allowed the identification of **critical issues due to the shear failure** (in accordance with the verification criteria provided by current regulations) **in the transverse walls corresponding to the first 4 spans**.

With regards the out of plan analysis, specific equilibrium assessments were carried out by identifying control sections, and for each of these the action that keeps the wall base completely compressed has been identified (identifying as "critic" the achievement of the "sectioning" condition of the base section).

This analysis reveals **systematic problems on all transverse walls** (especially those orthogonal to the central nave) and in the **longitudinal perimeter walls**.



ALMA MATER STUDIORUM
UNIVERSITA' DI BOLOGNA

DICAM

Dipartimento di Ingegneria Civile,
Chimica, Ambientale e dei Materiali

MiChE

Mitigating the Impacts of natural hazards on Cultural Heritage
sites, structures and artefacts

Based on the results summarized above, the values of peak ground horizontal accelerations that activate the different limit state SL are here summarized:

- SLO=0.02g
- SLD=0.05g
- SLV=0.15g
- SLC=0.25g

3.2.2 Fragility curves and performance curve

The results of the structural analysis allowed to obtain the fragility curves related to the four considered damage state.

Figures 2.3.2 and 2.3.3 show the fragility curves related to the four identified damage states and the performance curve obtained from the combination of the four fragility curves according to the following relationship:

$$P(pga) = \sum_i D_i(pga) \cdot Ds_i$$

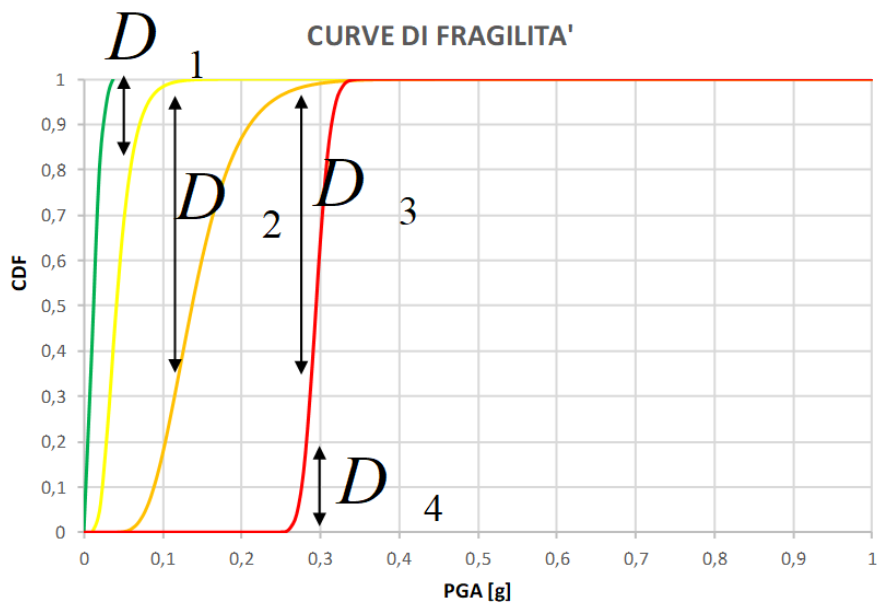


Figure 2.3.2: Fragility curves for Modena Cathedral corresponding to pre-intervention conditions.

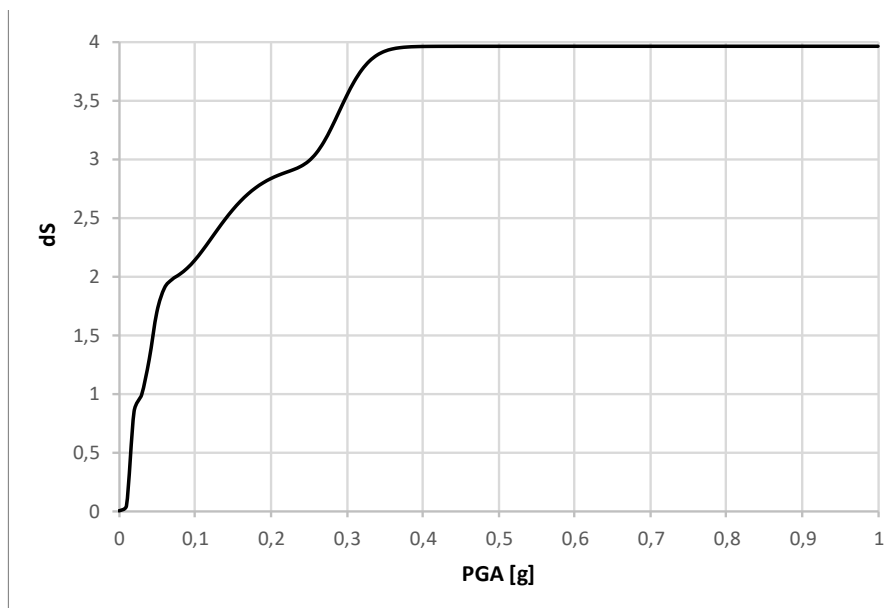


Figure 2.3.3: Performance curve for Modena Cathedral corresponding to pre-intervention conditions.



3.3 Vulnerability curves

In the following sub-sections the relevant information used to obtain the vulnerability curves are reported. For the sake of conciseness, the attention has been paid to the following factors:

- L1: economic losses due to structural damage;
- L4: non-usability;
- L5: economic losses due to non-usability;
- L7: fatalities;
- L8: economic losses due to fatalities;

Vulnerability curve L1: economic losses due to structural damage

The following table summarize the main values of selected points of the vulnerability curve L1 corresponding to the four relevant values of the damage state variable (e.g. ds=1, 2, 3, 4). The table provides information regarding the evaluation of the specific values.

| Damage State [ds] | variable V | Structural damage [€] | Considerations |
|---------------------------|--|-----------------------|---|
| 1 SLO PGA=0,02g | No damage | 0 € | / |
| 2 SLD PGA=0,05g | Cracks to arches and vaults | 250.000 € | From costs of retrofit Interventions after 2012 Earthquake |
| 3 SLV PGA=0,15g | Extended cracks, first collapses of vaults | 1.400.000€ | Estimated (800 euros/ mq) |
| 4 SLC PGA=0,30g | Extended collapses | 14.000.000€ | Based on data from the reconstruction of Collemaggio Chatedral* |

*adjusted considering actual surfaces

The following figure provides the vulnerability curve L1.

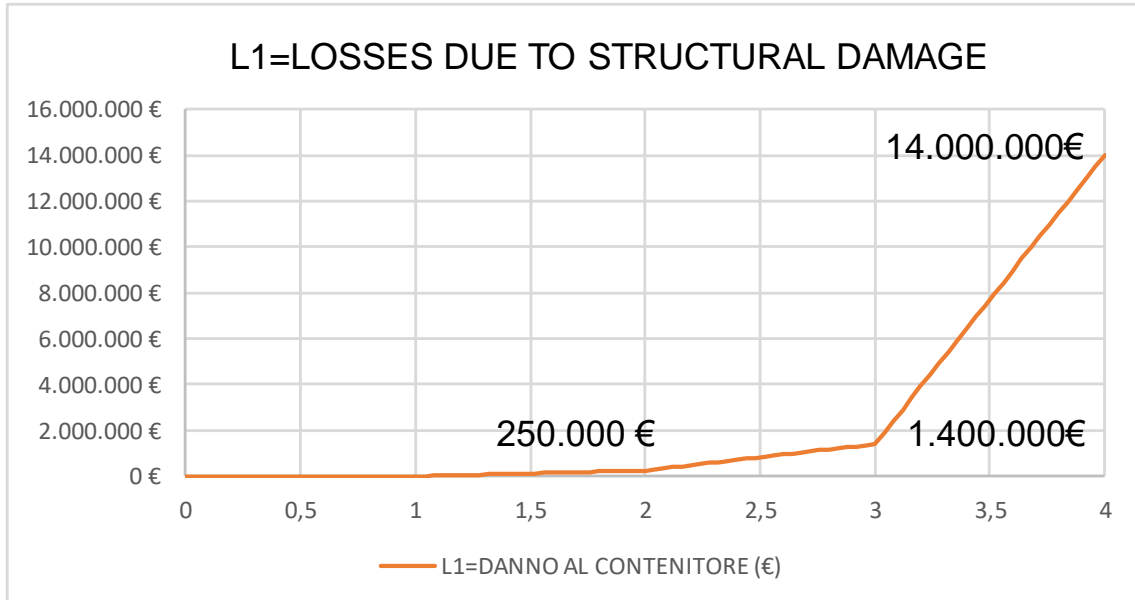


Figure 2.3.4: Vulnerability curve L1 for Modena Cathedral.

Vulnerability curve L4: non-usability

The following table summarizes the main values of selected points of the vulnerability curve L4 corresponding to the four relevant values of the damage state variable (e.g. ds=1,2,3,4). The table provides information regarding the evaluation of the specific values.

| Damage State [ds] | variable V | Months of non-usability [months] | Considerations |
|--------------------|------------------------------------|----------------------------------|---|
| 1 SLO PGA=0,02g | No interruptions | 0 | |
| 2 SLD PGA=0,05g | Partial interruptions | 3 mesi | From retrofit Interventions after 2012 Earthquake |
| 3 SLV PGA=0,15g | Interruptions due to strengthening | 48 mesi | From retrofit Interventions after 2012 Earthquake |
| 4 SLC PGA=0,30g | Reconstruction period | 60 mesi | From reconstruction of Collemaggio Cathedral |

The following figure provides the vulnerability curve L4.

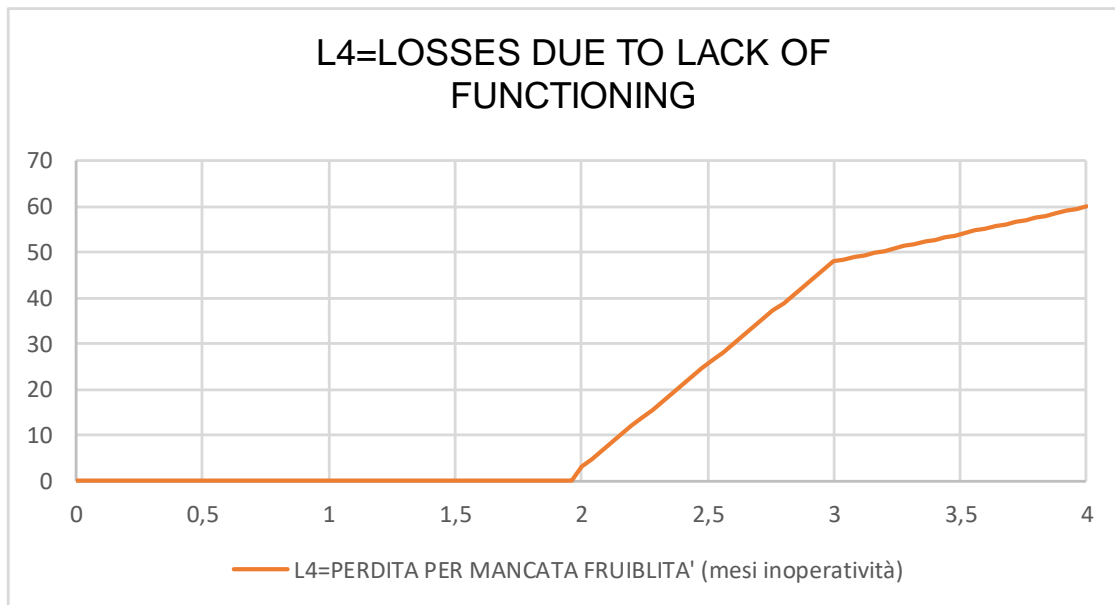


Figure 2.3.5: Vulnerability curve L4 for Modena Cathedral

Vulnerability curve L5: economic losses due to non-usability

The following table summarize the main values of selected points of the vulnerability curve L5 corresponding to the four relevant values of the damage state variable (e.g. ds=1, 2, 3, 4). The table provides information regarding the evaluation of the specific values.

| Damage State [ds] | Variable V | losses [€] | Considerations |
|---------------------------|--|-------------|--|
| 1 SLO PGA=0,02g | No interruptions | 0 | / |
| 2 SLD PGA=0,05g | Losses due to Partial interruptions | 187.000 € | Estimate based on the economic loss associated to the average number of visitors during the months of non-use. |
| 3 SLV PGA=0,15g | Losses due to Interruptions due to strengthening | 6.000.000 € | Estimate based on the economic loss associated to the average number of visitors during the months of non-use. |
| 4 SLC PGA=0,30g | Losses due to Reconstruction period | 7.500.000 € | Estimate based on the economic loss associated to the average number of visitors during the months of non-use. |



The following figure provides the vulnerability curve L5.



Figure 2.3.6: Vulnerability curve L5 for Modena Cathedral.



Vulnerability curve L7: fatalities

The following table summarize the main values of selected points of the vulnerability curve L7 corresponding to the four relevant values of the damage state variable (e.g. ds=1, 2, 3, 4). The table provides information regarding the evaluation of the specific values.

| Damage State [ds] | Variable V | Life losses | Considerations |
|--------------------|---|-------------|--|
| 1 SLO PGA=0,02g | No fatalities | 0 | |
| 2 SLD PGA=0,05g | No fatalities | 0 | Estimate based on average number of visitors and on contemporaneity issues |
| 3 SLV PGA=0,15g | Fatalities due to a partial collapse (10% of surface) | 2 | Estimate based on average number of visitors and on contemporaneity issues |
| 4 SLC PGA=0,30g | Fatalities due to total collapse | 17 | Estimate based on average number of visitors and on contemporaneity issues |



Vulnerability curve L8: economic losses due to fatalities

The following table summarizes the main values of selected points of the vulnerability curve L8 corresponding to the four relevant values of the damage state variable (e.g. ds=1,2,3,4). The table provides information regarding the evaluation of the specific values.

| Damage State [ds] | Variable V | Economic losses [€] | Considerations |
|--------------------|--|---------------------|--|
| 1 SLO PGA=0,02g | Losses due to no fatalities | 0 | Estimate based on the economic loss associated to fatalities |
| 2 SLD PGA=0,05g | Losses due to no fatalities | 0 | Estimate based on the economic loss associated to fatalities |
| 3 SLV PGA=0,15g | Losses associated to Fatalities due to a partial collapse (10% of surface) | 2.000.000 € | Estimate based on the economic loss associated to fatalities |
| 4 SLC PGA=0,30g | Losses associated to Fatalities due to total collapse | 17.000.000 € | Estimate based on the economic loss associated to fatalities |

The following figure provides the vulnerability curve L8.

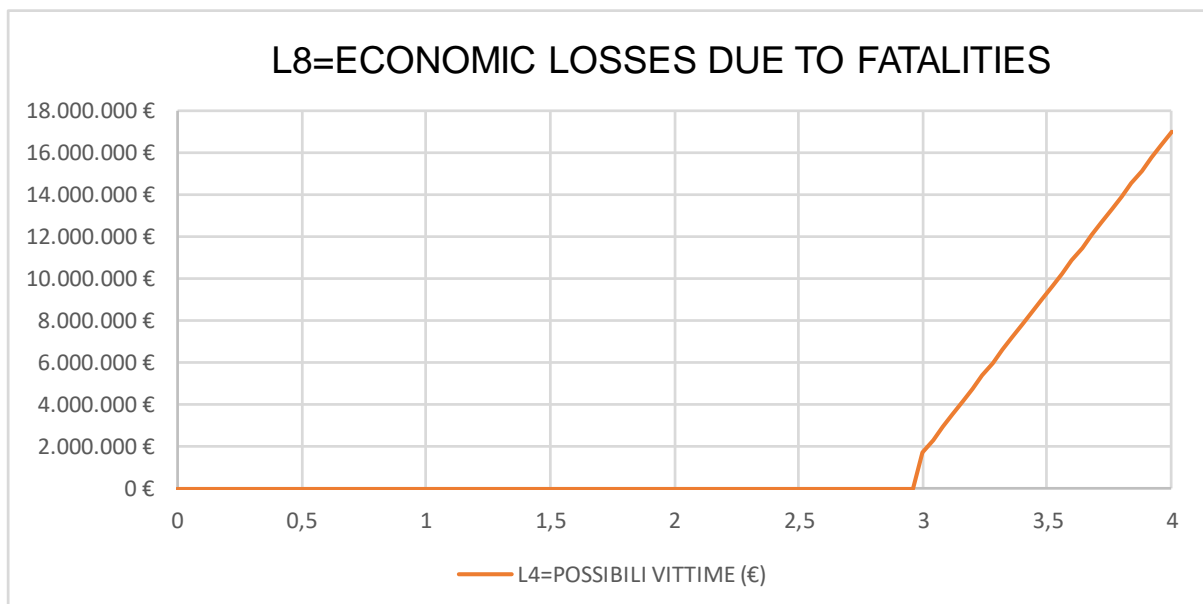


Figure 2.3.7: Vulnerability curve L8 for Modena Cathedral.

3.4 Risk curve L1

The risk due to economic losses associated to structural damage L1 has been evaluated according to the framework (Figure 2.3.8) introduced in part 1 of the present report.

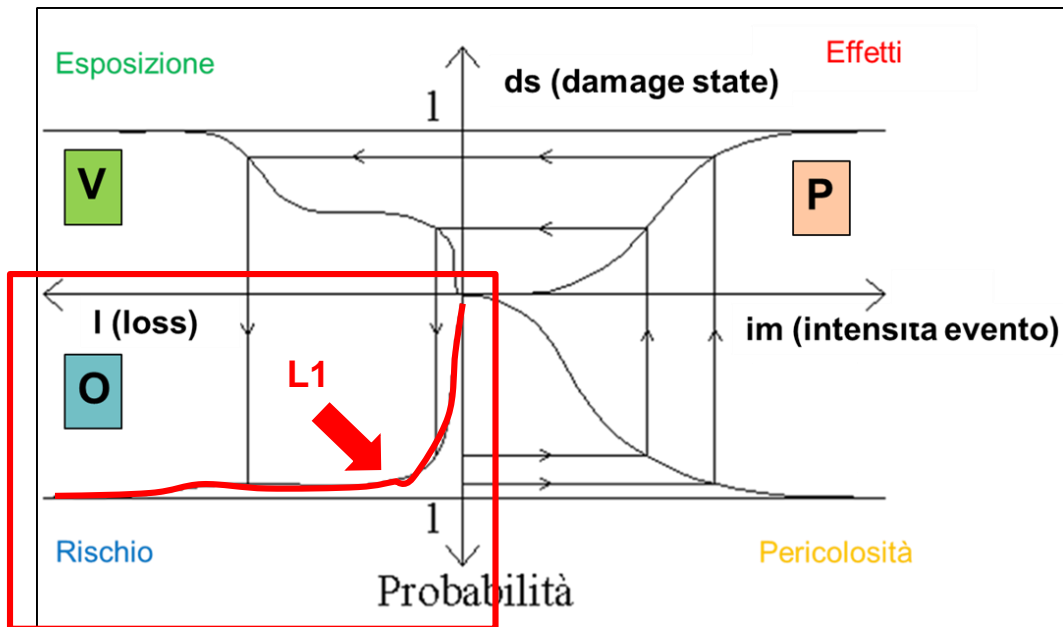
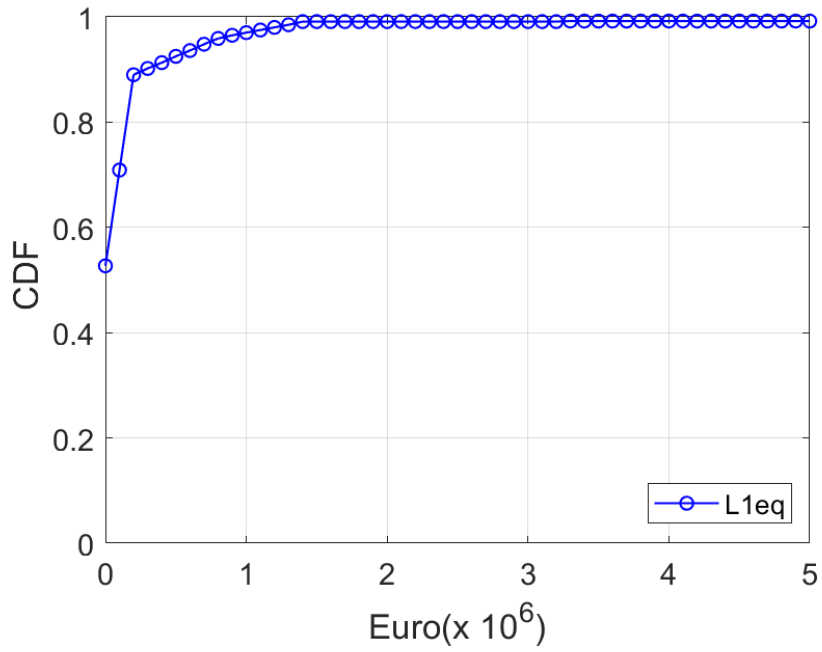
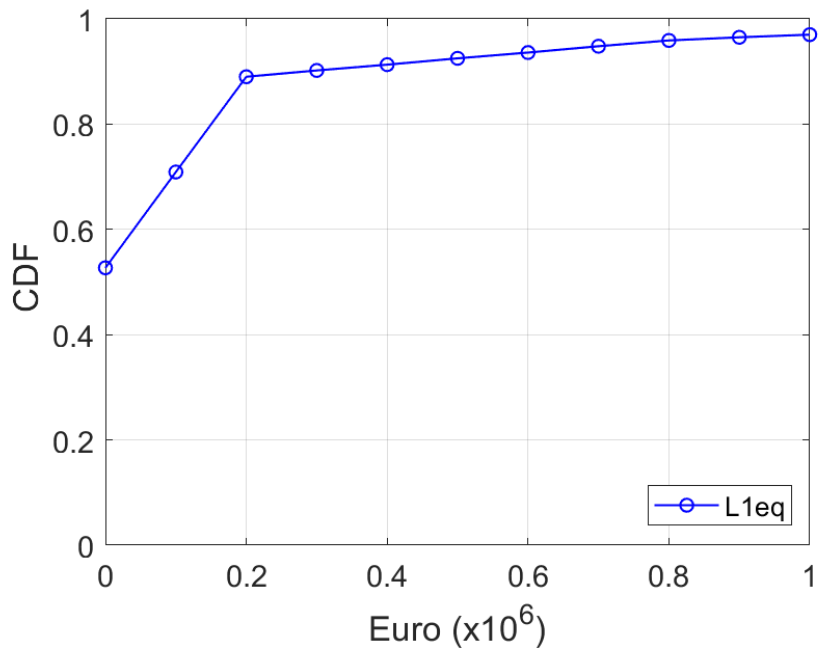


Figure 2.3.8: Vulnerability curve L8 for Modena Cathedral.

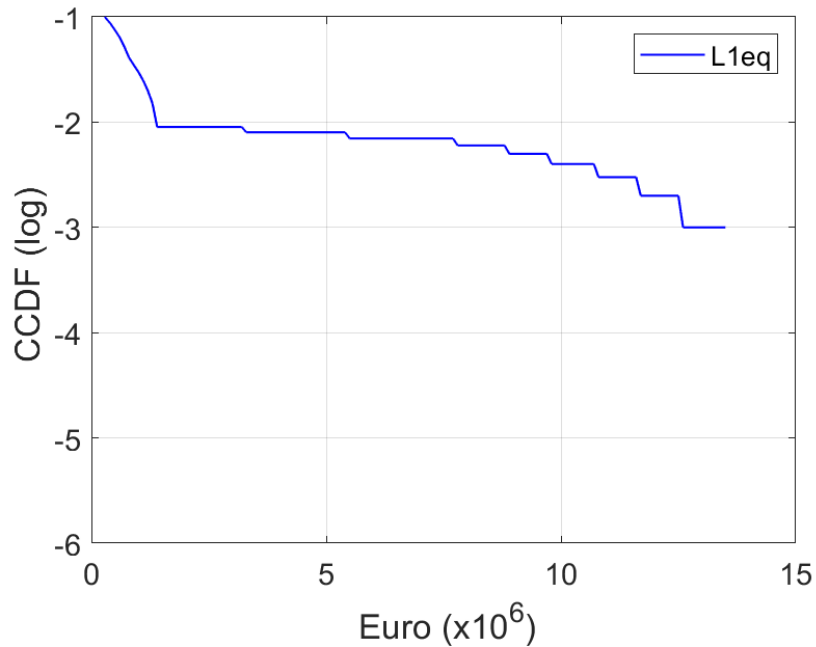
Figure 2.3.9 provides the cumulative distribution functions CDF and complementary cumulative distribution curves CCDF of risk curve L1 related to earthquake hazard.



(a)



(b)



(c)

Figure 2.3.9: Risk curve L1 for Modena Cathedral corresponding to pre-intervention conditions: (a) CDF; (b) CCDF and (c) CCDF in log scale.

The following main considerations can be drawn:

- A loss of around 1 million euro is associated with a quite large probability (around 10^{-2}).
- A loss of around 10 million euros is associated to a probability of occurrence of around 10^{-3} .



4 Multi-risk assessment

As mentioned in chapter 3 of part 2, the seismic risk has been here quantitatively compute with respect to direct losses L1 only, namely losses associated to structural damages. However, the same procedure can be easily extended to the other identified risks.

4.1 Summary of Fire risk analysis

As detailed in the final report of the Uniroma1 unit, the fire risk curve for the Modena Cathedral are carried out by adopting the scenario-based approach with reference to four fire scenarios (characterized by different intensity measure values). For each scenario the Cause-consequence (or “scenario”) analysis is carried out by defining event-tree diagrams similar to the example one shown in Figure 2.3.10 below. The fire ignition point has been assumed as located in the loft zone above the Inlaid wooden “pontile” art masterpiece (Figure 2.3.11), the fire ignition is assumed to be caused by an electrical short circuit. In addition to the “No Damage” state, four damage/loss severity levels are identified (increasing in severity: 1) Limited damages to the roof; 2) Average damages to the roof wooden elements and partial loss of it; 3) Considerable damages to the roof wooden elements and loss of a considerable amount of it; 4) Complete loss of the wooden roof and significant damages to the content. Peculiarities of both the Low-Probability-High-Consequence (LPHC) events like fire, and of the heritage buildings (related to specific vulnerabilities to fire) are taken into account. As final result, the procedure produces a fire risk curve to a reference to a pre-defined return period T_r which, for fire hazard, has to be set to 50 years at least.

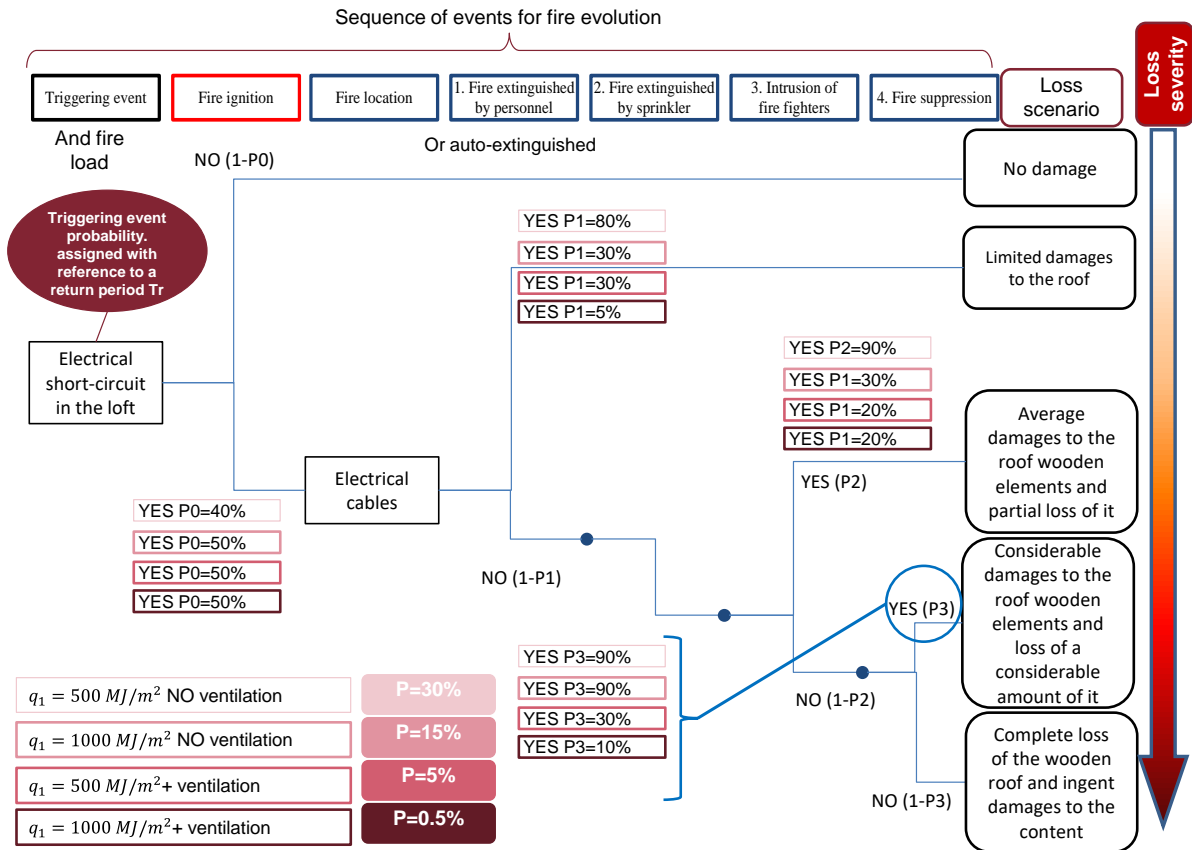


Figure 2.3.10: Example of event-tree diagram for fire risk analysis of the Modena Cathedral

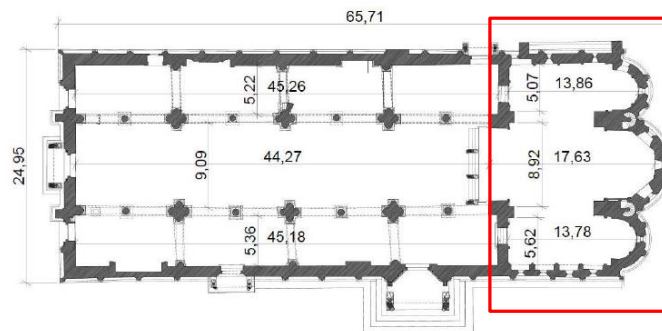


Figure 2.3.11: Fire ignition zone (loft compartment).

The obtained fire risk curve is shown in Figure 2.3.12, representing the complementary cumulative distribution function (CCDF) probability in the return period $Tr=50$ years, which is also interpolated by an exponential equation. If the loss severities are expressed in monetary terms, the risk curves constitutes the classical output of a single hazard risk analysis.

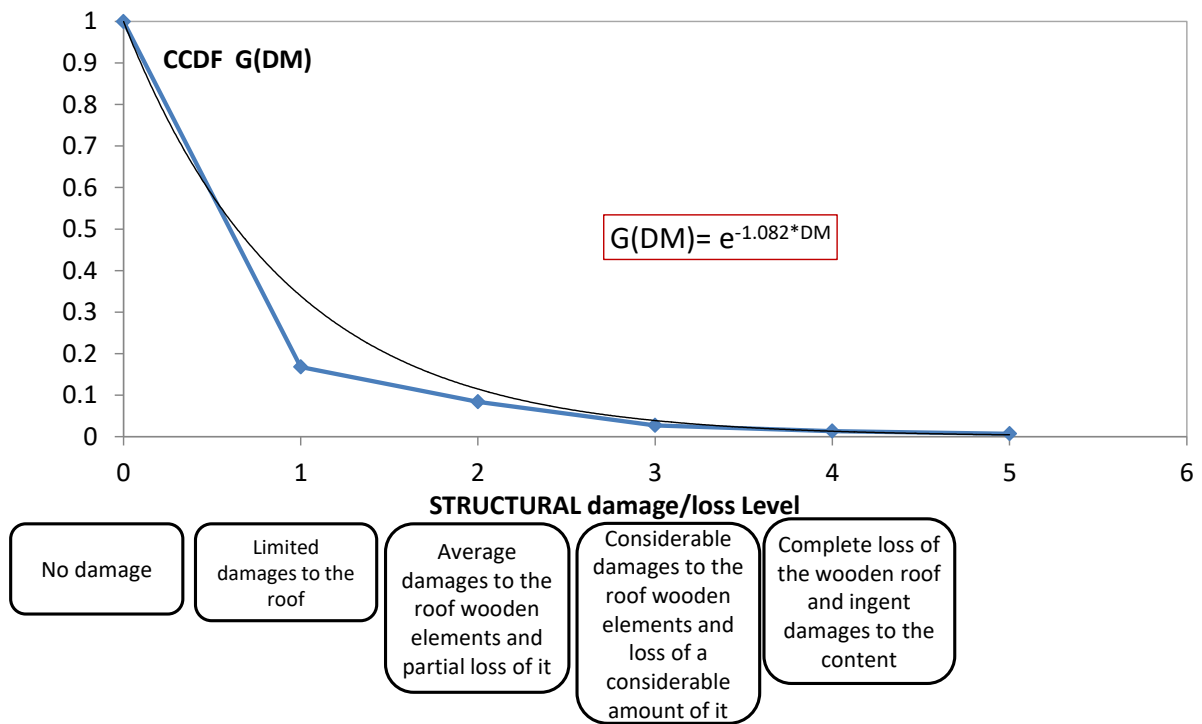


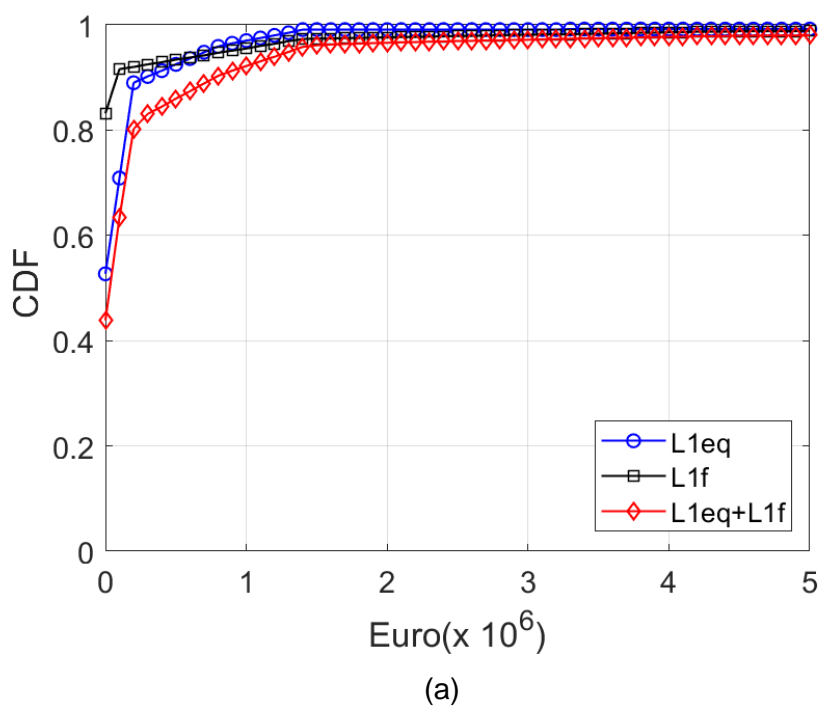
Figure 2.3.12: Obtained fire risk curve for the loft compartment with reference to $T_r=50$ years.

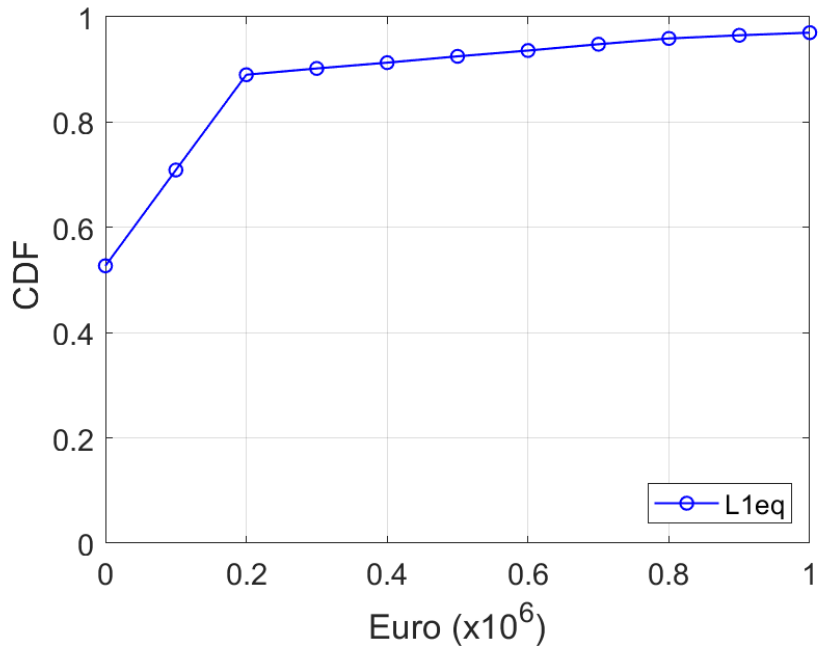


4.2 Total risk curve L1

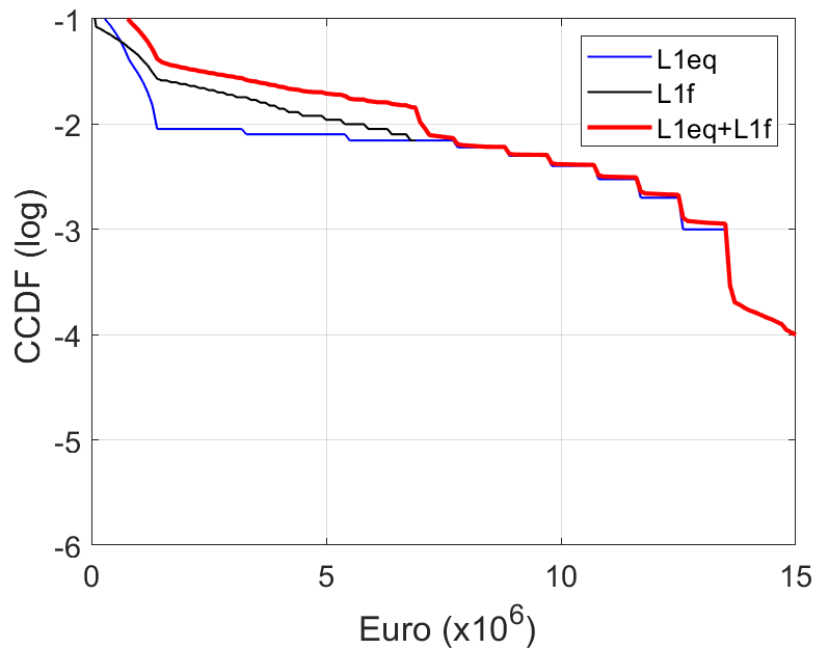
The “total risk” curve has been obtained by combining the risk curve related to each considered hazard according to the procedure introduced in part1.

Figure 2.3.13 provides the cumulative distribution functions CDF and complementary cumulative distribution curves CCDF of risk curve L1 related to the combination of earthquake and fire hazards.





(b)



(c)

Figure 2.3.13: Loss curves L1 considering fire and earthquake hazards: (a) CDF; (b) CDF, zoom; (c) CCDF in log scale.



ALMA MATER STUDIORUM
UNIVERSITA' DI BOLOGNA

DICAM

Dipartimento di Ingegneria Civile,
Chimica, Ambientale e dei Materiali

MiChE

Mitigating the Impacts of natural hazards on Cultural Heritage
sites, structures and artefacts

The total risk curve L1 (red thick curve) provides the economic losses associated to structural damages due to earthquake and fires. The following observations can be drawn:

- An economic loss of around 1 million euro has a quite large probability of occurrence (10% within an observation period of 50 years).
- An economic loss of around 15 million euro has probability of occurrence of around 10^{-4} within an observation period of 50 years.



ALMA MATER STUDIORUM
UNIVERSITA' DI BOLOGNA

DICAM

Dipartimento di Ingegneria Civile,
Chimica, Ambientale e dei Materiali

MiChE
Mitigating the Impacts of natural hazards on Cultural Heritage
sites, structures and artefacts

PART 3: MITIGATION

Part 3 deals with mitigation strategies to reduce risks due to earthquakes and fire with specific reference to the case study of Modena Cathedral. Chapter 1 gives a summary of the main structural vulnerabilities that have guided through the identification of the proposed strategies of intervention. Intervention solutions are then described in chapters 2 and 3. After the development of the mono-risk analysis associated to each single hazard (e.g. earthquake and fire), the total risk due to the combination of the two hazards is evaluated applying the simplified procedure here proposed (chapter 4).



1 Main vulnerabilities related to earthquake and fire risks

1.1 Vulnerabilities from earthquake-risk analysis

Starting from the knowledge acquired by the integrated approach, the structural behaviour of the Cathedral has been investigated in order to identify the more vulnerable elements of the building.

The results of the static analyses have been used to interpret the cracking patterns as obtained from in situ surveys and the deformations related to changes in the geometrical configuration.

The static analysis has been developed through simple limit schematizations and finite element models with increasing complexity (2D models, 3D models, models with fixed base, models accounting for the soil-structure interaction).

The different finite element models, validated through simple patterns, are then compared with the “survey” of the actual state of the building. The most representative one of the structural behaviour of the Cathedral is the model considering the soil-structure interaction.

On this model, various analyses have been carried out in order to identify the seismic behaviour of the monument. The local collapse mechanisms and the global seismic response of the structure have been studied.

From the static analyses and the knowledge, it can be recognized that the main vulnerabilities are:

- the tendency of the longitudinal perimeter walls to develop out-of-plane movements, as revealed by the 3D laser scanner, probably due to the unconstrained thrusts of the arches and differential settlements;
- the overall rotation movement towards the Ghirlandina Tower, caused by the strong interaction between the Cathedral and the Tower, that promotes differential soil settlements (note that the portion of the apses is significantly heavier than the other portions);
- the concentration of cracks in the portion coinciding with the location of the old Cathedrals;

Instead, the masonry arches, that link the Cathedral and the Tower, contrast the rotation movement of the Cathedral creating a critical point on the longitudinal wall.

Regarding the seismic behaviour, the results of the local analyses reveal that the main local vulnerabilities are the facade mechanisms, the failures of the cross vaults (as confirmed by the damages observed after the seismic sequence that hit Modena in the May 2012), the out-of-plane behaviour of the apse walls and the pinnacles

Moreover, the results of the global analyses reveal vulnerabilities of the perimeter walls with respect to out-of-plane overturning.



1.2 Vulnerabilities from fire-risk analysis

Main general factors that induce vulnerabilities to fire for the Modena Cathedral can be classified and identified as below:

- *Massive presence of wooden structural and non-structural elements (or other elements vulnerable to fire).* The roof structure (both beams and trusses) is in wood, while walls are made in massive masonry.
- *Valuable content.* A number of Artworks, are present in the Modena Cathedral (for an exhaustive list of valuable content please see (http://www.unesco.modena.it/en/plan-your-visit/cathedral?set_language=en and https://it.wikipedia.org/wiki/Duomo_di_Modena). The most important point is that all these contents can be damaged or get lost due to fire.
- *Absence of active protection and of adequate compartmentations.* Although a fire suppression system is not present in the Cathedral, there is a smoke detection system, important for decreasing the firefighters' intervention time. As for large part of cathedrals around the world, two main (large) compartments are individuated in the Modena one: the main hall for religious functions is the first compartment (which is relevant for evacuation studies), while the loft (the service/ storage cubature under the roof, which is relevant for fire development due to the presence of the wooden roof) is the second one.
- *Storage of flammable substances or unsuitability of electrical installations.* The short electricity circuit is considered the most suitable fire source in the Modena Cathedral, especially in the loft, where electrical cables and stations are present.
- *Presence of a large amount of people (churches and museums).* The possible in the Modena Cathedral, something that can be critical for the safety of people in fire.

Regarding the vulnerabilities of the Modena Cathedral with reference to the urban scale:

- *Difficulties of be approached by rescue vehicles.* This is a fairly relevant vulnerability for the case study. In fact, the Firefighters station it is quite near to the Modena Cathedral (3 km) but it is also located in historical center with narrow access ways;
- *Possible indirect involvement due to vulnerability of other units of the building cluster which can make the single heritage building subjected to fire spread or collapse spread.* The Cathedral Museum is stored in a building located adjacently the case study. The museum is characterized by a significant combustible load due to the presence of the library.



2 Solution strategies for seismic risk mitigation

In order to mitigate the main structural vulnerabilities the following types of interventions have been carried out:

1. Strengthening of vaults;
2. Insertion of steel chains
3. Local strengthening of walls and improvement of connections between orthogonal walls.
4. Intervention at roof level to realize a horizontal diaphragms;
5. Strengthening of pinnacles.

2.1 Interventions

The structural analyses have allowed identifying the main vulnerabilities of the Cathedral of Modena and thus the elements, which need a priority of strengthening. As well known, for the restoration of the historical monuments the intervention techniques and the used materials merit special care on account of their individual historical and architectural importance, or their significance as surviving representatives of an earlier tradition.

Beyond being the basis for a robust structural analysis, the importance of the integrated knowledge rises also from the possibility of identifying compatible materials and intervention techniques able to preserve the aesthetic and historical value of the monument.

In light of this, a strengthening design aimed at increase the safety level of the Cathedral preserving its integrity has been developed and will be effected in the next years. In particular, regarding the vaults several interventions have been planned.

The extrados of the vaults will be consolidated by a removal of the existing layer and re-filling through injections of lime. At their intrados, there is a decorated plaster dating back to the beginning of the XX century, with false paintings bricks. The project includes the fill of the cracks with a compatible lime and the consolidation of the plaster with the use of pigments of the same colors (Figure 3.2.1). Furthermore, the reinforcement of the vaults will be also achieved by attenuating the discontinuities (through the extension of the “frenelli” and the insertion of “diatoni” bricks, Figure 3.2.2) and/or putting a 5cm-thick layer of lime added with eco-pozzolana and reinforced with carbon-fiber mesh (Figure 3.2.2).



Figure 3.2.1: Consolidation of the decorated plaster with using compatible pigments

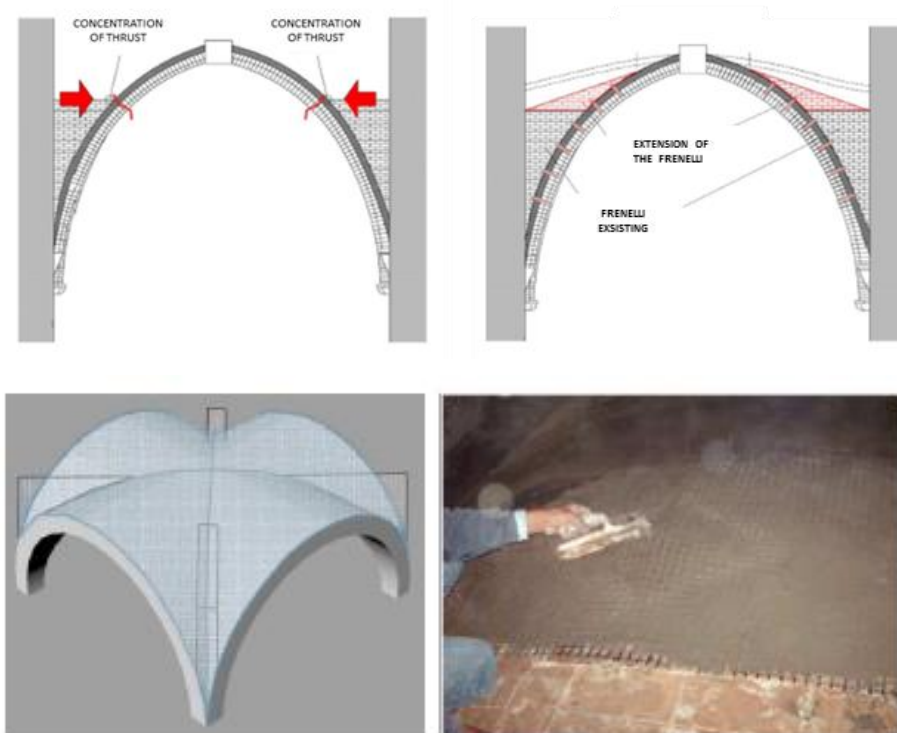


Figure 3.2.2: Interventions for strengthening the vaults: a) extension of the “frenelli”; b) layer of lime added with eco-pozzolana and reinforced with carbon-fiber mesh

The out-of-plane overturning of the perimeter walls and the façade can be contrasted with the insertion/ add of adequately dimensioned transversal and longitudinal tie rods. In particular, the strengthening design includes 36-millimeter tie rods at two different level: at 5.86 meter and at 13.28 meter. Figure 3.2.3 shows the cross section of the Cathedral and the blue lines represent the existing tie-rods while the red lines indicates the tie-rods planned at 5.86 meters height in order to contrast

the thrust due to the arches. Similarly, the Figure 3.2.4 shows in red lines the added tie-rods at 13.28 meters height in order to avoid the out-of-plane overturning of the perimeter walls and of the façade.

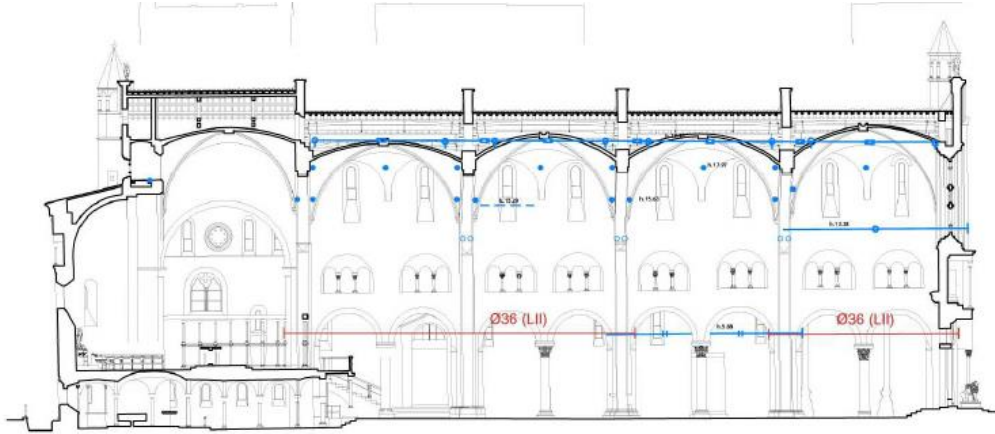


Figure 3.2.3: Tie-rods to contrast the thrust due to the arches

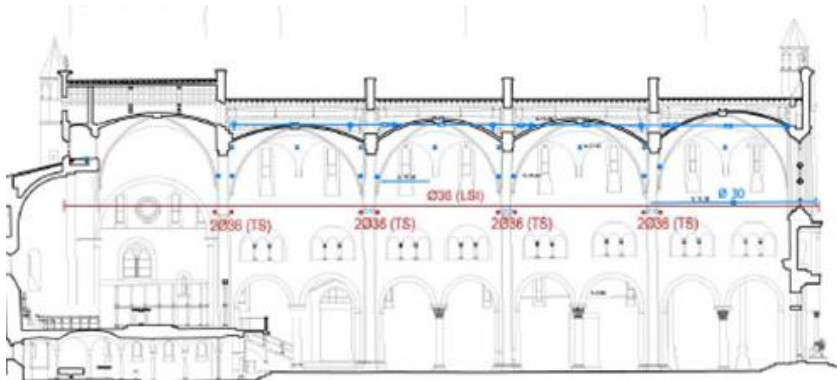


Figure 3.2.4: Tie-rods for avoiding the overturning mechanisms of the facade and of the perimeter walls

In order to ensure a box behaviour, an important concept to increase the seismic behaviour of the Cathedral, the connections between the orthogonal walls will be improved through insertions of new diatons and injections of compatible lime.

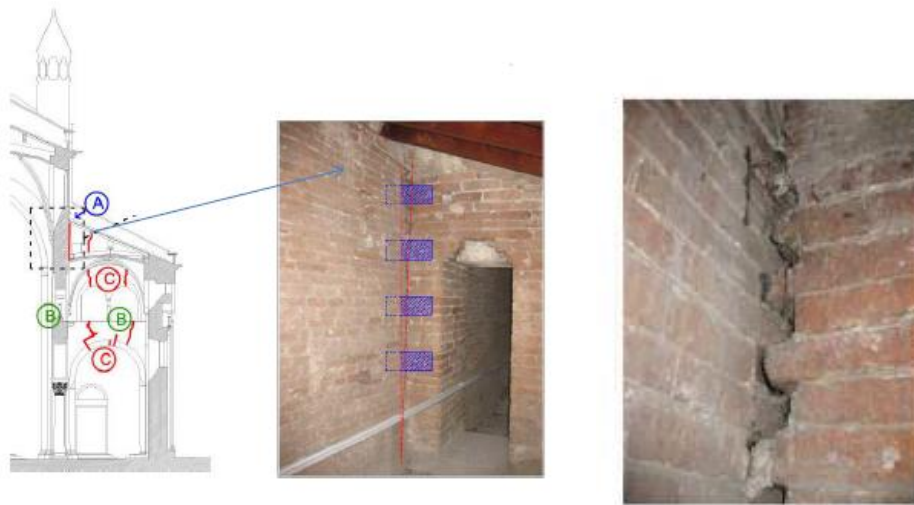


Figure 3.2.5: Connection of the orthogonal walls

The effectiveness of the existing tie-rods and end-plate anchors will be re-established in order to ensure a suitable safety against the overturning of the façade and of its top part (Figure 3.2.6). Moreover, a steel mesh grid has been placed internally and externally around the rose window to prevent the eventual out of plane mechanisms.

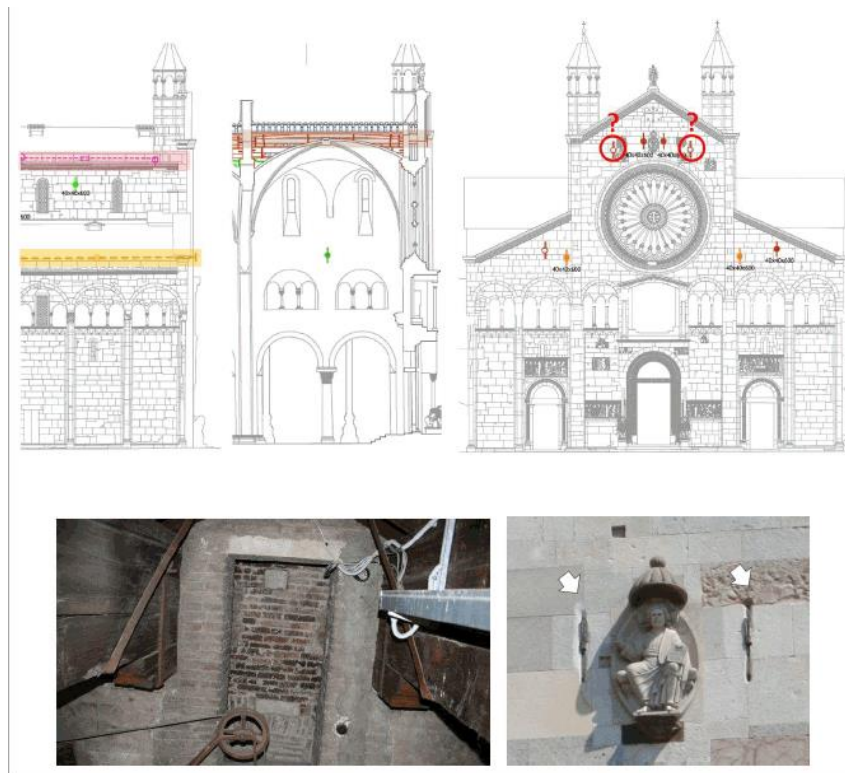


Figure 3.2.6: Reactivation of the existing tie-rod and plate anchors to contrast the overturning of the facade

Finally, the strengthening of the slender pinnacles will be carried out by inserting into the internal cavity a steel core, Figure 3.2.7.

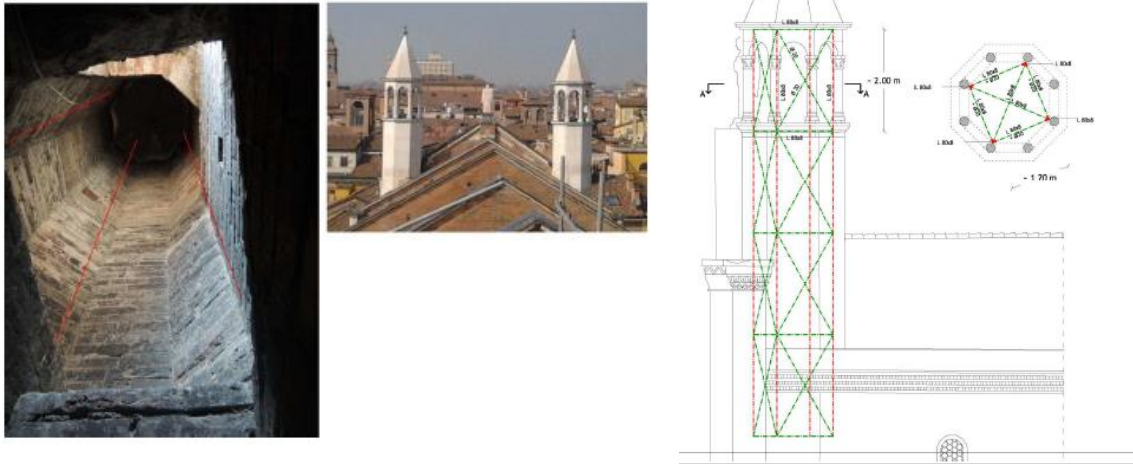


Figure 3.2.7: Strengthening of the slender pinnacles

2.1 Performance curve

The main objective of the structural interventions described in the previous sections was to mainly increase the structural performances at **ds1 (SLO)**, **ds2 (SLD)** and **ds3 (SLV)**.

The structural performances of the interventions have been assessed using both global and local analysis according to the methods described in part 2. For the sake of conciseness the details regarding the results of the structural analysis are not reported in the present report.

The values of ground accelerations that activate the different limit state SL in the post-intervention conditions are here summarized:

- SLO=0.12g
- SLD=0.15g
- SLV=0.25g
- SLC=0.30g

From the results of the structural analysis, the fragility curves corresponding to the four damage states have been obtained. The performance curve is then obtained from the combination of the four fragility curves according to the following relationship: $P(pga) = \sum_i D_i(pga) \cdot Ds_i$.

Figure 3.2.8 compares the performance curve for pre-intervention and post-intervention conditions.

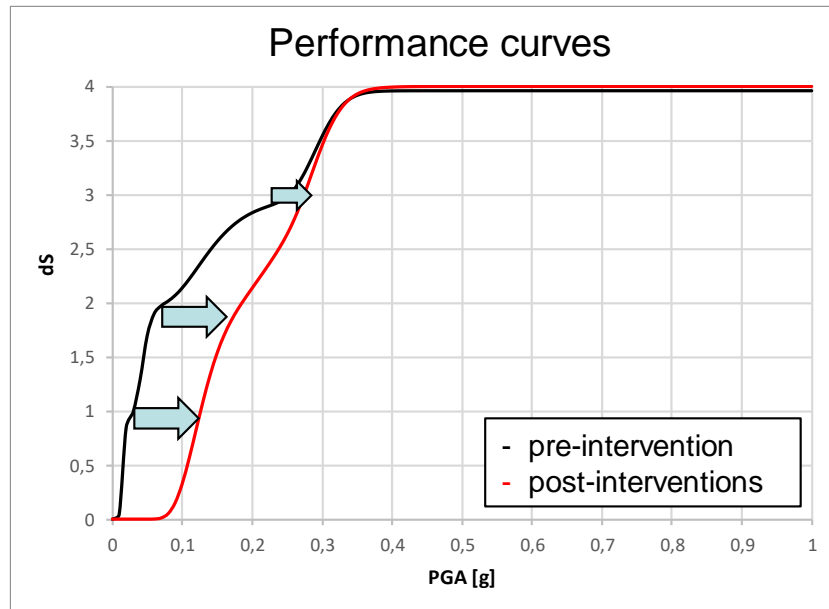


Figure 3.2.8: Performance curves representative of pre- and post-intervention conditions.

As expected, the interventions are able to significantly reduce the vulnerabilities due to earthquake hazard corresponding to damage states 1, 2 and 3.

2.2 Risk curve L1

The risk due to earthquake hazard has been evaluated combining the hazard curve, the performance curve and the vulnerability curve according to the procedure introduced in part 1.

Figure 3.2.9 provides the cumulative distribution functions CDF and complementary cumulative distribution curves CCDF of risk curve L1 related to earthquake hazard.

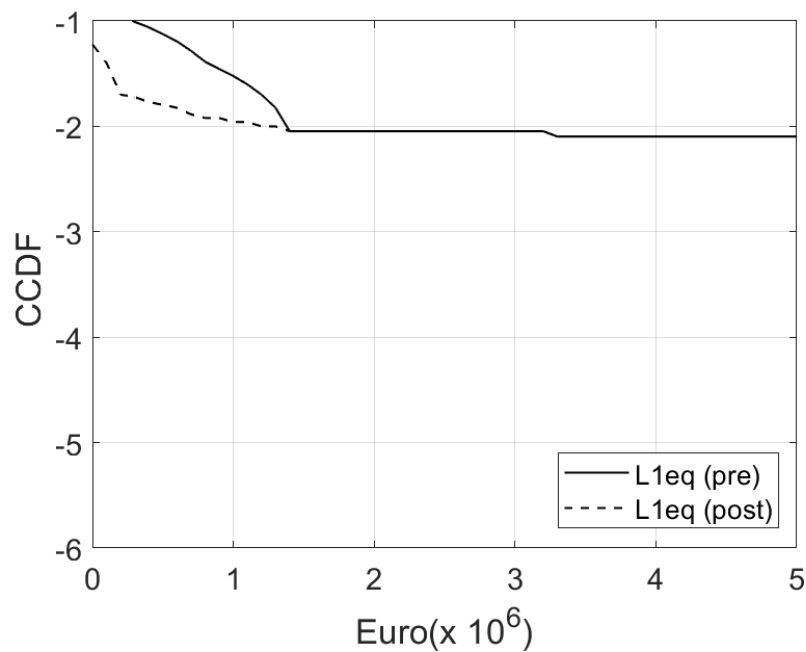


Figure 3.2.9 : Risk curve for earthquake hazard: comparison pre vs post intervention.

It can be noted that the interventions are quite effective in reducing losses associated to high probability of occurrence. This is consistent with the solution strategy adopted that aims at mitigating the main vulnerabilities associated with the operational and life-safety limit states.



3 Solution strategies for fire risk mitigation

3.1 Interventions

Different fire risk mitigation measures are available for ordinary buildings. They can be grouped in three main typologies:

- *prevention measures* consist pre-fire working measures like limitation of ignition sources and of human hazardous measures or instruction of occupants about emergency procedures and evacuation. Such kind of measures mainly attain to the management (e.g. vigilance and instruction) and architectural design procedure (e.g. proper design of evacuation paths);
- *protection measures* consist in appropriate measures to decrease the vulnerability of the structures to fire (e.g. protective paints), or the fire hazard intensity (e.g. sprinkler automatic fire suppression system). Protection measures can be subdivided in active and passive protection measures. Active protection measures implies the automatized intervention or the technological activation (electricity is often needed) of an hazard suppression system (e.g. sprinklers or automatic fire doors), while passive protections mainly do not require any technological or electricity-dependent activation. It is important to say that active measures are effective only in the ignition (pre-flashover) phase of fire, while passive measure are effective in both pre-flashover and flashover phases;
- *structural robustness*. The last measure which is able to mitigate the effects of fire on buildings and structure, consist in designing the structural system to retard as much as possible the occurring of significant (global or semi-global) collapses due to prolonged fire expositions. This last measure aims to avoid the propagation of losses from the fire compartment to the rest of the building: for example, if fire occurs in a floor of a high rise building, that is a single compartment, also if the flashover cannot be avoided and, consequently, all the contents and non-structural parts in the floor are lost (together with the life of the occupants in that floor), the structural components of the floor (and of the rest of

the structure designed as a whole) have to be designed for not developing the progressive collapse mechanisms which can involve other floors, and then propagate the losses to the rest of the building. Structural robustness requirement is a matter of structural design.

Then, the effectiveness of the different fire risk mitigation measures can be strictly related with the different fire development phases as described above and shown in Figure 3.3.1.

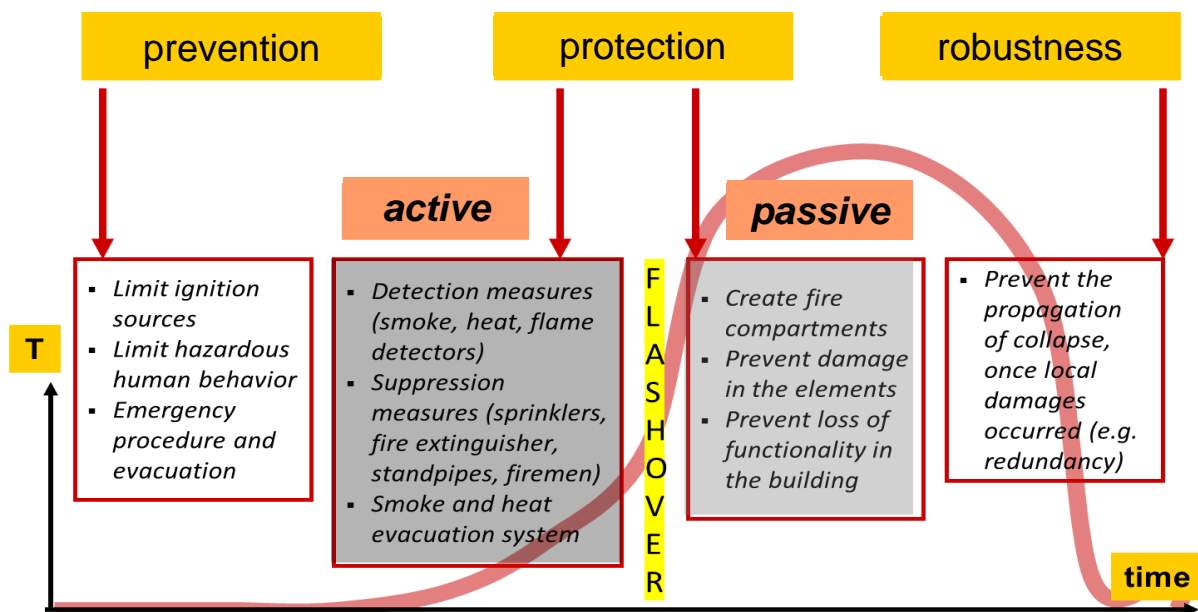


Figure 3.3.1 -. Effective fire mitigation measures in different phases of the fire development process.

In what follow, some more details are provided regarding the active protection put in place by mean of sprinkler system, which is the measure that has been applied to the case study in the MiChe project.

3.1.1 Sprinkler system

A fire sprinkler system consists of a water supply system, providing adequate pressure and flowrate to a water distribution piping system, until the arrival of the flux to water spatial diffusors (sprinklers), which are usually connected at the compartment roof. The sprinkler automatic fire suppression plant is a complicate system, which implies complex pipes assembly and high-pressure pumps, as schematically represented in Figure 3.3.2.

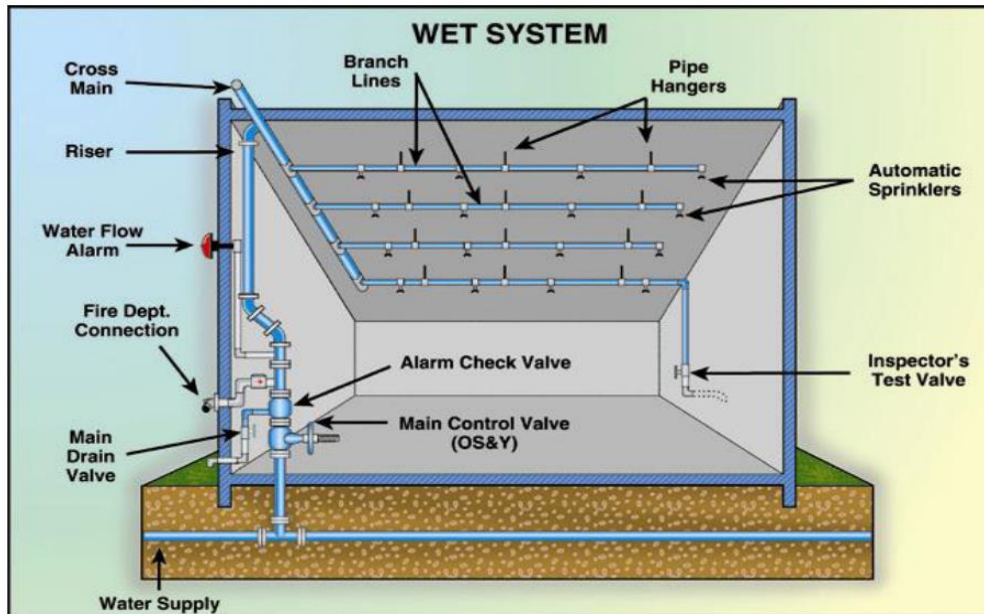


Figure 3.3.2 -. Schematic representation of automatic fire suppression system by sprinkler (after Marotta 2013).

Sprinkles (final component of the line for water rain diffusion) produces paraboloid jet falling on the fire for suppression purposes (Figure 3.3.3).

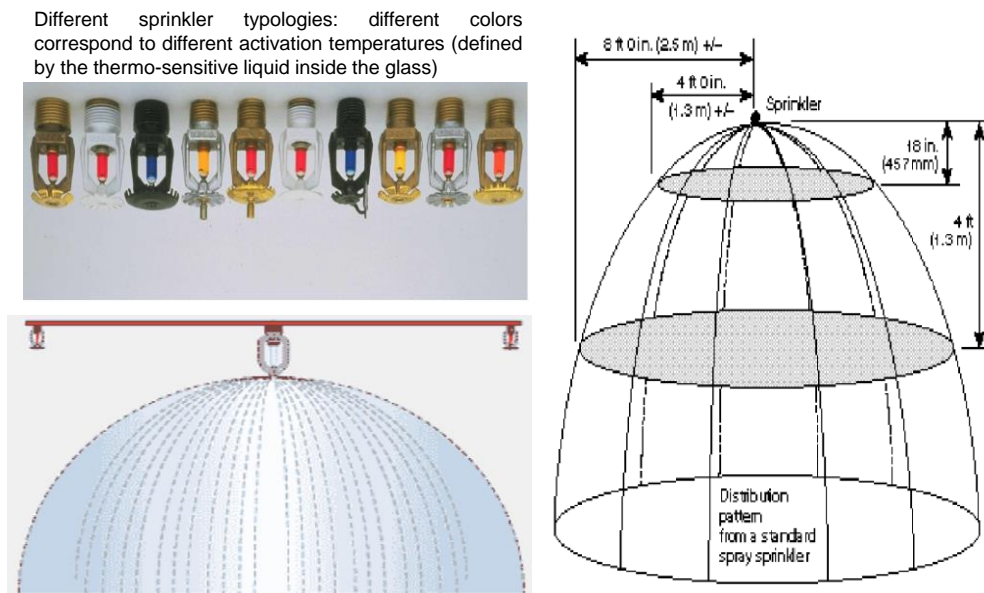


Figure 3.3.3 . Parabolic sprinkler diffusion area (after Marotta 2013).

Design of the sprinkler system consist in determining the number of water diffusion sprays to cover the compartment surface on the basis of the floor roof height, paraboloid dimensions and the required system water pressure.

3.2 Fire risk assessment

The installation of sprinkler automatic fire suppression system with an activation temperature of 60°C is considered as mitigation measure for fire risk. The effect of the sprinklers is shown by comparing (Figure 3.3.4) the fire development at the same time step as obtained without sprinklers and with them. The main effect of installing the sprinklers is then decreasing the air temperature around the structural elements and confining the fire extension.

In terms of risk, the installation of sprinkler automatic fire suppression systems has a significant effect in reducing risk mainly for the most catastrophic scenarios (tails of the risk curve). The change of the risk curve due to the installation of sprinklers is shown in Figure 3.3.5.

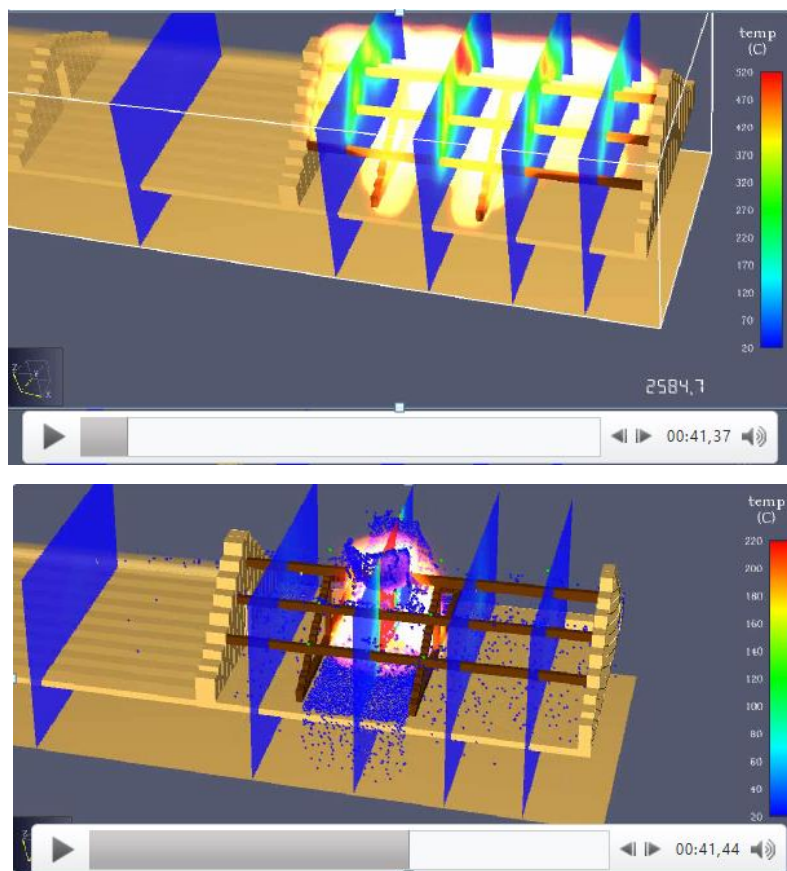


Figure 3.3.4: Effects of the sprinklers fire development in the loft.

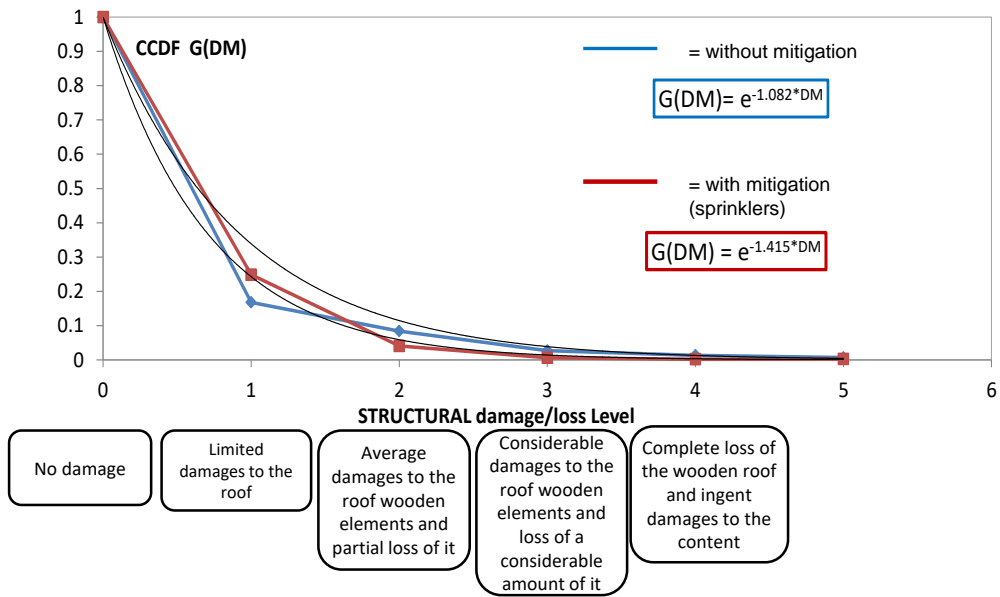


Figure 3.3.5: Fire risk curve with and without mitigation measures.

Figure 3.3.6 compares the loss curve due to fire hazard in pre-intervention and post-interventions conditions.

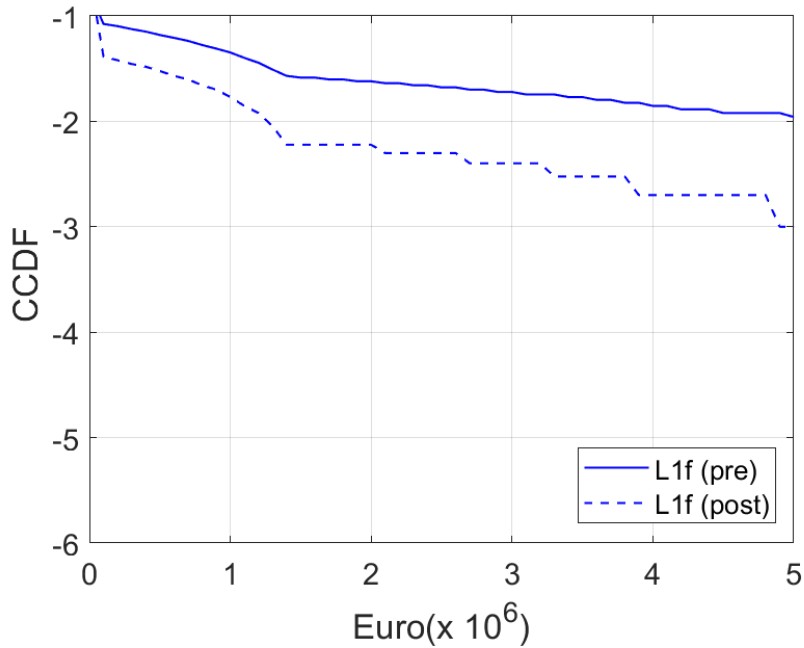


Figure 3.3.6 -. Loss curves L1 considering fire hazard.



ALMA MATER STUDIORUM
UNIVERSITA' DI BOLOGNA

DICAM

Dipartimento di Ingegneria Civile,
Chimica, Ambientale e dei Materiali

MiChE

Mitigating the Impacts of natural hazards on Cultural Heritage
sites, structures and artefacts

It can be noticed that the proposed interventions are effective in reducing risks within the entire range of probabilities.

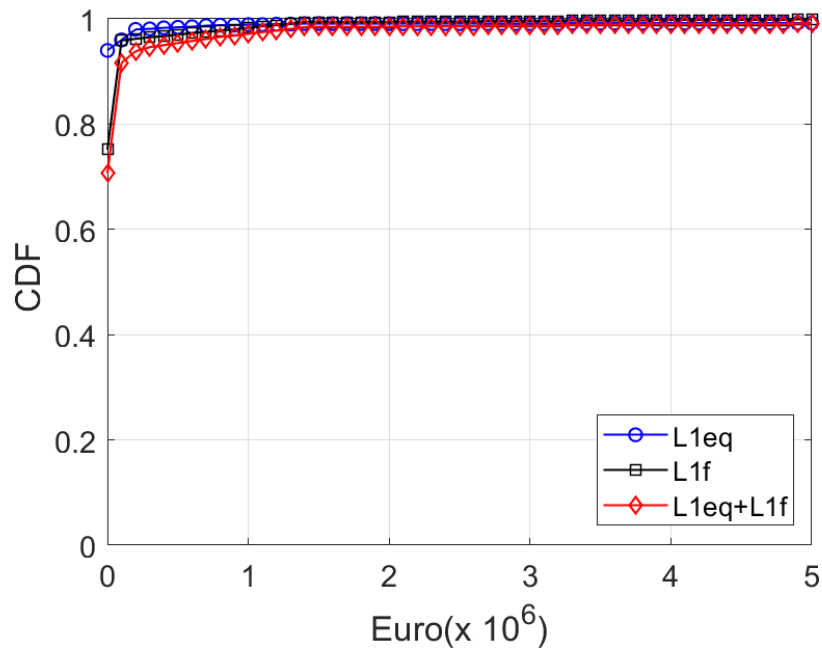


4 Multi-risk assessment due to earthquake and fire hazard

4.1 Total risk curve L1

The “total risk” curve has been obtained by combining the risk curves related to each considered hazard according to the procedure introduced in part 1.

Figure 3.4.1 provides the cumulative distribution functions CDF and complementary cumulative distribution curves CCDF of risk curve L1 related to the combination of earthquake and fire hazards.



(a)

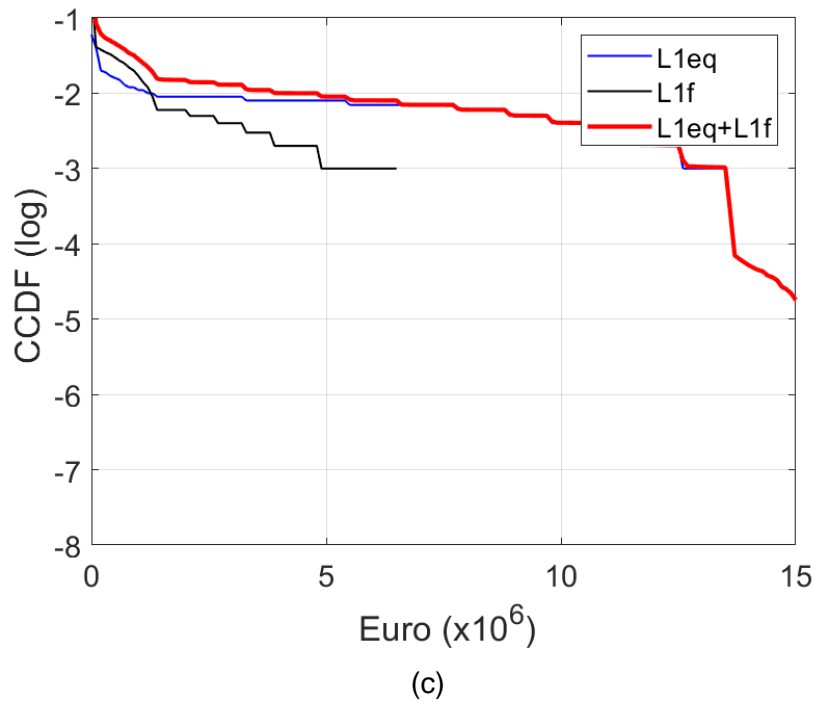
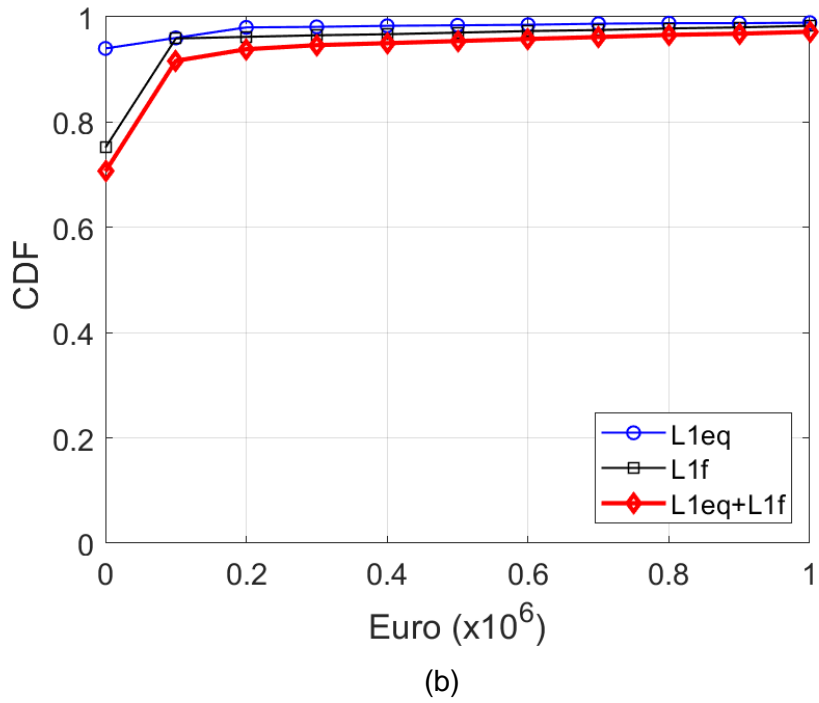


Figure 3.4.1: Total risk curves: (a) CDF, (b) CDF, zoom; (c) CCDF in log scale.

The following figure compares the total risk curve L1 associated to pre-intervention and post-interventions conditions

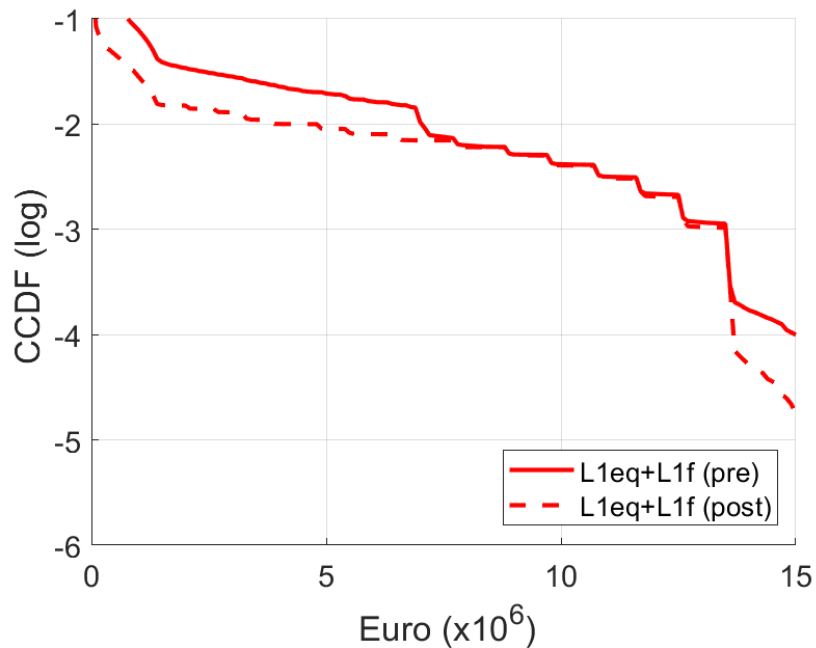


Figure 3.4.2: Total risk curves: comparison pre vs post intervention.

A significant reduction of losses can be noticed in two regions:

- High probabilities (probabilities larger than 10^{-2}).
- small probabilities (probabilities less than 10^{-4}).

Based on the obtained results it can be concluded that the envisaged mitigation interventions are effective in reducing the economic losses associated to both earthquake and fire hazards.



Bibliography

- [1] ISCARSAH (International Scientific Committee for Analysis and Restoration of Structures of Architectural Heritage), "Recommendations for the analysis, conservation and structural restoration of Architectural Heritage," *Icomos*, no. June, pp. 3–6, 2003.
- [2] P. Lourenço, "Computations of historic masonry structures," *Struct. Eng. Mater.*, 2002.
- [3] Guidelines for Evaluation and Mitigation of Seismic Risk to Cultural Heritage, "Guidelines for Evaluation and Mitigation of Seismic Risk to Cultural Heritage," *Gazz. Uff.*, vol. 47, 2011.
- [4] ISCARSAH, "Recommendations for the analysis, conservation and structural restoration of Architectural Heritage," *Icomos*, no. June. pp. 3–6, 2003.
- [5] C. Blasi and E. Coïsson, "The importance of historical documents for the study of stability in ancient buildings: The french Panthéon case study," *Asian J. Civ. Eng. (Building Housing)* 7, 2006.
- [6] J. Burland, M. Jamiolkowski, and C. Viggiani, "Leaning Tower of Pisa: Behaviour after Stabilization Operations," *169*, vol. 1, no. 3, pp. 156–169, 2009.
- [7] J. B. Burland, M. Jamiolkowski, and C. Viggiani, "Stabilising the leaning tower of Pisa," *Bull. Eng. Geol. Environ.*, vol. 57, no. 1, pp. 91–99, 1998.
- [8] G. Fiorentino *et al.*, "Seismic reassessment of the leaning tower of Pisa: Dynamic monitoring, site response, and SSI," *Earthq. Spectra*, vol. 35, no. 2, pp. 703–736, 2019.
- [9] G. Fiorentino *et al.*, "Leaning Tower of Pisa : Recent Studies on Dynamic Response and Soil-Structure Interaction," *16th Eur. Conf. Earthq. Eng. Thessaloniki 18-21 June*, no. July, pp. 1–12, 2018.
- [10] G. Gottardi, A. Lionello, M. Marchi, and P. P. Rossi, "Monitoring-driven design of a multiphase intervention for the preservation of the Frari bell tower in Venice," *Riv. Ital. di Geotec.*, vol. 49, no. 1, pp. 45–64, 2015.
- [11] A. Lionello, C. Rossi, and P. P. Rossi, "Testing and monitoring for the control of strengthening interventions of Santa Maria Gloriosa Dei Frari in Venice," *Res. Dev.*, pp. 113–125, 2015.
- [12] G. De Felice and A. Mauro, "On Overturning of the Façade in Churches with Single Nave : Some Case Studies from L ' Aquila , Italy , 2009 Earthquake," *Adv. Mater. Res.*, vol. 134, pp. 807–812, 2010.
- [13] A. Dazio, "The effect of the boundary conditions on the out-of-plane behaviour of unreinforced masonry walls," *Proc. 14th World Conf. Earthq. Eng.*, 2009.
- [14] M. R. Valluzzi, E. Garbin, M. Dalla Benetta, and C. Modena, "In-plane strengthening of timber floors for the seismic improvement of masonry buildings," *11th World Conf. Timber Eng. 2010*,



WCTE 2010, vol. 2, pp. 1752–1757, 2010.

- [15] M. Gentilini, C. Marzani, A. Mazzotti, “Nondestructive characterization of tie-rods by means of dynamic testing, added masses and genetic algorithms,” *J. Sound Vib.*, pp. 76–101, 2013.
- [16] S. Baraccani, G. Dan, A. Di Tommaso, and T. Trombetti, “Reducing seismic out of plane vulnerability of masonry church façades through optimization of capacity spectrum by tie rods,” *Key Eng. Mater.*, vol. 817 KEM, pp. 325–333, 2019.
- [17] B. Silva, M. Dalla Benetta, F. Da Porto, and C. Modena, “Experimental assessment of in-plane behaviour of three-leaf stone masonry walls,” *Constr. Build. Mater.*, vol. 53, pp. 149–161, 2014.
- [18] M. R. Valluzzi, F. Da Porto, and C. Modena, “Behavior and modeling of strengthened three-leaf stone masonry walls,” *Mater. Struct. Constr.*, vol. 37, no. 267, pp. 184–192, 2004.
- [19] M. Corradi, C. Tedeschi, L. Binda, and A. Borri, “Experimental evaluation of shear and compression strength of masonry wall before and after reinforcement: Deep repointing,” *Constr. Build. Mater.*, vol. 22, no. 4, pp. 463–472, 2008.
- [20] M. Dolce, D. Nigro, F. C. Ponzio, and R. Marnetto, “the Cam System for the Retrofit of Masonry Structures,” *7th Int. Semin. Seism. Isol. Passiv. Energy Dissipation Act. Control Vib. Struct.*, no. October, pp. 2–3, 2001.
- [21] E. Ferretti and G. Pascale, “Some of the latest active strengthening techniques for Masonry Buildings: A critical analysis,” *Materials (Basel)*, vol. 12, no. 7, 2019.
- [22] E. Zanello, “Miglioramento sismico con trefoli in acciaio inox. La torre nord del Castello di Compiano,” *J. Chem. Inf. Model.*, vol. 53, no. 9, pp. 1689–1699, 2013.
- [23] P. Napoli, “Rinforzo Di Archi E Volte.” pp. 1–17.
- [24] G. Croci, “General methodology for the structural restoration of historic buildings: The cases of the Tower of Pisa and the Basilica of Assisi,” *J. Cult. Herit.*, vol. 1, no. 1, pp. 7–18, 2000.
- [25] L. Ferrario, M. Alessandra, V. Andreis, S. Zanotti, P. Riva, and E. Giuriani, “Behavior and retrofitting of single-leaf vaults under distributed horizontal forces,” in *Structural Analysis of Historical Constructions –*, 2012.
- [26] L. Jurina, “The ‘reinforced arch method’: a new technique in static consolidation of arches and vaults.,” in *Proc. of the European Conference “Innovative Technologies and Materials for the Protection of Cultural Heritage.”*, 2003.
- [27] P. Foraboschi, “Strengthening of Masonry Arches with Fiber-Reinforced Polymer Strips,” no. June, pp. 191–202, 2004.
- [28] D. V. Oliveira, I. Basilio, and P. B. Loureño, “Experimental behavior of FRP strengthened masonry arches,” *J. Compos. Constr.*, vol. 14, no. 3, pp. 312–322, 2010.



- [29] M. R. Valluzzi, M. Valdemarca, and C. Modena, "Behavior of Brick Masonry Vaults Strengthened by FRP Laminates," *J. Compos. Constr.*, vol. 5, no. 3, pp. 163–169, 2002.
- [30] M. Corradi, A. Borri, G. Castori, and K. Coventry, "Experimental analysis of dynamic effects of FRP reinforced masonry vaults," *Materials (Basel)*, vol. 8, no. 12, pp. 8059–8071, 2015.
- [31] G. Ramaglia, G. P. Lignola, A. Balsamo, A. Prota, and G. Manfredi, "Seismic Strengthening of Masonry Vaults with Abutments Using Textile-Reinforced Mortar," *J. Compos. Constr.*, vol. 21, no. 2, pp. 1–16, 2017.
- [32] F. G. Carozzi, C. Poggi, E. Bertolesi, and G. Milani, "Ancient masonry arches and vaults strengthened with TRM, SRG and FRP composites: Experimental evaluation," *Compos. Struct.*, vol. 187, no. October 2017, pp. 466–480, 2018.
- [33] L. Garmendia, P. Larrinaga, R. San-Mateos, and J. T. San-José, "Strengthening masonry vaults with organic and inorganic composites: An experimental approach," *Mater. Des.*, vol. 85, pp. 102–114, 2015.
- [34] L. De Lorenzis, R. Dimitri, and A. La Tegola, "Reduction of the lateral thrust of masonry arches and vaults with FRP composites," *Constr. Build. Mater.*, vol. 21, no. 7, pp. 1415–1430, 2007.
- [35] A. Avorio, A. Borri, and M. Bottardi, "Theoretical Analysis and a case study of historical masonry vault strengthened by using advanced FRP," in *3rd International Conference Advanced Composite Materials in Bridge and Structures*, 2000.
- [36] A. Borri, M. Corradi, and A. Vignoli, "Seismic upgrading of masonry structures with FRP," ... *'Degli Stud. di Perugia, Fac. di ...*, 2002.
- [37] A. Avorio, A. Borri, M. Corradi, A. Barbieri, and A. Di Tommaso, "Comportamento dinamico di volte in muratura rinforzate con FRP-materials: primi risultati," in *X Congresso Nazionale "L'ingegneria Sismica in Italia" ANIDIS*, 2001, no. January 2016.
- [38] E. Nora and A. Ghioni, "Alluvioni e terremoti. Principali rischi naturali di Modena nel Novecento"., *La città e l'ambiente. Le trasformazioni Ambient. e urbane a Modena nel Novecento*, 2009.
- [39] A. E. R. – S. Idro-Meteo-clima, "Rapporto dell'evento meteo dal 15 al 19 novembre 2019", 2019.
- [40] W. Qiusheng, H. Liu, S. Wang, B. Yu, R. Beck, and K. Hinke, "A Localized Contour Tree Method for Deriving Geometric and Topological Properties of Complex Surface Depressions Based on High-Resolution Topographical Data," *International J. Geogr. Inf. Sci.*, 2015.
- [41] S. Rossi, "Mappatura della pericolosità idraulica da nubifragio mediante l'analisi di modelli digitali delle quote del terreno ad elevata risoluzione orizzontale," 2015.
- [42] T. Rossetto, I. Ioannou, and D. N. Grant, "Existing Empirical Fragility and Vulnerability



- Relationships: Compendium and Guide for Selection," *GEM Tech. Rep.*, vol. 01, p. 77, 2015.
- [43] D. Labate, "Il contributo dell'archeologia alla lettura di un monumento, in *La torre Ghirlandina. Un progetto per la Conservazione*," L. Sossella, Ed. 2009.
- [44] Cadigliani, R., *La torre Ghirlandina. Un progetto per la Conservazione*. 2009.
- [45] G. Bertoni, "La cattedrale modenese preesistente all'attuale: Primo ragguaglio sugli scavi del Duomo, agosto-settembre 1913/Giulio Bertoni.," Orlandini, Ed. 1914.
- [46] P. Frankl, "Der Dom in Modena, in 'Jahrbuch fur Kunstwissenschaft,'" SIFET., 1927.
- [47] A. Peroni, "Architettura e scultura: Aggiornamenti, in *Wiligelmo e Lanfranco nell'Europa romanica*," 1989.
- [48] A. Peroni, "Il Duomo di Modena. L'architettura, in *Il Duomo di Modena*," F. C. Panini, Ed. *Mirabilia Italiae* 9., 1999.
- [49] S. Lomartire, "Paramenti murari del Duomo di Modena. Materiali per un 'edizione critica, in *Wiligelmo e Lanfranco nell'Europa romanica*," 1989.
- [50] M. Armandi, "Copie e originali. Il repertorio di mensole figurate del Duomo di Modena," in *Il Duomo di Modena*, C.FRUGONI, Ed. Franco Cosimo Panini., 1999.
- [51] E. Silvestri, "Una rilettura delle fasi costruttive del Duomo di Modena," 2013.
- [52] A. K. Porter, "Lombard Architecture," H. and Milford, Eds. Yale University Press, 1917.
- [53] A. Dondi, "Il Duomo di Modena, notizie storiche ed artistiche," 1896.
- [54] and M. D. Castagnetti, C., E. Bertacchini, A. Capra, "Il laser scanning terrestre per l'analisi di edifici di interesse storico ed artistico," in *Geomatica - le radici del futuro*, 2011.
- [55] R. Lancellotta, "Geotechnical Engineering," T. and Francis, Ed. 2009.
- [56] R. Lancellotta, "Aspetti geotecnici nella salvaguardia della torre Ghirlandina.," in *La Torre Ghirlandina. Un progetto per la conservazione*, 2009.
- [57] R. Lancellotta, "La torre Ghirlandina: Una storia di interazione strutturaterreno," *Riv. Ital. di Geotec.*, 2013.
- [58] S. Lugli, "La Pietra Ringadora in Piazza Grande a Modena: Caratterizzazione geologica, provenienza, fenomeni di degrado e valorizzazione didattico-divulgativa," 2011.
- [59] M. Palermo, S. Silvestri, G. Gasparini, S. Baraccani, and T. Trombetti, "An approach for the mechanical characterisation of the Asinelli Tower (Bologna) in presence of insufficient experimental data," *J. Cult. Herit.*, vol. 16, no. 4, pp. 536–543, 2015.
- [60] T. P. Tassios, "Meccanica delle murature," Liguori, Ed. 1988.
- [61] A. W. Hendry, "Structural masonry," 1990.
- [62] Istruzioni CNR-DT 206, "Istruzioni CNR-DT 206/2007.Istruzioni per la Progettazione, l'Esecuzione ed il Controllo di Strutture di Legno, Cons. Nazionale delle Ricerch." 2007.



- [63] Cornell C.A, "Engineering seismic risk analysis," *Bull. Seismol. Soc. Am.*, 1968.
- [64] Krinitzsky E.L., "Deterministic versus probabilistic seismic hazard analysis for critical structures," *Eng. Geol.*, 1995.
- [65] F. Sabetta and A. Pugliese, "Attenuation of Peak Horizontal Acceleration and Velocity from Italian Strong - motion Records," *Bull. Seismol. Soc. Am.*, 1987.
- [66] B. Gutenberg and Richter ,C. F., "Seismicity of the Earth," 1949.
- [67] M. Dolce *et al.*, "The Emilia Thrust Earthquake of 20 May 2012 (Northern Italy): Strong Motion and Geological Observations - Report 1 -," vol. 2012, pp. 1–12, 2012.
- [68] D. M. Norme Tecniche per le Costruzioni, "Italian Ministerial Decree of 14 January 2008," *Gazzetta Ufficiale* n. 29 of 04 Feb 2008, 2008.
- [69] F. Parisi, F. De Luca, F. Petruzzelli, R. De Risi, and E. Chioccarelli, "Field inspection after the May 20th and 29th 2012 Emilia-Romagna earthquakes," 2012.
- [70] J. Heyman, *The stone skeleton: structural engineering of masonry architecture*. Cambridge University Press, 1995.
- [71] J. McInerney and M. DeJong, "Discrete Element Modeling of Groin Vault Displacement Capacity," *Int. J. Archit. Herit.*, vol. 9, no. 8, pp. 1037–1049, 2015.
- [72] S. Silvestri, G. Gasparini, M. Palermo, and S. Baraccani, "Analysis and Interpretation of the Structural Behavior of the Rose Window of the Cathedral of Modena (Italy)," in *9th International Conference on Structural Analysis of Historical Constructions*, 2014, no. October, pp. 14–17.
- [73] S. Baraccani, "Monitoring and Real Field Data for Understanding the Structural Behaviour and Health of Historical Buildings," 2017.